Charles University in Prague
Faculty of Science

Ph.D. study program: Modelling of Chemical Properties of Nano- and Biostructures

RNDr. Lukáš Grajciar

Quantum-chemical study of adsorption in microporous materials

Dissertation

Supervisor:
prof. RNDr. Petr Nachtigall, Ph.D.

Prague, 2013

Univerzite Karlova v Praze
Přírodovědecká fakulta

Doktorský studijní program: Modelování chemických vlastností nano- a biostruktur

RNDr. Lukáš Grajciar

Kvantově-chemické studium adsorpce v mikroporézních materiálech

Disertační práce

Školitel:
prof. RNDr. Petr Nachtigall, Ph.D.

Praha, 2013

Declaration of Authorship

I, LUKÁŠ GRAJCIAR, declare that this dissertation titled, 'QUANTUM-CHEMICAL STUDY OF ADSORPTION IN MICROPOROUS MATERIALS' and the work presented in it are my own. All the literature is properly cited, and I have not been yet awarded any other academic degree or diploma for this thesis or its substantial part.

Signed: _____

Date: _____

To my parents and Lucie

Abstract

Microporous materials play a crucial role in a wide range of applications in chemical engineering, chemistry, material science or lately even in medicine. Zeolites and metal-organic frameworks (MOFs) take a prominent place among them. The most important fields of applications include gas separation, purification or gas storage. A detailed understanding of adsorption properties of these materials represents a long-standing effort from experimental as well as computational chemistry community. However, accurate computational description of adsorption in microporous materials represents a significant challenge for computational chemists as: (i) unit cells of the crystalline microporous materials are typically large, (ii) dispersion interactions are of importance, and (iii) there are metal cations, often with open-shell electronic structure, present in the framework interacting strongly and specifically with adsorbing molecules. Despite a significant progress made in theoretical description of adsorption mechanisms in both zeolites and MOFs in last decade, there is a number of applications and systems for which the commonly used computational approaches fail to provide a needed accuracy. A whole class of such systems is represented, for example, by MOFs containing transition metal coordinatively unsaturated metal sites, the cus sites. Herein, we focused on proposing a computational scheme that can improve accuracy specifically for these systems or applications.

The aim of the dissertation is accurate description of adsorption in microporous materials that would allow for improved understanding of adsorption mechanism in these materials and could then lead to a rational design of adsorbents with desirable properties. The thesis includes a methodological section in which a previously proposed DFT/CC correction scheme was modified specifically to this end. The extended DFT/CC scheme was then applied for investigation of two types of microporous materials MOFs containing cus sites and zeolites.

Adsorption of various small molecules (H_2O, CO_2, CH_4, C_3H_6, C_3H_8 and CO) in the CuBTC MOF was studied. The suitability of various density functional theory (DFT) based methods for the description of adsorption on cus sites was analyzed first. Both standard DFT and dispersion corrected DFT (DC-DFT) functionals were found to be unable to yield sufficiently accurate results. Therefore, an extension of system-specific DFT/CC approach for accurate calculations of adsorbent-adsorbate interaction was proposed for description of adsorption in CuBTC. Importantly, the results obtained with this new approach were found to be in almost perfect agreement with available experimental data (errors $\sim$ 1 kJ.mol^{-1}) showing superior accuracy of DFT/CC over standard DFT or DC-DFT methods.

Adsorption of an environmentally consequential adsorbent, the carbon dioxide, in various zeolitic materials, was also studied. Specifically, a link between CO_2 adsorption heats and zeolite framework topology and composition was established based on the accurate DFT/CC calculations. Key factors influencing the stability of CO_2 adsorption complexes were identified following a very good agreement between available experimental and computational results.

The DFT/CC correction scheme was thus shown to be a viable approach for obtaining accurate description of the adsorption processes in various microporous materials even if a rather problematic systems or applications are considered. This method outperformed other DC-DFT methods commonly used in the field.

Abstrakt

Mikroporézní materiály hrají významnou roli v mnoha oblastech aplikace chemického inženýrství, chemie, materiálového výzkumu a v poslední době dokonce i v oblasti medicíny. Nejvýznamnější z nich jsou zeolity a mikroporézní koordinační polymery (angl. Metal Organic Frameworks, zkráceně MOF), které se používají především k rozdělování plynů, jejich čištění a k jejich uskladňování. Dlouhodobým cílem experimentálních a výpočetních chemiků je pochopit mechanismus adsorpce v těchto materiálech. Nicméně přesný popis tohoto procesu představuje velkou výzvu, protože (i) jednotkové cely krystalických forem těchto materiálů jsou obvykle velké, (ii) disperzní interakce musí být zohledněny, (iii) ve struktuře jsou přítomny kationty kovů, často s otevřenou elektronovou slupkou, které interagují silně a specificky s adsorbujícími se molekulami. Přes významný pokrok v teoretickém popisu mechanismu adsorpce v zeolitech a MOFech zaznamenaný v posledních letech, stále zůstává množství aplikací a systémů, pro které obecně používané výpočetní přístupy selhávají. Příkladem celé třídy takovýchto systému jsou MOFy obsahující v adsorpčních místech přechodné kovy, které jsou koordinačně nesaturované, t.j. *cus* adsorpční místa (z angl. coordinatively unsaturated sites). V této práci jsem hledal a vyvíjel výpočetní schéma, které by dokázalo zlepšit přesnost výpočtů právě pro tyto druhy systémů, a jeho následnou aplikací na studovanou problematiku.

Cílem disertační práce je přesný popis procesu adsorpce v mikroporézních materiálech, který by umožnil zlepšit pochopení mechanismu adsorpce v těchto materiálech a mohl by tak vést k návrhu adsorbentů požadovaných vlastností. Disertační práce obsahuje metodologickou část, ve které je představena modifikovaná DFT/CC (z angl. Density Functional Theory corrected for Coupled Clusters accuracy) metoda pro tyto účely. V další části je ukázána aplikace modifikované DFT/CC korekce ve výzkumu dvou typů mikroporézních materiálů: MOFů obsahujících *cus* adsorpční místa a zeolitů.

U systému CuBTC MOF, zástupce MOFů obsahujících *cus* adsorpční místa, byla studována adsorpce různých malých molekul (H_2O, CO_2, CH_4, C_3H_6, C_3H_8 a CO). Nejprve byla zkoumána vhodnost metod založených na teorií funkcionálu hustoty (DFT, z angl. Density Functional Theory) pro popis adsorpce v tomto systému. Bylo zjištěno, že ani standardní DFT, ani korigované DFT na zahrnutí disperze (DC-DFT, z angl. Dispersion Corrected Density Functional Theory) nejsou schopny poskytnout výsledek požadované přesnosti. Proto byl modifikován systémově specifický DFT/CC přístup tak, aby byl schopen poskytnout přesný výpočet interakce adsorbent-adsorbát, čímž se umožnil popis adsorpce v CuBTC MOFu. Je nutné zdůraznit, že výsledky získané pomocí nového přístupu byly téměř shodné s dostupnými experimentálními daty (rozdíl ~ 1 kJ.mol^{-1}), což ukazuje na vysokou přesnost modifikovaného DFT/CC oproti DFT a DC-DFT metodám.

Druhá část výzkumu se zabývala adsorpcí oxidu uhličitého v různých typech zeolitů. Především pak na základě přesných DFT/CC výpočtů byla teoreticky popsána závislost mezi adsorpčním teplem oxidu uhličitého a topologií a složením zeolitů. Díky vyborné shodě mezi dostupnými experimentálními daty a vypočtenými hodnotami byly určeny klíčové faktory ovlivňující stabilitu komplexů s adsorbovaným CO_2.

Disertační práce tak ukázala schopnost DFT/CC přesně popsat adsorpční procesy v různých mikroporézních materiálech, dokonce i v těch problematických. Tato metoda se ukázala být lepší než ostatní obecně používané DC-DFT metody v této oblasti.

Contents

List of Figures

List of Tables

Abbreviations

AQCC	**A**veraged **Q**uadratic **C**oupled **C**lusters
CBS	**C**omplete **B**asis **S**et limit
CCSD(T)	**C**oupled **C**lusters with **S**ingles, **D**oubles and perturbative **T**riples
DC-DFT	**D**ispersion **C**orrected **D**ensity **F**unctional **T**heory
DFT	**D**ensity **F**unctional **T**heory
DFT-D	**D**ensity **F**unctional **T**heory with empirical **D**ispersion
DFT/CC	**D**ensity **F**unctional **T**heory corrected for **C**oupled **C**lusters accuracy
GCMC	**G**rand **C**anonical **M**onte **C**arlo
GGA	**G**eneralized **G**radient **A**pproximation
LDA	**L**ocal **D**ensity **A**pproximation
MOF	**M**etal **O**rganic **F**ramework
MP2	**M**øller **P**lesset second order perturbation theory
MRE	**M**ean **R**elative **E**rror
RMSD	**R**oot **M**ean **S**quare **D**eviation
PES	**P**otential **E**nergy **S**urface
TD-DFT	**T**ime **D**ependent **D**ensity **F**unctional **T**heory
vdW	**v**an **d**er **W**aals
vdW-DF	**v**an **d**er **W**aals **D**ensity **F**unctional
vdW-TS	**v**an **d**er **W**aals correction by **T**katchenko and **S**cheffler
XDM	e**X**change hole **D**ipole **M**oment

Chapter 1

Introduction

Microporous materials play a crucial role in a wide range of applications in chemical engineering, chemistry, materials science or lately even in medicine. Specifically, the great potential for gas separation and purification, gas storage, shape/size selective catalysis, sensing or e.g., drug delivery has attracted a lot of attention in both industry and academia [1–3]. A prominent place among these material is reserved for zeolitic materials which have been around in industry for couple of decades now and are widely used as catalysists in petrochemical industry, as detergents or interestingly as ion exchangers in nuclear waste processing. These crystalline (alumino)silicates form a well-defined rigid three-dimensional structures with very similar chemical composition differing mostly in their pore topologies. An important feature of zeolites is the presence of extra-framework cations which balance the negative charge of zeolitic framework and act as the reaction/adsorption centers. However, the exact location of extra-framework cations in the framework is difficult to control or tune for a specific application. Similarly, the tunability of the pore dimensions (pore openings between $\sim 3 - 10$ Å) or surface chemistry is rather limited although more then 200 unique zeolitic frameworks have been reported so far along with many frameworks where aluminium in the structure was replaced by phosphorus, germanium, gallium or boron [4]. These drawbacks are however often outweighed by their low production cost[1] and high thermal stability.

Contrary to zeolites, the metal-organic frameworks (MOFs) represent a rather recent addition to the class of microporous materials. These microporous crystalline solids are composed of organic bridging ligands (e.g., carboxylates or azoles) coordinated to metal-containing nodes to form a three-dimensional extended network with uniform pore diameters typically in the range between 3 to 20 Å. Importantly, structures and properties of MOFs (e.g., pore size, structure flexibility, ligand connectivity, ligand functionalization, metal ion type) can be well-designed and systematically tuned by appropriate choice of

[1] Around 50 naturally occurring zeolites have been identified, many of which are rather abundant in nature.

the building blocks, i.e. organic linkers and metal-containing nodes. In this way, for example, in crystalline materials unprecedented internal surfaces areas, high void volumes and low framework densities were observed [5] with a large impact on applicability of MOFs in gas storage, gas separation and catalysis of bulkier molecules. Contrary to zeolites, location and density of active adsorption/reaction sites in the crystalline MOF structure is well-defined and easily controlled. Another interesting feature of MOFs is the occurrence of flexible frameworks which are envisioned to work in sensing devices or as the drug delivery systems [6]. Despite an apparent potential of MOFs for large-scale application there are two important issues that need to be addressed in future, namely the production cost and thermal and chemical stability; a significant progress has been achieved in these directions but there is still a lot of room for improvement.

One of the best adsorption and catalytic performances among MOFs were reported for a large group of MOFs where metal cations are not coordinatively saturated by organic linkers, i.e. the MOFs containing the coordinatively unsaturated sites (*cus* sites). These sites are in as-synthesized samples usually occupied by solvent molecule which can be removed by thermal activation without degradation of the sample. Activated *cus* sites then show enhanced adsorbate-framework interaction and interesting catalytic activities. Amongst the reported MOFs containing the *cus* site, the HKUST-1 MOF, Cu_3(1,3,5-benzenetricarboxylate)$_2$, often referred to as CuBTC, has become a reference MOF material that has often been investigated both experimentally and computationally [7, 8]. Therefore, this specific *cus*-containing MOF was a natural choice for a subsequent computational study discussed in detail in Section 3.1.

Obviously, application potential of both zeolites and MOFs has drawn a lot of attention from computational chemistry community. Various characteristics of these materials were investigated computationally (structure flexibility, catalytic properties, adsorption properties *etc.*). This thesis however focuses on adsorption properties only as: (i) the gas separation, storage or purification are some of the main applications of either zeolites or MOFs, (ii) understanding of the adsorbate-framework interaction is important for other investigations as well (e.g., catalysis), and quite importantly (iii) the *ab initio* computational approaches employed in this thesis and referred to throughout can provide *consequential* results in reasonable time. Typically, adsorption on both zeolites or MOFs is in either physisorption (i.e. below $\sim$ 50 kJ.mol^{-1}) or only weakly chemisorption regime and therefore requirements on the computational method accuracy are more stringent. Nevertheless, in many instances like alkane adsorption in high-silica zeolites [9] or adsorption of simple gas molecules in MOFs that do not contain *cus* sites [10], molecular simulations employing simple empirical force fields (FF) were found to provide reasonable agreement with experimental data. In general however, the suitability of empirical FF-based approaches for the description of more complex system such as MOFs with *cus* sites is at least questionable [11, 12]. It is therefore understandable

that interaction of various adsorbates with zeolites and MOFs was investigated at the density functional theory (DFT) level. However, for example in case of MOFs with *cus* sites, it has been found that interaction of small molecules with MOFs was typically overestimated when local exchange-correlation functionals (LDA) were employed and it was underestimated when semi-local generalized gradient approximation (GGA) type functionals were used [13–15].

Poor DFT performance and a surprisingly good one of empirical force fields in some cases is attributed to a non-negligible effect of van der Waals (vdW) interactions on the overall stabilization. Inability of local or semilocal DFT functionals to include long-range van der Waals (vdW) interactions is well-known and a number of dispersion-corrected DFT (DC-DFT) methods were proposed to address this deficiency and they are discussed in more detail in Section 2.1. Several attempts at including dispersion effects in zeolites and MOFs are included in the reference list ranging from empirically corrected DFT functionals (Section 2.1.2) and explicit vdW DFT functionals (Section 2.1.1) to random phase approximation with DFT wave-functions and hybrid MP2:DFT calculations [15–19].

While the DC-DFT approaches are (to some extent) capable to correct for missing dispersion interaction in DFT, other DFT deficiencies must be expected when adsorption on transitional metals cations with open-shell electronic structure takes place; such systems are represented by transition metal cation exchanged zeolites or MOFs containing transition metal *cus* sites. Besides, the metal-containing nodes of MOF structure often contain multiple transition metal cations which makes accurate description even more challenging; spin-coupling between unpaired electrons on individual transitional metal ions needs to be considered which have to be accompanied by validation of the applicability of standard single-reference DFT approach [20]. Indeed, it is demonstrated in Section 3.1.1 that when adsorption on transitional metal *cus* sites is considered there can be observed sizable DFT errors that are not related to dispersion.

Construction of a general approach that could correct for lacking dispersion and other DFT deficiencies in computationally tractable way is a very difficult and complicated task. In this thesis, one of the possible routes towards obtaining accurate results in a computationally feasible way for a subset of systems of interest is investigated, namely the extension of DFT/CC correction scheme [21, 22] (Section 2.2). DFT/CC scheme was initially proposed for description of the vdW complexes representing a generalization of standard empirical atom-atom corrected DFT methods, however herein, its extension for other than vdW-dominated adsorption complexes is proposed and applied specifically for adsorption of: (i) carbon dioxide on various zeolites (Section 3.2), and (ii) a range of small gas molecules on a specific and much studied *cus* site containing MOF, the CuBTC (Section 3.1). Importantly, results of computational investigation are complemented and discussed with respect to the experimental measurements carried out mostly by our

colleagues (the group of Prof. Philip L. Llewellyn at Marseille University, the group of Prof. Carlos Otero Areán at University of the Balearic Islands and the group of Prof. Jiří Čejka at the IPC AS CR).

The following thesis is divided into three sections. An overview of DC-DFT methods and of DFT/CC scheme in particular is given in Section 2. Results and discussion of computational investigations of adsorption mechanism in CuBTC MOF and various zeolites are provided in Section 3: (i) reliability of DFT and DC-DFT methods for the description of adsorption on *cus* sites is investigated in Section 3.1.1, (ii) adsorption mechanism of a number of gas molecules (water, carbon dioxide, methane, propane, propylene and carbon monoxide) in CuBTC MOF is elucidated in Section 3.1.2 based on the DFT/CC calculations, and (iii) in Section 3.2, a general model for carbon dioxide adsorption in zeolites of various topologies and chemical composition is proposed in the light of the DFT/CC results. Finally, Section 4 summarizes the results and draws general recommendations for future applications and developments.

Chapter 2

Methods

2.1 Overview of the DC-DFT methods

2.1.1 Explicit van der Waals DFT functionals

The inability of standard DFT exchange-correlation functionals (LDA, GGA, meta-GGA) to account for long-ranged, van der Waals interactions, stems from their local or at best semilocal dependence on the electron density. As dispersion interaction is by definition a non-local correlation effect[1] due to fluctuating densities in separated regions in space, an inherently non-local functional of density is needed for its inclusion. The development of non-local functionals was pioneered by Rutgers-Chalmers collaboration [23–25] who in 2004 proposed first computationally affordable non-local density functional for general geometries, dubbed vdW-DF functional [24]. In this approach the non-local correlation (dispersion) energy $E_{\mathrm{c}}^{\mathrm{nl}}$ is considered as an extra term in the exchange-correlation functional, namely

$$E_{\mathrm{xc}}[\rho] = E_{\mathrm{xc}}^{0}[\rho] + E_{\mathrm{c}}^{\mathrm{nl}}[\rho] = E_{\mathrm{x}}^{\mathrm{GGA}}[\rho] + E_{\mathrm{c}}^{\mathrm{LDA}}[\rho] + E_{\mathrm{c}}^{\mathrm{nl}}[\rho] \tag{2.1}$$

where short-ranged exchange and correlation terms are evaluated at the GGA and LDA level, respectively. The final form of the $E_{\mathrm{c}}^{\mathrm{nl}}$ is following:

$$E_{\mathrm{c}}^{\mathrm{nl}} = \frac{1}{2}\iint \rho(\mathbf{r})\Phi(\mathbf{r},\mathbf{r}')\rho(\mathbf{r}')d\mathbf{r}d\mathbf{r}' \tag{2.2}$$

where the non-local kernel Φ, itself a double-integral, is a complex function of electron density as well; more precisely, $\Phi(\mathbf{r},\mathbf{r}') = \Phi(k_0(\mathbf{r}), k_0(\mathbf{r}'))$, $\quad k_0(\mathbf{r}) = k_0(\rho(\mathbf{r}), \nabla\rho(\mathbf{r}))$. The parameter k_0 is constrained by the requirement that the exchange-correlation energy density of homogenous electron gas under vdW-DF approximation (see below and Ref. [26]), $\epsilon_{\mathrm{xc}}^{0} = -\frac{3e^2}{4\pi}k_0$, corresponds to the energy density obtained using the gradient

[1] Although HF method, and therefore also hybrid DFT functionals, are non-local, the non-locality is due to exchange and not the correlation part of the exchange-correlation energy.

corrected LDA functional prescription, the so-called *internal functional*:

$$\epsilon_{\rm xc}^{0} = \epsilon_{\rm xc}^{\rm LDA} - \epsilon_{\rm xc}^{\rm LDA}\left[\frac{Z_{\rm ab}}{9}\left(\frac{\nabla\rho}{2k_{\rm F}\rho}\right)^{2}\right] \tag{2.3}$$

where $k_{\rm F}^3 = 3\pi^2\rho$ is the Fermi wave vector and $Z_{\rm ab} = -0.8491$ is determined from the gradient expansion for slowly varying electron gas. Note that *internal functional* is used solely to impart constraints to k_0 and a combination of GGA exchange and LDA correlation is used for evaluation of short-range exchange-correlation energy in Eq. 2.1.

Most importantly, the $\Phi(\mathbf{r},\mathbf{r}')$ of Eq. 2.2 can be recast as function of two variables only $\Phi(D,\delta)$, easily tabulated for a set of (D_i,δ_j) values and interpolated when needed in (2.2). Moreover, an efficient implementation of the $E_{\rm c}^{\rm nl}$ in Fourier space [27] made its evaluation only marginally more computationally expensive than a regular GGA. However, a computationally tractable form of Equation 2.2 is an outcome of a number of approximations (e.g., full potential approximation - FPA, generalized plasmon-pole model of dielectric function ϵ *etc.*) made along the way starting from an exact adiabatic-connection fluctuation-dissipation formula for exchange-correlation energy [28]:

$$E_{xc} = \frac{1}{2}\int_0^1 d\lambda \iint d\mathbf{r}d\mathbf{r}'\frac{1}{|\mathbf{r}-\mathbf{r}'|}\left\{\int_0^\infty \chi_\lambda(\mathbf{r},\mathbf{r}',iu)\frac{du}{\pi} - \delta(\mathbf{r}-\mathbf{r}')\rho(\mathbf{r})\right\}, \tag{2.4}$$

where χ_λ is the density response to the external potential at the coupling strength λ.[2] A detailed analysis of the approximations employed is beyond the scope of this introductory section and can be found in Refs. [26, 29]. Note however that the choice of simplified formulas enabling analytical integration over some variables of (2.4) was done in a way to satisfy several known conservation laws, limits, sum rules and invariances [24].

A selection of specific exchange and correlation functionals for short-range $E_{\rm xc}^0$ term deserves few comments. First, the LDA has been used for short-range correlation as, within the vdW-DF formalism,[3] there should be only minimal correlation double counting contrary to GGAs. However, the accuracy of LDA exchange is not optimal and therefore GGA functionals are employed for exchange part. The choice of a specific GGA was guided by the requirement to minimize "spurious" binding from exchange alone that was observed, for example, in rare gas dimers for several standard GGAs [30]. In this respect, the revPBE functional of Zhang and Yang [31] was found to perform the best being closest to the exact HF exchange predictions and thus it was selected for use within the vdW-DF framework. Despite a sizable improvement in describing dispersion for several benchmark systems [32], the overall accuracy of vdW-DF was found to be insufficient even with respect to the empirical atom-atom dispersion correction

[2] $\lambda = 1$ represents the fully interacting system, while $\lambda = 0$ corresponds to non-interacting limit, i.e. to the Kohn-Sham system.

[3] Under FPA $E_{\rm c}^{\rm nl} = 0$ for uniform system, that is, one is correctly left with the $E_{\rm c}^{\rm LDA}$ term only.

schemes (see Section 2.1.2). Specifically, the vdW-DF has a tendency to underestimate the hydrogen-bond strength [33] and overestimate equilibrium binding distances [32] or the corresponding lattice constants in solids [34]. Therefore, a number of approaches based on the vdW-DF theoretical framework were proposed aiming at improving its performance for various systems of interest.

Both semi-local E_{xc}^{0} and non-local $E_{\mathrm{c}}^{\mathrm{nl}}$ terms were an object of revision, with especially the exchange $E_{\mathrm{x}}^{\mathrm{GGA}}$ part of E_{xc}^{0} being recognized to play a prominent role in determining the overall accuracy [35]. The largest overhaul of the vdW-DF framework came with a series of studies by Vydrov and Van Voorhis (VV) who developed three new vdW-DF-type functionals, namely the vdW-DF-09 [36], VV09 [37], and VV10[38]. Going from vdW-DF-09 to VV10 functional, progressively simplified analytical formulas with respect to the original vdW-DF were used for derivation of the $E_{\mathrm{c}}^{\mathrm{nl}}$ term. In this way, integral in Equation 2.2 can be evaluated more efficiently which was later used with benefit for development of both the generalization to a spin-polarized systems [37] or self-consistent implementations. Furthermore, few adjustable parameters (three or less for each VV-type functional) were introduced within the whole VV scheme which were fitted to reproduce either accurate molecular C_6 coefficients or binding/dissociation energies of a training set. Besides the modification in $E_{\mathrm{c}}^{\mathrm{nl}}$ term, the short-range E_{xc}^{0} contribution was altered as well; both range-separated hybrid functionals and standard semi-local GGAs were considered for $E_{\mathrm{x}}^{\mathrm{GGA}}$ while LDA and specifically PBE correlation functionals were used for $E_{\mathrm{c}}^{\mathrm{LDA}}$.

A large variance in the functionals used for the E_{xc}^{0} term is rather symptomatic of the vdW-DF-type functional development and this "degree of freedom" was exploited also by a second version of the vdW-DF functional, dubbed vdW-DF2 [25]. However, only minor physically motivated changes with respect to the original vdW-DF functional were carried out: (i) revPBE was replaced by revised PW86 (rPW86) [35] exchange functional as rPW86 was found to provide superior agreement with the exact HF exchange results, and (ii) Z_{ab} parameter of Eq. 2.3 was set to $Z_{\mathrm{ab}} = -1.887$ corresponding to large-N asymptote gradient correction that is more appropriate for use in molecular calculations [25]. Although being minor, the changes in the construction of the vdW-DF2 functional were shown to considerably improve the accuracy of original vdW-DF functional for several dispersion-dominated and hydrogen-bonded systems including the ones forming S22 set. Similarly, the VV10 functional of Vydrov and Van Voorhis provided significantly improved performance over vdW-DF being even superior to vdW-DF2. The accuracy of VV10 was actually observed to be on par with the best-performing empirical dispersion schemes like DFT-D3 [39] and therefore it was recommended as a general-use DC-DFT method [40].

Interestingly, a significant accuracy improvement was achieved upon simple refitting of GGA exchange functionals used in conjunction with the non-local vdW-DF functional

[34, 41, 42]. Specifically, Klimeš *et al.* studied the performance of several standard GGA exchange functionals coupled with vdW-DF for the binding energies of S22 benchmark set. They noticed that most of the dimers are underbound with revPBE-vdW but overbound with PBE-vdW. Furthermore, the enhancement factor F_{x} appearing in exchange energy density expression $\epsilon_{\mathrm{x}} = \epsilon_{\mathrm{x}}^{\mathrm{LDA}} F_{\mathrm{x}}$ has the same form for both revPBE and PBE:

$$F_{\mathrm{x}} = 1 + \frac{\mu s^2}{1 + \mu s^2/\kappa}, \tag{2.5}$$

where κ, μ are parameters and $s = \nabla\rho/2k_{\mathrm{F}}\rho$ is reduced density gradient. Hence a simple refitting of the enhancement factor parameters κ, μ was carried out on the S22 set, with the vdW-DF non-local energy included. The resulting GGA exchanged functional was labeled optPBE-vdW and exhibited improved accuracy not only for the S22 set but also for solid-state properties such as lattice constants, bulk moduli or atomization energies [34]. Besides optPBE, Klimeš *et al.* proposed other modified GGA exchange functionals as well, namely optB88, parameterized similarly to optPBE on the S22 set, and optB86b which was constructed using two constraints: (i) the small s behavior of enhancement factor F_{x} matches the one of PBEsol [43] which was reported to provide accurate lattice constants, and (ii) for large s, F_{x} should have $s^{2/5}$ behavior which was suggested as optimal in Ref. [35]. Performance of both optB88-vdW and optB86b-vdW was found to be superior not only with respect to standard vdW-DF and vdW-DF2 functionals but also with respect to optPBE [34].

Recently, an intriguing study by Wellendorf *et al.* attempted at a brand new parameterization of a general-purpose density functional including GGA exchange and LDA, PBE and vdW-DF2 correlation contributions [44]. Machine-learning techniques were employed in order to obtain robust well-behaved fit in a given model space that includes the previously discussed approaches as special cases. Moreover, as a number of very different benchmark databases (vdW complexes, reaction energies and barriers, solid state properties *etc.*) were used for parameterization, Wellendorf *et al.* were able to investigate the transferability of particular fits for description of different types of interactions or properties. Besides providing the *best general-purpose* vdW-DF-type functional labeled BEEF-vdW (containing 60% of PBE, 40% of LDA and 100% of vdW-DF2 non-local correlation), the study: (i) uncovered the bias of various GGA exchange parametrizations (optB88, vdW-DF2) towards certain types of properties, and (ii) highlighted the fact that database used for parameterization of the vdW-DF-type functional greatly influences the optimal GGA fit. Therefore, it is understandable that while BEEF-vdW represents the best compromise for the databases considered, there are the (already developed) vdW-DF-type functionals which perform better for a specific type of interactions. In other words, presently used vdW-DF model space is not flexible enough to

enable further accuracy improvement. Thus either fundamentally new approaches need be developed or the system-specific schemes should be applied.

2.1.2 Atom-atom dispersion correction schemes

A more straightforward approach to include dispersion terms to DFT is established via the following pair-wise atom-atom functional form:

$$E_{disp}[\rho] = -\sum_{i>j}\sum_{n\geq 6} C_n^{ij}(\rho) R_{ij}^{-n} f_{damp}^n(R_{ij},\rho), \tag{2.6}$$

where i and j are atom labels, $C_n^{ij}[\rho]$ are, in general, density-dependent dispersion coefficients between atomic pair ij, R_{ij} is the interatomic separation and $f_{damp}^n(R_{ij},\rho)$ is the damping function. Then the total dispersion corrected energy is expressed as a sum of DFT electronic energy, E_{DFT}, and (dispersion) correction term, E_{disp}, or generally ΔE:

$$E_{tot} = E_{DFT} + E_{disp} = E_{DFT} + \Delta E \tag{2.7}$$

The series of the $\sum_{n\geq 6} C_n R^{-n}$ form used in Equation 2.6 can be derived from the well-known second-order perturbation theory expression for dispersion energy between isolated molecules A and B [45],

$$E_{disp}^{AB} = -\sum_{m}^{A}\sum_{n}^{B} \frac{\left|\left\langle m^A n^B \left|\hat{V}_{AB}\right| 0^A 0^B \right\rangle\right|^2}{\omega_m^A + \omega_n^B}, \tag{2.8}$$

where $\hat{V}_{AB}$ is the electrostatic interaction operator between molecules A and B, $\left|0^A\right\rangle$ and $\left|m^A\right\rangle$ are the ground and mth excited states of the molecule A, and ω_m^A is the corresponding excitation energy, with similarly defined quantities for molecule B [46]. However, a general expression for intermolecular C_n coefficients stemming from Equation 2.8 is of a rather complex nature being given in terms of imaginary frequency integrals of the product of fragment polarizabilities multiplied by spherical harmonics which are used to account for the anisotropic character of C_n. Furthermore, transition from intermolecular C_n^{AB} to atom-atom (or domain-domain) C_n^{ij} dispersion coefficients, i.e. from monosite to multisite multipole expansion, needs to be established in order to arrive to Equation 2.6. Lastly, the $\sum_{n\geq 6} C_n R^{-n}$ series can be convergent only if the interacting fragments are well-separated which is often not the case for molecular complexes routinely considered within the DC-DFT framework.[4] Hence, the damping function, which is suggested to be n-order dependent [45], is introduced to avoid the divergence for short intermolecular distances.

[4] In fact, the atom centered multisite multipole expansion was found to converge much better than the monosite molecular multipole expansion [45].

A large number of approaches of the form (2.6) has been devised varying in the extent of approximations made; while the local response dispersion (LRD) method of Sato and Nakai [46] sum the contributions up to $n = 10$, retain the density-dependence and anisotropy of C_n^{ij} and even consider the system- and n-order dependence of damping function, the empirical DFT-D1 approach of Grimme [47] truncates the expansion (2.6) already at $n = 6$ and uses isotropic density-independent C_n^{ij} coefficients. Two of the most applied and computationally efficient approaches that take into account the density dependence of the interatomic C_n^{ij} coefficients were proposed by Becke and Johnson [48, 49] and Tkatchenko and Scheffler [50].

Becke and Johnson suggested a simple "semiclassical" model, dubbed the XDM model, in which instaneous dipole moment of (electron plus its) exchange hole generates a dispersion interaction between nonoverlapping systems. This rather heuristic model was derived later from first-principles by Ángyán [51] highlighting a number of approximations and simplification made along the way. The XDM method considers dispersion coefficients up to order $n = 10$ which are evaluated according to[5]

$$C_{2n+4}^{ij}(\rho) = C_{2n+4}^{ij}(\alpha_i, \alpha_j, \langle M_1^2 \rangle_i, \ldots, \langle M_n^2 \rangle_i, \langle M_1^2 \rangle_j, \ldots, \langle M_n^2 \rangle_j), n = 1, 2, 3, \qquad (2.9)$$

where α_i is the effective atom-in-molecule polarizability for atom i, estimated from a Hirshfeld partitioning of the molecular density and $\langle M_\ell^2 \rangle_i$ is the atomic expectation value of the squared and angular averaged (isotropic) ℓ-th multipole moment defined using the exchange hole dipole moment $d_{X\sigma}$ by

$$\langle M_\ell^2 \rangle = \sum_\sigma \int \rho_\sigma(\mathbf{r})[r^\ell - (r - d_{X\sigma})^\ell]^2 d^3\mathbf{r}]. \qquad (2.10)$$

The exchange-hole dipole moment $d_{X\sigma}$ can be easily calculated using either occupied Kohn-Sham orbitals being the one-electron property [48] or alternatively using the density-functional reformulation depending on the total density, the gradient, Laplacian of density and kinetic-energy density [49] (i.e., within the meta-GGA formalism). A simple rational damping function employing effective vdW radii is applied

$$E_{disp} = -\sum_{i>j} \sum_{n=6,8,10} \frac{C_n^{ij}}{R_{vdW,ij}^n + R_{ij}^n}, \qquad (2.11)$$

$$R_{vdW,ij}^n = a_1 R_{c,ij} + a_2, R_{c,ij} = (C_8^{ij}/C_6^{ij})^{1/2} \qquad (2.12)$$

with a_1 and a_2 being the (only) universal parameters determined by least-square fit to binding energies of 45 intermolecular complexes [53]. Basically the same damping is

[5] Odd order dispersion coefficients are zero for isotropic dispersion corrections or arise from higher than second-order perturbation theory treatment [45, 52].

suggested for use with the DFT-D3 method [39, 54] of Grimme (see below). The intermolecular C_n coefficients determined by the XDM approach (as a sum of atomic C_n's) were found to be on average $10-20\%$ off the experimental or many-body perturbation theory values [50, 53]. Similar discrepancies were observed for description of binding energies of a set of vdW intermolecular complexes [55]. Interestingly, the contribution of higher-order C_8 and C_{10} terms to the overall dispersion energy reached as much as 40% in some cases investigated emphasizing the importance of their inclusion in the dispersion correction models. Similar observation regarding the importance of higher-order contributions was made by Krishtal *et al.* employing their anisotropic DC-DFT method [52] and by Sato and Nakai with their local response dispersion (LRD) method [46]. It implies that within the atom-atom DC-DFT methods retaining the C_6 terms only, the strength and/or damping of the C_6 interactions needs to effectively account for the missing higher-order terms as well.

The method of Tkatchenko and Scheffler [50], labeled vdW-TS, represents another atom-atom DC-DFT approach capable of reflecting the bonding environment of an atom in molecule employing the density-dependent C_6 coefficients as well as the density-dependent damping function. However, the vdW-TS scheme restricts itself to C_6 terms contrary to either XDM or DFT-D3 approach. First, the reference free-atom $C_6^{ii,\text{free}}$ coefficients and static polarizability $\alpha_i^{0,\text{free}}$ values are obtained from self-interaction corrected TD-DFT calculations (using the Casimir-Polder formula for isotropic C_6's) scaled to reproduce accurate all-order many-body calculations for rare gases, alkalis, and alkaline earth atoms. Next, a number of approximations is employed in order to obtain the system-dependent effective $C_6^{ij,\text{eff}}$ coefficients [50]:

- A Casimir-Polder formula[6]

$$C_6^{AB} = \frac{3}{\pi}\int_0^\infty \alpha_A(i\omega)\alpha_B(i\omega)d\omega, \tag{2.13}$$

  where $\alpha_i(i\omega)$ is the average dipole frequency-dependent polarizability of system i, is analytically integrated using however only the leading term in the Padé series for $\alpha_i(i\omega)$ yielding a well-known approximate London formula [45]

$$C_6^{AB} = \frac{3}{2}\alpha_A^0\alpha_B^0[\eta_A\eta_B/(\eta_A+\eta_B)] \tag{2.14}$$

$$C_6^{AA} = \frac{3}{4}(\alpha_A^0)^2\eta_A, \quad \text{for} \quad A=B, \tag{2.15}$$

  where α_i^0 is the average dipole static polarizability and η_i is an effective frequency of system i.

[6]The Casimir-Polder formula being itself derived from Equation 2.8 using the constrain of spherical symmetry of the interacting systems, or for arbitrary systems averaging over all orientations is needed for the Equation 2.13 to hold [45].

- A (qualitative) proportionality relation between volume and polarizability is exploited next [56], with a Hirshfeld partitioning of the electron density being employed for the volume[7]

$$\frac{\kappa_i^{\text{eff}}}{\kappa_i^{\text{free}}}\frac{\alpha_i^{\text{eff}}}{\alpha_i^{\text{free}}} = \frac{V_i^{\text{eff}}}{V_i^{\text{free}}} = \left(\frac{\int r^3 w_i(\mathbf{r})\rho(\mathbf{r})d^3\mathbf{r}}{\int r^3 \rho_i^{\text{free}}(\mathbf{r})d^3\mathbf{r}}\right), \tag{2.16}$$

  where κ_i^l is the proportionality constant between volume and polarizability for the free-atom and atom-in-molecule, $w_i(\mathbf{r})$ is the Hirshfeld atomic partitioning weight for the atom i, and $\rho(\mathbf{r})$ and $\rho_i^{\text{free}}(\mathbf{r})$ is the total electron density and electron density of the free atom i, respectively. Using now the Equations 2.14, 2.15 and 2.16 the dependence of the C_6 coefficient on the electron density is established

$$C_6^{ii,\text{eff}} = \frac{\eta_i^{\text{eff}}}{\eta_i^{\text{free}}}\left(\frac{\kappa_i^{\text{free}}}{\kappa_i^{\text{eff}}}\right)^2\left(\frac{V_i^{\text{eff}}}{V_i^{\text{free}}}\right)^2 C_6^{ii,\text{free}}. \tag{2.17}$$

- The proportionality constant $\frac{\eta_i^{\text{eff}}}{\eta_i^{\text{free}}}\left(\frac{\kappa_i^{\text{free}}}{\kappa_i^{\text{eff}}}\right)^2$ was set to unity which turned out to be a reasonable simplification [50]. A formula for obtaining corresponding heteroatomic coefficients $C_6^{ij,\text{free}}$ can be easily derived using Equations 2.14 and 2.15.

Despite a several simplifications made, the intermolecular C_6 (a sum of atomic C_n's) coefficients calculated at the vdW-TS level were found to be very accurate; benchmarking on a database of 1225 experimental intermolecular C_6 coefficients showed a mean absolute relative error of only 5.5% which is e.g., approximately a factor of $1.5 - 2$ more accurate than the accuracy observed for the computationally more involved XDM method or broadly parametrized DFT-D3 method. Use of a *relative* change of atomic polarizabilities with respect to the very accurate reference free-atom polarizabilities is presumably critical for a fine performance of vdW-TS in C_6 determination. The coupling of the vdW-TS scheme with the underlying exchange-correlation functional for shorter distances is achieved using a Fermi-type damping function

$$f_{damp}(R_{ij}, R_{ij,\text{eff}}^0) = \frac{1}{1 + exp[-d(\frac{R_{ij}}{s_R R_{ij,\text{eff}}^0} - 1)]}, \tag{2.18}$$

where $R_{ij,\text{eff}}^0$ is a sum of atomic vdW radii $R_{ii,\text{eff}}^0$ of constituent atoms, while d and s_R are free parameters. The value of parameter d,[8] adjusting the steepness of the damping function, is set to $d = 20$ and s_R is fitted using the S22 database of Jurečka *et al.* [58]. The effective atomic vdW radii $R_{ii,\text{eff}}^0$ are determined from free-atom vdW radii $R_{ii,\text{free}}^0$ using the relation between the effective- and free-atomic volume of Equation 2.16 with $R_{ii,\text{free}}^0$

[7] This point actually represent two approximations taken at the same time.

[8] A range of d values were investigated and optimal d value was chosen. Grimme uses the same d value within the DFT-D2 method [57].

value taken as the radius of a specific electron density contour value for the (spherical) free atom. Thus, the damping function defined by Equation 2.18, similarly to the C_6 coefficients, to some extent reflects the environment of an atom in molecule. The performance of the vdW-TS scheme, coupled with the PBE exchange-correlation functional, for binding energies of the S22 set was found to be similar or better than the one observed for the most popular empirical atom-atom DFT-Dn ($n = 1, 2, 3$) methods of Grimme [39, 47, 57] discussed below in more detail.[9] Recently, Tkatchenko *et al.* developed an extension of the vdW-TS method including both the screening effects and treatment of the many-body vdW energy to infinite order [59], i.e. evaluation of terms (within an approximate model) beyond the second-order perturbation treatment of Equation 2.8 was considered. The screened many-body dispersion energy is obtained from the solution of Schrödinger equation for a model system of coupled quantum harmonic oscillators placed at the positions of atoms in the monomers[10] which could be solved rather straightforwardly (within a fraction of DFT calculation time) as the Hamiltonian of the system is in quadratic (bilinear) form. Improvement over the original vdW-TS approach was observed with the role of screening and many-body effects emphasized for the large (supramolecular) dense systems [60]. This observation was later confirmed by Grimme who investigated interaction energies of twelve large organic dimers and quantified the effect of three-body interactions (included semi-empirically within the framework of his DFT-D3 method) to be between 2.3 to 14.6% for the particular systems [61].

A very pragmatic approach to include the dispersion interaction within the DFT framework is the empirical atom-atom correction scheme, often denoted as the DFT-D, DFT with dispersion. Contrary to previously discussed methods, neither C_n coefficients nor damping function of Equation 2.6 are explicitly electron density dependent.[11] This has to be compensated for by an (often) extensive fitting procedure using large training sets in order to obtain optimized values of a number of free parameters for a particular DFT-D model. The DFT-D type of approach was first suggested by various groups in the early 2000's [30, 62, 63] and later gradually developed by Grimme [39, 47, 57] to an efficient computational scheme applicable to systems containing almost any element of the periodic table. The empirical dispersion correction E_{disp} within the Grimme's DFT-D framework is given by

$$E_{disp} = -\sum_{i>j}\sum_{n\geq 6} s_n C_n^{ij} R_{ij}^{-n} f_{damp}^n(R_{ij}), \tag{2.19}$$

[9] Note that in both cases, i.e. for vdW-TS and DFT-Dn schemes, the S22 set was used for fitting of their free parameters. Hence, the comparison of their performance for the S22 set is reasonable.

[10] The overall many-body vdW energy is, similarly to the previous discussion, partitioned to the individual n-body vdW interaction between atoms.

[11] Obviously, an effective dependence on "averaged" atomic density is introduced by atom typing.

where compared to Equation 2.6 the dependence on the electron density is dropped and a global scaling parameters s_n, optimized individually for each exchange-correlation functional, are introduced. First DFT-D type method proposed by Grimme, denoted as DFT-D1 [47], was limited only to systems containing few atomic types (hydrogen, carbon, nitrogen, oxygen, fluorine and neon) as for most of these, reasonably accurate atomic C_6 coefficients were available from work of Wu and Yang [63]. Within the DFT-D1 method only the $n = 6$ order terms were retained and a Fermi-type damping function (compare with Equation 2.18) was adopted

$$f_{damp}(R_{ij}, R_{ij}^0) = \frac{1}{1 + exp[-d(\frac{R_{ij}}{R_{ij}^0} - 1)]}. \tag{2.20}$$

The vdW radii $1/2R_{ii}^0$ were determined, similarly as the $R_{ii,\text{free}}^0$ vdW radii within the vdW-TS method, as the radius of a specific (and rather *ad hoc* defined) electron density contour value for the free atom. The value of steepness parameter d was set to 23 being taken from Wu and Yang who determined its value by requiring $f_{damp} = 0.99$ at $R_{ij} = 1.2R_{ij}^0$. The heteronuclear C_6^{ij} coefficients were obtained using a simple combination rule

$$C_6^{ij} = 2\,\frac{C_6^{ii} C_6^{jj}}{C_6^{ii} + C_6^{jj}} \tag{2.21}$$

as it was argued that the effect of using more sophisticated combination rules on the overall DFT-D1 performance was only minor. Eventually, only the s_6 global scaling factor was determined from a training set of eighteen vdW complexes for the BLYP, BP86 and PBE functionals. Note however that several approximations were made along the way with a few parameters set "manually". Nevertheless, a sizable improvement over "standard" DFT was observed for the vdW complexes investigated; observed errors with respect to the reference data being about $10 - 30\%$.

An extension of the DFT-D1 method, the DFT-D2 method [57], was introduced in a short succession and addressed a large shortcoming of the DFT-D1 method, namely the lack of reliable and consistently obtained atomic C_6 coefficients for most elements of the periodic table. Therefore, in the DFT-D2 approach, the atomic C_6 coefficients are calculated by a heuristically altered London formula (see Equation 2.15 for comparison):

$$C_6^{ii} = 0.05 N I \alpha_i^0 \tag{2.22}$$

where N has values 2, 10, 18, 36 and 54 for atoms from rows 1-5 of the periodic table. Atomic ionization potentials I and static polarizabilities α_i^0 are calculated at the DFT/PBE0 level of theory. The proportionality constant 0.05 was adjusted to reproduce previously used C_6 values for H, C-Ne and other related properties [57]. However, for elements from group I and II and transition metals, the differences between the free

atom and the atom in typical bonding situations is large. Therefore, the C_6 coefficient for e.g., K-Zn were obtained by averaging the C_6 coefficients of preceding rare gas and the following group III element.[12] Heteronuclear C_6^{ij} coefficients were, contrary to DFT-D1, obtained from geometrical mean of homonuclear C_6^{ii} as it yielded much better results.[13] As the s_6 parameters represent a scaling of the C_6 coefficients, a determination of new s_6 parameters for exchange-correlation functionals was also required; new s_6 values were obtained using a training set of forty vdW complexes (e.g., the $s_6 = 0.75$ for PBE functional). Similarly, the R_{ii}^0 and d parameters of the Fermi-type damping function (Equation 2.20) were modified/rescaled with respect to the DFT-D1 method for optimal performance. Although the amount of empiricism in the DFT-D2 approach is sizable, its simplicity combined with a reasonable accuracy observed for a wide variety of systems have made it a first choice DC-DFT method when the role of dispersion in the investigated systems is assumed to be non-negligible.

A significantly revised DFT-D model, dubbed DFT-D3, was proposed by Grimme *et al.* in 2010 [39]. It incorporated an additional C_8 term in the dispersion energy series, made adjustments to damping function and formulas used for atomic C_n calculations and most importantly introduced a geometry (coordination number) dependent C_n coefficients incorporating thus some awareness of the chemical environment into the DFT-D3 scheme. First, the often criticized density functional dependent s_6 scaling factors were set to unity being replaced by functional-dependent s_8 global scaling factor and $s_{R,6}$ scaling factor of the vdW radii R_{ij}^0 used within a yet new form of damping function

$$f_{damp}(R_{ij}, R_{ij}^0) = \frac{1}{1 + 6(\frac{R_{ij}}{s_{R,n} R_{ij}^0})^{-d_n}}. \tag{2.23}$$

The steepness parameters were set to $d_6 = 14, d_8 = 16$ and vdW radii R_{ij}^0 for a particular (ij) were determined directly from atomic pair DFT calculations using consistent but a rather heuristic approach (see Ref. [39] for more details). Next, the (generally heteronuclear) C_6^{ij} coefficients were calculated using the Casimir-Polder formula (2.13) employing TD-DFT[14] approach to obtain frequency-dependent polarizabilities. Subsequently, the C_8^{ij} coefficients were computed using known recursion relations. In order to mimic the effect of environment on particular C_n^{ij} coefficients, besides the TD-DFT calculations on a pair of free atoms (ij), the environment-dependent $C_n^{ij,\text{eff}}$ coefficient were obtained from calculations on hydrides $I_m H_n$ and $J_k H_l$ by removing the contribution of

[12] Similar averaging was employed also for determination of vdW radii R_{ij}^0 of transitional metals.

[13] It was proved that geometrical mean is the upper bound of the exact C_6^{ij} [64].

[14] A specific "flavor" of PBE0 functional was utilized, labeled PBE38, with the amount of exact exchange changed from 1/2 to 3/8 as it was observed to yield much better excitation energies [65].

the hydrogens, i.e.,

$$C_6^{ij,\text{eff}} = \frac{3}{\pi}\int_0^\infty \frac{1}{m}\left[\alpha_{I_m H_n}(i\omega) - \frac{n}{2}\alpha_{H_2}(i\omega)\right] \times \frac{1}{k}\left[\alpha_{J_k H_l}(i\omega) - \frac{l}{2}\alpha_{H_2}(i\omega)\right] d\omega. \quad (2.24)$$

In this way a number of reference molecule-dependent coefficients were obtained. For a general structure, the actual $C_6^{ij,\text{eff}}$ is determined by interpolation between several reference values based upon (fractional) coordination number (CN) extracted from the molecular structure. However, three further global *ad hoc* parameters were required for either CN definition or C_6 interpolation [39]. The performance of proposed procedure for obtaining environment-dependent atomic C_6 coefficients was assessed on molecular C_6 coefficients; a mean percentage error of approximately 10% was seen which is similar to both vdw-TS or XDM methods discussed above. Inclusion of leading three-body (Axilrod-Teller-Muto) term was also considered but was not recommended for a default use. Note however, that recently, the importance of many-body terms for large systems was reported [60, 61]. In the end, only the s_8 and $s_{R,6}$ parameters were fitted using an extensive training sets containing extended S22 set, tripeptides, sugars, alkanes and cysteine conformers, and rare gas dimers. Regarding the performance of the DFT-D3 method, it was argued [39] that DFT-D3 method achieves results which are typically within 10% from CCSD(T) values and that the mean absolute error decreases by $0-30\%$ compared to the previous DFT-D2 method. Recently, further (minor) refinement of results was achieved upon using Becke-Johnson damping function of Equation 2.12 which is now a recommended damping function for use within the DFT-D3 scheme [54].[15]

Despite an improvement observed, the DFT-D3 still represents a rather heuristic correction with a number of "manually" or "by chemical reasoning" set parameters besides the ones fitted directly. Furthermore, the fitting of (especially) DFT-D methods is performed with respect to the accurate structural parameters or binding energies obtained at CCSD(T) level and not with respect to a "dispersionless" DFT. And lastly, the effect of either the higher-order or many-body corrections to the truly dispersion correction, which is shown to be non-negligible (see discussion above), are often neglected or to some extent effectively included in the lower-order pair-wise terms. Therefore, the E_{disp} within the DFT-D formalism is very much a model-dependent quantity [47] with a limited physical (dispersion) meaning and it likely incorporates errors related to other deficiencies of DFT besides dispersion description. Interestingly enough, the errors of DFT-D or density-dependent vdW-TS and XDM methods are already within $10-20\%$ [66] from reference values and we believe that further improvement is possible either via the refinement of underlying exchange-correlation functional or by changing focus from

[15] Improvement can be understood on the basis of the fact that Becke-Johnson damping introduces another free parameter.

universal "dispersion" correction to the one tailored specifically for a given application. The latter route is pursued in the following section.

2.2 The DFT/CC correction scheme

The DFT/CC approach [21, 22] formally falls within the class of empirically atom-atom corrected DFT methods, however, there are several important differences between DFT/CC correction scheme and "standard" DFT-D approaches. First, the artificial assumption about the particular form of the E_{disp} or rather ΔE correction (see Equation 2.7) is lifted; instead, the deficiencies of the DFT are corrected for using a robust Reciprocal Power Reproducing Kernel Hilbert Space (RP-RKHS) interpolation method designed specifically for construction of smooth molecular potential energy surfaces [67].[16] Second, rather than attempting to obtain a universal correction parameters using a large and heterogeneous training set of accurate post-HF data, the DFT-CC scheme focuses on the accurate description of a limited number of (extended) systems for which a careful selection of a suitable reference set (equivalent of a training set) is made. While each DFT/CC scheme application is accompanied with a rather involved generation of the reference system set, the DFT/CC also represents a framework for analysis of the DFT error in a specific system of interest (see Section 3.1.1). Next, the benchmark calculation used in the literature as the training set are often reported only for equilibrium distances, but within the DFT/CC approach one-dimensional scans through the PES of a particular molecular complex in the reference set are utilized. This practice is assumed to deliver a more consistent description of larger portions of the PES in question. And lastly, the basis set dependence of the ΔE correction is circumvented by using as converged DFT and reference theory data with respect to the basis set size as possible, i.e. the DFT/AVQZ and CCSD(T)/CBS (see Attachments for details on the basis sets definition).

The DFT/CC computational strategy begins the with evaluation of the inter-molecular energy[17] correction ΔE for reference set of molecules as the difference between DFT and CCSD(T)/CBS interaction energies

$$\Delta E = E_{CCSD(T)} - E_{DFT}. \tag{2.25}$$

The correction surface ΔE is assumed, similarly to Equation 2.19, to be pairwise atom-atom representable

$$\Delta E(R, \Omega) = \sum_{i=1}^{N_a} \sum_{j=1}^{N_b} \epsilon_{ij}^{\Omega}(r_{ij}), \tag{2.26}$$

[16] Within the DFT/CC scheme, the DFT error is evaluated with respect to some high-level post-HF method for a *range* of non-equilibrium inter-molecular distances, contrary to e.g. the DFT-D2 method.

[17] No intra-molecular corrections are considered within the DFT/CC scheme.

where Ω denotes the angular parameters, ϵ_{ij}^{Ω} are the Ω-dependent atom-atom pairwise correction functions and r_{ij} is the distance between atoms i and j belonging to different monomers. The correction functions ϵ_{ij}^{Ω} are then represented using one-dimensional reproducing kernels $q^{[n,m]}(x, x')$ for distance-like variables [67] of the form [68]

$$q^{[n,m]}(r, r') = \frac{1}{r_>^{m+1}} \sum_{k=0}^{n-1} \beta_k^{[n,m]} \frac{r_<^k}{r_>^k}, \tag{2.27}$$

where $r_< = min(r, r')$, $r_> = max(r, r')$ and the coefficients $\beta_k^{[n,m]}$ are implicitly given in Ref. [67]. These kernel functions possess an important *reproducing* property [67] which enables effective extraction of the smooth potential energy representation from gridded *ab initio* data points in the following form:

$$V(r) = \sum_{i=1} \alpha_i^{[n,m]} q^{[n,m]}(r, r_i). \tag{2.28}$$

where r_i are arbitrary selected grid points. The values of the $\alpha_i^{[n,m]}$ coefficients are then found by solving the system of linear equations

$$V(r_j) = \sum_{i=1} \alpha_i^{[n,m]} q^{[n,m]}(r_j, r_i). \tag{2.29}$$

where $V(r_j)$ are the values of the gridded *ab initio* data points.[18]

For the application within the DFT/CC scheme the $n = 2$ is used as it was shown that it is desirable to keep n as low as possible for numerical stability [69]. Furthermore, the m is set to 2 and kernel function $q^{[n,m]}(x, x')$ is interpolated with respect $x = r^2$ to both prevent the contamination of the long-range part of the correction functions by odd-order terms and to obtain specifically the "standard" r^{-6} asymptotic behavior. Thus we arrive at the final RP-RKHS functional form used for the ϵ_{ij}^{Ω} correction functions (compare with Equation 2.29)

$$\epsilon_{ij}^{\Omega}(r_{ij}) = \sum_{k=1} \alpha_k^{\Omega,ij} q(r_{ij}^2, r_k^2) \tag{2.30}$$

with the kernel function

$$q(r_{ij}^2, r_k^2) = \frac{1}{3r_>^6} - \frac{r_<^2}{5r_>^8}. \tag{2.31}$$

[18] Obviously, in order to solve the system of linear equation defined by Equation 2.29 the number of r_i grid points and thus the number of $\alpha_i^{[n,m]}$ coefficients should correspond to the number of *ab initio* data points. The r_i grid points are usually selected to cover the distance range of the *ab initio* data points.

Substitution of the Equation 2.30 into (2.26) then leads to a general prescription for ΔE similar to the Equation 2.28

$$\Delta E(R,\Omega) = \sum_{i=1}^{N_a}\sum_{j=1}^{N_b}\sum_{k=1}\alpha_k^{\Omega,ij} q(r_{ij}^2, r_k^2). \tag{2.32}$$

This equation can be also understood as a transformation of ΔE correction surface from R, Ω to the r_{ij}, Ω_{ij} coordinate space. Given a sufficient number of *ab initio* data points inversion of Equation 2.32 for various values of Ω is possible and presumably an accurate representation of the ΔE correction surface can be achieved. However, except from numerical stability issues [67], the transferability of the correction functions for systems outside the reference set will be problematic. Therefore in practice a number of changes and simplifications to the model has been made:

Anisotropy of the correction functions, i.e. the orientation- or Ω-dependence, is assumed to be negligible. The effect was however explicitly considered in Ref. [21] for various complexes of hydrogen, ethylene and benzene where it was found to be of low importance especially in the vdW minimum region. It was also concluded that a suitable choice of the reference systems is more important than the effect of anisotropy.

Atomic types are introduced, i.e. the ϵ_{ij} are replaced by the "averaged" correction functions for all the atoms of the same atomic type found in the respective monomers (e.g., hydrogen-hydrogen correction function ϵ_{HH}). The Equation 2.32 therefore reads now

$$\Delta E(R) = \sum_{i\in\mathbf{A}}\sum_{j\in\mathbf{B}}\sum_{k=1}\alpha_k^{At(i)At(j)} q(r_{ij}^2, r_k^2), \tag{2.33}$$

$$\Delta E(R) = \sum_{i\in\mathbf{A}}\sum_{j\in\mathbf{B}}\epsilon_{At(i)At(j)}, \tag{2.34}$$

where **A** and **B** stand for sets of atoms in fragments A and B and $At(k)$ is the atom type of atom k. Actually, the very recently developed extension of the DFT/CC method, dubbed vdW-DF/CC [70], is able to obtain reasonably transferable correction functions for all the atomic types present in the interacting monomers already using Equation 2.33, i.e. from a single reference system or more precisely from a single one-dimensional scan (see below). It was achieved by relating the coefficients α_k^{ij} for various combination of atomic types via their relative contribution to the overall vdW-DF non-local contribution [29, 70].

A single atomtype-atomtype correction function per reference system or per a one-dimensional scan[19] is obtained within the DFT/CC scheme. Thus, the number of reference models needed is equal to the number of distinct atomtype-atomtype correction functions generated.

In order to construct transferable correction functions for a target (extended) system containing various atomic types two rather tedious procedures had to be devised, namely the *sequential* and *iterative* procedure, which are usually combined for a specific application. In both cases a series of reference models with gradually (by one only if possible) increasing number of atomic types is generated until all the atomic types found in the target system are accounted for. In a *sequential* procedure only one atomtype-atomtype contact is added in one step of sequence with the new correction function derived by subtracting the contributions from other atomic types correction functions which were obtained in previous steps. For example, the correction curves for hydrogen-graphene interaction, i.e. the ϵ_{HH} and ϵ_{CH}, are obtained from $H_2 \cdots H_2$ and $H_2 \cdots$ benzene reference models, respectively. The total correction energy for $H_2 \cdots$ benzene reference model is expressed as a sum of the two terms corresponding to the H-H and C-H pair-wise interactions

$$\Delta E(R) = \Delta E_{\mathrm{CH}}(R) + \Delta E_{\mathrm{HH}}(R), \tag{2.35}$$

where $E_{\mathrm{HH}}(R)$ is calculated using the correction functions ϵ_{HH} obtained from $H_2 \cdots H_2$ reference system. The C-H contribution are then evaluated as

$$\Delta E_{\mathrm{CH}}(R) = \Delta E(R) - \Delta E_{\mathrm{HH}}(R), \tag{2.36}$$

from which the ϵ_{CH} correction functions can be readily acquired. The *sequential* procedure only was also used for generating correction curves for methane-CuBTC interaction (see Section 3.1.2).

A more elaborate procedure, the *iterative* one, can deal with more atomtype-atomtype contacts added in a sequence of reference systems. However, the number of added atomtype-atomtype contacts needs to be matched by the number of distinct monomer-monomer orientations of the respective reference system. For example, in case of two atomtype-atomtype (ij, kl) contacts added the procedure then proceeds as follows: (i) generate ϵ_{ij} for first monomer-monomer orientation and set the ϵ_{kl} to zero, (ii) generate ϵ_{kl} for second monomer-monomer orientation using the ϵ_{ij} obtained in the previous step, (iii) refine ϵ_{ij} for first monomer-monomer orientation using the ϵ_{kl} from previous step, and (iv) cycle over steps '(ii)' and '(iii)'until convergence or 'maxstep'is reached. It is

[19] In many instances, several correction functions are obtained for a single reference system where different monomer orientations are considered. For obtaining the correction function for a specific monomer orientation, a one-dimensional scan along a favorable monomer-monomer coordinate is carried out.

important to note that in order to obtain optimal transferability the monomer orientations are chosen in a way that dominant atomtype-atomtype contact ij (i.e. usually the shortest) is the one from which the respective ϵ_{ij} is obtained. Figure 2.1 depicting the reference set used for generation of the water-CuBTC correction curves (see Section 3.1.2) serves as an example for an extensive use of the *iterative* procedure, namely the correction functions for $(H_w - H_{MOF}, O_w - H_{MOF})$, $(H_w - C_{MOF}, O_w - C_{MOF})$, $(H_w - O_{MOF}, O_w - O_{MOF})$ and $(H_w - Cu_{MOF}, O_w - Cu_{MOF})$ atomtype-atomtype contacts are constructed in this way.

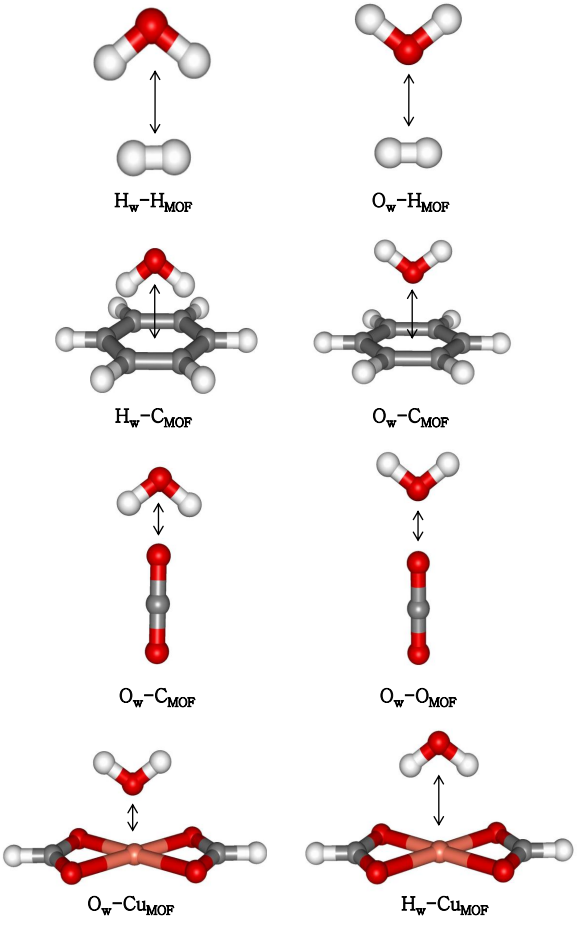

FIGURE 2.1: The reference set employed in order to obtain atomictype-atomictype correction functions for water-CuBTC interaction. Direction of the one-dimensional PES scans utilized for this purpose is shown by arrow. The subscripts indicate whether the respective atomic type belongs to water ('w') or CuBTC ('MOF').

Before applying the correction functions for a system of interest their transferability is thoroughly tested, i.e. stabilization of other[20] molecular complexes that were not included in the reference set is evaluated at the CCSD(T)/CBS level and compared with the DFT/CC results. If the agreement between reference and DFT/CC values is satisfactory, the correction function are used for the target system (for which CCSD(T)/CBS

[20]Usually larger and conveniently selected molecular complexes for a given problem are used.

values cannot be obtained). Otherwise, an adjustment of the reference set is made until reasonable accuracy of the DFT/CC results is achieved. An example of successful transferability checks carried out within the adsorption study of small molecules in CuBTC MOF is depicted in Figure 3.4.

The DFT/CC correction scheme can be summarized as follows:

- Selection of the reference set of molecular complexes, which represents a parameterization of the resulting DFT/CC model
- Generation of atomtype-atomtype correction functions ϵ_{ij} from reference set on tha basis of RP-RKHS interpolation
- Test the transferability of resulting correction functions for a larger molecular complex not included in the reference set and for which it is still feasible to carry out high-level post-HF calculations
- Application of DFT/CC to the (extended) system of interest

Until now the DFT/CC method has been successfully employed for description of gas-phase complexes [71], dispersion-bound molecular crystals [72] and for various adsorption complexes [73, 74]. Although it was developed primarily for accurate description of weakly (dispersion-dominated) interacting systems, its flexible form allows for extension to the systems where the stabilization was found to be stronger. This possibility was thoroughly explored in the thesis for the case of adsorption in MOFs and zeolites.

Chapter 3

Results and Discussion

3.1 Adsorption in CuBTC MOF

Computational investigations of adsorption properties of MOFs mostly rely on the empirical inter-atomic potential functions (IPF, often referred to as force field) used in Grand Canonical Monte Carlo (GCMC) simulations [10]. Although these IPFs do surprisingly well for many MOFs [75, 76], the suitability of IPF-based approaches for the description of MOFs with *cus* sites has been shown to be at least questionable [11, 12]. However, an adoption of more involved but yet computationally tractable approach, namely the DFT theory, does not lead to an improved description of adsorption in MOFs with *cus* sites. Rather a large variance between the performance of various DFT approximations (LDA, GGA) and functionals was observed [13–15].

3.1.1 Reliability of the standard (DC-)DFT approaches

A systematic study aimed at understanding the failure of standard exchange-correlation DFT functionals is presented first as an unavoidable step towards the accurate description of adsorption in *cus*-containing MOFs. In order to decrease dimensionality of the investigation a single representative of the *cus*-containing MOFs was chosen, namely the CuBTC (often denoted as HKUST-1) [77], for which a large amount of experimental data is available and which is undoubtedly the most often computationally investigated MOF [7, 8]. Moreover, the paddlewheel-like metal cluster containing a pair of Cu^{2+} ions with open-shell electronic structure in close proximity (see Figure 3.1) was itself an object of a number of experimental and computational studies [78–80].

Copper(II) formate cluster model

The reliability of various DFT based methods, including dispersion-corrected DFT, for the adsorbate-*cus* interaction was first investigated using the copper(II) formate, i.e. $Cu(HCOO)_2$, cluster model (Figure 3.1). The small size of this model enables the

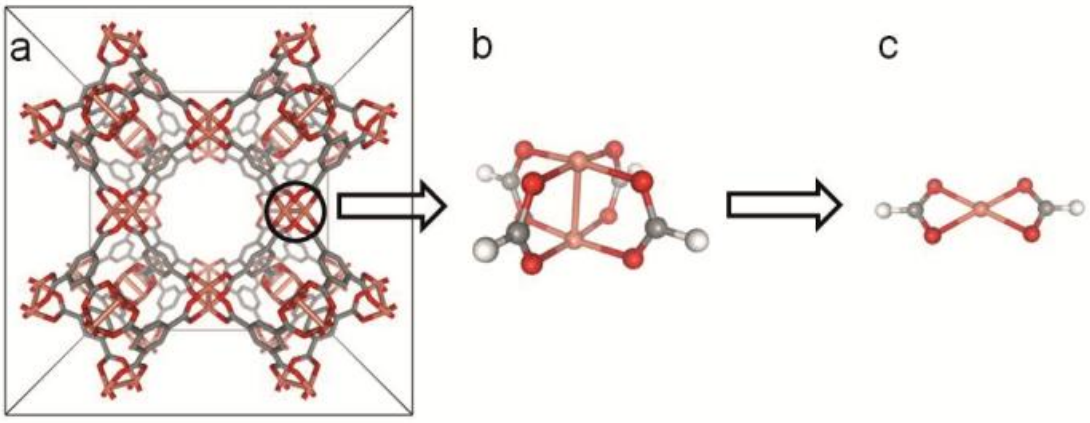

FIGURE 3.1: (a) CuBTC unit cell, (b) paddle-wheel (PDWL) unit, and (c) copper(II) formate model.

benchmarking of DFT functionals with respect to the highly accurate CCSD(T) results for a number of adsorbents (CH_4, H_2, N_2, CO_2, CO, H_2O and NH_3); different types of adsorbate-adsorbent interactions, including dispersion, electrostatic, and partially covalent bonding, are represented in this set.

Interaction energies of the above listed small molecules with the $Cu(HCOO)_2$ cluster model in the PBE/AVTZ equilibrium geometry were first evaluated for several commonly used LDA, GGA and hybrid functionals (Figure 3.2). For all the molecules considered the interaction energy is underestimated with all exchange-correlation functionals tested except for the LDA functional, which, on the contrary, systematically overestimates interaction energies. In terms of RMSD values the hybrids (B3LYP, BHLYP and PBE0) are on average more accurate then GGA (PBE, PW91, RPBE and BLYP) functionals with RMSD values in the range of $3.5 - 9.5$ and $6.7 - 15.7$ kJ.mol^{-1}, respectively. Note however, that e.g. a very popular B3LYP has larger RMSD than PBE, PW91, or even LDA. Since none of these functionals accounts for long-range dispersion interaction, it is not surprising that even for BHLYP (having the lowest RMSD) the relative errors are larger than 40% for adsorbates where the stabilization by the dispersion interaction is dominant (CH_4, H_2, N_2). However, even for H_2O and NH_3, where dispersion does not constitute dominant contribution to the stabilization, the underestimation larger than 30% (and in case of RPBE and BLYP as large as 80%) is observed for most of the DFT functionals considered with the exception of BHLYP, PBE0 and LDA. Nonetheless, a notable systematic improvement, which has been also reported for Cu^{2+} cation interaction with other ligands [81, 82], could be observed for the DFT functionals formed by the B88 exchange and LYP correlation functionals; the increasing amount of the exact HF exchange (BLYP<B3LYP<BHLYP) leads to an improvement in the performance with the BHLYP functional providing the best description.

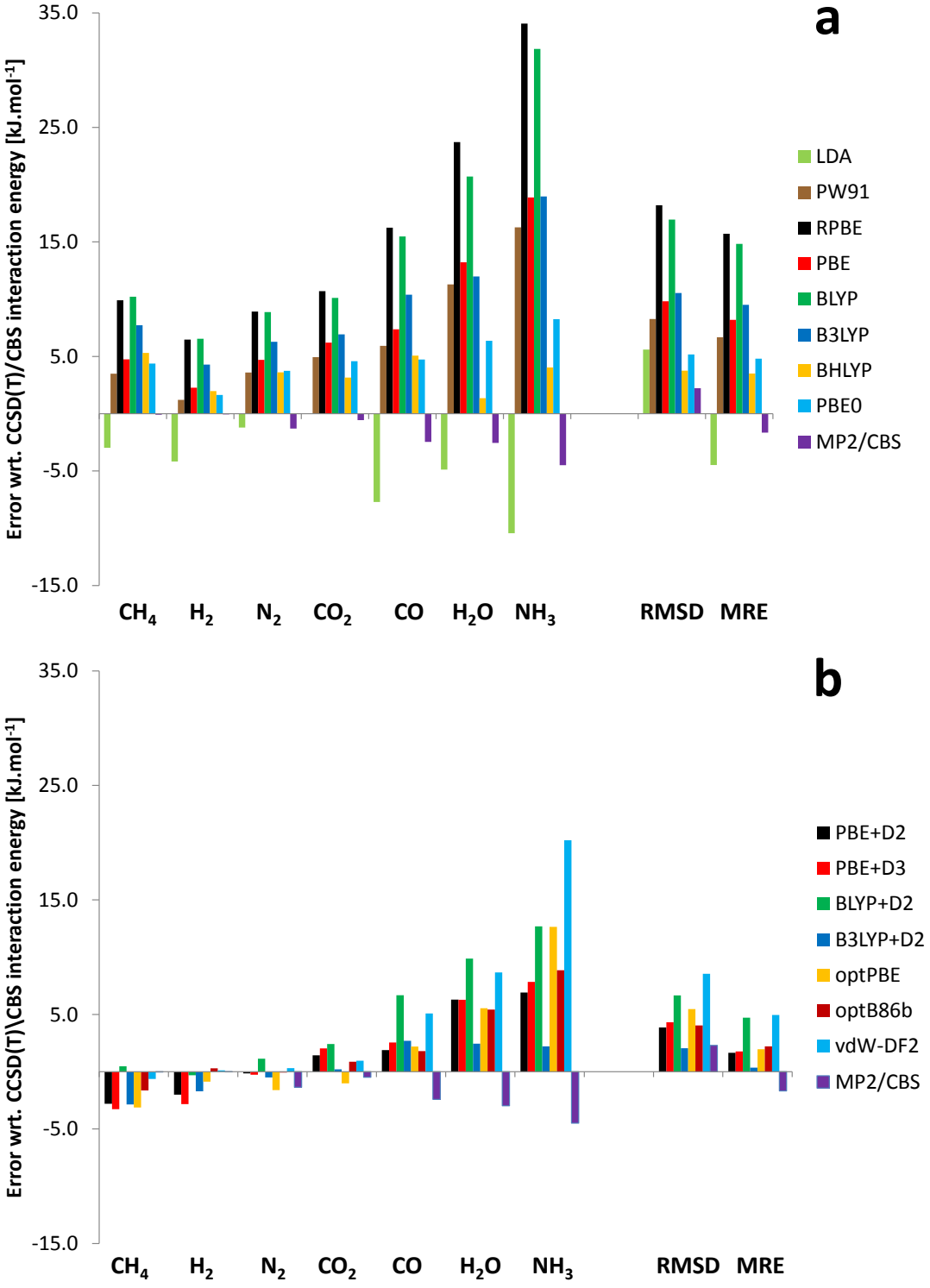

FIGURE 3.2: Error in interaction energies (in kJ.mol^{-1}) with respect to CCSD(T)/CBS results. Interaction energies of various molecules with the $Cu(HCOO)_2$ model were calculated with the (a) DFT and (b) dispersion corrected DFT functionals. MP2/CBS results included for comparison.

Therefore, two different DFT schemes accounting for the dispersion interaction, either via the semi-empirical pairwise C_6 approach by Grimme (DFT-D2 or DFT-D3) [39, 57] or by the construction of non-local correlation functionals which capture long-range dispersion forces (vdW-DF2, optPBE, optB86b) [25, 34, 42], have been tested (see Section 2). The inclusion of semi-empirical dispersion corrections led to a substantial improvement over the dispersion-uncorrected functionals (Fig. 3.2) with B3LYP-D2 providing the best performance outperforming even the MP2 method. The performance of the nonlocal functionals is comparable to the semi-empirically corrected standard GGA/hybrid functionals; nonlocal functionals providing somewhat better results for the dispersion-dominated adsorption complexes (CH_4, H_2) while being inferior for systems where covalent bonding (and charge transfer, see Table 1.2 in Attachment **A**) between adsorbate and adsorbent is non-negligible (CO, H_2O, NH_3). However, the improvement over the dispersion-uncorrected DFT functionals depends on the type of the adsorption complex; different functionals appears to be optimal for individual adsorbates. The following observations can be drawn: (i) the stability of dispersion-dominated complexes (H_2 and CH_4 in particular) is overestimated, (ii) interaction energies of N_2 and CO_2 are accurately described at the DFT-D level, and (iii) the interaction between the *cus* site and CO, H_2O, and NH_3 molecules is severely underestimated (except for the B3LYP-D2 level). This implies that inclusion of dispersion interaction improves the interaction energies only partially and that other effects (errors) besides a missing dispersion play a role as well.

There have already been studies aimed at elucidating the shortcomings of standard DFT for similar adsorption complexes, namely the Cu^{2+} cation interacting with small neutral ligands as H_2O, H_2O_2 or H_2S_2 [81–84]. An unrealistically large spin and charge delocalization, which was attributed to the incomplete cancellation of self-interaction included in the Coulomb energy by the exchange-correlation functional, was observed for GGA functionals in particular [81, 82]. Interestingly, this artificial delocalization was found to decrease with the increasing amount of the exact exchange mixed in hybrid exchange-correlation functionals. Similar dependence of the spin and charge delocalization on the amount of the HF exchange was reported also for adsorption complexes of small gas molecules with $Cu(HCOO)_2$ cluster model (see Table 1.2 in Attachment **A**). Description of the electron density improves from LDA to GGA and to hybrid functionals with respect to the reference high level ab initio averaged quadratic coupled-cluster (AQCC) densities. All the DFT functionals considered, with the exception of the BH-LYP, overestimate the spin and charge delocalization which leads to artificially large electron density (and incorrect electronic structure description) on Cu^{2+} cation.

In order to quantify the DFT error due to an incorrect electron density we have evaluated the density functionals on the pre-calculated AQCC densities for all the adsorption complexes considered. The use of the AQCC electron densities resulted in only minor

and often non-favorable (less than 1 kJ.mol^{-1}) changes in the interaction energies for all the adsorption complexes with the exception of the water and ammonia complexes where electrostatic and partially covalent bonding is of most importance; for these complexes a larger effect in the range of $1 - 8$ kJ.mol^{-1} (around $5 - 15\%$ of the CCSD(T)/CBS interaction energy) was observed. Furthermore, in the case of water and ammonia the AQCC densities led to an improvement of the interaction energies (see Figure 3.3) with the more pronounced effect on the GGA than hybrid functionals (results for LDA are actually worsened) which is in line with the fact that the densities obtained using the hybrid functional are closer to the reference AQCC electron density. Figure 3.3 further exemplifies the cumulative favorable effect of both dispersion and electron density corrections on the interaction energies for water and ammonia complexes; a few-fold decrease in error is observed for GGA functionals upon adding up both corrections with the error bars almost reaching the chemical accuracy level of 4 kJ.mol^{-1}.

It can be concluded that although the discrepancy between reference CCSD(T)/CBS and DFT interaction energies can be to a sizable extent attributed to either a missing part of the dispersion interaction or unrealistic charge distribution on the $Cu(HCOO)_2$ cluster model, non-negligible uncertainties remain. These can be related to the quality of the underlying exchange-correlation functional, the transferability of the semiempirical dispersion corrections (DFT-D) and finally to the robustness of the combination of exchange-correlation functional with the scheme accounting for the dispersion (long-range correlation). It follows that different functionals appear to be optimal for individual system; the B3LYP-D2 gives the lowest RMSD among the functionals considered herein, however, the accuracy results from partial error cancellation.

Paddlewheel cluster model

The cluster model that more closely represents the *cus* site in CuBTC, the paddle-wheel (PDWL) unit (Fig. 3.1), was adopted in the follow-up study. The electronic structure of the PDWL unit is rather complicated as the unpaired electrons on each Cu^{2+} dimer are either antiferromagnetically (spin-up-spin-down) or ferromagnetically (spin-up-spin-up) coupled leading to the singlet and triplet state, respectively [78, 79] (see Attachments **A**, **B** and **F** for further discussion). While the electronic ground state of the PDWL unit, namely the singlet state, has a multi-reference character (and thus it makes the benchmarking significantly more computationally demanding) a single-reference-dominated lowest triplet state was used in the investigation of the reliability of DFT methods with respect to the reference CCSD(T) approach (see Attachments). Note however, that the interaction energies for the multi-reference singlet and single-reference triplet states were

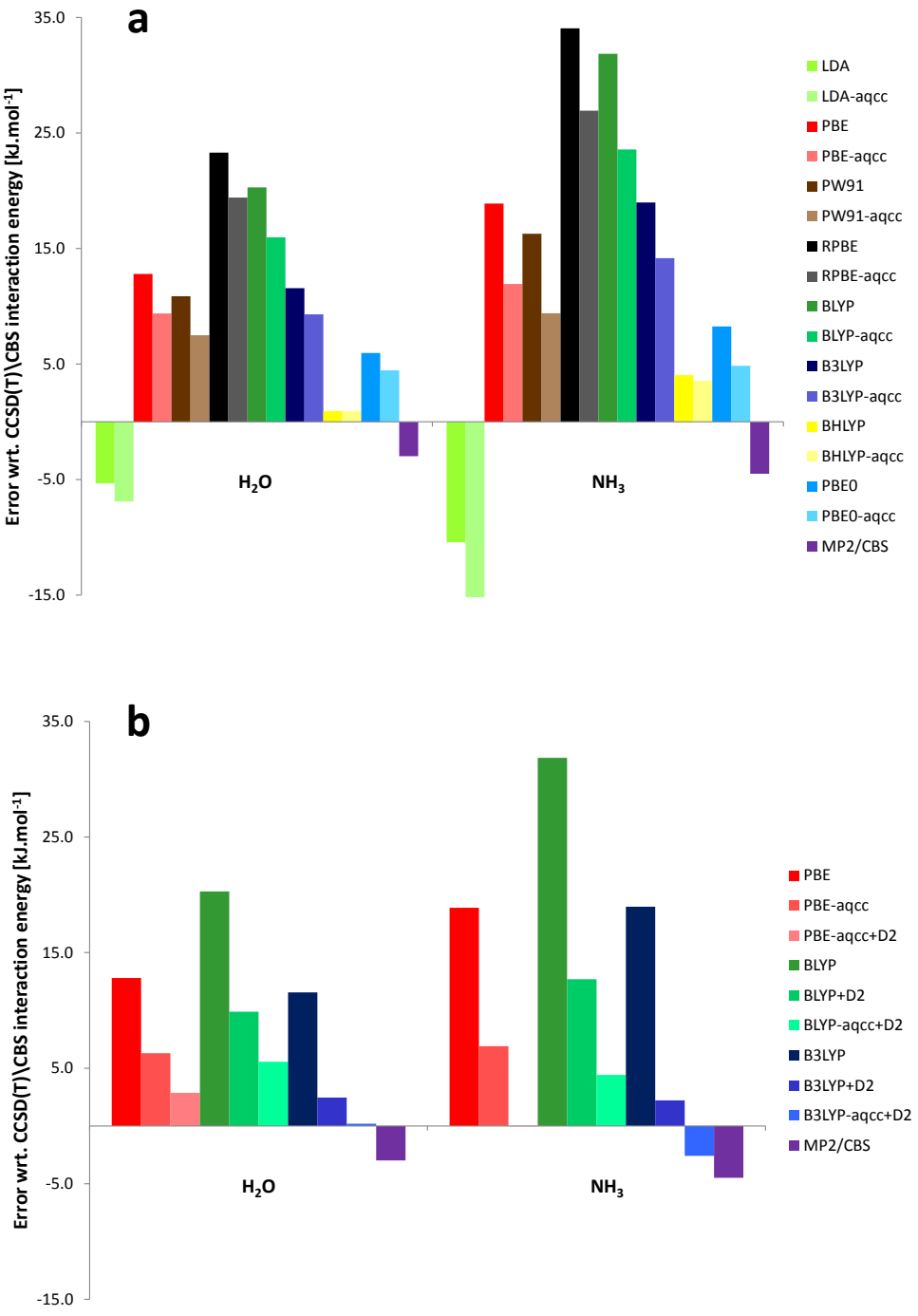

FIGURE 3.3: Error in interaction energies (in kJ.mol^{-1}) with respect to CCSD(T)/CBS results. Interaction energies of various molecules with the $Cu(HCOO)_2$ model were calculated on DFT and AQCC densities using (a) DFT and (b) dispersion corrected DFT functionals.

Functional type	Functional name	Dispersion correction		
		None	D2	D3
GGA	PBE	-32.4	-39.5	-39.7
	RPBE	-19.2	-31.0	-33.1
	B-LYP	-23.7	-35.0	-38.1
meta-GGA	TPSS	-30.2	-39.6	-40.2
hybrid	B3LYP	-34.8	-44.7	-46.7
	BH-LYP	-47.6	-	-57.4

TABLE 3.1: Interaction energies (in kJ.mol^{-1}) of water with PDWL model evaluated for various GGA, meta-GGA and hybrid DFT functionals. The corresponding value obtained at the reference level of theory, CCSD(T)/CBS, is -51.2 kJ mol^{-1}.

found to be almost identical [85, 86].[1] First, the transferability of the findings obtained for the smaller $Cu(HCOO)_2$ cluster model regarding the performance of various DFT-based methods was tested for the interaction of water molecule with the PDWL unit (see Figure 3.4 and Table 3.1). The observation about (insufficient) accuracy of DFT for description of the interaction of water with $Cu(HCOO)_2$ model reported above holds also for the interaction with PDWL model; neither standard (meta-)GGA nor hybrid exchange-correlation functionals (with or without dispersion correction) provide satisfactory results. However, reliable CCSD(T) calculations cannot be performed on larger cluster models nor on a periodic model of MOF.

Thus, there was a need for a computationally tractable yet reliable method for the description of MOFs with transition-metal *cus* sites for which the non-dispersion-like inaccuracies play a significant role. Such an approach, represented e.g. by the DFT/CC scheme (see Section 2.2), should be able to incorporate all the errors associated with the given exchange-correlation functional. Although it has to be admitted that refitting the above mentioned dispersion-correction methods particularly for the adsorbate-*cus* interaction would definitely improve their performance, the DFT/CC scheme is by its construction as a robust functional-form-free and interpolation-based scheme well-suited for the task of obtaining the best representation of the CCSD(T)/CBS reference data for the adsorption on the *cus* site.

For the H_2O, CO and ethylene molecules, which represent different types of interaction with the *cus* site, the reliability of the DFT/CC scheme interaction energies was tested for the full dissociation curves (Fig. 3.4) while only single-point energy calculations were

[1] Within the periodic DFT framework, both antiferromagnetic and ferromagnetic coupling between the unpaired electrons on Cu^{2+} dimers, corresponding to the broken-symmetry singlet and triplet states of the PDWL units within the molecular DFT, were considered. However, due to convergence issues and minor dependence of the interaction energy on the copper dimer coupling, the ferromagnetic (or even the spin-unpolarized) solution was used for periodic DFT calculations.

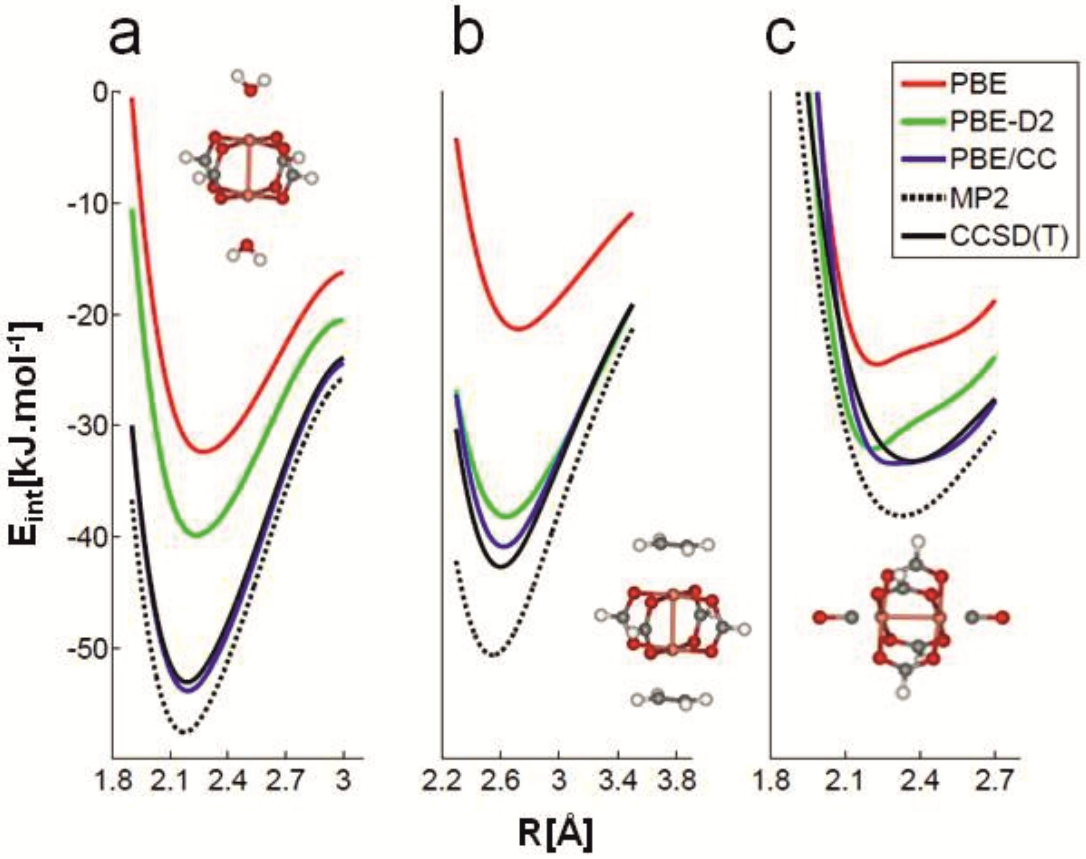

FIGURE 3.4: (a) PDWL-H_2O, (b) PDWL-Ethane and (c) PDWL-CO 1-D dissociation curves evaluated at various levels of theory.

carried out for CO_2, H_2 and CH_4. Interaction energies calculated at the PBE-optimized geometry of PDWL complexes with CO_2, H_2 and CH_4 molecules are -18.8, -9.0 and -13.5 kJ.mol^{-1}, respectively, at the reference CCSD(T)/CBS level and they are -19.0, -9.7 and -13.5 kJ.mol^{-1}, respectively, at the DFT/CC level. Similarly encouraging agreement between DFT/CC and CCSD(T) data was observed for the H_2O, CO and ethylene dissociation curves with the errors smaller than 2 kJ.mol^{-1} (see Figure 3.4). It can be summarized that DFT/CC scheme represents a viable route for accurate description of adsorption on the *cus* sites and while the DFT/CC computational overhead (with respect to DFT) is negligible it can be readily used within the periodic DFT calculations and its predictions can be compared with the available experimental data. More information is provided in Attachment **A**.

3.1.2 A periodic CuBTC model: DFT/CC scheme extension

Water adsorption on the cus site: Methodological study

As-synthesized CuBTC contains water molecules relatively firmly attached to *cus* sites; thus, the activation, i.e. prolonged outgassing at elevated temperatures ($100-150\,^{\circ}$C), is

required prior to the adsorption measurements of other probe molecules [87]. Moreover, the CuBTC has shown a considerable instability upon extended exposure to the high humidity [88, 89] which makes the accurate determination of character and strength of the water interaction with CuBTC of great importance. Further motivation for choosing water adsorption as the case study on the reliability of the DFT, DC-DFT and most importantly the DFT/CC method for description of interaction with *cus* sites was following: (i) single-crystal X-ray diffraction data on the H_2O/CuBTC system are available (the water is bound just on top of the Cu^{2+} ion at the distance of $R_{Cu\text{-}water} = 2.17$ Å), (ii) although rather scarce, the experimental adsorption enthalpies, namely the data ($-\Delta H_{ads}(313\text{ K}) = 50.7 \pm 2.9$ kJ.mol^{-1}) from Henninger *et al.* [89] , are reported and (iii) a rather poor performance of DFT and DC-DFT methods for water interaction with $Cu(HCOO)_2$ model of the *cus* site discussed at length in Section 3.1.1 was observed.

In case of standard DFT and DC-DFT methods a sizable underestimation of the water-*cus* interaction was observed already for PDWL model (see Section 3.1.1) and this observation was supported by other computational studies employing both cluster [90] and periodic [91] CuBTC models. However, the DFT/CC correction scheme was able to provide much better performance for both structural characteristics ($R_{Cu\text{-}water} = 2.19$ Å) and adsorption enthalpy ($-\Delta H_{ads}(0\text{ K}) = 49$ kJ.mol^{-1} at the zero coverage limit), see Table 3.2. However, it must be noted that a degree of uncertainty with respect to this comparison remains stemming from the fact that experimental measurements of adsorption heats were carried out at finite (and a rather high) temperature and for higher water coverage [89]; effects of the finite temperature along with coverage-dependence of the adsorption heats were investigated in the subsequent studies on the adsorption of carbon dioxide and methane (see below). The interaction energy calculated for a single water molecule in CuBTC was found to be very similar to the value observed for the PDWL cluster only (differ by less than 10%) which indicates that the long-range interactions are small. It also suggests that the cluster model of PDWL unit is a suitable representation of the *cus* site in CuBTC. It is also worth noting that upon adsorption of the second water molecule on the same PDWL unit the water-*cus* stabilization drops by approximately 5 kJ.mol^{-1}; this indicates the presence of two nonequivalent adsorption sites at the paddle-wheel unit, the free paddle-wheel and the paddle-wheel with the one copper center occupied by the adsorbed molecule. This behavior, attributed to the structural changes (pyramidalization)[2] of the paddle-wheel unit upon adsorption, was observed also for other molecules with larger contribution from covalent bonding, namely the propylene and carbon monoxide molecules (see Attachments **E** and **F**). More information on water adsorption in CuBTC is provided in Attachment **B**.

[2]Pyramidalization is defined as the distance of the Cu^{2+} cation from the plane defined by adjacent carboxylic oxygen atoms

Adsorbate	DFT/CC / site type			Experiment
	cus	cage	window	
H_2O	49.0	-	-	50.7 ± 2.9[a]
CO_2	28.2	23.2	23.1	29.0[b]
CH_4	17.4	19.6	20.5	20.5[c]
C_3H_8	24.3	43.3	31.0	44.3[d]
C_3H_6	56.4	44.7	34.0	58.4[d]
CO	33.3	-	-	29.0[e]

[a]Ref. [89]. [b]Ref. [92]. [c]Ref. [93]. [d]Ref. [94]. [e]Ref. [86].

TABLE 3.2: Adsorption heats (in kJ.mol^{-1}) for low coverage regime.

Carbon dioxide adsorption on the cus site: Coverage dependence of adsorption heats

Metal-organic frameworks in general and CuBTC material in particular have shown a great potential for CO_2 storage where excellent adsorption properties have been assigned to a combination of large surface areas and significant density of high-affinity-adsorption sites, such as *cus* sites [95]. In this respect, the CuBTC has shown superior performance specifically for lower-pressure (< 1.2 bar) adsorption capacities which are of importance for post-combustion CO_2 capture. While the adsorption at lower-pressure and thus lower-coverage range is largely a function of the binding strength of the strongest binding site within the material, understanding of the fine CuBTC performance for the CO_2 capture can be achieved only through a thorough evaluation of CO_2 adsorption over the entire coverage range. Therefore the adsorption of CO_2 in CuBTC has been investigated in a number of experimental studies [14, 96–100] which unfortunately reported a rather broad variation in adsorption heats ($25 - 35$ kJ.mol^{-1}). This observation has been attributed to the differences in sample synthesis and activation and/or the method used for obtaining the value of adsorption heat (e.g., Clausius-Clapeyron [98, 100] or temperature-dependent isotherm equation [99]). Interestingly, a weak dependence of the adsorption heats on the coverage was observed in most of the experimental studies which suggested a presence of homogenous adsorption sites in CuBTC. However, a completely different interpretation was given based on a systematic investigation of CO_2 adsorption mechanism in CuBTC at the DFT/CC level for a wide range of coverages (from zero-coverage limit to the CO_2 loading as high as 9 mmol.g^{-1}).

An important prerequisite for reliability of the following discussion on CO_2 adsorption mechanism is the observation regarding the agreement between DFT/CC calculations and available experimental data: (i) the calculated DFT/CC adsorption enthalpies were

well in range determined from various experimental studied and most importantly a great agreement with very accurate microcalorimetry measurements has to be noted, (ii) structural features of CO_2 adsorption sites (see below) as well as the sequence of adsorption site occupation as obtained from the neutron diffraction data [14] were in line with DFT/CC data. Calculations yield three types of adsorption sites in CuBTC: *cus*, the cage center and the cage window sites (Figure 3.5). Interaction energies calculated for the zero coverage limit (Table 3.2) show that the most stable CO_2 adsorption complex is the one formed on the *cus* site (28.2 kJ.mol^{-1}) whereas the adsorption complexes in the cage window and in the cage center are almost isoenergetic being about 5 kJ.mol^{-1} less stable than the complex on the *cus* site. Hence in the low-coverage regime (up to roughly one CO_2 per Cu or 5 mmol.g^{-1}), CO_2 molecules adsorb onto *cus* sites. At higher coverages, both secondary adsorption sites, the cage window and cage center sites, should be occupied but due to a favorable topology of the CuBTC material the CO_2 complexes in cage window sites (contrary to the cage center sites) are stabilized by the lateral interaction (5 kJ.mol^{-1}) with already adsorbed CO_2 molecules on the *cus* sites (see Figure 3.5). Therefore at CO_2 loadings between $5 - 8$ mmol.g^{-1} the cage windows site are occupied preferentially. Surprisingly, while the stabilization due to lateral interactions to a large extent offsets the differences as observed at the zero-coverage limit, differential adsorption enthalpies should remain almost unchanged up to 8 mmol.g^{-1} although different types of adsorption sites are being occupied. At even higher coverages, CO_2 molecules adsorb in the center of small cages and in large cages. Again the lateral interactions between these molecules and those already adsorbed in *cus* sites and cage windows sites (amounting to almost 10 kJ.mol^{-1}) are behind a small increase (1-3 kJ.mol^{-1}) in adsorption enthalpies in this high-coverage regime which was also observed experimentally.

In summary, a very good agreement between DFT/CC and experimental results implies that applicability of the DFT/CC correction scheme is not limited to the accurate description of adsorbate-*cus* interaction but is able to provide a balanced description of CO_2 adsorption at rather different sites (electrostatic interaction with the *cus* site versus purely dispersion driven interaction in cage center site) and that it can properly account also for lateral interactions. Although the performance of the DFT/CC scheme is encouraging, some degree of uncertainty remains as the temperature effects were not considered (in the calculations); this issue has been addressed in the following study on methane adsorption. More information on carbon dioxide adsorption in CuBTC is provided in Attachment **C**.

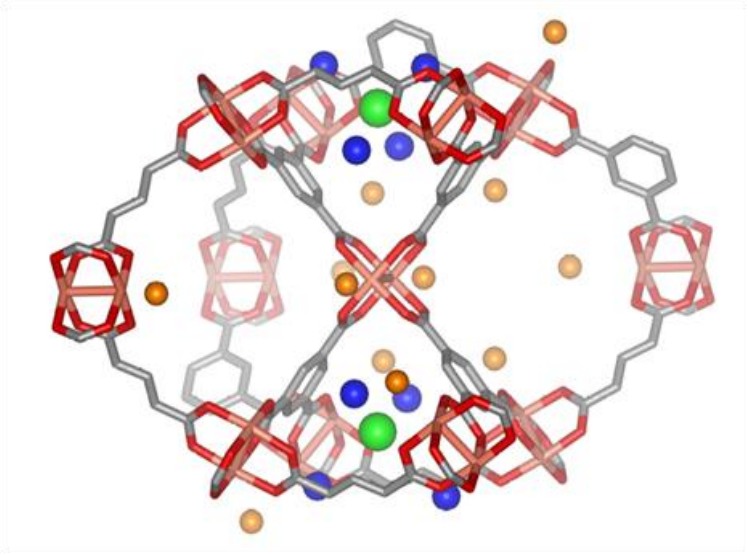

FIGURE 3.5: CuBTC adsorption sites: the 12 *cus* sites in the unit cell (indicated by orange spheres) are located just above the Cu^{2+} cations; there are two small cages, each of them with one cage center site (green sphere) and four cage window sites (blue spheres).

Methane adsorption in CuBTC: GCMC study employing DFT/CC interaction potential

The adsorption of methane in CuBTC has received a considerable attention due to a high methane storage capacities which were attributed, based on the data obtained from the neutron diffraction studies of Wu *et al.* [101] and Kaskel *et al.* [102], to both the presence of the *cus* sites and favorable structure of the CuBTC containing small pockets (cages) significantly enhancing the vdW interaction. Moreover, it has been observed [101, 102] that the grand-canonical Monte Carlo (GCMC) simulations employing standard empirical force fields fail to correctly describe the interaction of the methane with the *cus* site and lead thus to prediction of an unrealistic adsorption mechanism (note the performance of Universal Force Field (UFF) depicted in Figure 3.6) [102, 103].

To address this deficiency a methane-CuBTC interaction potential was constructed using DFT/CC approach. The methane-CuBTC potential energy surface (PES) was represented on a pre-calculated three-dimensional Cartesian grid neglecting the orientation dependence of the interaction potential (which is small, as methane is a spherical molecule) and keeping the CuBTC framework rigid. The final grid constructed from about 2000 explicitly calculated grid points was then implemented in the standard GCMC simulations (Figure 3.6). In this way a direct comparison with the experimentally observed characteristics of the adsorption process obtained at finite temperature (as e.g. adsorption isotherms, adsorption heats or occupations of adsorption sites derived from (neutron, X-ray) diffraction) is readily available. It simultaneously represents

a difficult test for the quality of the whole DFT/CC derived adsorbent-adsorbate PES as at the elevated temperatures large segments of the adsorbent-adsorbate PES are sampled within the GCMC simulations. Therefore, a very good agreement of simulations with experimental adsorption isotherms (and also adsorption heats [93, 101]) is of great importance (see Figure 3.6 and Table 3.2). In addition, the DFT/CC-PES based simulations quantitatively captured the experimentally determined occupancies of adsorption sites (see Table 1 in Attachment **D**), including the *cus* sites for which the simulated average methane-copper distance of 3.097 Å is well in line with the experimental value of 3.075 Å [102].

It should be noted that choice of the computational method used for adsorbate-adsorbent interaction is critical as neither PBE, PBE-D2, nor PBE-D3 derived PES lead to a correct prediction of the adsorption isotherm (Figure 3.6) with their under- or overestimation tendencies reflecting the trends observed for small $Cu(HCOO)_2$ cluster calculations (see Figure 3.2). Regarding the actual CH_4 adsorption mechanism, contrary to the CO_2 molecule, methane adsorbs preferentially in the center or openings (windows) leading to the small cages where dispersion interaction with the framework is optimal. Only at higher pressure (higher loading) the *cus* and other less-stable adsorption sites become occupied. Hence the favorable properties of CuBTC for methane adsorption could be indeed understood on the basis of combination of specific high-affinity sites (*cus* site) and van der Waals potential pocket sites present in the same structure. More information on methane adsorption in CuBTC is provided in Attachment **D**.

Propane and Propylene adsorption in CuBTC: An application study

The CuBTC has been considered for propane/propylene separation and therefore it has been extensively studied both experimentally and theoretically [104–108]. However, most of the theoretical studies used empirical force-field-based GCMC simulations to predict adsorption isotherms. In line with the observation made in case of methane adsorption (see above), the commonly used empirical potentials fail to describe the interaction with *cus* sites. The attempts to improve standard empirical force-fields focused on improving description of the partially dative bond between Cu^{2+} and π-electron density on propylene [104, 105]. However, simple rescaling of Lennard-Jones parameters for $Cu^{2+}-C(sp^2)$ interaction [106] or parameterizations based on the GGA functionals [108] do not yield a desired accuracy which is not surprising in light of the results presented in Figure 3.4 (PDWL-ethylene interaction).

Adsorption enthalpies of propane and propylene calculated for the zero-coverage limit are summarized in Table 3.2. The agreement between DFT/CC predictions and experimentally measured adsorption enthalpy (neglecting however temperature effects) is reasonable with a small underestimation observable for propylene adsorption on the *cus* site which seems to be consistent with the PDWL model results discussed above (see

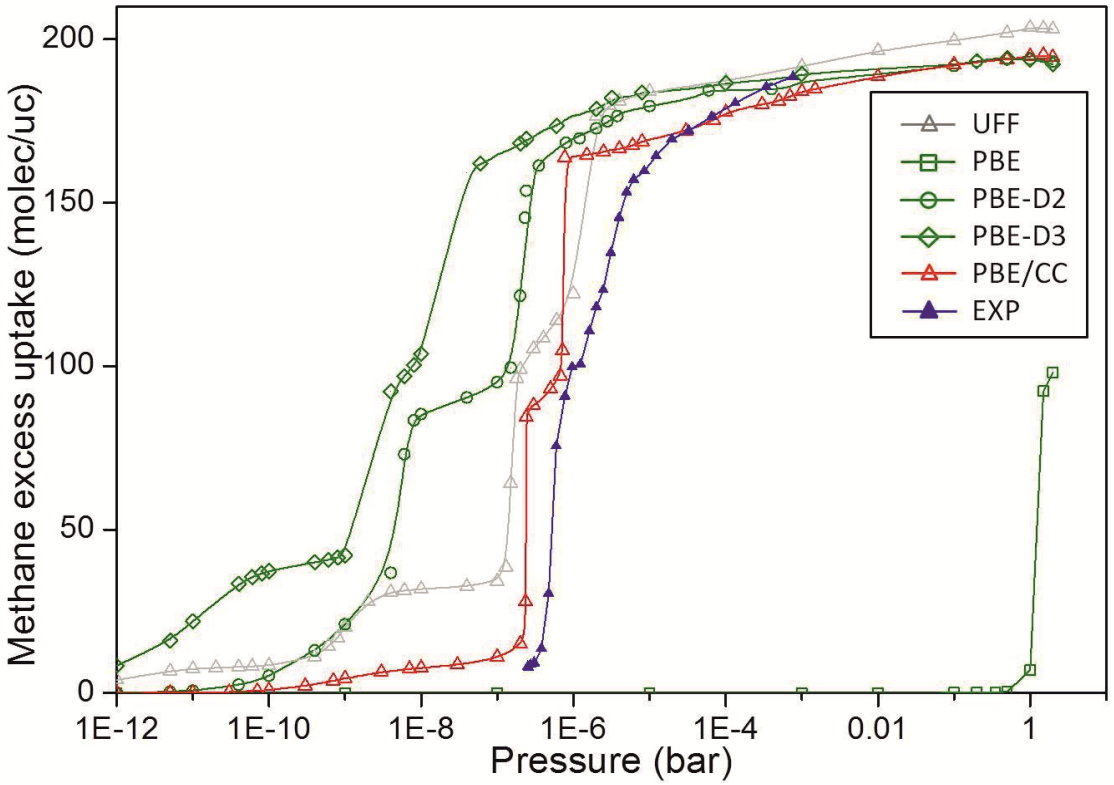

FIGURE 3.6: Methane adsorption isotherms in CuBTC at 77 K in semi-log scale calculated using various interaction potentials

Figure 3.4). Similarly to the CH_4 and CO_2 case three types of (primary) adsorption sites were identified (*cus*, cage center and cage window). Although adsorption enthalpies for both cage center and cage widow sites (where the role of dispersion interactions is dominant) do not differ significantly for propane/propylene, the interaction with *cus* site is markedly (by 30 kJ.mol^{-1}) different due to the formation of partial dative bond in case of propylene [94]. This results in qualitatively different adsorption mechanism for propane and propylene; while propane behaves like methane, preferentially adsorbing at the cage center sites first, followed by adsorption at cage window and *cus* sites, the propylene adsorption pattern resembles rather that of CO_2 (or H_2O)[3] molecule with propylene preferably (and rather strongly $-\Delta H_{ads} \sim 58$ kJ.mol^{-1}) interacting with the *cus* sites. Although the observation made for the low-coverage was encouraging for the CuBTC potential in propane/propylene separation further investigation for higher coverage demonstrated that due to the topology of CuBTC, stabilizing lateral interactions were significantly larger among the adsorbates located at the cage center and cage window sites (populated in the case of propane) than among adsorbates at the *cus* and cage center sites (populated in the case of propylene) (see Attachment **E**).

[3]Calculations also indicated that upon adsorption of second propylene molecule on the same PDWL unit the adsorption enthalpy decreases by 9 kJ.mol^{-1}. This indicates that with increasing propylene loading the *cus* sites are no longer equivalent. Similar observation was made also in case of H_2O adsorption.

It can be concluded, that while the presence of *cus* site is beneficial for good separation of propane and propylene, the presence of small cages (where molecules in cage center and cage window sites show favorable lateral interactions) makes the material much less efficient for propane/propylene separation. More information on propane/propylene adsorption in CuBTC is provided in Attachment **E**.

Carbon monoxide adsorption in CuBTC: A problematic case

The CO molecule serves as a powerful infra-red (IR) spectroscopy probe molecule for characterization of active sites (e.g. *cus* site) [109], in particular in microporous materials like CuBTC MOF where the use of many powerful surface characterization tools is precluded [110]. The advantage of CO molecule lies in the fact that CO stretching frequency is highly sensitive to different chemical environments. Therefore, also the CuBTC became an object of IR investigations where the assignment of relatively rich spectra in CO stretching region has been discussed [111–114]; nevertheless, not all of the IR features were conclusively interpreted. There is an agreement on the interpretation of the main band located at about $2170-2178$ cm^{-1} that is assigned to carbonyl complexes formed on Cu^{2+} sites in CuBTC [111, 113, 114]. However, there are various suggestions to explain the shift of this band from 2178 cm^{-1} to lower frequencies with increasing CO coverage [112–114] or to explain other features of the IR spectra.

An accurate computational description of CO interaction with the *cus* sites as well as theoretical assignment of the IR features proved to be rather complicated tasks. Besides the already observed deficiencies of the standard DFT(GGA) description, namely the lack of dispersion interactions and artificial charge delocalization (see Section 3.1.1), another shortcoming of the GGA performance has been manifested for CO interaction with the PDWL unit model; large geometrical differences between the reference MP2 and PBE structures were observed.[4] The overestimation of the σ-donation from CO to Cu or/and π back-donation from Cu to CO was suggested as the possible reasons for this behavior. However, it can be also related to the artificial electron density increase on the copper. A large deformation of the PDWL unit upon interaction with the CO molecule is observed at the PBE level (much larger than in case of water or propylene) which results in significant pyramidalization of the PDWL unit manifested in increase of Cu-Cu distance and decrease of the Cu-C distance. Hence the reference Cu-C distances are about 0.2 longer than the PBE ones. As a result, interaction energies at the PBE level are only slightly ($2-5$ kJ.mol^{-1}) underestimated as the lack of dispersion interactions is compensated by (artificially) increased strength of the Cu-C bonding. While DFT/CC

[4]MP2/aug-cc-pVDZ interaction energies were found to be in the best agreement with CCSD(T)/CBS values for fixed geometries. While full CCSD(T) geometrical optimization was prohibitive, the MP2/aug-cc-pVDZ were employed instead. Note however that MP2/CBS overestimated the CCSD(T)/CBS values by about 5 kJ.mol^{-1}(see Figure 3.4) and thus fine performance of MP2/aug-cc-pVDZ is based on a fortuitous error cancellation.

scheme assumes that error of DFT description is not significantly altered upon changes in monomer geometries in the complex,[5] application of the DFT/CC scheme is more problematic than in the previous cases. Nevertheless, the adsorption enthalpies evaluated at the DFT/CC level for the first (-33 kJ.mol^{-1}) and the second (-31 kJ.mol^{-1}) CO molecule on one PDWL unit of CuBTC (a periodic model is employed) are only a little overestimated with respect to the experimental data at low coverage (see Table 3.2). In addition, the DFT/CC scheme is capable to partially improve (lengthen) the Cu-C distance.

As the effect of long-range interactions was found to be very small (based on the comparison of DFT/CC interaction energies evaluated for periodic and cluster PDWL model) and PBE was found to provide rather inconsistent results for frequency shifts (see Attachment **F**), the theoretical assignment of the IR features was done using the PDWL cluster model at the MP2 level. Calculations showed that only the band in the IR spectra at $2170 - 2178$ cm^{-1} is due to the CO adsorption on regular *cus* sites in CuBTC, while the other bands observed experimentally must be due to the defect sites (most probably Cu^+-CO species [112]) or to physisorbed CO. The small red shift of the band at 2178 cm^{-1} at increased CO coverage can be explained by populating both *cus* sites of PDWL unit with CO molecules; frequency lowering is due to the smaller PDWL unit pyramidalization. More information on carbon monoxide adsorption in CuBTC is provided in Attachment **F**.

3.2 Carbon dioxide adsorption in zeolites

Although the MOFs nowadays constitute the main focus of CO_2 capture research, zeolites continue to represent an attractive target materials due to their low cost, high thermal stability and easy cation exchange, which facilitates the tuning of the gas-solid interaction [95, 115]. The strength of the CO_2-zeolite interaction and its dependence on the zeolite topology and composition (Si/Al ratio and extra-framework cations) are the main factors to consider in order to find the most suitable zeolitic framework for a particular application. Therefore a number of computational investigations aimed at establishing the link between CO_2 adsorption heats and zeolite topology/composition were carried out [116–125]. However, similarly to MOFs, a significant portion of studies employed either empirical interatomic potentials (force fields) [122–125] or standard DFT (GGA) functionals [116–121]. While the empirical force fields were successful at describing the CO_2 adsorption in siliceous zeolites [122, 123] performance for metal-exchanged

[5] A monomer geometry-dependence of the ϵ_{ij} correction functions could be principally incorporated into the DFT/CC scheme but this route was not investigated.

zeolite was questionable [124, 125]. On the other hand, standard DFT (GGA) functionals are capable to describe the CO_2-(alkali-)metal interaction reasonably well [121],[6] but their inability to properly account for dispersion interactions can lead to a significant underestimation of the overall CO_2 adsorption heats (see below for details). Hence to achieve an accurate description for a whole range of zeolite compositions (various Si/Al ratios) more involved approach, namely the DFT/CC correction scheme, was required.

3.2.1 Carbon dioxide adsorption heats in zeolites: Role of zeolite topology and composition

In order to analyze the role of different factors that determine the CO_2 adsorption heats, zeolites belonging to the four structural types (MFI, FER, FAU and LTA) were investigated. These structural types were chosen because there are experimental results available and these zeolites cover entire range of allowed Si/Al ratios (from 1 to ∞). A model of CO_2 adsorption in zeolites taking into account the key factors influencing the stability of CO_2 adsorption complexes at the molecular level was proposed:

- Effect from bottom: This effect accounts for (predominantly electrostatic) interaction of CO_2 with the primary extra-framework (alkali-)metal cation. The strength of the interaction increases with increasing charge/ionic radius ratio , and decreasing coordination of extra-framework cations to the zeolite framework [74] (see also Table 3.3 and Figures 3.7 and 3.8). The adsorption site where CO_2 molecule interacts with only one extra-framework cation was denoted as the single cation (SC) site.

- Effect from top: When two extra-framework cations are separated by a distance between 5 to 10 Å (depending on cation size and charge), the CO_2 molecule can interact with both cations simultaneously (see Figure 3.8); such site was denoted as the dual cation (DC) site. Obviously, for very low Si/Al ratios (high extra-framework concentration) the CO_2 molecule can interact simultaneously with multiple cations (e.g., Na-LTA), i.e. the multiple cation (MC) are present [126].

- Dispersion interactions: This effect is of importance as in the microporous channels the CO_2 molecule is surrounded by a large number framework atoms in favorable distance for dispersion interactions to contribute [74] (see Figure 3.8) .

Based on a very good agreement between experimental and computational results:[7] the experimental (as well as computational) results were evaluated with respect to the

[6] In the DFT/CC model employed, the interaction between the alkali-metal and CO_2 was not corrected, i.e. the pure DFT(PBE) description was used.

[7] The DFT/CC estimates are within few kJ.mol^{-1} from experimental low-coverage adsorption heats for various zeotypes and Si/Al ratios considered (see Attachment **G** for more details).

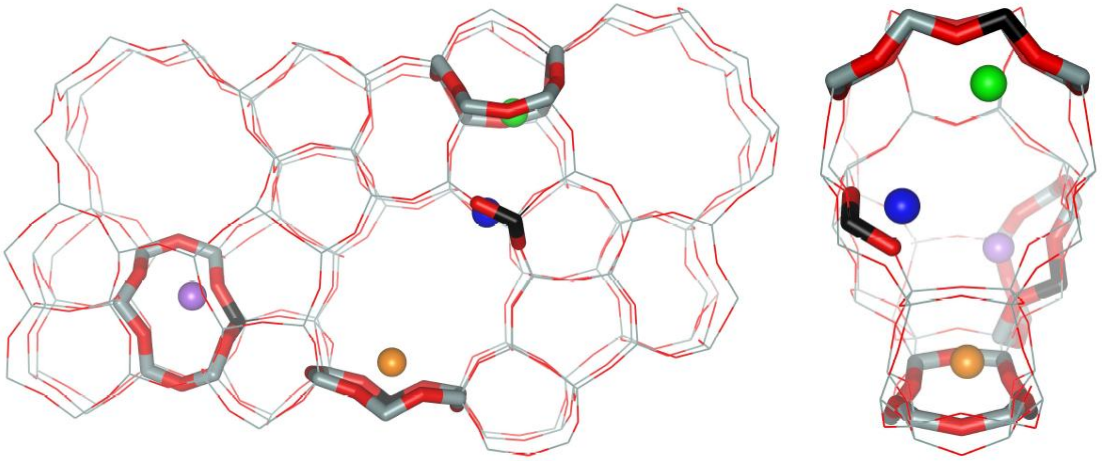

FIGURE 3.7: Extra-framework sites for Na^+ cation in Na-ZSM-5, viewed along the main (left) and zigzag channels (right). The Na^+ cation located in Z8, Z6, M6, and I2 sites depicted as green, violet, orange, and blue ball, respectively. The Z8 and Z6 sites are located in the zigzag channel, whereas the M6 site is in the main channel; the I2 site is in the channel intersection. Framework Si, Al, and O atoms depicted in gray, black, and red color, respectively.

proposed model. For a particular zeolite topology, CO_2 adsorption heats in general increase with increasing Si/Al ratio (cation concentration); however, for various zeolite topologies with similar Si/Al ratios sizable differences in adsorption heats can be observed (see below). Nevertheless, it is beneficial to classify zeolitic materials with respect to their composition: (i) purely siliceous materials (Si/Al $\rightarrow \infty$), (ii) high-silica zeolites (Si/Al ≥ 10) and (iii) low-silica zeolites (Si/Al ≤ 10).

Purely siliceous zeolites (no extra-framework cation) represent a particularly convenient model to reveal the character and importance of CO_2 interactions with the zeolitic framework. Calculations show that the interaction between CO_2 and siliceous zeolites is dominated by dispersion interaction,[8] that account for at least 80% of the overall interaction. Consequently, the CO_2 molecules are adsorbed in the vicinity of the channel walls maximizing the number of van der Waals contacts with framework atoms. Regarding the effect of topology on CO_2 adsorption heats, it was observed that adsorption heats increase with decreasing size of the channel or cavity and with increasing thickness of the channel wall; hence LTA exhibits the smallest (22 kJ.mol^{-1}) and MFI the largest (28 kJ.mol^{-1}) adsorption heats out of the zeotypes considered.

In case of high-silica zeolites the concentration of extra-framework cations is expected to be too low to allow the formation of DC or MC sites (effect from top). Therefore the interaction of CO_2 with zeolite is driven by the (specific) electrostatic interaction with the extra-framework cations at SC sites (effect from bottom) and is further increased

[8] Although the DFT/CC scheme is defined as global correction scheme (not only dispersion interaction), for systems investigated herein the dominant part of the DFT/CC correction accounts for missing dispersion interaction. Therefore, in the following discussion the DFT/CC corrections are considered to be a measure of dispersion interactions between CO_2 molecule and zeolite.

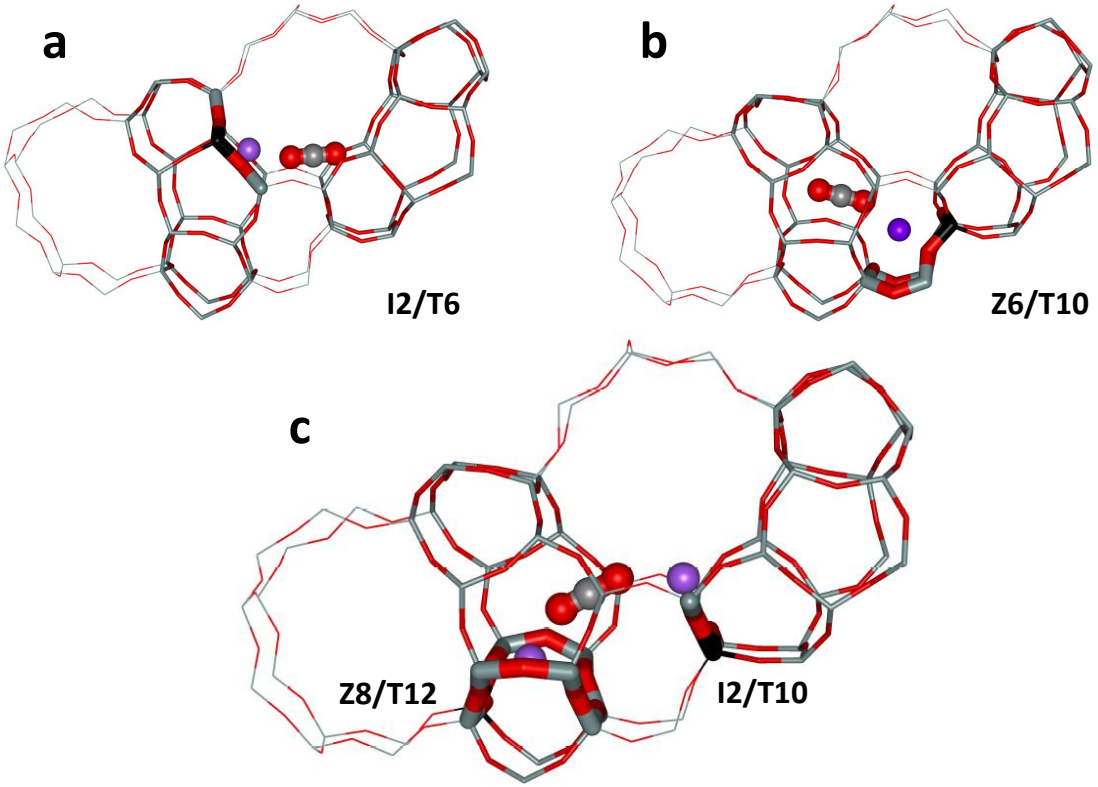

FIGURE 3.8: CO_2 adsorption complexes on Na-ZSM-5. CO_2 and Na^+ cations are depicted as balls, see caption of Fig. 3.7 for coloring scheme. ZSM-5 is viewed along the main channel; the zigzag channel surface is shown in tube mode. The CO_2 adsorption complexes on the Na^+ cation in the channel wall site Z6/T10 (a) and in the intersection site I2/T6 (b) are shown, together with the adsorption complex on a DC site (c).

by the (nonspecific) dispersion interaction with the zeolite framework. Results obtained for the model of Na-ZSM-5 zeolite (Si/Al = 95) summarized in Table 3.3 illustrate[9] a rather general behavior observed with minor differences also for other alkali-metals [127] and zeotypes (FER [74]): (i) a (negative) correlation between cation coordination with the framework and its ability to bind CO_2 is obtained (effect from bottom), i.e. the I2/T6 and Z6/T10 sites (see also Figs. 3.7 and 3.8) are characterized by largest and smallest values of $-\Delta E_{\mathrm{DFT}}$, respectively, (ii) dispersion component of the CO_2-zeolite interaction ($\Delta E_{\mathrm{DFT/CC}}$) is maximized when CO_2 molecule is located as far as possible from intersection of channel system, specifically the interior of the MFI zigzag channel (see Figure 3.8) is the most favorable in this respect as the number of framework atoms in van der Waals contact around the CO_2 is maximal, (iii) dispersion interaction is comparable (at least 30% of the overall interaction in case of MFI) to the DFT contribution only. Consequently, overall CO_2-zeolite interaction is a result of a rather delicate balance between the dispersion ($\Delta E_{\mathrm{DFT/CC}}$) and predominantly electrostatic

[9]While the exact location of the alkali-metal cation in the channel system is not known (as a consequence of the unknown aluminium distribution) it is a standard practice to report the adsorption heats at least for the most stable cationic sites in the vicinity of all the crystallographically unique T atoms.

Al position	Na^+ site[a]	CO_2 location	r(Na-O_f) [Å][b]	r(Na-CO_2) [Å]	E_{int}(DFT) [kJ.mol^{-1}]	$\Delta E_{DFT/CC}$ [kJ.mol^{-1}]	ΔH_{ads}(0K) [kJ.mol^{-1}]
SC site							
T10	Z6	CH	2.36, 2.39, 2.40, 2.68	2.326	-22.4	-24.2	-45
T4	Z6	CH	2.29, 2.34, 2.63, 2.69	2.324	-25.7	-24.2	-48
T11	M6	I	2.31, 2.32, 2.49, 2.51	2.320	-27.6	-19.2	-45
T12	Z8	I	2.33, 2.33, 2.63	2.347	-31.0	-17.4	-46
T6	I2	W	2.28, 2.29	2.345	-32.2	-20.3	-51
DC site							
T10	I2		2.24, 2.27	2.397	-47.1	-18.4	-64
T12	Z8		2.31, 2.33, 2.55	2.424			

[a]For notation see Figure 3.7. [b]Distance between the Na^+ cation and framework oxygen atoms.

TABLE 3.3: Calculated characteristics of CO_2 adsorption complexes formed in the Na-ZSM-5 zeolite. Location of the CO_2 molecule within the zeolite channel system; CH, I, and W represent the CO_2 molecule in the channel, on the intersection, and on the wall at the channel crossing, respectively.

interactions (ΔE_{DFT}) making a straightforward conclusion about the CO_2 preference for a specific types of adsorption sites (e.g. "least coordinated" or "located in the channels") problematic. It can be concluded that presence of the SC site (extra-framework cation) in the zeolitic structure sizably strengthens CO_2-zeolite interaction by few tens of kJ.mol^{-1} depending on the (alkali-)metal cation exchanged.

As the Si/Al ratio decreases further (low-silica zeolite) besides the SC sites (effect from bottom), the DC (see Figure 3.8) and MC sites become present in the zeolitic structure (effect from top). It should be noted that the ratio between SC and DC (or MC) cation sites depends, in addition to cation concentration, on the zeolite topology and even (in some cases) on the synthesis procedure (see Section 3.2.2). A role of topology was nicely exemplified on CO_2 adsorption in two Al-rich zeolites, namely the Na-A (Si/Al = 1) [126] and Na-FAU (Si/Al = 2.7) [120, 128]; there are only DC and MC sites in Na-A while there are only SC sites in Na-FAU. This rather surprising result can be understood as follows: (i) Only some Na^+ cations in Na-FAU are accessible for the CO_2 molecules; hence the effective Na^+ concentration is significantly lower than the actual Si/Al ratio corresponding to the zeolite chemical composition. (ii) For a broad range of Si/Al ratios, accessible Na^+ cations are almost 10 Å apart from each other rendering the formation of the DC site impossible. Note however that already for the K-FAU (Si/Al = 2.7) a formation of the DC site is observed [120] as the K^+ cations are due to their size moved further from the framework and closer to each other, enough to constitute a DC site for CO_2. In general, formation of the DC or MC sites leads to increased stabilization of the CO_2 adsorption complexes; this stabilization however strongly depends on the zeolite topology and (alkali-)metal cation involved, e.g., 3 kJ.mol^{-1} for K-FER (Si/Al = 8) [74] or as much as $20 - 30$ kJ.mol^{-1} for Na-A (Si/Al = 1) [126].

Some recommendations related to the potential of zeolites for CO_2 capture can be drawn. For applications requiring large CO_2 adsorption heats, zeolites showing the maximal effect from bottom or/and zeolites with a large number of DC sites should be used. For cases where constant adsorption heats are required, it becomes more complicated to find a suitable zeolite; a lower cation concentration should be used (to avoid formation of DC sites) and a specific (with suboptimal cation-cation distances for DC formation) distribution of extra-framework cations is desirable. The second option is discussed in detail in the following section. More information on this topis is provided in Attachment **G**.

3.2.2 Understanding the effect of synthesis conditions

Recently a synthesis strategy capable of tailoring the distribution of acid sites, i.e. distribution of specific extra-framework cations H^+, in FER zeolite has been reported based on the use of suitable organic structure directing agents (SDA) in the absence of alkaline cations [129]. Specifically, pyridine adsorption measurements showed that the distribution of acid sites between for pyridine non-accessible FER cage and the accessible 10-ring main channel in FER samples is strongly dependent on the SDA used in the synthesis. Note that coordination and location of the extra-framework cations (H^+ in this case) are, for the particular zeolite topology and extra-framework cation, determined by the Al distribution in the framework. Therefore, the above mentioned observation implies that such synthesis strategy can lead to preparation of zeolite samples with a specific and (in some respect) regular Al distribution - an object of the long-standing effort in the zeolite community.

In order to further elucidate the "regularity" of the Al distribution adsorption of CO_2 in Na-FER[10] samples (both with the same Si/Al = 15.4) prepared employing the above mentioned synthesis procedure were investigated experimentally [130]; results depicted in Figure 3.9 illustrate that while one of the samples (FER/B) exhibited a typical dependence [128] of adsorption heats on CO_2 coverage (a gradual decrease with increasing CO_2 dose) a significantly different situation was observed for the second sample considered (FER/A), for which the adsorption heat is almost constant from the onset of the adsorption up to the adsorbed CO_2 amount of $\sim$ 22.3 $cm^3.g^{-1}$ for which the number of adsorbed CO_2 molecules is equal to the number of extra-framework cations (surface coverage $\theta = 1$).

Based on the CO_2 adsorption heats calculated employing the DFT/CC correction scheme (see Table 1 in Attachment **H**), the explanation of the experimental results was proposed on the basis of different involvement of dual cation sites in the adsorption of CO_2 molecules in each FER sample. FER/B sample was assumed to contain a significant

[10]First the acid from (H-FER) of the FER zeolite was prepared according to the procedure reported in Ref. [129]. Subsequently, the sodium form (Na-FER) was prepared by ion-exchange.

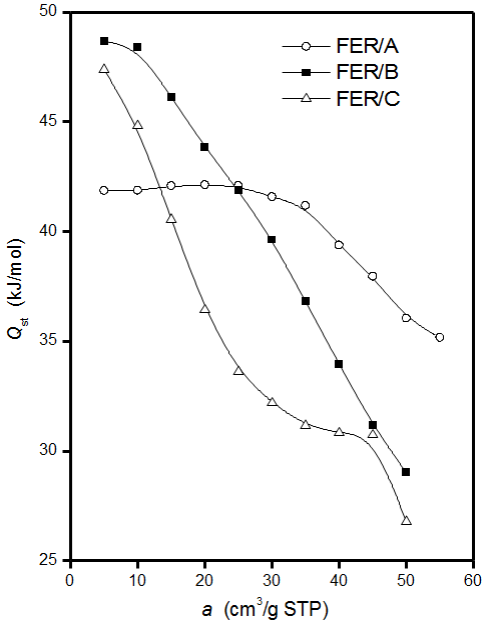

FIGURE 3.9: Dependence of isosteric heats on the adsorbed amount of CO_2 for samples FER/A, FER/B (both with Si/Al $\approx$ 15) and FER/C. Sample FER/C with lower aluminium content (Si/Al = 26.8) is shown for comparison.

fraction of DC sites contrary to the FER/A sample where only a negligible amount of DC sites should be found. The differences between experimental results for two FER samples is explained as follows: (i) Large values of adsorption enthalpies at low CO_2 coverage for FER/B can be attributed to the formation of CO_2 adsorption complexes on dual cation sites as these are about 10 kJ.mol^{-1} more stable than the corresponding single cation sites. (ii) Since the CO_2 molecule adsorbed on the DC site interacts with two Na^+ cations simultaneously, number of the available Na^+ sites diminishes faster with the CO_2 loading and once the Na^+ cations are occupied additional CO_2 molecules cannot interact directly with the extra-framework cations. Consequently, the presence of DC (in FER/B) leads to a larger decrease (with respect to the FER/A sample) in the adsorption heats for larger coverage.[11] A lack of the DC sites for FER/A sample implies that Al distribution is such that it precludes formation of the DC sites, i.e. the distance between two neighboring Na^+ cations is too large for CO_2 molecule to fit in between. In any case a regularity in the Al distribution of FER/A sample is apparent. Therefore, it can be summarized that computational investigation presented above provided an evidence that the synthesis strategy presented in Ref. [129] indeed allows the control

[11]The actual mechanism of adsorption in both samples involves also the formation of geminal CO_2 complexes (two CO_2 molecules interacting with a single Na^+ cation) where the adsorption enthalpy of the second CO_2 molecule on the Na^+ cation is 3$-$7 kJ.mol^{-1} smaller than the corresponding value for the mono-CO_2 adsorption complex (note the drop of approximately 5 kJ.mol^{-1} for FER/A sample at $\theta > 1$ which nicely corresponds with the presumable formation of the germinal CO_2 adsorption complexes). However, the general idea about saturation of the favorable Na^+ interactions sites due to the formation of DC site holds.

of the aluminum distribution in FER zeolite which can have an important application potential. More information on the topic is provided in Attachment **H**.

Chapter 4

Conclusions

The aim of the presented thesis was to extend the understanding of adsorption properties of selected microporous materials, namely the MOFs and zeolites. Despite significant progress made in theoretical description of adsorption mechanism in both zeolites and MOFs in last decade, there are numerous applications and systems for which the commonly used computational approaches fail to deliver needed accuracy. MOFs containing transitional metal *cus* sites represent a whole class of such systems where accurate description of both dispersion and open-shell metal electronic structure is needed to obtain reasonable overall performance. While the performance of standard DC-DFT approaches is in general much less problematic for alkaline or alkali earth metal containing zeolites, further improvement of accuracy is beneficial and in many application outright vital. Therefore, investigations discussed in the thesis focused on providing very accurate results specifically for the problematic systems or applications. Hence, the largest contribution to the current state of knowledge in adsorption on microporous materials can be achieved.

In the first part of the thesis, adsorption of various small molecules in a model *cus* containing MOF, the CuBTC, was studied. Initially, the suitability of various DFT-based methods for description of the *cus* site present in CuBTC was analyzed and both standard DFT and DC-DFT schemes were found to be unable to yield sufficiently accurate results. Therefore, an extension of previously developed DFT/CC approach, capable of effectively correcting for most of DFT deficiencies, was proposed for adsorption in CuBTC. The application potential of the DFT/CC scheme was tested for six different adsorbents (H_2O, CO_2, CH_4, C_3H_6, C_3H_8 and CO) with each molecule used to elucidate different aspects of adsorption mechanism in CuBTC: (i) zero-coverage limit adsorption heats on *cus* site only (all molecules), (ii) vibrational frequencies of species adsorbed on *cus* site (CO), (iii) component separation potential on *cus* site (C_3H_6, C_3H_8), (iv) coverage dependence of adsorption heats (CO_2, CH_4, C_3H_6, C_3H_8), i.e. consideration of various adsorption sites simultaneously. Finally, in case of methane more or less complete picture of temperature-dependent adsorption mechanism was uncovered thanks to

a direct implementation of DFT/CC-based methane-CuBTC PES into GCMC simulations. Thus, a direct acquisition of adsorption isotherms, coverage- and temperature-dependent adsorption heats and adsorption site occupations was made possible. But most importantly, DFT/CC results were found to be in almost perfect accord with available experimental data showing, where available, superior accuracy over standard DFT or DC-DFT methods.

In the second part of the thesis, the attention was focused on understanding adsorption of a single but environmentally consequential adsorbent, the carbon dioxide, in various zeolitic materials. Specifically, an attempt to establish a link between CO_2 adsorption heats and zeolite framework topology and composition (Si/Al ratio, i.e. the concentration of extra-framework cations) based on the DFT/CC calculations was made. Key factors influencing the stability of CO_2 adsorption complexes were identified following a very good agreement between experimental and computational results. Based on the identified key factors, a general model of CO_2 adsorption in zeolites was proposed which enabled to draw recommendations for optimal combination of zeolite topology and composition for a particular CO_2-related application.

In summary, the DFT/CC correction scheme proved to be a viable approach for obtaining accurate description of the adsorption processes in various microporous materials. However, currently applied strategy to obtain DFT/CC correction functions relies on a careful selection of the reference systems accompanied with extensive testing of the their transferability which is both computationally quite demanding as high level post Hartree Fock methods are used in the process and difficult to readily implement in the black-box fashion. Nevertheless, these drawbacks are outweighed in cases where standard empirical force fields, DFT or DC-DFT methods fail significantly which was observed above especially for MOFs containing the *cus* sites (and to some extent also in case of zeolites). Furthermore, a new and more readily applicable approach along the lines of DFT/CC scheme is being developed at present in our group [70].

Bibliography

[1] Auerbach, S. M., Carrado, K. A., Dutta, P. K., Eds. *Handbook of Zeolite Science and Technology*; Marcel Dekker, 2004.

[2] Čejka, J., van Bekkum, H., Corma, A., Schüth, F., Eds. *Introduction to Zeolite Molecular Sieves*; Elsevier, 2007.

[3] Long, J. R.; Yaghi, O. M. *Chem. Soc. Rev.* **2009**, *38*, 1213.

[4] Database of Zeolite Structures. `http://www.iza-structure.org/databases/`.

[5] Eddaoudi, M.; Kim, J.; Rosi, N.; Vodak, D.; Wachter, J.; O'Keeffe, M.; Yaghi, O. M. *Science* **2002**, *295*, 469.

[6] Keskin, S.; Kizilel, S. *Ind. Eng. Chem. Res.* **2011**, *50*, 1799.

[7] Lee, J.; Farha, O. K.; Roberts, J.; Scheidt, K. A.; Nguyen, S. T.; Hupp, J. T. *Chem. Soc. Rev.* **2009**, *38*, 1450.

[8] Li, J.-R.; Kuppler, R. J.; Zhou, H.-C. *Chem. Soc. Rev.* **2009**, *38*, 1477.

[9] Smit, B.; Maesen, T. L. M. *Chem. Rev.* **2008**, *108*, 4125.

[10] Düren, T.; Bae, Y.-S.; Snurr, R. Q. *Chem. Soc. Rev.* **2009**, *38*, 1237.

[11] Krishna, R.; van Baten, J. M. *Phys. Chem. Chem. Phys.* **2011**, *13*, 10593.

[12] García-Pérez, E.; Gascón, J.; Morales-Flórez, V.; Castillo, J. M.; Kapteijn, F.; Calero, S. *Langmuir* **2009**, *25*, 1725.

[13] Xiang, S.; Zhou, W.; Gallegos, J. M.; Liu, Y.; Chen, B. *J. Am. Chem. Soc.* **2009**, *131*, 12415.

[14] Wu, H.; Simmons, J. M.; Srinivas, G.; Zhou, W.; Yildirim, T. *J. Phys. Chem. Lett.* **2010**, *1*, 1946.

[15] Rana, M. K.; Koh, H. S.; Hwang, J.; Siegel, D. J. *J. Phys. Chem. C* **2012**, *116*, 16957.

[16] Tuma, C.; Sauer, J. *Phys. Chem. Chem. Phys.* **2006**, *8*, 3955.

[17] Kerber, T.; Sierka, M.; Sauer, J. *J. Comput. Chem.* **2008**, *29*, 2088.

[18] Göltl, F.; Hafner, J. *J. Chem. Phys.* **2011**, *134*, 064102.

[19] Sillar, K.; Hofmann, A.; Sauer, J. *J. Am. Chem. Soc.* **2009**, *131*, 4143.

[20] Cohen, A. J.; Mori-Sánchez, P.; Yang, W. *Chem. Rev.* **2012**, *112*, 289.

[21] Rubeš, M.; Soldán, P.; Nachtigall, P.; Bludský, O. *Open Chem. Phys. J.* **2008**, *1*, 1.

[22] Bludský, O.; Rubeš, M.; Soldán, P.; Nachtigall, P. *J. Chem. Phys.* **2008**, *128*, 114102.

[23] Andersson, Y.; Langreth, D.; Lundqvist, B. *Phys. Rev. Lett.* **1996**, *76*, 102.

[24] Dion, M.; Rydberg, H.; Schröder, E.; Langreth, D.; Lundqvist, B. *Phys. Rev. Lett.* **2004**, *92*, 22.

[25] Lee, K.; Murray, E. D.; Kong, L. Z.; Lundqvist, B. I.; Langreth, D. C. *Phys. Rev. B* **2010**, *82*, 081101.

[26] Dion, M. van der Waals forces in density functional theory. Ph.D. thesis, Rutgers University, 2004.

[27] Román-Pérez, G.; Soler, J. *Phys. Rev. Lett.* **2009**, *103*, 096102.

[28] Langreth, D.; Perdew, J. *Phys. Rev. B* **1977**, *15*, 2884.

[29] Hermann, J. Nonlocal correlation in density functional theory. M.Sc. thesis, Charles University in Prague, 2013.

[30] Wu, X.; Vargas, M. C.; Nayak, S.; Lotrich, V.; Scoles, G. *J. Chem. Phys.* **2001**, *115*, 8748.

[31] Zhang, Y.; Yang, W. *Phys. Rev. Lett.* **1998**, *80*, 890.

[32] Langreth, D. C.; Lundqvist, B. I.; Chakarova-Käck, S. D.; Cooper, V. R.; Dion, M.; Hyldgaard, P.; Kelkkanen, A.; Kleis, J.; Kong, L.; Li, S.; et al., *J. Phys. Condens. Matter* **2009**, *21*, 084203.

[33] Gulans, A.; Puska, M.; Nieminen, R. *Phys. Rev. B* **2009**, *79*, 201105.

[34] Klimeš, J.; Bowler, D.; Michaelides, A. *Phys. Rev. B* **2011**, *83*, 195131.

[35] Murray, E. D.; Lee, K.; Langreth, D. C. *J. Chem. Theory Comput.* **2009**, *5*, 2754.

[36] Vydrov, O. A.; Van Voorhis, T. *J. Chem. Phys.* **2009**, *130*, 104105.

[37] Vydrov, O. A.; Van Voorhis, T. *Phys. Rev. Lett.* **2009**, *103*, 063004.

[38] Vydrov, O. A.; Van Voorhis, T. *J. Chem. Phys.* **2010**, *133*, 244103.

[39] Grimme, S.; Antony, J.; Ehrlich, S.; Krieg, H. *J. Chem. Phys.* **2010**, *132*, 154104.

[40] Hujo, W.; Grimme, S. *J. Chem. Theory Comput.* **2011**, *7*, 3866.

[41] Cooper, V. R. *Phys. Rev. B* **2010**, *81*, 161104.

[42] Klimeš, J.; Bowler, D.; Michaelides, A. *J. Phys. Condens. Matter* **2010**, *22*, 022201.

[43] Armiento, R.; Mattsson, A. *Phys. Rev. B* **2005**, *72*, 085108.

[44] Wellendorff, J.; Lundgaard, K. T.; Møgelhøj, A.; Petzold, V.; Landis, D. D.; Nørskov, J. K.; Bligaard, T.; Jacobsen, K. W. *Phys. Rev. B* **2012**, *85*, 235149.

[45] Kaplan, I. *Intermolecular Interactions: Physical Picture, Computational Methods and Model Potentials*; John Wiley & Sons, Ltd., 2006.

[46] Sato, T.; Nakai, H. *J. Chem. Phys.* **2009**, *131*, 224104.

[47] Grimme, S. *J. Comput. Chem.* **2004**, *25*, 1463.

[48] Becke, A. D.; Johnson, E. R. *J. Chem. Phys.* **2005**, *122*, 154104.

[49] Becke, A. D.; Johnson, E. R. *J. Chem. Phys.* **2005**, *123*, 154101.

[50] Tkatchenko, A.; Scheffler, M. *Phys. Rev. Lett.* **2009**, *102*, 6.

[51] Angyán, J. G. *J. Chem. Phys.* **2007**, *127*, 024108.

[52] Krishtal, A.; Vannomeslaeghe, K.; Geldof, D.; Van Alsenoy, C.; Geerlings, P. *Phys. Rev. A* **2011**, *83*, 024501.

[53] Becke, A. D.; Johnson, E. R. *J. Chem. Phys.* **2006**, *124*, 14104.

[54] Grimme, S.; Ehrlich, S.; Goerigk, L. *J. Comput. Chem.* **2011**, *32*, 1456.

[55] Johnson, E. R.; Becke, A. D. *J. Chem. Phys.* **2006**, *124*, 174104.

[56] Brinck, T.; Murray, J. S.; Politzer, P. *J. Chem. Phys.* **1993**, *98*, 4305.

[57] Grimme, S. *J. Comput. Chem.* **2006**, *27*, 1787.

[58] Jurečka, P.; Šponer, J.; Černý, J.; Hobza, P. *Phys. Chem. Chem. Chem. Phys.* **2006**, *8*, 1985.

[59] Tkatchenko, A.; DiStasio, R. A.; Car, R.; Scheffler, M. *Phys. Rev. Lett.* **2012**, *108*, 236402.

[60] Tkatchenko, A.; Alfè, D.; Kim, K. S. *J. Chem. Theory Comput.* **2012**, *8*, 4317.

[61] Risthaus, T.; Grimme, S. *J. Chem. Theory Comput.* **2013**, *9*, 1580.

[62] Elstner, M.; Hobza, P.; Frauenheim, T.; Suhai, S.; Kaxiras, E. *J. Chem. Phys.* **2001**, *114*, 5149.

[63] Wu, Q.; Yang, W. *J. Chem. Phys.* **2002**, *116*, 515.

[64] Tang, K. T. *J. Chem. Phys.* **1968**, *49*, 4727.

[65] Dierksen, M.; Grimme, S. *J. Phys. Chem. A* **2004**, *108*, 10225.

[66] Burns, L. A.; Vázquez-Mayagoitia, A.; Sumpter, B. G.; Sherrill, C. D. *J. Chem. Phys.* **2011**, *134*, 084107.

[67] Ho, T.-S.; Rabitz, H. *J. Chem. Phys.* **1996**, *104*, 2584.

[68] Soldán, P.; Hutson, J. *J. Chem. Phys.* **2000**, *112*, 4415.

[69] Ho, T.-S.; Hollebeek, T.; Rabitz, H.; Harding, L. B.; Schatz, G. C. *J. Chem. Phys.* **1996**, *105*, 10472.

[70] Hermann, J.; Bludský, O. *J. Chem. Phys.* **2013**, Accepted.

[71] Rubeš, M.; Bludský, O.; Nachtigall, P. *ChemPhysChem* **2008**, *9*, 1702.

[72] Bludský, O.; Rubeš, M.; Soldán, P. *Phys. Rev. B* **2008**, *77*, 092103.

[73] Rubeš, M.; Kysilka, J.; Nachtigall, P.; Bludský, O. *Phys. Chem. Chem. Phys.* **2010**, *12*, 6438.

[74] Zukal, A.; Pulido, A.; Gil, B.; Nachtigall, P.; Bludský, O.; Rubeš, M.; Čejka, J. *Phys. Chem. Chem. Phys.* **2010**, *12*, 6413.

[75] Dzubak, A. L.; Lin, L.-c.; Kim, J.; Swisher, J. A.; Poloni, R.; Maximoff, S. N.; Smit, B.; Gagliardi, L. *Nat. Chem.* **2012**, *4*, 810.

[76] Getman, R. B.; Bae, Y.-S.; Wilmer, C. E.; Snurr, R. Q. *Chem. Rev.* **2012**, *112*, 703.

[77] Chui, S. S.; Lo, S. M.-F.; Charmant, J. P. H.; Orpen, A. G.; Williams, I. D. *Science* **1999**, *283*, 1148.

[78] Kahn, O. *Molecular Magnetism*; VCH, New York, 1993.

[79] Rodríguez-Fortea, A.; Alemany, P.; Alvarez, S.; Ruiz, E. *Chem. Eur. J.* **2001**, *7*, 627.

[80] Ruiz, E.; Llunell, M.; Alemany, P. *J. Solid State Chem.* **2003**, *176*, 400.

[81] Poater, J.; Solà, M.; Rimola, A.; Rodríguez-Santiago, L.; Sodupe, M. *J. Phys. Chem. A* **2004**, *108*, 6072.

[82] Jeanvoine, Y.; Spezia, R. *J. Mol. Struct. THEOCHEM* **2010**, *954*, 7.

[83] El-Nahas, A. A. M.; Tajima, N.; Hirao, K. *Chem. Phys. Lett.* **2000**, *318*, 333.

[84] Ducéré, J.-M.; Goursot, A.; Berthomieu, D. *J. Phys. Chem. A* **2005**, *109*, 400.

[85] Grajciar, L.; Bludský, O.; Nachtigall, P. *J. Phys. Chem. Lett.* **2010**, *1*, 3354.

[86] Rubeš, M.; Grajciar, L.; Bludský, O.; Wiersum, A. D.; Llewellyn, P. L.; Nachtigall, P. *ChemPhysChem* **2012**, *13*, 488.

[87] Chowdhury, P.; Bikkina, C.; Meister, D.; Dreisbach, F.; Gumma, S. *Microporous Mesoporous Mater.* **2009**, *117*, 406.

[88] Küsgens, P.; Rose, M.; Senkovska, I.; Fröde, H.; Henschel, A.; Siegle, S.; Kaskel, S. *Microporous Mesoporous Mater.* **2009**, *120*, 325.

[89] Henninger, S.; Schmidt, F.; Henning, H.-M. *Appl. Therm. Eng.* **2010**, *30*, 1692.

[90] Lukose, B.; Supronowicz, B.; St. Petkov, P.; Frenzel, J.; Kuc, A. B.; Seifert, G.; Vayssilov, G. N.; Heine, T. *Phys. Status Solidi B* **2012**, *249*, 335.

[91] Watanabe, T.; Sholl, D. S. *J. Chem. Phys.* **2010**, *133*, 094509.

[92] Grajciar, L.; Wiersum, A. D.; Llewellyn, P. L.; Chang, J.-S.; Nachtigall, P. *J. Phys. Chem. C* **2011**, *115*, 17925.

[93] Getzschmann, J.; Senkovska, I.; Fairen-Jimenez, D.; Düren, T.; Kaskel, S. *unpublished results*

[94] Rubeš, M.; Wiersum, A. D.; Llewellyn, P. L.; Grajciar, L.; Bludský, O.; Nachtigall, P. *J. Phys. Chem. C* **2013**, *117*, 11159.

[95] Sumida, K.; Rogow, D. L.; Mason, J. A.; McDonald, T. M.; Bloch, E. D.; Herm, Z. R.; Bae, T.-h.; Long, J. R. *Chem. Rev.* **2012**, *112*, 724.

[96] Min Wang, Q.; Shen, D.; Bülow, M.; Ling Lau, M.; Deng, S.; Fitch, F. R.; Lemcoff, N. O.; Semanscin, J. *Microporous Mesoporous Mater.* **2002**, *55*, 217.

[97] Liang, Z.; Marshall, M.; Chaffee, A. L. *Energy Fuels* **2009**, *23*, 2785.

[98] Farrusseng, D.; Daniel, C.; Gaudillère, C.; Ravon, U.; Mirodatos, C.; Schuurman, Y.; Dubbeldam, D.; Frost, H.; Snurr, R. Q. *Langmuir* **2009**, *25*, 7383.

[99] Aprea, P.; Caputo, D.; Gargiulo, N.; Iucolano, F.; Pepe, F. *J. Chem. Eng. Data* **2010**, *55*, 3655.

[100] Moellmer, J.; Moeller, A.; Dreisbach, F.; Glaeser, R.; Staudt, R. *Microporous Mesoporous Mater.* **2011**, *138*, 140.

[101] Wu, H.; Simmons, J. M.; Liu, Y.; Brown, C. M.; Wang, X.-S.; Ma, S.; Peterson, V. K.; Southon, P. D.; Kepert, C. J.; Zhou, H.-C.; Yildirim, T.; Zhou, W. *Chem. Eur. J.* **2010**, *16*, 5205.

[102] Getzschmann, J.; Senkovska, I.; Wallacher, D.; Tovar, M.; Fairen-Jimenez, D.; Düren, T.; van Baten, J. M.; Krishna, R.; Kaskel, S. *Microporous Mesoporous Mater.* **2010**, *136*, 50.

[103] Chen, L.; Grajciar, L.; Nachtigall, P.; Düren, T. *J. Phys. Chem. C* **2011**, *115*, 23074.

[104] Lamia, N.; Jorge, M.; Granato, M. A.; Almeida Paz, F. A.; Chevreau, H.; Rodrigues, A. E. *Chem. Eng. Sci.* **2009**, *64*, 3246.

[105] Yoon, J.-W.; Jang, I.-T.; Lee, K.-Y.; Hwang, Y.-K.; Chang, J.-S. *Bull. Korean Chem. Soc.* **2010**, *31*, 220.

[106] Jorge, M.; Lamia, N.; Rodrigues, A. E. *Colloids Surf., A* **2010**, *357*, 27.

[107] Ferreira, A. F.; Santos, J. C.; Plaza, M. G.; Lamia, N.; Loureiro, J. M.; Rodrigues, A. E. *Chem. Eng. J.* **2011**, *167*, 1.

[108] Fischer, M.; Gomes, J. R. B.; Fröba, M.; Jorge, M. *Langmuir* **2012**, *28*, 8537.

[109] Hadjiivanov, K. I.; Vayssilov, G. N. *Adv. Catal.* **2002**, *47*, 307.

[110] Zecchina, A.; Areán, C. O. *Chem. Soc. Rev.* **1996**, *25*, 187.

[111] Alaerts, L.; Séguin, E.; Poelman, H.; Thibault-Starzyk, F.; Jacobs, P. A.; De Vos, D. E. *Chem. Eur. J.* **2006**, *12*, 7353.

[112] Prestipino, C.; Regli, L.; Vitillo, J. G.; Bonino, F.; Damin, A.; Lamberti, C.; Zecchina, A.; Solari, P. L.; Kongshaug, K. O.; Bordiga, S. *Chem. Mater.* **2006**, *18*, 1337.

[113] Bordiga, S.; Regli, L.; Bonino, F.; Groppo, E.; Lamberti, C.; Xiao, B.; Wheatley, P. S.; Morris, R. E.; Zecchina, A. *Phys. Chem. Chem. Phys.* **2007**, *9*, 2676.

[114] Drenchev, N.; Ivanova, E.; Mihaylov, M.; Hadjiivanov, K. *Phys. Chem. Chem. Phys.* **2010**, *12*, 6423.

[115] D'Alessandro, D. M.; Smit, B.; Long, J. R. *Angew. Chem. Int. Ed.* **2010**, *49*, 6058.

[116] Bonelli, B.; Civalleri, B.; Fubini, B.; Ugliengo, P.; Areán, C. O.; Garrone, E. *J. Phys. Chem. B* **2000**, *104*, 10978.

[117] Garrone, E.; Bonelli, B.; Lamberti, C.; Civalleri, B.; Rocchia, M.; Roy, P.; Otero Areán, C. *J. Chem. Phys.* **2002**, *117*, 10274.

[118] Galhotra, P.; Navea, J. G.; Larsen, S. C.; Grassian, V. H. *Energy Environ. Sci.* **2009**, *2*, 401.

[119] Plant, D.; Maurin, G.; Deroche, I.; Gaberova, L.; Llewellyn, P. *Chem. Phys. Lett.* **2006**, *426*, 387.

[120] Pirngruber, G. D.; Raybaud, P.; Belmabkhout, Y.; Čejka, J.; Zukal, A. *Phys. Chem. Chem. Phys.* **2010**, *12*, 13534.

[121] Pulido, A.; Nachtigall, P.; Zukal, A.; Domínguez, I.; Čejka, J. *J. Phys. Chem. C* **2009**, *113*, 2928.

[122] Akten, E. D.; Siriwardane, R.; Sholl, D. S. *Energy Fuels* **2003**, *17*, 977.

[123] Hirotani, A.; Mizukami, K.; Miura, R.; Takaba, H.; Miya, T.; Fahmi, A.; Stirling, A.; Kubo, M.; Miyamoto, A. *Appl. Surf. Sci.* **1997**, *120*, 81.

[124] Maurin, G.; Llewellyn, P. L.; Bell, R. G. *J. Phys. Chem.. B* **2005**, *109*, 16084.

[125] Plant, D.; Maurin, G.; Deroche, I.; Llewellyn, P. *Microporous Mesoporous Mater.* **2007**, *99*, 70.

[126] Zukal, A.; Areán, C.; Delgado, M.; Nachtigall, P.; Pulido, A.; Mayerová, J.; Čejka, J. *Microporous Mesoporous Mater.* **2011**, *146*, 97.

[127] Bulánek, R.; Frolich, K.; Frýdová, E.; Čičmanec, P. *J. Therm. Anal. Calorim.* **2010**, *105*, 443.

[128] Grajciar, L.; Čejka, J.; Zukal, A.; Otero Areán, C.; Turnes Palomino, G.; Nachtigall, P. *ChemSusChem* **2012**, *5*, 2011.

[129] Pinar, A.; Márquez-Álvarez, C.; Grande-Casas, M.; Pérez-Pariente, J. *J. Catal.* **2009**, *263*, 258.

[130] Nachtigall, P.; Grajciar, L.; Pérez-Pariente, J.; Pinar, A. B.; Zukal, A.; Čejka, J. *Phys. Chem. Chem. Phys.* **2012**, *14*, 1117.

List of Attached Publications

This thesis is based on the following articles and book chapter:

Attachment A:
Grajciar, L., Rubeš, M., Bludský, O., Nachtigall, P. (2013): Accurate ab Initio Description of Adsorption on Coordinatively Unsaturated Sites in MOFs. Book chapter in: *Metal-Organic Frameworks: Materials Modeling towards Engineering Applications.* Pan Stanford Publishing, Singapore.

Attachment B:
Grajciar, L., Bludský, O., Nachtigall, P. (2010): Water Adsorption on Coordinatively Unsaturated Sites in CuBTC MOF. In: *Journal of Physical Chemistry Letters*, 1, 3354-3359.

Attachment C:
Grajciar, L., Wiersum, A. D., Llewellyn, P. L., Chang, J. S., Nachtigall, P. (2011): Understanding CO_2 Adsorption in CuBTC MOF: Comparing Combined DFT-ab Initio Calculations with Microcalorimetry Experiments. In: *Journal of Physical Chemistry C*, 115, 17925-17933.

Attachment D:
Chen, L. J., **Grajciar, L.**, Nachtigall, P., Düren, T. (2011): Accurate Prediction of Methane Adsorption in a Metal-Organic Framework with Unsaturated Metal Sites by Direct Implementation of an ab Initio Derived Potential Energy Surface in GCMC Simulation. In: *Journal of Physical Chemistry C*, 115, 23074-23080.

Attachment E:
Rubeš, M., Wiersum, A. D., Llewellyn, P. L., **Grajciar, L.**, Bludský, O., Nachtigall, P. (2013): Adsorption of Propane and Propylene on CuBTC MOF: Combined Theoretical and Experimental Investigation. In: *Journal of Physical Chemistry C*, 117, 11159-11167.

Attachment F:
Rubeš, M., **Grajciar, L.**, Bludský, O., Wiersum, A. D., Llewellyn, P. L., Nachtigall, P. (2012): Combined Theoretical and Experimental Investigation of CO Adsorption on Coordinatively Unsaturated Sites in CuBTC MOF. In: *ChemPhysChem*, 13, 488-495.

Attachment G:

Grajciar, L., Čejka, J., Zukal, A., Areán, C. O., Palomino, G. T., Nachtigall, P. (2012): Controlling the Adsorption Enthalpy of CO_2 in Zeolites by Framework Topology and Composition. In: *ChemSusChem*, 5, 2011-2022.

Attachment H:

Nachtigall, P., **Grajciar, L.**, Pérez-Pariente, J., Pinar, A. B., Zukal, A., Čejka, J. (2012): Control of CO_2 Adsorption Heats by the Al Distribution in FER Zeolites: Effect of Synthesis Conditions. In: *Physical Chemistry Chemical Physics*, 14, 1117-1120.

Attached Publications

Attachment A

Chapter One

Accurate Ab Initio Description of Adsorption on Coordinatively Unsaturated Sites in MOFs

Lukáš Grajciar, Miroslav Rubeš, Ota Bludský and Petr Nachtigall
Department of Physical and Macromolecular Chemistry, Faculty of Science, Charles University in Prague, Hlavova 8, 128 43, Prague, Czech Republic
petr.nachtigall@natur.cuni.cz

Accurate *ab initio* description of the adsorbate–adsorbent interactions in MOFs containing coordinatively unsaturated transition metal sites represents a significant challenge for computational chemists. The following complications are often faced: (i) spin-coupling between the unpaired electrons on individual transition metal ions, (ii) complicated electronic structure of individual transition metal ions or metal-oxo-clusters resulting in multi-reference character of corresponding wavefunction, and (iii) the importance of dispersion interaction between adsorbate and adsorbent. As a consequence, a reliability of computational methods based on popular density functional theory (DFT) is often insufficient. The suitability, reliability, and accuracy of DFT methods for the description of adsorption in MOFs is discussed in this chapter based on the comparison with highly accurate wavefunction-based methods and with accurate experimental data.

1.1 INTRODUCTION

Book Title
First Author & Second Author

www.panstanford.com

There is a large group of MOFs where transition metal cations are not coordinatively saturated by organic linkers. Consequently, these MOFs contain coordinatively unsaturated sites (*cus*) that exhibit unique adsorption properties. CuBTC [36], CPO-27 [60], MIL-100 [19], or MIL-101 [20], are only few examples of MOFs with *cus* sites. Computational investigations of adsorption properties of MOFs mostly rely on the empirical inter-atomic potential functions (IPF, often referred to as force field) used in Grand Canonical Monte Carlo (GCMC) simulations [15]. While there are many successful applications of IPF giving adsorption isotherms in good agreement with experiments [16,24], the suitability of IPF-based approaches for the description of MOFs with *cus* sites is at least questionable [23,43]. It is therefore understandable that interaction of various adsorbates with *cus* sites was investigated at the density functional theory (DFT) level. Not surprisingly it has been found that interaction of small molecules with MOFs was typically overestimated when local exchange-correlation functionals (LDA) were employed and it was underestimated when semi-local generalized gradient approximation (GGA) type functionals were employed [59,69-70]. There are two reasons for the failure of traditional exchange-correlation functionals (LDA and GGA) to describe adsorbate interactions with the *cus*-containing MOFs: firstly, the inability of these functionals to describe the van der Waals interactions that are critical for correct description of adsorption in porous materials and, secondly, the inaccuracy of DFT when describing the electronic structure of transition metal cations, in particular those with open-shell electronic structure. While the former deficiency can be reasonably well overcome using either semi-empirical dispersion corrections [29-30] or nonempirical vdW density functionals [41,46], the latter deficiency is more serious for MOFs containing transition metal *cus* sites.

The accurate *ab initio* calculations employing the reliable post Hartree-Fock methods such as Coupled Cluster (CC) have been used for the description of adsorbate-*cus* interactions (*e. g.*, Refs. [27,34]) employing relatively small cluster models representing the *cus* site. While the results obtained are highly accurate for the model used, they cannot be directly compared with experimental results since they cannot account for the long-range interactions. Instead, the results of CC (or similar) highly accurate calculations for cluster models can serve as

important benchmark for evaluation of the accuracy of more approximate methods, such as DFT or empirical force-fields.

The extent of this Chapter does not allow for a broad overview of large number of applications of *ab initio* methods in the investigation of adsorption phenomenon in many different MOFs. Instead, this Chapter is focused on one particular MOF, HKUST-1 (often denoted as CuBTC) [36], for which a large amount of experimental data is available and which is likely the most often computationally investigated MOF. The computational methods discussed within the Chapter are described first. The computational difficulties related to the spin coupling issues are described next on the example of the Cu^{2+}-Cu^{2+} interaction in the CuBTC paddlewheel. The reliability of computational methods is thoroughly discussed in Section X.3.2, comparing cluster model results obtained at the CC level of theory with those obtained with less accurate electronic structure methods. The results obtained for water, CO, CO_2, CH_4, and C_3 hydrocarbons are reviewed in Sections X.4.1, X.4.2, X.4.3, X.4.4, and X.4.5, respectively.

1.2 METHODS AND MODELS

1.2.1 *Cluster and periodic models of CuBTC*

The *cus* site in CuBTC consists of a pair of Cu^{2+} ions in close proximity (about 2.5 Å) connected with four carboxylic groups (a paddle-wheel model, PDWL, see Figure 1.1b). The PDWL unit represents the smallest model capturing the electronic properties of the *cus* site.

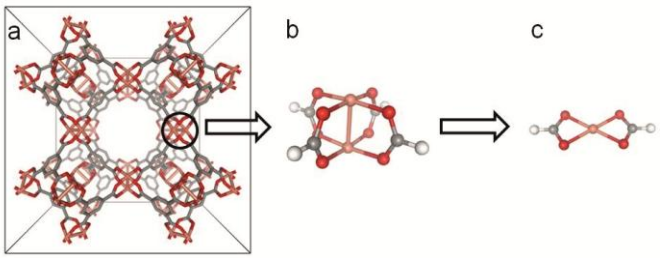

Figure 1.1. (a) CuBTC unit cell, (b) PDWL unit and (c) $Cu(HCOO)_2$ model.

In situations where the coupling of unpaired electrons on Cu^{2+} can be neglected (such as physisorption of small molecules on *cus* site, see Section X.3.1), a much smaller model, $Cu(HCOO)_2$ constrained at the geometry of PDWL, can be employed (Figure 1.1c). The size of this model enables the benchmarking of density functionals (see Section X.2.2.1) used in periodic calculations with respect to the reference level of theory (typically coupled cluster theory, Section X.2.2.2).

While cluster models described above are extremely useful for explaining a rather complex electronic structure and properties of *cus* sites, an accurate description of adsorbate-MOF interactions accounting for long range dispersion and electrostatic contributions can only be obtained within the periodic model. The CuBTC structure was modeled either using the experimental rhombohedral primitive cell [36] containing 156 framework atoms (RPC; a=b=c=18.627 Å, α=β=γ=60°) or by the optimized RPC cell obtained from fitting the polynomial to the E(V) curve calculated at different volumes relaxing the cell shape and fractional coordinates (a=b=c=18.774 Å, α=β=γ=60°) [27,34].

1.2.2 *Methods*

1.2.2.1 *Density functional theory*

The cluster DFT calculations were carried out with several commonly used density functionals (LDA, GGA, hybrid, and non-local exchange-correlation functionals, Figure 1.2). The interaction energies were calculated using the supermolecular approach:

$$E_{\text{int}} = E_{AB} - E_A - E_B \tag{1.1}$$

corrected for the basis set superposition error (BSSE) by the counterpoise correction of Boys and Bernardi [9] within the frozen monomer approximation. The pseudopotential-based correlation-consistent valence-X-ζ basis set with polarization functions by Peterson *et al.* [54], cc-pVXZ-PP, were employed for Cu atoms while the standard Dunning's correlation-consistent valence-X-ζ basis sets with polarization functions[14], cc-pVXZ, were used for other atoms. The corresponding augmented correlation-consistent basis sets were also employed, aug-cc-pVXZ-PP and aug-cc-pVXZ for Cu and other atoms, respectively.

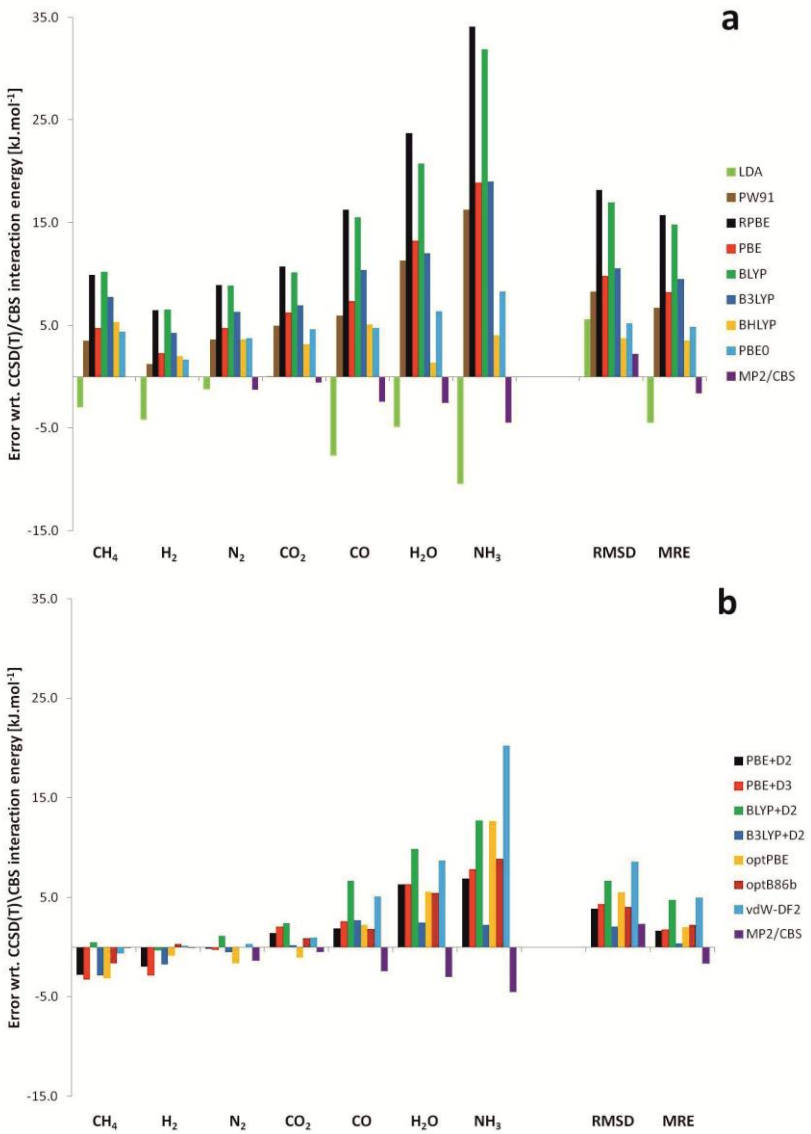

Figure 1.2. (a) Interaction energies (in kJ.mol^{-1}) of various molecules with the $Cu(HCOO)_2$ model calculated at the (a) DFT and (b) dispersion corrected DFT functionals. MP2/CBS is included for comparison.

The above mentioned mixed basis sets are denoted throughout the text as VXZ and AVXZ for the standard and augmented basis sets, respectively. The periodic DFT calculations were performed with the Perdew-Burke-Ernzerhof (PBE) functional [53] for the ferromagnetic case (all unpaired spins on 12 copper atoms in the unit call were aligned in the same direction). The projector augmented wave (PAW) [6] and the kinetic energy cutoff of 600 eV were used. The Γ-point sampling of the first Brillouin zone was found to be sufficient to yield converged results.

1.2.2.2 *Post-Hartree–Fock methods*

The coupled cluster method [11] with explicit single and double and perturbative triple excitations, CCSD(T), is currently the most reliable quantum-chemical method for the accurate description of the adsorbate–adsorbent interactions. Thanks to the recent progress in parallelizing CC equations, the CCSD(T) method is applicable even to moderately large systems. The only sizable errors in CCSD(T) calculations come from the basis set incompleteness (BSI). Two commonly employed approaches for dealing with the BSI error are the explicitly correlated coupled-cluster method[1] and the extrapolation to the CBS limit [32]. Since the extrapolation technique requires the use of truly large basis sets, the actual CCSD(T)/CBS calculations for large cluster models (see Section X.2.1) are usually performed in combination with more approximative (and less reliable) methods such as MP2. For models of the MOF adsorption complexes the estimation of the BSI error is performed at the MP2 level typically using the AVXZ (X=T,Q) basis sets.

An accurate theoretical description of the *cus* site in CuBTC by single reference methods (such as CCSD(T)) is complicated by the presence of Cu^{2+} ions with open-shell electronic structure. The multireference character of the singlet wavefunction and the stability in the corresponding singlet (S) and triplet (T) electronic states for the $Cu_2(HCOO)_4$ cluster model (see Fig. 1.1b) was investigated by the complete active space second-order perturbation theory (CASPT2).

1.2.2.3 *DFT/CC method*

Reliable coupled cluster and multi-reference methods described in Section X.2.2.2 cannot be applied directly neither to large cluster models nor to a periodic model of MOFs. Thus, there is a need for a computationally tractable yet reliable method for description of MOFs with transition metal *cus's*. Density functional theory (DFT) has been used extensively for description of molecular sieves. The GGA-type functionals, however, do not account for dispersion interactions (always important in extended systems). Various types of dispersion corrected density functionals were employed for the periodic calculations of MOFs ranging from the nonlocal functionals to GGA-type functionals with damped r^{-6} dispersion corrections. However, the problem of DFT for the description of *cus* sites involves often unrealistically large spin and charge delocalization and cannot be fixed simply by adding a dispersion component.

Recently, a parameter-free DFT/CC correction scheme has been proposed for precise calculations (close to CCSD(T) accuracy) of weakly bound molecular systems [7]. The correction scheme has been successfully applied to the physical adsorption of molecules on graphene and various molecular sieves. The DFT/CC method is based on the pair-wise representability of DFT error, ΔE, defined as

$$\Delta E = E_{CCSD(T)} - E_{DFT} \tag{1.2}$$

where $E_{CCSD(T)}$ and E_{DFT} is the interaction energy calculated at the CCSD(T)/CBS and DFT/AVQZ levels of theory, respectively. Therefore, the DFT/CC method can be used also for systems where the nature of the DFT error is more general than just a lack of non-local correlation. Within the DFT/CC method, the DFT error ΔE is expressed as a sum of atom-atom correction functions $\varepsilon_{ij}(R_{ij})$,

$$\Delta E = \sum_{ij} \varepsilon_{ij}(R_{ij}) \tag{1.3}$$

where R_{ij} is the distance between atoms i and j. No explicit functional form for ε_{ij} correction functions is assumed, instead a Reproducible Kernel Hilbert Space interpolation [63] is used. In addition to the assumption about pair-wise representability of DFT error, Eq. (1.3), the transferability of the correction functions from the reference system to

the system of interest is assumed. Correction functions ε_{ij} are evaluated from one-dimensional potential energy curves of suitably chosen reference complexes including complexes of the $Cu(HCOO)_2$ model described in Section X.2.1 with small adsorbate molecules (CH_4, H_2, N_2, CO_2, CO, H_2O and NH_3). The choice of the reference system is just critical for the reliability of DFT/CC method. For example, the water-CuBTC correction functions ε_{OH} (ε_{HH}), ε_{OC} (ε_{HC}), ε_{OO} (ε_{HO}), and ε_{OCu} (ε_{HCu}) were evaluated from H_2O-H_2, H_2O-C_6H_6, H_2O-CO_2, and H_2O-$Cu(HCOO)_2$ complexes, respectively [27]. Details about the construction of other correction functions can be found elsewhere [28,34,61]. The assumption of the correction function transferability was tested by CCSD(T)/CBS and DFT/CC calculations carried out for the $Cu_2(HCOO)_4$ cluster model and they are discussed below.

1.3 ELECTRONIC STRUCTURE OF COORDINATIVELY UNSATURATED SITES IN CUBTC

1.3.1 *Spin-coupling in CuBTC*

The PDWL units in CuBTC closely resemble some well known molecular complexes of dimeric Cu^{2+} carboxylates, which show paramagnetic behavior at a room temperature. The temperature lowering leads to a steady transition from paramagnetic to the antiferromagnetic couplings of the two unapaired electrons on each Cu^{2+} pair [39-40,49]. Thus the ground state of the PDWL unit is a singlet state (diamagnetic) and the excited triplet state (paramagnetic) starts to be populated with increasing temperature. The experimental singlet-triplet splitting for such complexes is usually in the range of -150 to -200 cm^{-1}.

In order to reliably calculate the singlet-triplet splitting ($\Delta E_{ST}=E_S-E_T$) in PDWL unit, the singlet and triplet states must be described with high accuracy. While the triplet state can be described with just a single Slater determinant, and thus "standard" methods of quantum chemistry such as CCSD(T), MP2 and DFT can be used, multireference wave function (i.e at least two Slater determinants) is required for the description of the singlet state [27,61]. Within the DFT approach the energy of the singlet state is often approximated with the broken-symmetry solution. The

calculated singlet-triplet splittings for PDWL and its complexes with H_2O and CO molecules are given in Table 1.1.

The ΔE_{ST} energy gap calculated at the CASPT2 level is consistent with experimental results and it does not change significantly upon the interaction with H_2O and CO. It follows that the calculated interaction energies for singlet and triplet states are very similar. Thus, the accurate interaction energies can be obtained for triplet electronic state for which the accurate approach such as CCSD(T) at the complete basis set limit (CBS) can be used.

The B3LYP and PBE functionals give correctly singlet state (broken-symmetry solution) below the triplet state and the ΔE_{ST} energy gaps are also not influenced significantly upon the interaction with H_2O or CO. The B3LYP results are clearly superior to the PBE ones considering the strong overestimation of ΔE_{ST} energy gap at the PBE level. Moreover in case of CO interaction with *cus* sites there is a large change in Cu-Cu distance at PBE level with respect to B3LYP and CASPT2 results. This artificially increased Cu-Cu distance results in the overestimated σ-bonding interaction [61]. It is apparent that mixing of the exact exchange into the functional leads to better results.

Table 1.1. Calculated singlet-triplet (S,T) splitting (ΔE_{ST}) for bare PDWL, CO\PDWL and H_2O\PDWL complexes along with optimized Cu-Cu equilibrium distances. The DFT (B3LYP, PBE) singlet corresponds to the broken-symmetry solution.

		r(Cu-Cu) [Å]			ΔE_{ST}[cm^{-1}]		
Complex[a,b]	State	CASPT2	B3LYP	PBE	CASPT2	B3LYP	PBE
PDWL	S	2.511	2.523	2.473	-155	-365	-953
	T	2.511	2.518	2.455			
H_2O\PDWL	S	2.600	2.618	2.548	-119	-300	-838
	T	2.600	2.614	2.532			
CO\PDWL	S	2.593	2.618	2.644	-135	-343	-1055
	T	2.593	2.614	2.604			

[a] The complexes has been described with standard cc-pVDZ basis set; for Cu the cc-pVDZ-PP basis set with pseudopotential has been used. The size of the basis set should not significantly influence the singlet-triplet splitting.[27] [b] All complexes have D_{2h} symmetry, which implies that two H_2O and CO molecules interact with each of the *cus* sites of the PDWL unit.

The B3LYP and PBE closed shell singlet state solutions are not reported in Table 1.1 since corresponding energies are above the triplet state and, in addition, they strongly depend on the adsorbed molecule and geometry used. The strong dependence of ΔE_{ST} energy gap upon adsorbed species and geometry can result in largely overestimated difference (as much as 17 kJ.mol^{-1}) between interaction energies for closed shell singlet and open-shell triplet (and properly described singlet) electronic states.

The experimental measurements on CuBTC indicated an antiferromagnetic coupling on each PDWL unit at low temperatures [72]. The magnetic susceptibility measurements further suggested a weak ferromagnetic coupling between PDWL units bellow 70 K probably modulated by organic linkers. However, it was pointed out by the subsequent experimental study that presence of paramagnetic extra framework Cu^{2+} cations can influence magnetic susceptibility measurements at very low temperatures [57].

It can be concluded that the antiferromagnetic solution in periodic DFT treatment is desirable. However, the presence of six PDWL units in the unit cell of CuBTC makes the convergence into the correct antiferromagnetic solution rather problematic. Corresponding convergence issues can be overcome by using a high-spin (ferromagnetic) solution, which can be taken as an analogy of the triplet state on each PDWL unit in the CuBTC unit cell. Considering a weak coupling between PDWL units the resulting adsorption enthalpies obtained for a well-defined high-spin solution do not differ significantly from the correct antiferromagnetic solution. Furthermore, spin un-polarized solutions yields interaction energies also in a good agreement (within 2 kJ.mol^{-1}) with the high-spin solution [27]. This apparent contradiction with the results obtained for the PDWL cluster (see above) is most likely due to different geometries of PDWL cluster and PDWL unit in CuBTC; some favorable error compensation takes place in CuBTC structure while such error cancellation it is not operative for the PDWL cluster. It follows that the calculations can be performed for adsorption of some adsorbates in CuBTC even with the spin-unpolarized wavefunction, however, spin-polarized solution should be preferred.

1.3.2 *Evaluation of method accuracy: $Cu(COOH)_2$ model*

The reliability of various density functional theory (DFT) based methods, including dispersion-corrected DFT, for the adsorbate-*cus* interaction was investigated using the $Cu(HCOO)_2$ cluster model (Figure 1.1c). The small size of this model enables the benchmarking of DFT functionals with respect to the highly accurate CCSD(T) results for a number of adsorbents (CH_4, H_2, N_2, CO_2, CO, H_2O and NH_3); different types of adsorbate-adsorbent interactions, including dispersion, electrostatic, and partially covalent bonding, are represented in this set.

Interaction energies of the above mentioned small molecules with the $Cu(HCOO)_2$ cluster model in the PBE/AVTZ equilibrium geometry were first evaluated for several commonly used LDA, GGA and hybrid functionals (Figure 1.2a). For all the molecules considered herein the interaction energy is underestimated with tested exchange-correlation functionals except for the LDA functional, which, on the contrary, systematically overestimates interaction energies. The RMSD values averaged for hybrid exchange-correlation functionals (B3LYP, BHLYP and PBE0) are lower than those for the GGA functionals (PBE, PW91, RPBE and BLYP), 7.1 and 14.0 $kJ.mol^{-1}$, respectively. Note however, that B3LYP has larger RMSD than PBE, PW91, and LDA. Since none of these functionals accounts for dispersion interaction, it is not surprising that even for BHLYP (having lowest RMSD) the relative errors are larger than 40% for adsorbates where the stabilization by the dispersion interaction is critical (CH_4, H_2, N_2). A notable trend, which has been also reported for Cu^{2+} cation interaction with other ligands [13,17,37,55], could be observed for the DFT functionals formed by the B88 exchange and LYP correlation functionals with an addition of a different amount of the exact HF exchange: the increasing amount of the exact HF exchange (BLYP<B3LYP<BHLYP) leads to improved accuracy.

The failure of the standard GGA or even hybrid functionals to provide reasonable agreement with the benchmarking data is not surprising as it is well-known that these DFT functionals do not account for dispersion interactions which should lead to a systematic underestimation of the interaction energies (Fig. 1.2a) Therefore, two different types of dispersion-correction schemes were adopted: the semiempirical pairwise C_6 approach by Grimme (DFT+D2 or DFT+D3) [3,30] and new nonlocal correlation functionals which capture long-range dispersion forces (vdW-DF2, optPBE, optB86b) [41-42,46]. The

inclusion of dispersion interactions led to an substantial improvement of the interaction energies (Fig 1.2b) with a RMSD value decreasing as much as 7.4 kJ.mol^{-1} upon adding the D2 correction; note that B3LYP+D2 has smaller RMSD than MP2. However the improvement is dependent on the type of the adsorption complex. The following observations can be drawn: (i) the stability of dispersion-dominated complexes (H_2 and CH_4 in particular) is overestimated, (ii) interaction energies of N_2 and CO_2 are accurately described at the DFT-D level, and (iii) the interaction between the *cus* site and CO, H_2O, and NH_3 molecules is severely underestimated (except for the B3LYP-D2 level). Thus, adding the

Table 1.2. Mulliken charges computed employing various exchange-correlation functionals and reference averaged-quadratic-coupled-cluster (AQCC) method.

System	Fragment	Molecule	DFT functional				AQCC
			LDA	GGA	hybrid		
				BLYP	B3LYP	BHLYP	
		CH_4	0.49	0.57	0.70	0.88	0.87
		H_2	0.49	0.57	0.70	0.88	0.87
		N_2	0.47	0.55	0.68	0.86	0.86
	Cu atom	CO_2	0.50	0.58	0.71	0.88	0.88
		CO	0.47	0.56	0.69	0.87	0.87
		H_2O	0.49	0.59	0.72	0.90	0.89
		NH_3	0.48	0.58	0.72	0.90	0.88
$Cu(COOH)_2$ molecule							
		CH_4	-0.01	0.00	0.00	0.00	0.00
		H_2	-0.01	0.00	0.00	0.00	0.00
		N_2	-0.04	-0.04	-0.03	-0.02	-0.02
	$Cu(COOH)_2$ monomer	CO_2	-0.02	-0.02	-0.02	-0.01	-0.01
		CO	-0.06	-0.04	-0.04	-0.04	-0.04
		H_2O	-0.09	-0.08	-0.07	-0.06	-0.06
		NH_3	-0.13	-0.11	-0.10	-0.09	-0.09
$Cu(COOH)_2$			0.49	0.57	0.69	0.87	0.86

dispersion correction leads to improved accuracy; however, missing dispersion is not the only deficiency of exchange-correlation functionals discussed herein and other effects (errors) play a role as well.

The accuracy of nonlocal functionals is somewhat disappointing; based on the RMSD values it appears to be even worse than the accuracy of some hybrid functionals without the dispersion correction (PBE0 and BHLYP in particular). A closer inspection of the vdW-DF2 results reveals that this non-local functional performs excellently for systems where covalent bonding (and charge transfer, see Table 1.2) between adsorbate and adsorbent is negligible (CH_4, H_2, N_2 and CO_2). The error of vdW-DF2 increases with increasing covalency of adsorbate-adsorbent interactions (5, 9 and 20 kJ mol^{-1} for CO, H_2O and NH_3, respectively).

The performance of dispersion-corrected functionals discussed above indicates that DFT cannot accurately described interaction of adsorbates with *cus* sites. A problematic description of the Cu^{2+} cation interactions with small ligands at the DFT level has been already reported [37,55]. An unrealistically large spin and charge delocalization, which is often connected with the incomplete cancellation of the self-interaction, was observed for GGA functionals in particular [37,55]. This artificial delocalization was found to decrease with the increasing amount of the exact exchange mixed in hybrid exchange-correlation functionals.

Similar dependence of the spin and charge delocalization on the amount of the HF exchange is reported in Table 1.2 for the adsorption complexes of small gas molecules with the $Cu(HCOO)_2$ cluster model. The description of the charge density improves from LDA to GGA and to hybrid functionals with respect to the reference high level *ab initio* averaged quadratic coupled-cluster (AQCC) densities. All the DFT functionals considered, with the exception of the BHLYP, overestimate the spin and charge delocalization which leads to a too large charge density (and incorrect electronic structure description) on Cu^{2+} that is responsible for a part of the DFT error. In order to quantify the DFT error due to an incorrect electronic density we have evaluated the density functionals on the precalculated AQCC densities for all the adsorption complexes considered. The use of the AQCC densities resulted in only minor (less than 1 kJ.mol^{-1}) changes in the interaction energies for all the adsorption complexes with the exception of the water and ammonia complexes where a larger effect in the range of 1-8 kJ.mol^{-1}

(around 5-15 % of the CCSD(T)/CBS interaction energy) was observed. Furthermore, in the case of water and ammonia the AQCC densities led to an improvement of the interaction energies with the more pronounced effect on the GGA than hybrid functionals which is in line with the fact that the densities obtained using the hybrid functional are closer to the reference AQCC density. Although the discrepancy between DFT and reference CCSD(T)/CBS interaction energies can be to some extent attributed to either a missing part of the dispersion interaction at the DFT level or unrealistic charge distribution on the $Cu(HCOO)_2$ cluster model, significant uncertainties remain which could be related to the quality of the underlying exchange-correlation functional, the transferability of the semiempirical dispersion corrections (DFT+D) and finally to the robustness of the combination of the exchange-correlation functional with the scheme accounting for the dispersion (long-range correlation).

1.3.3 *Paddlewheel model*

The assessment of various DFT methods presented in the previous section shows that none of the commonly used density functionals (local, semilocal, and non-local) provides satisfactory accuracy for the adsorbate-*cus* site interaction. Adding dispersion correction is not sufficient since the DFT deficiency stems not only from the lack of dispersion in the exchange-correlation functionals, but also from an incorrect electronic structure description of the *cus* site. The DFT/CC method described in Section X.2.2.3 represents a viable alternative to the "standard" DFT approaches. While formally very similar to well established DFT-D methods, the DFT/CC approach can be used also for the description of adsorbate-*cus* interaction since it does not assume any explicit functional form (such as r^{-6}).

The transferability of correction functions defined in Eq. (1.3) and obtained using the adsorbate-$Cu(HCOO)_2$ complexes was evaluated for the significantly more realistic paddlewheel model (see Fig. 1.1b). Full dissociation curves were considered for H_2O, CO and ethylene molecules (Fig. 1.3) while only single-point energy calculations were carried out for CO_2, H_2 and CH_4. Interaction energies calculated at the PBE-optimized geometry of PDWL complexes with CO_2, H_2 and CH_4 molecules are -

18.8, -9.0 and -13.5 kJ.mol^{-1}, respectively, at the reference CCSD(T)/CBS level and they are -19.0, -9.7 and -13.5 kJ.mol^{-1}, respectively, at the DFT/CC level.

The dissociation curves of water/PDWL model (Fig. 1.3a) calculated at the DFT/CC and reference CCSD(T)/CBS levels are in excellent agreement for a whole range of intersystem distances. Results obtained with the semi-empirical dispersion correction schemes show only partial improvement, being in an 10 kJ mol^{-1} error (Table 1.3). The dissociation curves for PDWL complexes with ethylene and carbon monoxide (Figs. 1.3b and 1.3c, respectively) also show a very good agreement between DFT/CC and CCSD(T)/CBS level (just slightly worse than in the case of water). The error of PBE-D2 for the ethylene/PDWL complex is about 4 kJ mol^{-1}; and it is even smaller for the CO/PDWL complex, however, too short equilibrium Cu-C distance (with respect to the CCSD(T)/CBS) observed for the PBE functional remains unchanged upon the augmentation with the D2 correction.

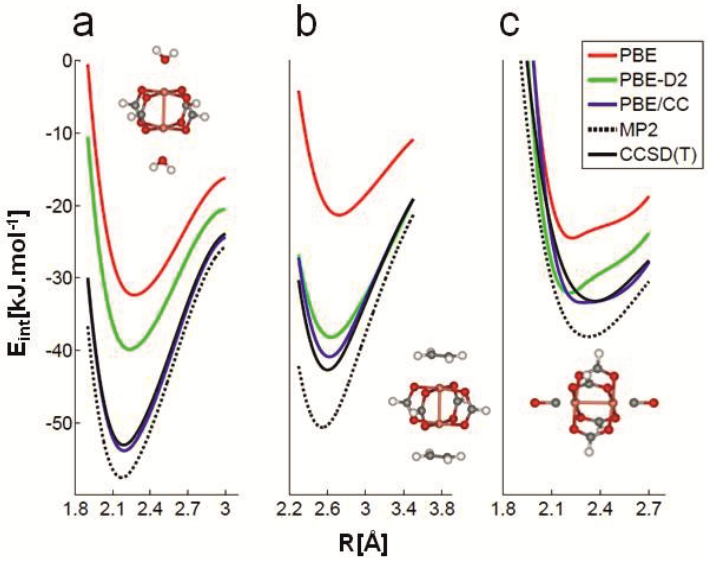

Figure 1.3. (a) PDWL/H2O, (b) CO and (c) Eth – 1-D dissociation curves at various levels of theory.

Table 1.3. Interaction energies (in kJ.mol^{-1}) of water with PDWL model evaluated for various GGA, meta-GGA and hybrid DFT functionals.[a]

Functional type	Functional name	Dispersion correction		
		None	D2	D3
GGA	PBE	-32.4	-39.5	-39.7
	RPBE	-19.2	-31	-33.1
	B-LYP	-23.7	-35	-38.1
meta-GGA	TPSS	-30.2	-39.6	-40.2
hybrid	B3LYP	-34.8	-44.7	-46.7
	BH-LYP	-47.6	-	-57.4

[a] The corresponding value obtained at the reference level of theory, CCSD(T)/CBS, is -51.2 kJ mol^{-1}.

In summary, based on PDWL results none of the exchange-correlation functionals (with or without dispersion corrections) can systematically describe the interaction between adsorbate and the *cus* site in CuBTC MOF. The dispersion correction accounted at the semi-empirical level (D2 or D3) appears to be slightly overestimated (*e.g.*, methane), however, the major source of error comes from the exchange part of the density functional. Increasing amount of the exact (Hartree-Fock) exchange mixed in the hybrid functional leads to improved accuracy. It follows that different functionals appear to be optimal for individual system; the B3LYP-D2 gives the lowest RMSD among the functionals considered herein, however, the accuracy results from partial error cancellation. It is concluded that the DFT/CC scheme outperforms other DFT methods and it can be used for the accurate description of the adsorption of application for the periodic model of CuBTC and compare its predictions with the available experimental data.

1.4 ADSORPTION IN CUBTC – ELECTROSTATIC VS. DISPERSION INTERACTIONS

1.4.1 H_2O

As synthesized CuBTC crystals contain H_2O molecules relatively firmly attached to the *cus* site [36]. The knowledge of the interaction energy of

H_2O with CuBTC is thus important, however, experimental determination of adsorption heats is complicated due to the instability of the CuBTC at high humidity [33,44]. Nevertheless, Henninger *et al.* [33] were able to obtain an adsorption enthalpy ($-\Delta H_{ads}$) of 50.7 ± 2.9 kJ.mol^{-1} at 313 K using the thermogravimetry and differential scanning calorimetry (TG/DSC). The geometry of the H_2O/CuBTC has been determined from the single-crystal X-ray diffraction [36]; water is bound just on top of the Cu^{2+} *cus* site at the distance $R_{Cu\text{-}water}$=2.17 Å. These experimental data can be used to evaluate the performance of various computational approaches. Structural characteristics of the water in CuBTC obtained at the DFT/CC level [27], $R_{Cu\text{-}water}$= 2.19 Å, are in very good agreement with experimental results. The adsorption heat of 49 kJ.mol^{-1} for the zero coverage limit has been obtained at the DFT/CC level; while this is in excellent agreement with experimental results (above) it must be noted that the TG/DSC measurements were carried out for the higher water coverage. The low coverage adsorption behavior was investigated in the grand canonical Monte Carlo simulation (GCMC) by Castillo *et al.* [10], who used interaction parameters fitted on the water adsorption isotherms in CuBTC from Wang et al. [50]; estimated adsorption enthalpy at the zero coverage limit was 48.0 ± 6.6 kJ.mol^{-1}.

The interaction energy of 52 kJ mol^{-1} was recently reported based on the cluster model DFT calculations employing the B3LYP functional [48]; that corresponds to $-\Delta H_{ads}$=46 kJ mol^{-1} (considering the zero-point vibrational energy correction, ZPVE, of -6 kJ mol^{-1}). Using the periodic model and DFT calculations employing PW91 functionals the interaction energies of 47.3 kJ.mol^{-1} was reported [66]; that corresponds to $-\Delta H_{ads}$=41 kJ mol^{-1}. These adsorption enthalpies based on DFT calculations are clearly underestimed (compared to experimental and DFT/CC values) which is understandable in the light of the results for the PDWL cluster model discussed in section X.3.2.; although the magnitude of the underestimation is smaller than expected.

1.4.2 *CO*

The active catalytic sites in microporous materials are often investigated by means of IR spectroscopy [31]. The CO molecule is especially powerful probe due to the sensitive changes of CO stretching frequency in different environments. Assignment of relatively rich spectra in the

CO stretching region in CuBTC has been discussed [2,8,12,58]; nevertheless, not all of the IR features were conclusively interpreted. There is an agreement on the interpretation of the main band located at about 2170–2178 cm^{-1} that is assigned to carbonyl complexes formed on Cu^{2+} sites in CuBTC [8,12]. The small red shift of this band with increasing CO coverage can be explained by populating both *cus* sites of each PDWL unit with CO molecules [61]. This conclusion is also supported by theoretical estimates of adsorption enthalpy ($-\Delta H_{ads}$) 30 kJ mol^{-1} and 28 kJ mol^{-1} for the first and the second CO molecule on one PDWL unit of CuBTC. Theoretical calculations further ruled out the presence of dicarbonyl species on *cus* sites of CuBTC. The quite characteristic band at 2125 cm^{-1} is usually assigned to Cu^{+}-CO species due to the confirmed presence of such defects in CuBTC and its persistence upon evacuation [58]. The origin of two characteristic bands around 2192 cm^{-1} and 2148 cm^{-1} is still unclear, but they should not arise as a result of CO interacting with regular *cus* sites of CuBTC framework.

1.4.3 CO_2

The adsorption of CO_2 in CuBTC was addressed in a number of experimental studies [4,18,28,47,50-51,69], including microcalorimetry [28] and the neutron diffraction study [69]. Thus the accuracy of computational approaches can be judged based on the comparison with experimental data. The adsorption mechanism of the CO_2 molecule in CuBTC was systematically investigated at the DFT/CC level for a wide range of coverages (from zero-coverage limit to the CO_2:Cu ratio of 21:12). Calculations show that there are three types of adsorption sites in CuBTC: *cus*, the cage center and the cage window sites (Fig. 1.4). Interaction energies calculated for the zero coverage limit (Table 1.4) show that the most stable CO_2 adsorption complex is the one formed on the *cus* site (28.2 $kJ.mol^{-1}$) whereas the adsorption complexes in the cage window and in the cage center are almost isoenergetic being about 5 $kJ.mol^{-1}$ less stable than the complex on the *cus* site (see Figure 1.4). Hence in the low-coverage regime (up to roughly one CO_2 per Cu), CO_2 molecules adsorb onto *cus* sites. Only one CO_2 molecule can interact with each *cus* site. CO_2 molecules on *cus* sites are tilted towards the adjacent

cus site, and their arrangement is such that the lateral interactions are maximized (Figure 1.5) [28].

At higher coverages, both secondary adsorption sites, the cage window and cage center sites, should be occupied but it was observed that due to a proximity of the cage window sites to the *cus* sites the CO_2 complexes in the cage window sites are stabilized by the lateral interaction with the already adsorbed CO_2 molecules on the *cus* sites to a larger extent than the ones in the cage center sites (Figure 1.5). Up to CO_2/CU=5:3 (the full occupation of *cus* and cage window sites), CO_2

Table 1.4. Adsorption heats (in kJ.mol^{-1}) for low coverage regime.

Adsorbate	Calculations/site type			Experiment
	cus	cage	window	
H_2O	49.0	-	-	50.7 ± 2.9[a]
CO	30.0	-	-	29.0[b]
CO_2	28.2	23.2	23.1	29.0[c]
CH_4	17.4	19.6	20.5	20.5[d]
C_3H_8	24.3	43.3	31.0	44.3[e]
C_3H_6	56.4	44.7	34.0	58.4[e]

[a] Ref. [33] [b] Ref. [61] [c] Ref. [28] [d] Ref. [25] [e] Ref. [62]

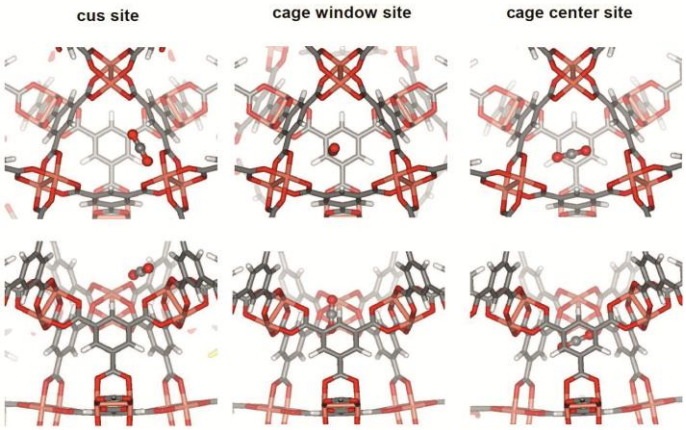

Figure 1.4. Site types in CuBTC – shown for CO_2 adsorption.

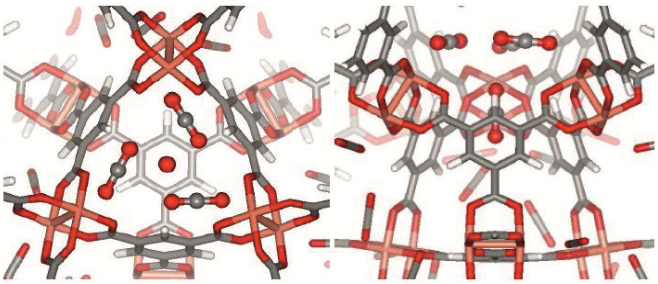

Figure 1.5. CO_2 – structure of adsorption complexes and lateral interactions.

molecules preferentially occupy sites in the cage windows of small cages. Lateral interactions between CO_2 molecules in cage window sites and those already adsorbed on *cus* sites (about 5 kJ.mol^{-1}) result in increased stability of CO_2 in cage windows sites and, as a result, the adsorption enthalpy remains unchanged compared to the low-coverage regime. At even higher coverages, CO_2 molecules adsorb in the center of small cages and in large cages. The lateral interactions between these molecules and those already adsorbed in *cus* sites and cage windows sites (amounting to almost 10 kJ.mol^{-1}) lead to a small increase (1-3 kJ.mol^{-1}) in adsorption enthalpies in the high-coverage regime.

In line with theoretical predictions the adsorption enthalpies obtained by microcalorimetry measurements [28] were found to remain almost unchanged at about 29 kJ.mol^{-1} for coverages up to almost two CO_2 molecules per *cus* site before increasing gradually by 2-3 kJ.mol^{-1} for even higher coverages.

There is a number of experimental studies reporting both adsorption isotherms and heats of adsorption for CO_2 on CuBTC at various coverages [4,18,47,50-51]; in many cases, the heats were obtained indirectly from adsorption isotherms measured at different temperatures using either the Clausius-Clapeyron equation [18,51] or a temperature-dependent isotherm equation [4]. Nevertheless, with the exception of Ref. [18], all of the values reported in the literature are close to the enthalpies obtained by microcalorimetry and calculations discussed above being in the range of 25-35 kJ.mol^{-1}. Furthermore the weak dependence of the adsorption heats on the coverage was observed in many studies, although some minor discrepancies were observed.

Further confirmation of the accuracy of the theoretical description is due to an excellent agreement with the neutron diffraction data by Yildrim *et al.* [69] who reported the occupancies of *cus*, cage window and cage center adsorption sites for two different CO_2 loadings (1.07 and 1.47 CO_2/Cu) along with the structural characteristics of the CO_2 adsorption complexes. The calculated interaction energy values of -33 and -7 kJ.mol^{-1} for the CO_2 interaction with the CuBTC at zero-coverage limit employing LDA and PBE functionals, respectively, were reported [69]. These values could be well understood in light of the results obtained for the CO_2 interaction with the $Cu(HCOO)_2$ model in the section X.3.2. Lately a study devoted to the comparison of the newly implemented non-local density functionals for CO_2 adsorption in MOFs (including CuBTC) by Siegel *et al.* [59] reported an improvement of the energetics of the CO_2 interaction upon using non-local functional (with the vdW-DF1 and optB86b performing the best). This is again in the agreement with the data for the CO_2 interaction with the $Cu(HCOO)_2$ model as shown in Fig. 1.2. But the closer inspection of this figure indicates that the improvement is not fully transferable to other molecules like water, ammonia or even methane.

In summary, a very good agreement between DFT/CC and experimental results along with the fact that the nature of the CO_2 adsorption is very different for *cus* (electrostatic) and cage window/center sites (van der Waals) implies that the DFT/CC method is able to provide a balanced description of complicated systems having various types of interactions.

1.4.4 *CH_4*

The adsorption of methane in CuBTC (besides other MOFs with the *cus* sites) has received a considerable attention due to a high methane storage capacities which were attributed, based on the data obtained from the neutron diffraction studies of Yildirim [68] and Kaskel [26], to both the presence of the *cus* sites and favorable structure of the CuBTC containing small pockets (cages) significantly enhancing the vdW interaction. It has been observed [26,68] that the grand-canonical Monte Carlo (GCMC) simulations employing standard empirical force fields fail to correctly describe the interaction of the methane with the cus site and leads thus to a prediction of an unrealistic adsorption mechanism [26,34].

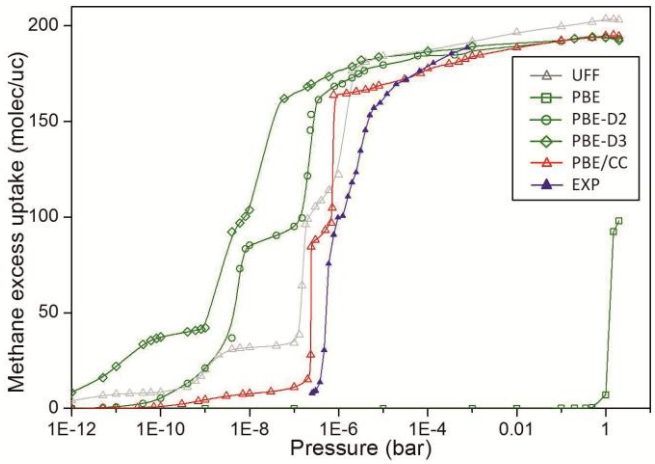

Figure 1.6. CH_4 adsorption isotherms in semi-log scale – calculated with various interaction potentials.

To address the problem of the interaction with the *cus* site and to take advantage of the detailed information about the adsorption sites available from the in situ neutron diffraction data and adsorption measurements by Kaskel [26], the potential energy surface (methane-framework interaction potential) calculated by the DFT/CC approach was directly implemented in the GCMC simulations (Figure 1.6). A very good agreement with the experimental adsorption isotherms was found. In addition, the DFT/CC-PES based simulations quantitatively capture the experimentally determined occupancies of the adsorption sites, including the open metal sites (Table 1.5) for which the simulated average methane-copper distance of 3.097 Å is well in line with the experimental value of 3.075 Å. It should be noted that neither DFT, DFT-D2, nor DFT-D3 derived PES lead to a correct prediction of the adsorption isotherm (Figure 1.6) with their under- or overestimation tendencies reflecting the trends observed for small cluster calculations (Figure 1.2). The adsorption enthalpies calculated for the zero coverage limit at the DFT/CC level (17.4, 19.6, and 20.5 kJ mol^{-1} for *cus*, cage, and window sites, respectively) are in good agreement with available experimental data (Table 1.4). Adsorption enthalpies calculated at the LDA level (25.5, 18.1 and 24.8 kJ.mol^{-1} for *cus*, cage and window sites, respectively) are clearly overestimated and they are in an incorrect order;

Table 1.5. Loading of CH4 molecules identified for each adsorption site at maximum loading.

Pore[a]	Location	176 molec/uc		
		DFT/CC	UFF	Exp.[b]
small/large	window	22.4	20.6	24.8
medium	corner	47.6	48.0	48.0
large	cus	46.3	0.0	44.6
medium/large	window	29.1	32.1	27.8
small	center	8.0	8.0	6.4
medium/large	window	4.9	19.9	4.0
small/large	window	10.1	12.2	11.8
large	center	3.5	31.3	4.0
medium	center	4.1	4.0	[c]

[a] For some sites the same characterization is used as those sites are close to each other. [b] Experimental results at 176 molecules/uc from Ref. [26] where a total of 171.21 molecules/uc were resolved. [c] Not reported in Ref.[26].

overestimated interaction with the *cus* site is in line with the results reported for cluster models (Fig. 1.2).

1.4.5 C_3H_8 and C_3H_6

The separation of propane/propylene mixture in CuBTC has been extensively studied experimentally and theoretically [21-22,38,45,71]. Most of the theoretical studies used GCMC simulations to predict adsorption isotherms. However, the commonly used empirical potentials fail to describe the interaction with *cus* sites. The theoretical attempts to improve "standard" empirical force-fields have been made. The main focus has been to improve description of the partially dative bond between Cu^{2+} and π-electron density on propylene. However, simple rescaling of Lennard-Jones parameters for Cu^{2+}-C(sp^2) interaction or parameterizations based on the GGA functionals do not yield a desired accuracy (Figure 1.3b). The interaction energy between ethylene and the *cus* site (represented by a PDWL cluster) calculated at the PBE level is

only about half of the reference CCSD(T)/CBS level value of -41.3 kJ mol^{-1}.

Adsorption enthalpies ($-\Delta H_{ads}$) of propane and propylene calculated for the zero-coverage limit are summarized in Table 1.4. The agreement between DFT/CC predictions and experimentally measured adsorption enthalpy is excellent. A small underestimation of the DFT/CC adsorption enthalpy on the *cus* sites is consistent with the cluster model results discussed above. Propylene preferably adsorbs on the *cus* sites ($-\Delta H_{ads} \approx$ 58 kJ.mol^{-1}) due to the formation of partial dative bond (Figure 1.7b). Calculations also indicated that upon adsorption of second propylene molecule on the same PDWL unit the adsorption enthalpy decreases by 9 kJ.mol^{-1}. This indicates that with increasing propylene loading the *cus* sites are not longer equivalent. For cage center and cage widow sites the propane and propylene adsorption enthalpies do not differ significantly. The adsorption of propane is driven by van der Waals interactions, thus, the topology of CuBTC framework determines the stability of each adsorption site. The most stable propane adsorption complex is formed in the cage center site ($-\Delta H_{ads} \approx$ 44 kJ.mol^{-1}) due to the favorable dimension (maximal dispersion interactions) of small CuBTC octahedral cage (Figure 1.7a). Once the cages in CuBTC are occupied by propane molecules the adsorption enthalpy decreases due to a smaller stability of adsorption complexes formed on other adsorption sites. However, the importance of lateral interactions increases at large propane loadings.

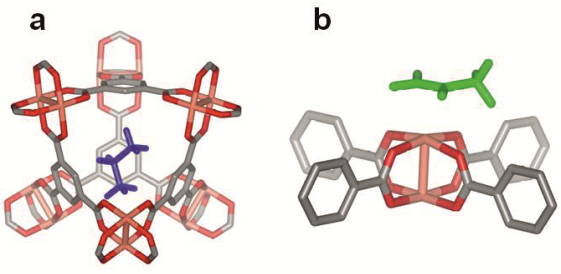

Figure 1.7. (a) Propan in the cage and (b) propylene on the cus site.

1.5 SUMMARY

The application of accurate post Hartree-Fock and DFT-based methods has been reviewed above for the particular case of CuBTC MOF. It is obvious that accurate description of MOFs having *cus* sites with partially filled d orbitals is rather involved. Accurate post Hartree-Fock methods are computationally too demanding to be routinely used for MOFs and computationally tractable DFT-based methods do not have sufficient accuracy. The dispersion interactions between adsorbate and MOF are no longer a problem; they can be relatively well described either by non-local exchange-correlation functionals or by one of the correction scheme (DFT-D or DFT/CC). The problematic part is the description of the transition metals with open-shell electronic structure. It is therefore always very important to verify the accuracy of the particular DFT method and it is clear that the accuracy decreases with the increasing complexity of the electronic structure of particular transition metal. All these conclusions are based on our systematic investigation of CuBTC MOF interaction with various adsorbates. They are in line with other calculations reported for CuBTC (*e.g.,* Refs. [59,66,69-70]) and for other MOFs (*e.g.*, Refs. [5,16,35,52,56,64-65,67]).

Acknowledgments

The research leading to these results has received funding from the Grant Agency of the Czech Republic (Center of Excellence – P106/12/G015) and from the European Community's Seventh Framework Programme (FP7/2007-2013) under grant agreement n° 228862. MACADEMIA is a Large-scale Integrating Project under the Nanosciences, Nanotechnologies, Materials and New Production Technologies Theme (www.macademia-project.eu).

1.6 REFERENCES AND CITATIONS

1. Adler, T. B. and Werner, H. J. (2009). Local explicitly correlated coupled-cluster methods: Efficient removal of the basis set incompleteness and domain errors, *J. Chem. Phys.*, **130**, pp. 241101.
2. Alaerts, L., Seguin, E., Poelman, H., Thibault-Starzyk, F., Jacobs, P. and De Vos, D. (2006). Probing the Lewis acidity and catalytic activity of the metal-organic framework $[Cu_3(btc)_2]$ (BTC=benzene-1,3,5-tricarboxylate), *Chem. Eur. J.*, **12**, pp. 7353-7363.
3. Antony, J. and Grimme, S. (2006). Density functional theory including dispersion corrections for intermolecular interactions in a large benchmark set of biologically relevant molecules, *Phys. Chem. Chem. Phys.*, **8**, pp. 5287-5293.
4. Aprea, P., Caputo, D., Gargiulo, N., Iucolano, F. and Pepe, F. (2010). Modeling carbon dioxide adsorption on microporous substrates: Comparison between Cu-BTC metal−organic framework and 13X zeolitic molecular sieve, *J. Chem. Eng. Data*, **55**, pp. 3655-3661.
5. Bae, Y. S., Lee, C. Y., Kim, K. C., Farha, O. K., Nickias, P., Hupp, J. T., Nguyen, S. T. and Snurr, R. Q. (2012). High propene/propane selectivity in isostructural metal-organic frameworks with high densities of open metal sites, *Angew. Chem. Int. Ed.*, **51**, pp. 1857-1860.
6. Blochl, P. E. (1994). Projector augmented-wave method, *Phys. Rev. B*, **50**, pp. 17953-17979.
7. Bludsky, O., Rubes, M., Soldan, P. and Nachtigall, P. (2008). Investigation of the benzene-dimer potential energy surface: DFT/CCSD(T) correction scheme, *J. Chem. Phys.*, **128**, pp. 114102.
8. Bordiga, S., Regli, L., Bonino, F., Groppo, E., Lamberti, C., Xiao, B., Wheatley, P., Morris, R. and Zecchina, A. (2007). Adsorption properties of HKUST-1 toward hydrogen and other small molecules monitored by IR, *Phys. Chem. Chem. Phys.*, **9**, pp. 2676-2685.
9. Boys, S. F. and Bernardi, F. (1970). Calculation of small molecular of small molecular interactions by differences of separate total energies - some procedures with reduced errors, *Mol. Phys.*, **19**, pp. 553-566.
10. Castillo, J. M., Vlugt, T. J. H. and Calero, S. a. (2008). Understanding water adsorption in Cu−BTC metal−organic frameworks, *J. Phys. Chem. C*, **112**, pp. 15934-15939.
11. Čížek, J. (1969) *On the Use of the Cluster Expansion and the Technique of Diagrams in Calculations of Correlation Effects in Atoms and Molecules*, Vol. 14., (John Wiley & Sons, Inc.).
12. Drenchev, N., Ivanova, E. and Mihaylov, M. (2010). CO as an IR probe molecule for characterization of copper ions in a basolite C300 MOF sample, *Phys. Chem. Chem. Phys.*, **12**, pp. 6423-6427.

13. Ducéré, J.-M., Goursot, A. and Berthomieu, D. (2005). Comparative density functional theory study of the binding of ligands to Cu^{+} and Cu^{2+}: Influence of the coordination and oxidation state, *J. Phys. Chem. A*, **109**, pp. 400-408.
14. Dunning, T. H. (1989). Gaussian-basis sets for use in correlated molecular calculations 1. The atoms boron through neon and hydrogen, *J. Chem. Phys.*, **90**, pp. 1007-1023.
15. Duren, T., Bae, Y.-S. and Snurr, R. Q. (2009). Using molecular simulation to characterise metal-organic frameworks for adsorption applications, *Chem. Soc. Rev.*, **38**, pp. 1237-1247.
16. Dzubak, A. L., Lin, L. C., Kim, J., Swisher, J. A., Poloni, R., Maximoff, S. N., Smit, B. and Gagliardi, L. (2012). Ab initio carbon capture in open-site metal-organic frameworks, *Nature Chemistry*, **4**, pp. 810-816.
17. El-Nahas, A. A. M., Tajima, N. and Hirao, K. (2000). Do $Cu^{2+}NH_3$ and $Cu^{2+}OH_2$ exist?: theory confirms `yes!', *Chem. Phys. Lett.*, **318**, pp. 333-339.
18. Farrusseng, D., Daniel, C., Gaudillère, C., Ravon, U., Schuurman, Y., Mirodatos, C., Dubbeldam, D., Frost, H. and Snurr, R. Q. (2009). Heats of adsorption for seven gases in three metal-organic frameworks: systematic comparison of experiment and simulation, *Langmuir*, **25**, pp. 7383-7388.
19. Férey, G., Serre, C., Mellot-Draznieks, C., Millange, F., Surblé, S., Dutour, J. and Margiolaki, I. (2004). A hybrid solid with giant pores prepared by a combination of targeted chemistry, simulation, and powder diffraction, *Angew. Chem. Int. Ed.*, **43**, pp. 6296-6301.
20. Férey, G., Mellot-Draznieks, C., Serre, C., Millange, F., Dutour, J., Surblé, S. and Margiolaki, I. (2005). A chromium terephthalate-based solid with unusually large pore volumes and surface area., *Science*, **309**, pp. 2040-2042.
21. Ferreira, A., Santos, J., Plaza, M., Lamia, N., Loureiro, J. and Rodrigues, A. (2011). Suitability of Cu-BTC extrudates for propane–propylene separation by adsorption processes, *Chem. Eng. J.*, **167**, pp. 1-12.
22. Fischer, M., Gomes, J. R. B., Froba, M. and Jorge, M. (2012). Modeling Adsorption in metal-organic frameworks with open metal sites: propane/propylene separations, *Langmuir*, **28**, pp. 8537-8549.
23. Garcia-Perez, E., Gascon, J., Morales-Florez, V., Castillo, J. M., Kapteijn, F. and Calero, S. (2009). Identification of adsorption sites in Cu-BTC by experimentation and molecular simulation, *Langmuir*, **25**, pp. 1725-1731.
24. Getman, R. B., Bae, Y. S., Wilmer, C. E. and Snurr, R. Q. (2012). Review and analysis of molecular simulations of methane, hydrogen, and acetylene storage in metal-organic frameworks, *Chem. Rev.*, **112**, pp. 703-723.
25. Getzschmann, J., Senkovska, I., Fairen-Jimenez, D., Düren, T. and Kaskel, S. unpublished results.
26. Getzschmann, J., Senkovska, I., Wallacher, D., Tovar, M., Fairen-Jimenez, D., Düren, T., van Baten, J. M., Krishna, R. and Kaskel, S. (2010). Methane

storage mechanism in the metal-organic framework $Cu_3(btc)_2$: An in situ neutron diffraction study, *Microporous Mesoporous Mater.*, **136**, pp. 50-58.

27. Grajciar, L., Bludsky, O. and Nachtigall, P. (2010). Water adsorption on coordinatively unsaturated sites in CuBTC MOF, *J. Phys. Chem. Lett.*, **1**, pp. 3354-3359.
28. Grajciar, L., Wiersum, A. D., Llewellyn, P. L., Chang, J.-S. and Nachtigall, P. (2011). Understanding CO_2 adsorption in CuBTC MOF: Comparing combined DFT–ab initio calculations with microcalorimetry experiments, *J. Phys. Chem. C*, **115**, pp. 17925-17933.
29. Grimme, S. (2006). Semiempirical GGA-type density functional constructed with a long-range dispersion correction, *J. Comput. Chem.*, **27**, pp. 1787-1799.
30. Grimme, S., Antony, J., Ehrlich, S. and Krieg, H. (2010). A consistent and accurate ab initio parametrization of density functional dispersion correction (DFT-D) for the 94 elements H-Pu, *J. Chem. Phys.*, **132**, pp. 154104.
31. Hadjiivanov, K. I. and Vayssilov, G. N. (2002). Characterization of oxide surfaces and zeolites by carbon monoxide as an IR probe molecule, *Adv. Catal.*, **47**, pp. 307-511.
32. Halkier, A., Helgaker, T., Jorgensen, P., Klopper, W. and Olsen, J. (1999). Basis-set convergence of the energy in molecular Hartree-Fock calculations, *Chem. Phys. Lett.*, **302**, pp. 437-446.
33. Henninger, S. K., Schmidt, F. P. and Henning, H.-M. (2010). Water adsorption characteristics of novel materials for heat transformation applications, *Appl. Therm. Eng.*, **30**, pp. 1692-1702.
34. Chen, L., Grajciar, L., Nachtigall, P. and Düren, T. (2011). Accurate prediction of methane adsorption in a metal–organic framework with unsaturated metal sites by direct implementation of an ab initio derived potential energy surface in GCMC simulation, *J. Phys. Chem. C*, **115**, pp. 23074-23080.
35. Chen, L., Morrison, C. A. and Düren, T. (2012). Improving Predictions of Gas Adsorption in Metal–Organic Frameworks with Coordinatively Unsaturated Metal Sites: Model Potentials, ab initio Parameterization, and GCMC Simulations, *J. Phys. Chem. C*, **116**, pp. 18899-18909.
36. Chui, S. S. Y., Lo, S. M. F., Charmant, J. P. H., Orpen, A. G. and Williams, I. D. (1999). A chemically functionalizable nanoporous material Cu-3(TMA)(2)(H_2O)(3) (n), *Science*, **283**, pp. 1148-1150.
37. Jeanvoine, Y. and Spezia, R. (2010). Cu^{2+} binding chalcogen–chalcogen bridges: A problematic case for DFT, *THEOCHEM*, **954**, pp. 7-15.
38. Jorge, M., Lamia, N. and Rodrigues, A. (2010). Molecular simulation of propane/propylene separation on the metal–organic framework CuBTC, *Colloids Surf., A*, **357**, pp. 27-34.

39. Jotham, R., Kettle, S. and Marks, J. (1972). Antiferromagnetism in transition-metal complexes. Part IV. Lowlying excited states of binuclear copper (II) carboxylate complexes, *J. Chem. Soc., Dalton Trans.*, pp. 428.
40. Kahn, O. (1993) *Molecular Magnetism*, (John Wiley & Sons, Inc.).
41. Klimes, J., Bowler, D. and Michaelides, A. (2010). Chemical accuracy for the van der Waals density functional., *J. Phys.: Condens. Matter*, **22**, pp. 022201.
42. Klimes, J., Bowler, D. and Michaelides, A. (2011). Van der Waals density functionals applied to solids, *Phys. Rev. B*, **83**, pp. 1-13.
43. Krishna, R. and van Baten, J. M. (2011). In silico screening of metal-organic frameworks in separation applications, *Phys. Chem. Chem. Phys.*, **13**, pp. 10593-10616.
44. Küsgens, P., Rose, M., Senkovska, I., Fröde, H., Henschel, A., Siegle, S. and Kaskel, S. (2009). Characterization of metal-organic frameworks by water adsorption, *Microporous Mesoporous Mater.*, **120**, pp. 325-330.
45. Lamia, N., Jorge, M., Granato, M., Almeida Paz, F., Chevreau, H. and Rodrigues, A. (2009). Adsorption of propane, propylene and isobutane on a metal–organic framework: Molecular simulation and experiment, *Chem. Eng. J.*, **64**, pp. 3246-3259.
46. Lee, K., Murray, E., Kong, L., Lundqvist, B. and Langreth, D. (2010). Higher-accuracy van der Waals density functional, *Phys. Rev. B*, **82**, pp. 081101.
47. Liang, Z., Marshall, M. and Chaffee, A. L. (2009). CO_2 adsorption-based separation by metal organic framework (Cu-BTC) versus zeolite (13X), *Energy & Fuels*, **23**, pp. 2785-2789.
48. Lukose, B., Supronowicz, B., St. Petkov, P., Frenzel, J., Kuc, A. B., Seifert, G., Vayssilov, G. N. and Heine, T. (2012). Structural properties of metal-organic frameworks within the density-functional based tight-binding method, P*hys. status solidi B*, **249**, pp. 335-342.
49. Melník, M. (1982). Structural isomerism of copper (II) compounds, *Coord. Chem. Rev.*, **47**, pp. 239-261.
50. Min Wang, Q., Shen, D., Bülow, M., Ling Lau, M., Deng, S., Fitch, F. R., Lemcoff, N. O. and Semanscin, J. (2002). Metallo-organic molecular sieve for gas separation and purification, *Microporous Mesoporous Mater.*, **55**, pp. 217-230.
51. Moellmer, J., Moeller, a., Dreisbach, F., Glaeser, R. and Staudt, R. (2011). High pressure adsorption of hydrogen, nitrogen, carbon dioxide and methane on the metal–organic framework HKUST-1, *Microporous Mesoporous Mater.*, **138**, pp. 140-148.
52. Peralta, D., Chaplais, G., Simon-Masseron, A., Barthelet, K., Chizallet, C., Quoineaud, A.-A. and Pirngruber, G. D. (2012). Comparison of the behavior of metal-organic frameworks and zeolites for hydrocarbon separations, *J. Am. Chem. Soc.*, **134**, pp. 8115-8126.

53. Perdew, J. P., Burke, K. and Ernzerhof, M. (1996). Generalized gradient approximation made simple, *Phys. Rev. Lett.*, **77**, pp. 3865-3868.
54. Peterson, K. A. and Puzzarini, C. (2005). Systematically convergent basis sets for transition metals. II. Pseudopotential-based correlation consistent basis sets for the group 11 (Cu, Ag, Au) and 12 (Zn, Cd, Hg) elements, *Theor. Chem. Acc.*, **114**, pp. 283-296.
55. Poater, J., Solà, M., Rimola, A., Rodríguez-Santiago, L. and Sodupe, M. (2004). Ground and low-lying states of Cu^{2+} $-H_2O$. A difficult case for density functional methods, *J. Phys. Chem. A*, **108**, pp. 6072-6078.
56. Poloni, R., Smit, B. and Neaton, J. B. (2012). CO2 capture by metal-organic frameworks with van der Waals density functionals, *J. Phys. Chem. A*, **116**, pp. 4957-4964.
57. Poppl, A., Kunz, S., Himsl, D. and Hartmann, M. (2008). CW and pulsed ESR spectroscopy of cupric ions in the metal-organic framework compound Cu3(BTC)2, *J. Phys. Chem. C*, **112**, pp. 2678-2684.
58. Prestipino, C., Regli, L., Vitillo, J., Bonino, F., Damin, A., Lamberti, C., Zecchina, A., Solari, P., Kongshaug, K. and Bordiga, S. (2006). Local structure of framework Cu(II) in HKUST-1 metallorganic framework: spectroscopic characterization upon activation and interaction with adsorbates, *Chem. Mat.*, **18**, pp. 1337-1346.
59. Rana, M. K., Koh, H. S., Hwang, J. and Siegel, D. J. (2012). Comparing van der Waals density functionals for CO2 adsorption in metal organic frameworks, *J. Phys. Chem. C*, **116**, pp. 16957-16968.
60. Rosi, N. L., Kim, J., Eddaoudi, M., Chen, B., O'Keeffe, M. and Yaghi, O. M. (2005). Rod packings and metal-organic frameworks constructed from rod-shaped secondary building units., *J. Am. Chem. Soc.*, **127**, pp. 1504-1518.
61. Rubeš, M., Grajciar, L., Bludský, O., Wiersum, A. D., Llewellyn, P. L. and Nachtigall, P. (2012). Combined theoretical and experimental investigation of CO adsorption on coordinatively unsaturated sites in CuBTC MOF, *Chemphyschem*, **13**, pp. 488-495.
62. Rubeš, M., Wiersum, A. D., Llewellyn, P. L., Grajciar, L. s., Bludský, O. and Nachtigall, P. (2013). Adsorption of Propane and Propylene on CuBTC MOF: Combined theoretical and experimental investigation, *J. Phys. Chem. C*, submitted.
63. Soldan, P. and Hutson, J. M. (2000). On the long-range and short-range behavior of potentials from reproducing kernel Hilbert space interpolation, *J. Chem. Phys.*, **112**, pp. 4415-4416.
64. Valenzano, L., Civalleri, B., Sillar, K. and Sauer, J. (2011). Heats of Adsorption of CO and CO2 in metal–organic frameworks: quantum

mechanical study of CPO-27-M (M = Mg, Ni, Zn), *J. Phys. Chem. C*, **115**, pp. 21777-21784.

65. Valenzano, L., Vitillo, J. G., Chavan, S., Civalleri, B., Bonino, F., Bordiga, S. and Lamberti, C. (2012). Structure–activity relationships of simple molecules adsorbed on CPO-27-Ni metal–organic framework: In situ experiments vs. theory, *Catal. Today*, **182**, pp. 67-79.
66. Watanabe, T. and Sholl, D. S. (2010). Molecular chemisorption on open metal sites in Cu(3)(benzenetricarboxylate)(2): A spatially periodic density functional theory study, *J. Chem. Phys.*, **133**, pp. 094509.
67. Watanabe, T. and Sholl, D. S. (2012). Accelerating applications of metal-organic frameworks for gas adsorption and separation by computational screening of materials., *Langmuir*, **28**, pp. 14114-14128.
68. Wu, H., Simmons, J. M., Liu, Y., Brown, C. M., Wang, X.-S., Ma, S., Peterson, V. K., Southon, P. D., Kepert, C. J., Zhou, H.-C., Yildirim, T. and Zhou, W. (2010). Metal-organic frameworks with exceptionally high methane uptake: where and how is methane stored?, *Chem. Eur. J.*, **16**, pp. 5205-5214.
69. Wu, H., Simmons, J. M., Srinivas, G., Zhou, W. and Yildirim, T. (2010). Adsorption sites and binding nature of CO_2 in prototypical metal−organic frameworks: A combined neutron diffraction and first-principles study, *J. Phys. Chem. Lett.*, **1**, pp. 1946-1951.
70. Xiang, S., Zhou, W., Gallegos, J. M., Liu, Y. and Chen, B. (2009). Exceptionally high acetylene uptake in a microporous metal-organic framework with open metal sites, *J. Am. Chem. Soc.*, **131**, pp. 12415-12419.
71. Yoon, J., Jang, I., Lee, K., Hwang, Y. and Chang, J. (2010). Adsorptive separation of propylene and propane on a porous metal-organic framework, copper trimesate, *Bull. Korean Chem. Soc.*, **31**, pp. 220-223.
72. Zhang, X. X., Chui, S. S.-Y. and Williams, I. D. (2000). Cooperative magnetic behavior in the coordination polymers [Cu3(TMA)2L3] (L=H2O, pyridine), *J. Appl. Phys.*, **87**, pp. 6007-6009.

Attachment B

THE JOURNAL OF PHYSICAL CHEMISTRY Letters

pubs.acs.org/JPCL

Water Adsorption on Coordinatively Unsaturated Sites in CuBTC MOF

Lukáš Grajciar,[†] Ota Bludský,[‡] and Petr Nachtigall*,[†]

[†]Department of Physical and Macromolecular Chemistry, Faculty of Science, Charles University in Prague, Hlavova 2030, CZ-128 40 Prague 2, Czech Republic, and [‡]Institute of Organic Chemistry and Biochemistry, AS CR, v.v.i., Flemingovo nám. 2, 16610 Prague 6, Czech Republic

ABSTRACT We report a theoretical study of water adsorption on coordinatively unsaturated sites (cus's) in a metal−organic framework (MOF) compound CuBTC. The reliability of the density functional theory (DFT)-based methods and dispersion-corrected DFT-D schemes for the description of cus sites was investigated with respect to the accurate reference CCSD(T)/CBS data. The accuracy of both DFT and DFT-D methods was found to be insufficient. The proposed DFT/CC correction scheme gave the results in excellent agreement with the reference CCSD(T)/CBS data. DFT/CC calculations performed for the periodic CuBTC model gave R_{Cu-OH_2} = 2.19 Å and $-\Delta H_{ads}$ = 49 kJ mol^{-1}, both in very good agreement with available experimental data. The interaction of the first water molecule with the paddle-wheel unit is about 5 kJ mol^{-1} stronger than the interaction of the second water molecule with the same paddle-wheel unit. The DFT/CC scheme provides an accurate description of the extended MOF systems, and the results obtained with periodic DFT/CC model can be used for the testing and improvement of the force fields for classical simulations.

SECTION Surfaces, Interfaces, Catalysis

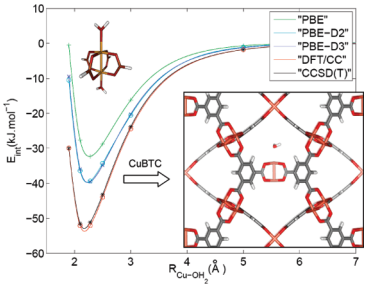

HKUST-1, Cu_3(1,3,5-benzenetricarboxylate)$_2$,[1] often denoted as CuBTC, is one of the most studied MOFs for adsorption and separation of gases[2−7] and even for catalytic[8−10] applications. Adsorption isotherms for various gases in CuBTC were successfully modeled;[11−15] nevertheless, the details of the adsorbate−adsorbent interactions at the low coverage limit and the role of coordinatively unsaturated sites (cus's) are not fully understood.[4] Calculations on CuBTC were typically performed at the molecular mechanics level[3,4,7] or at the density functional theory (DFT) level.[15−17] However, the reliability of these calculations for characterization of adsorption complexes on cus's in CuBTC has not been established. For example, the interaction energy of CO_2 with CuBTC (at the zero-coverage limit) depends on the level of theory used. The local density approximation (LDA) and a generalized gradient approximation (GGA) give −33 and −7 kJ/mol, respectively,[17] while the *NVT* simulation employing a combination of DREIDING and TraPPE force fields gives −17 kJ/mol for molecules in a large pore.[3] The reported experimental heats of adsorption for CO_2 in CuBTC at low coverage are also somewhat ambiguous; the gravimetric and pulse response experiments in the temporal analysis of products (TAP) reactor gave −12.1 ± 0.3 and −14.6 ± 0.5 kJ mol^{-1}, respectively,[3] while the differential thermal analysis (DTA) and the sorption−isosteric method arrived at values of −30 and −35 kJ mol^{-1}, respectively.[18,19] It is therefore important to investigate the reliability of computational methods and models for the description of adsorbates' interaction with cus's in MOFs.

An accurate theoretical description of adsorption properties of CuBTC is complicated by the large size of the unit cell (UC) and by the presence of pairs of coordinatively unsaturated Cu^{II} ions with open-shell electronic structure.[20] The water adsorption on Cu^{II} cus's in CuBTC has been chosen as the case study for the following reasons: (i) Crystallographic data on H_2O/CuBTC are available; (ii) water is usually present in the CuBTC samples, and it must be removed during the sample activation; (iii) the interaction of water with cus's in CuBTC is relatively strong; (iv) CuBTC is often used as a reference MOF, and a large amount of experimental and computational data are available in the literature; and (v) a pair of Cu^{II} cations in close proximity (about 2.5 Å) represents a particularly challenging problem due to the presence of two unpaired electrons, one on each Cu cation. The accuracy of methods for the description of water interaction with the Cu^{II} cus in CuBTC is first discussed based on the calculations performed for the copper formate ($Cu_2(HCOO)_4 + 2H_2O$) cluster model, and a selected method is then used in calculations employing a periodic model of CuBTC. The copper formate model has a paddle-wheel structure (inset

Received Date: October 6, 2010
Accepted Date: November 9, 2010
Published on Web Date: November 12, 2010

DOI: 10.1021/jz101378z | *J. Phys. Chem. Lett.* **2010**, *1*, 3354–3359

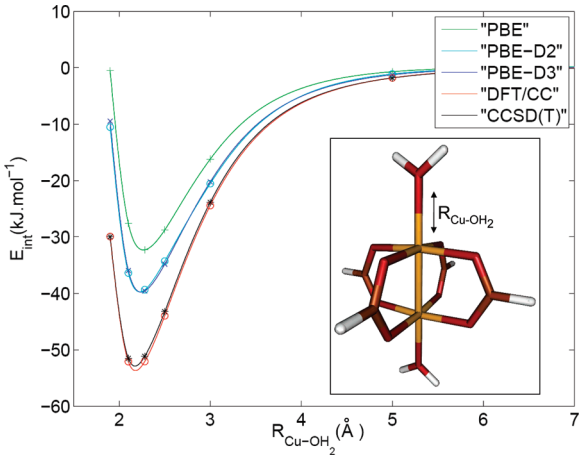

Figure 1. The interaction energy of H_2O with the $Cu_2(HCOO)_4$ cluster model (depicted in the inset) calculated at different levels of theory as a function of the R_{Cu-OH_2} distance. DFT calculations without (PBE) and with empirical dispersion corrections (PBE-D2 and PBE-D3), the DFT/CC correction scheme, and the coupled cluster CCSD(T), method were used. Cu, O, C, and H atoms are depicted in yellow, red, orange, and white colors, respectively.

of Figure 1) that closely resembles the local environment of the cus in CuBTC.

The coupling of unpaired electrons on two Cu^{II} cations in one paddle-wheel can be either ferromagnetic or antiferromagnetic. The stability of $Cu_2(HCOO)_4$ in the singlet (S) and triplet (T) electronic states was calculated at the multireference level (CASPT2/ANO-VQZP); the singlet state was found to be about 200 cm^{-1} below the triplet state. Similarly, for the $Cu_2(HCOO)_4(H_2O)_2$ model, where one molecule is coordinated to each Cu^{II} cation, the singlet state is 176 cm^{-1} below the triplet state. Thus, the S/T gap remains relatively unchanged when water molecules interact with Cu^{II} cations. It follows that the electronic interaction energy between H_2O and $Cu_2(HCOO)_4$ does not depend on the spin state of copper formate; the interaction energy, defined as

$$\frac{1}{2}Cu_2(HCOO)_4 + H_2O \leftrightarrow \frac{1}{2}Cu_2(HCOO)_4(H_2O)_2 \qquad (1)$$

is −52.6 and −52.7 kJ mol^{-1} for the S and T states, respectively (at the CASPT2/ANO-VQZP level). It is therefore possible to investigate the reliability of the method with respect to the single-reference coupled cluster method (explicitly considering single and double excitations and treating the effect of triple excitations at the perturbation theory level, CCSD(T) method) in a triplet electronic state. All of the calculations on $Cu_2(HCOO)_4(H_2O)_n$ clusters reported below were performed for the triplet state only.

The interaction energy of H_2O with the $Cu_2(HCOO)_4$ cluster model (defined by eq 1) as a function of R_{Cu-OH_2} distance is shown in Figure 1. Calculations performed with a highly accurate coupled cluster method at the complete basis set limit (CCSD(T)/CBS) serve as benchmark calculations that can be used to evaluate the accuracy of other methods. The interaction energy is strongly (over 20 kJ/mol) underestimated at the DFT/AVQZ level (employing GGA type Perdew−Burke−Ernzernhof, PBE,[21,22] exchange−correlation functional).

Table 1. Interaction Energies (in kJ mol^{-1}) of Water with the Paddle-Wheel Cluster Model (inset of Figure *1*) Evaluated with Various GGA, meta-GGA, and Hybrid DFT Functionals[a]

		dispersion correction		
functional type	functional name	none	D2	D3
GGA	PBE	−32.4	−39.5	−39.7
	RPBE	−19.2	−31.0	−33.1
	BLYP	−23.7	−35.0	−38.1
meta-GGA	TPSS	−30.2	−39.6	−40.2
hybrid	B3LYP	−34.8	−44.7	−46.7
	BHLYP	−47.6		−57.4

[a] The corresponding value obtained at the reference level of theory, CCSD(T)/CBS, is −51.2 kJ mol^{-1}.

It is well-known that GGA-type functionals do not account for dispersion interactions and that they need to be modified or augmented for the description of dispersion-stabilized complexes. Results obtained with the empirical dispersion correction schemes of Grimme (denoted as D2[23] and D3[24]) are also shown in Figure 1. Clearly, the dispersion component accounts only for a fraction of the discrepancy between the PBE and CCSD(T) results. Besides the inability of DFT functionals to describe dispersion interactions, a problematic description of the Cu^{2+} cation with small ligands at the DFT level has been also reported.[25−28] An unrealistically large spin and charge delocalization, which is often connected with the incomplete cancellation of the self-interaction included in the Coulomb energy by the exchange−correlation functional, was observed for GGA functionals in particular.[26,28] This artificial delocalization decreases with the increasing amount of the exact exchange mixed in hybrid exchange−correlation functionals.[26,28] Similar dependence of the spin and charge delocalization on the amount of the HF exchange is reported in Table S1 in the Supporting Information for $Cu(HCOO)_2$ and $H_2O\cdots Cu(HCOO)_2$ cluster models. This overestimated spin and charge delocalization leads to a too large charge density (and incorrect electronic structure description) on Cu^{2+} that is responsible for part of the DFT error in the description of the water adsorption on Cu^{2+} sites in CuBTC.

Interaction energy, defined by eq 1, was evaluated for several commonly used GGA, meta-GGA, and hybrid functionals at the PBE/AVTZ equilibrium geometry (Table 1). Interaction energy is underestimated (compared to the reference level CCSD(T)/CBS value of −51.2 kJ mol^{-1}) with all exchange−correlation functionals tested, except LDA, which gives a too large value of −57.5 kJ mol^{-1}. The interaction energy increases with increasing amount of HF exchange in the functionals ($-E_{int}$(BLYP) < $-E_{int}$(B3LYP) < $-E_{int}$(BHLYP)). Dispersion interactions evaluated as described in refs 23 and 24 for individual functionals are in the range from −10 to −14 kJ mol^{-1}, except for PBE, where it is only about −7 kJ mol^{-1}. The interaction energies calculated at the DFT-D level for GGA and meta-GGA type functionals are at least 10 kJ mol^{-1} underestimated. Calculations based on hybrid functionals corrected for the dispersion interaction give results in better agreement with the reference CCSD(T)/CBS result. The interaction energies calculated at the B3LYP-D3 and BHLYP-D3 levels are 5 kJ mol^{-1}

DOI: 10.1021/jz101378z | J. Phys. Chem. Lett. 2010, 1, 3354–3359

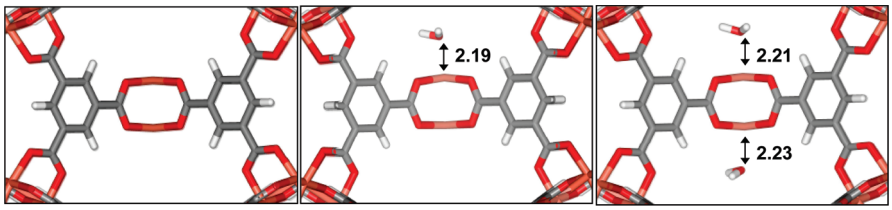

Figure 2. The structures of CuBTC without any water (a), with one water molecule adsorbed on the paddle-wheel unit (b), and with two adsorbed water molecules on the single copper paddle-wheel unit (c) of CuBTC (distances between the framework and adsorbed water molecules, in Å, are also shown). Cu, O, C, and H atoms are depicted in orange, red, gray, and white colors, respectively.

underestimated and 6 kJ mol^{-1} overestimated, respectively. Apparently, the discrepancy between the DFT and CCSD(T) interaction energies is to a large extent due to two effects, the missing part of the dispersion interaction at the DFT level and artificial spin and charge delocalization on the paddle-wheel cluster model.

Reliable CCSD(T) calculations cannot be performed on larger cluster models nor on a periodic model of MOF; thus, there is a need either for an accurate force field or for a computationally tractable (DFT-type) yet reliable method for the description of MOFs with transition-metal cus's. Empirically corrected DFT-D methods account for the dispersion contribution in a parametric way, adding an r^{-6} (and r^{-8} in some cases) dispersion term. However, the problem of DFT for the description of the H_2O interaction with $Cu_2(HCOO)_4$ is not just a lack of dispersion (see above); therefore, it is beneficial to use a more general correction scheme that does not assume any functional form for the DFT error rather than to use a standard DFT-D correction that assumes a particular functional form suitable for adding a missing dispersion contribution. A recently proposed DFT/CC method[29−31] is based on the pairwise representability of DFT error, ΔE, defined as

$$\Delta E = E_{CCSD(T)} - E_{DFT} \quad (2)$$

where $E_{CCSD(T)}$ and E_{DFT} are the interaction energies calculated at the CCSD(T)/CBS and DFT/AVQZ levels of theory, respectively. Therefore, the DFT/CC method can be applied also for systems where the DFT error is more general than just a lack of dispersion interaction. An extension of the DFT/CC method for the H_2O/CuBTC system is described below, and the results are compared with available experimental data.

Within the DFT/CC method, the DFT error ΔE is expressed as a sum of atom−atom correction functions $\varepsilon_{ij}(R_{ij})$

$$\Delta E = \sum_{ij} \varepsilon_{ij}(R_{ij}) \quad (3)$$

where R_{ij} is the distance between atoms i and j. No explicit functional form for ε_{ij} correction functions is assumed; instead, a reproducible kernel Hilbert space interpolation is used.[32] In addition to the assumption about pairwise representability of DFT error, eq 3, the transferability of the correction functions from the reference system to the system of interest is assumed. The choice of the reference system is critical for the reliability of the DFT/CC method. Correction functions ε_{OH} (ε_{HH}), ε_{OC} (ε_{HC}), ε_{OO} (ε_{HO}), and ε_{OCu} (ε_{HCu}) were evaluated from one-dimensional potential energy curves of $H_2O\cdots H_2$, $H_2O\cdots C_6H_6$, $H_2O\cdots CO_2$, and $H_2O\cdots Cu(HCOO)_2$ complexes, respectively. Details about the construction of correction functions are presented in Supporting Information, while the more detailed description of the DFT/CC method can be found elsewhere.[29,33] The assumption of the correction transferability was tested by calculations carried out for a larger $(H_2O)_2\cdots Cu_2(HCOO)_4$ cluster model, depicted in Figure 1, at the CCSD(T)/CBS level. The interaction energy of the water with the $Cu_2(HCOO)_4$ cluster model, eq 1, calculated at the DFT/CC level is in excellent agreement with CCSD(T)/CBS results in a whole range of intersystem distances R_{Cu-OH_2} (Figure 1). It is also worth mentioning that the computational demands of the DFT/CC scheme are comparable to those of the DFT-D methods.

The interaction of H_2O with CuBTC was investigated within the periodic DFT/CC model (details below). The adsorption of a single water molecule as well as the adsorption of two water molecules on the single paddle-wheel unit was considered. DFT/CC-optimized structures of the adsorbed water molecules in CuBTC are depicted in Figure 2. (i) The R_{Cu-OH_2} distance is 2.19 Å for one H_2O and 2.21 and 2.23 Å for two water molecules per paddle-wheel, in good agreement with the experimental value[1] of 2.17 Å, and it is significantly improved compared to the DFT (2.27 and 2.31 Å for one and two water molecules, respectively). (ii) Upon the interaction of the paddle-wheel unit with just one water molecule, the Cu^{II} cation interacting with water is pulled slightly above the paddle-wheel ring, and as a result, a small pyramidalization is observed for this Cu^{II} cation. Also, the second Cu^{II} cation of the paddle-wheel unit is pulled in the same direction but to a smaller extent; correspondingly, the Cu−Cu bond is elongated from 2.48 to 2.51 Å upon the first water molecule adsorption. When two water molecules interact with one paddle-wheel, the Cu−Cu distance is further elongated to 2.55 Å; however, the pyramidalization of Cu^{II} cations is smaller than that in the case of single water molecule adsorption. (iii) The C_2 axis of the adsorbed water molecule does not coincide with the C_4 axis of a paddle-wheel unit; instead, hydrogen atoms of water molecules are tilted toward the carboxylic oxygen atoms (Figure 2).

The interaction energy calculated for one water molecule on the paddle-wheel at the DFT and DFT/CC levels is −34.6 and −55.3 kJ mol^{-1}, respectively. The large difference of about 20 kJ mol^{-1} between the DFT and DFT/CC approaches could be (within the pairwise DFT error representation) traced to water interaction with the nearest paddle-wheel unit, $Cu_2(CO_2)_4$, which accounts for more than 90% of the DFT error,

DOI: 10.1021/jz101378z | J. Phys. Chem. Lett. 2010, 1, 3354–3359

while the long-range contribution from the CuBTC framework is relatively small. The interaction energies calculated for the second water molecule (see Figure 2c for the structure) on a paddle-wheel unit at the DFT and DFT/CC levels of theory are −30.6 and −50.3 kJ mol^{-1}, respectively. Hence, the interaction with the second water molecule is about 5 kJ mol^{-1} weaker; this indicates the presence of two nonequivalent adsorption sites, the free paddle-wheel and the paddle-wheel with the one copper center occupied by the adsorbed molecule.

The zero-point vibrational energy (ZPVE) correction was calculated within the harmonic approximation using a numerical Hessian (±0.005 Å displacements) and assuming a rigid framework except for atoms of the water molecule and the nearest paddle-wheel unit. The calculated ZPVE (6.3 kJ mol^{-1} for one water molecule) led the adsorption enthalpy at 0 K of −49.0 kJ mol^{-1}. Although the CuBTC is often used as a reference MOF for various experimental studies, the experimental data on the water adsorption are scarce. The reason is the instability of the CuBTC at high humidity levels.[2,34] Despite that, Henninger et al.[34] were able to obtain an adsorption enthalpy of −50.7 ± 2.9 kJ mol^{-1} at 313 K using the thermogravimetry and differential scanning calorimetry (TG/DSC). These experimental data are in excellent agreement with calculations reported here; however, it must be pointed out that the calculations are reporting the adsorption enthalpy at 0 K for the low coverage limit while the TG/DSC measurements were carried out for the higher water coverage. The low coverage adsorption behavior was considered in grand canonical Monte Carlo simulations (GCMC) by Castillo et al.,[11] who used interaction parameters fitted on the water adsorption isotherms in CuBTC from Wang et al.;[19] the estimated adsorption enthalpy at the zero coverage limit was −48.0 ± 6.6 kJ mol^{-1}, again in very good agreement with the results reported here. Although the above-mentioned adsorption enthalpy estimates cannot be straightforwardly compared to our DFT/CC values, a good agreement is noteworthy.

Recently, also, the periodic DFT calculations by Watanabe et al.[15] employing PW91-GGA exchange−correlation functional have been reported; the interaction energies of adsorption of the first and second water molecules on the paddle-wheel unit were −47.3 and −33.8 kJ mol^{-1}, respectively. Reported interaction energies have not been corrected for ZPVE; therefore, they should be compared with −55.3 and −50.3 kJ mol^{-1} values, respectively, reported above. The discrepancy between the DFT/CC results reported here and DFT results from ref 15 is thus understandable in light of the benchmarking calculations reported in Table 1.

In summary, the suitability of the various theoretical methods and models for the description of the coordinatively unsaturated transition-metal sites in MOFs was analyzed for the water adsorption in CuBTC. Both DFT and empirical dispersion-corrected DFT-D schemes were found to be unable to reliably describe the interaction of water with the cus's in CuBTC. The DFT/CC method was extended to correct the DFT error in the description of the transition-metal site; DFT/CC results were in excellent agreement with CCSD(T)/CBS ones. DFT/CC calculations performed for the periodic CuBTC model gave $-\Delta H_{ads}$ = 49 kJ mol^{-1}, in good agreement with available experimental data. We conclude that the DFT/CC correction scheme provides an accurate description of the CuBTC MOF that can be used for testing of other methods and for possible improvement of existing force fields.

COMPUTATIONAL METHODS

The pseudopotential-based correlation-consistent valence-X-ζ basis set with polarization functions by Peterson et al.,[35] cc-pVXZ-PP, was employed for Cu atoms, while the standard Dunning's correlation-consistent valence-X-ζ basis sets with polarization functions,[36] cc-pVXZ, was used for other atoms. The corresponding augmented correlation-consistent basis sets were also employed, aug-cc-pVXZ-PP and aug-cc-pVXZ for Cu and other atoms, respectively. The above-mentioned mixed basis sets are denoted throughout the text as VXZ or AVXZ for the standard and augmented basis sets, respectively.

The CCSD(T)/CBS estimates of the interaction energies of the $Cu_2(HCOO)_4(H_2O)_2$ model system were obtained using correlation energy dependence on the cardinal number X ($E_X = E_{CBS} + AX^{-3}$). The HF/VQZ energy was taken as the CBS limit for the uncorrelated part of the energy. The interaction energies were calculated at the CCSD(T)/VTZ level, and the CCSD(T)/CBS was obtained from

$$\text{CCSD(T)/CBS} = \text{(CCSD(T)/VTZ)} + \text{(MP2/CBS)} - \text{(MP2/VTZ)} \quad (4)$$

using the MP2/CBS estimate obtained from MP2/VQZ and MP2/VTZ by means of the same extrapolation formula mentioned above.

The multireference level CASPT2 calculations of the $Cu_2(HCOO)_4(H_2O)_n$ (n = 0 and 2) model system were performed with the relativistic full electron basis sets of atomic natural orbitals (ANO-RCC)[37] using the quadruple-ζ contraction denoted in the text as ANO-VQZP. The geometry of the model system is provided in the Supporting Information.

The DFT calculations on the $Cu_2(HCOO)_4(H_2O)_2$ cluster model reported in Table 1 employed the VTZ basis set and were performed at the PBE/AVTZ geometry, which is provided in the Supporting Information for reference.

The periodic DFT calculations of the interaction of the water molecule with CuBTC were modeled using the rhombohedral primitive cell (RPC) of CuBTC containing 156 framework atoms. The optimized RPC lattice parameters were obtained from fitting the polynomial to the $E(V)$ curve obtained from DFT calculations at different volumes relaxing the cell shape and fractional coordinates ($a = b = c$ = 18.774 Å, $\alpha = \beta = \gamma$ = 60°, and V = 4678.71 Å^3). The projector augmented wave approximation (PAW)[38] and the plane wave basis set with a kinetic energy cutoff of 600 eV were used; Brillouin zone sampling was restricted to the Γ-point. The Perdew−Burke−Ernzerhof (PBE) exchange−correlation functional was employed. The periodic structures of the CuBTC with adsorbed water molecules were optimized with respect to all atomic positions considering fixed RPC lattice parameters. Single- and multireference calculations with cluster models and calculations with periodic models were performed with Molpro09,[39] MOLCAS 7.2,[40] and VASP 5.2[41] program suites, respectively.

DOI: 10.1021/jz101378z | J. Phys. Chem. Lett. 2010, 1, 3354–3359

SUPPORTING INFORMATION AVAILABLE

The details about the construction of the DFT/CC correction functions (reference systems, CCSD(T)/CBS extrapolation scheme, etc.), spin and charge density analysis, and the geometries of the $Cu_2(HCOO)_4(H_2O)_2$ model systems are provided. This material is available free of charge via the Internet at http://pubs.acs.org.

AUTHOR INFORMATION

Corresponding Author:

*To whom correspondence should be addressed. E-mail: petr.nachtigall@molecular.cz.

ACKNOWLEDGMENT This work is (partly) funded by MACADEMIA (www.macademia-project.eu). MACADEMIA is a 4-year Large-scale Integrating Collaborative Project, funded under the EU Seventh Framework Programme for Research and Development, under the Nanosciences, Nanotechnologies, Materials and New Production Technologies Theme ([FP7/2007-2013] under Grant 228862). P.N. and L.G. acknowledge the support of ME CR (Grants 7E09111 and MSM0021620835); O.B. thanks Research Project Z4 055 0506.

REFERENCES

(1) Chui, S. S. Y.; Lo, S. M. F.; Charmant, J. P. H.; Orpen, A. G.; Williams, I. D. A Chemically Functionalizable Nanoporous Material $[Cu_3(TMA)_2(H_2O)_3]_n$. *Science* **1999,** *283*, 1148–1150.

(2) Küsgens, P.; Rose, M.; Senkovska, I.; Fröde, H.; Henschel, A.; Siegle, S.; Kaskel, S. Characterization of Metal–Organic Frameworks by Water Adsorption. *Microporous Mesoporous Mater.* **2009,** *120*, 325–330.

(3) Farrusseng, D.; Daniel, C.; Gaudillère, C.; Ravon, U.; Schuurman, Y.; Mirodatos, C.; Dubbeldam, D.; Frost, H.; Snurr, R. Q. Heats of Adsorption for Seven Gases in Three Metal–Organic Frameworks: Systematic Comparison of Experiment and Simulation. *Langmuir* **2009,** *25*, 7383–7388.

(4) Getzschmann, J.; Senkovska, I.; Wallacher, D.; Tovar, M.; Fairen-Jimenez, D.; Düren, T.; van Baten, J. M.; Krishna, R.; Kaskel, S. Methane Storage in CuBTC. *Microporous Mesoporous Mater.* **2010**, *136*, 50–58.

(5) Hamon, L.; Jolimaître, E.; Pirngruber, G. D. CO_2 and CH_4 Separation by Adsorption Using Cu–BTC Metal–Organic Framework. *Ind. Eng. Chem. Res.* **2010,** *49*, 7497–7503.

(6) Peterson, V. K.; Liu, Y.; Brown, C. M.; Kepert, C. J. Neutron Powder Diffraction Study of D_2 Sorption in Cu_3(1,3,5-benzenetricarboxylate)$_2$. *J. Am. Chem. Soc.* **2006,** *128*, 15578–15579.

(7) Keskin, S. Molecular Simulation Study of CH_4/H_2 Mixture Separations Using Metal Organic Framework Membranes and Composites. *J. Phys. Chem. C* **2010,** *114*, 13047–13054.

(8) Schlichte, K.; Kratzke, T.; Kaskel, S. Improved Synthesis, Thermal Stability and Catalytic Properties of the Metal–Organic Framework Compound $Cu_3(BTC)_2$. *Microporous Mesoporous Mater.* **2004,** *73*, 81–88.

(9) Alaerts, L.; Séguin, E.; Poelman, H.; Thibault-Starzyk, F.; Jacobs, P. A.; De Vos, D. E. Probing the Lewis acidity and catalytic activity of the Metal–Organic Framework $[Cu_3(btc)_2]$ (BTC = benzene-1,3,5-tricarboxylate). *Chem.—Eur. J.* **2006,** *12*, 7353–7363.

(10) Pérez-Mayoral, E.; Čejka, J. $[Cu_3(BTC)_2]$: A Metal–Organic Framework Catalyst for the Friedländer Reaction. *ChemCatChem* **2010**, doi:10.1002/cctc.201000201.

(11) Castillo, J. M.; Vlugt, T. J. H.; Calero, S. Understanding Water Adsorption in Cu–BTC Metal–Organic Frameworks. *J. Phys. Chem. C* **2008,** *112*, 15934–15939.

(12) García-Pérez, E.; Gascón, J.; Morales-Flórez, V.; Castillo, J. M.; Kapteijn, F.; Calero, S. Identification of Adsorption Sites in Cu–BTC by Experimentation and Molecular Simulation. *Langmuir* **2009,** *25*, 1725–1731.

(13) Liu, J. C.; Culp, J. T.; Natesakhawat, S.; Bockrath, B. C.; Zande, B.; Sankar, S. G.; Garberoglio, G.; Johnson, J. K. Experimental and Theoretical Studies of Gas Adsorption in $Cu_3(BTC)_2$: An Effective Activation Procedure. *J. Phys. Chem. C* **2007,** *111*, 9305–9313.

(14) Düren, T.; Bae, Y.-S.; Snurr, R. Q. Using Molecular Simulation to Characterise Metal–Organic Frameworks for Adsorption Applications. *Chem. Soc. Rev.* **2009,** *38*, 1237–1247.

(15) Watanabe, T.; Sholl, D. S. Molecular Chemisorption on Open Metal Sites in Cu_3(benzenetricarboxylate)$_2$: A Spatially Periodic Density Functional Theory Study. *J. Chem. Phys.* **2010,** *133*, 094509.

(16) Liu, D. H.; Zhong, C. L. Characterization of Lewis Acid Sites in Metal–Organic Frameworks Using Density Functional Theory. *J. Phys. Chem. Lett.* **2010,** *1*, 97–101.

(17) Wu, H.; Simmons, J. M.; Srinivas, G.; Zhou, W.; Yildirim, T. Adsorption Sites and Binding Nature of CO_2 in Prototypical Metal–Organic Frameworks: A Combined Neutron Diffraction and First-Principles Study. *J. Phys. Chem. Lett.* **2010,** *1*, 1946–1951.

(18) Liang, Z.; Marshall, M.; Chaffee, A. L. CO_2 Adsorption-Based Separation by Metal Organic Framework (Cu–BTC) versus Zeolite (13X). *Energy Fuels* **2009,** *23*, 2785–2789.

(19) Wang, Q. M.; Shen, D. M.; Bülow, M.; Lau, M. L.; Deng, S. G.; Fitch, F. R.; Lemcoff, N. O.; Semanscin, J. Metallo-Organic Molecular Sieve for Gas Separation and Purification. *Microporous Mesoporous Mater.* **2002,** *55*, 217–230.

(20) Rodríguez-Fortea, A.; Alemany, P.; Alvarez, S.; Ruiz, E. Exchange Coupling in Carboxylato-Bridged Dinuclear Copper(II) Compounds: A Density Functional Study. *Chem.—Eur. J.* **2001,** *7*, 627–637.

(21) Perdew, J. P.; Burke, K.; Ernzerhof, M. Generalized Gradient Approximation Made Simple. *Phys. Rev. Lett.* **1996,** *77*, 3865–3868.

(22) Perdew, J. P.; Burke, K.; Ernzerhof, M. Errata: Generalized Gradient Approximation Made Simple. *Phys. Rev. Lett.* **1997,** *78*, 1396.

(23) Grimme, S. Semiempirical GGA-Type Density Functional Constructed with a Long-Range Dispersion Correction. *J. Comput. Chem.* **2006,** *27*, 1787–1799.

(24) Grimme, S.; Antony, J.; Ehrlich, S.; Krieg, H. A Consistent and Accurate Ab Initio Parametrization of Density Functional Dispersion Correction (DFT-D) for the 94 Elements H–Pu. *J. Chem. Phys.* **2010,** *132*, 154104.

(25) El-Nahas, A. M.; Tajima, N.; Hirao, K. Do Cu_2+NH_3 and Cu_2+OH_2 Exist? Theory Confirms 'Yes!'. *Chem. Phys. Lett.* **2000,** *318*, 333–339.

(26) Poater, J.; Sola, M.; Rimola, A.; Rodriguez-Santiago, L.; Sodupe, M. Ground and Low-Lying States of Cu^{2+}–H_2O. A Difficult Case for Density Functional Methods. *J. Phys. Chem. A* **2004,** *108*, 6072–6078.

(27) Ducéré, J. M.; Goursot, A.; Berthomieu, D. Comparative Density Functional Theory Study of the Binding of Ligands to Cu^+ and Cu^{2+}: Influence of the Coordination and Oxidation State. *J. Phys. Chem. A* **2005,** *109*, 400–408.

(28) Jeanvoine, Y.; Spezia, R. Cu^{2+} Binding Chalcogen–Chalcogen Bridges: A Problematic Case for DFT. *J. Mol. Struct.: THEOCHEM* **2010,** *954*, 7–15.

(29) Bludský, O.; Rubeš, M.; Soldán, P.; Nachtigall, P. Investigation of the Benzene-Dimer Potential Energy Surface: DFT/CCSD(T) Correction Scheme. *J. Chem. Phys.* **2008,** *128*, 114102.

DOI: 10.1021/jz101378z | *J. Phys. Chem. Lett.* **2010,** *1*, 3354–3359

(30) Rubeš, M.; Kysilka, J.; Nachtigall, P.; Bludský, O. DFT/CC Investigation of Physical Adsorption on a Graphite (0001) Surface. *Phys. Chem. Chem. Phys.* **2010,** *12*, 6438–6444.
(31) Zukal, A.; Pulido, A.; Gil, B.; Nachtigall, P.; Bludský, O.; Rubeš, M.; Čejka, J. Experimental and Theoretical Determination of Adsorption Heats of CO_2 over Alkali Metal Exchanged Ferrierites with Different Si/Al Ratio. *Phys. Chem. Chem. Phys.* **2010,** *12*, 6413–6422.
(32) Soldán, P.; Hutson, J. M. On the Long-Range and Short-Range Behavior of Potentials from Reproducing Kernel Hilbert Space Interpolation. *J. Chem. Phys.* **2000,** *112*, 4415–4416.
(33) Bludský, O.; Rubeš, M.; Soldán, P. Ab Initio Investigation of Intermolecular Interactions in Solid Benzene. *Phys. Rev. B* **2008,** *77*, 092103.
(34) Henninger, S. K.; Schmidt, F. P.; Henning, H. M. Water Adsorption Characteristics of Novel Materials for Heat Transformation Applications. *Appl. Therm. Eng.* **2010,** *30*, 1692–1702.
(35) Peterson, K. A.; Puzzarini, C. Systematically Convergent Basis Sets for Transition Metals. II. Pseudopotential-Based Correlation Consistent Basis Sets for the Group 11 (Cu, Ag, Au) and 12 (Zn, Cd, Hg) Elements. *Theor. Chem. Acc.* **2005,** *114*, 283–296.
(36) Dunning, T. H. Gaussian-Basis Sets for Use in Correlated Molecular Calculations 0.1. the Atoms Boron Through Neon and Hydrogen. *J. Chem. Phys.* **1989,** *90*, 1007–1023.
(37) Roos, B. O.; Lindh, R.; Malmqvist, P. A.; Veryazov, V.; Widmark, P. O. New Relativistic ANO Basis Sets for Transition Metal Atoms. *J. Phys. Chem. A* **2005,** *109*, 6575–6579.
(38) Blöchl, P. E. Projector Augmented-Wave Method. *Phys. Rev. B* **1994,** *50*, 17953–17979.
(39) *MOLPRO* is a package of ab initio programs written by Werner, H.-J.; Knowles, P. K.; Manby, F. R.; Schütz, M.; Celani, P.; Knizia, G.; Korona, T.; Lindh, R.; Mitrushenkov, A.; Rauhut, G.; Adler, T. B.; Amos, R. D.; Bernhardsson, A.; Berning, A.; Cooper, D. L.; Deegan, M. J. O.; Dobbyn, A. J.; Eckert, F.; Goll, E.; Hampel, C.; Hesselmann, A.; Hetzer, G.; Hrenar, T.; Jansen, G.; Köppl, C.; Liu, Y.; Lloyd, A. W.; Mata, R. A.; May, A. J.; McNicholas, S. J.; Meyer, W.; Mura, M. E.; Nicklass, A.; Palmieri, P.; Pflüger, K.; Pitzer, R.; Reiher, M.; Shiozaki, T.; Stoll, H.; Stone, A. J.; Tarroni, R.; Thorsteinsson, T.; Wang, M.; Wolf, A. MOLPRO, version 2009.1; A Package of Ab Initio Programs; University College Cardiff Consultants Limited: Wales, U.K., 2009.
(40) Aquilante, F.; De Vico, L.; Ferré, N.; Ghigo, G.; Malmqvist, P. å.; Neogrády, P.; Pedersen, T. B.; Pitoňák, M.; Reiher, M.; Roos, B. O.; Serrano-Andrés, L.; Urban, M.; Veryazov, V.; Lindh, R. MOLCAS 7: The Next Generation. *J. Comput. Chem.* **2009,** *31*, 224–247.
(41) Kresse, G.; Hafner, J. Ab-Initio Molecular-Dynamics for Open-Shell Transition-Metals. *Phys. Rev. B* **1993,** *48*, 13115–13118.

DOI: 10.1021/jz101378z | *J. Phys. Chem. Lett.* **2010,** *1*, 3354–3359

Attachment C

THE JOURNAL OF PHYSICAL CHEMISTRY C

ARTICLE

pubs.acs.org/JPCC

Understanding CO_2 Adsorption in CuBTC MOF: Comparing Combined DFT−ab Initio Calculations with Microcalorimetry Experiments

Lukáš Grajciar,[†] Andrew D. Wiersum,[‡] Philip L. Llewellyn,[‡] Jong-San Chang,[§] and Petr Nachtigall[†,*]

[†]Department of Physical and Macromolecular Chemistry, Faculty of Science, Charles University in Prague, Hlavova 2030, CZ-128 40, Prague 2, Czech Republic

[‡]Laboratoire Chimie Provence, Université d'Aix-Marseille I, II et III - CNRS (UMR 6264), Centre de St Jérôme, 13397 Marseille Cedex 20, France

[§]Research Group for Nanocatalyst, Biorefinery Research Center, Korea Research Institute of Chemical Technology (KRICT), P.O. Box 107, Yusung, Daejeon 305-600, Korea

Supporting Information

ABSTRACT: A combined experimental and theoretical investigation of CO_2 adsorption in the metal−organic framework CuBTC is presented. Adsorption enthalpies were measured as a function of coverage up to 13 mmol g^{-1} adsorbed amount (corresponding roughly to CO_2/Cu = 5:2) by a Tian−Calvet-type microcalorimeter. Experimetal data are interpreted based on accurate calculations employing a combined DFT−ab initio computational scheme. CO_2 molecules adsorb preferentially on coordinatively unsaturated sites for coverages below CO_2/Cu = 1:1; at higher coverages (up to CO_2/Cu = 5:3), CO_2 adsorbs in cage window sites; and at higher coverages, the sites in cage centers and in large cages start to be occupied. Experimental adsorption enthalpies are almost constant (−29 kJ mol^{-1}) up to the CO_2/Cu = 5:3 coverage, suggesting a homogeneity of adsorption sites. However, calculations clearly show that adsorption sites in CuBTC are rather heterogeneous. The experimentally observed independence of adsorption enthalpies with respect to coverage is due to the cancellation of two effects: the decrease in the adsorbate−adsorbent interaction is compensated by an increase in the lateral interactions.

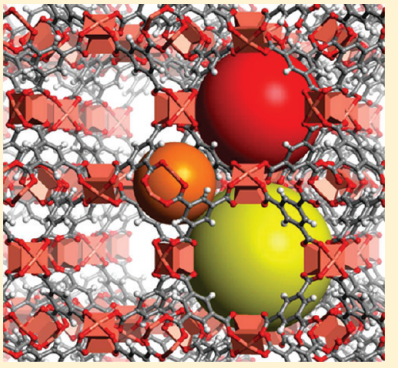

INTRODUCTION

Metal−organic frameworks (MOFs) are a recent addition to the class of microporous and mesoporous materials. Made up of metal clusters connected by organic ligands, they form crystalline materials presenting surface areas and pore volumes that are able to compete with activated carbons while having a far more varied structure and adaptable surface chemistry even than zeolites.[1] They are seen as potential replacements for activated carbons and zeolites in applications such as adsorption[2] and catalysis.[3,4]

CuBTC, also known as HKUST-1, is one of the earliest reported stable MOFs with a very high surface area. Based on the well-known copper "paddlewheel",[5] it is formed of large interconnecting square channels surrounded by small tetrahedral side pockets (Figure 1) and presents a number of coordinatively unsaturated (cus) copper metal sites. This makes it particularly suited to the adsorption of gases, as the small cages and open metal sites provide strong adsorption sites at low pressure whereas the large channels allow high uptakes through pore filling at higher pressures.[6,7] Because of its relatively straightforward synthesis and high adsorption capacity, CuBTC has been widely studied both experimentally and theoretically and can be considered a reference MOF. Early studies focused mainly on its potential for storing H_2[8−11] and CO_2,[12] whereas more recently, CuBTC has been considered for gas separations, such as the removal of CO_2 from carbon monoxide[13] and methane,[14] and even for catalysis.[15] Several groups have also worked on different synthesis routes leading to higher surface areas,[16−18] resulting in the data published in the literature being highly dependent on the quality of the sample.

Adsorption on CuBTC has been modeled for a number of gases using both grand-canonical Monte Carlo (GCMC)[7,13,14,19−22] and density functional theory (DFT)[20,22] simulations, and the results have been used to investigate the adsorption mechanism and location of adsorbed species in CuBTC. However, both of these models are limited by the difficulties in accurately reproducing the interactions of adsorbed molecules with unsaturated metal sites at low coverages.[7,20,23] In particular, large discrepancies have been observed in the calculated heats of adsorption. Recently, the DFT/coupled-cluster (CC) method,[24−26] a combined DFT−ab initio computational scheme, has been shown to successfully model the interactions of water with CuBTC[23] and will be used here to investigate the adsorption of CO_2 on CuBTC.

Received: June 26, 2011
Revised: August 2, 2011
Published: August 02, 2011

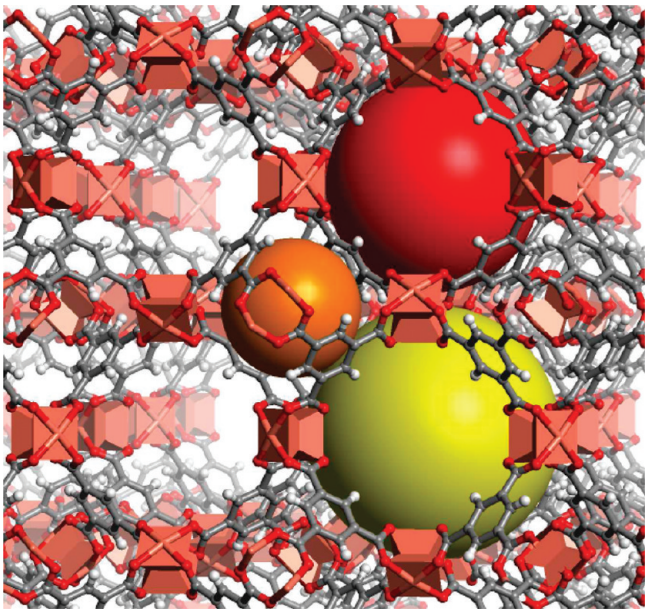

Figure 1. View of the structure and connectivity of CuBTC containing three pores (cages): a small tetrahedral pore shown as an orange sphere and two large octahedral pores approximately depicted as red and yellow spheres. Cu, O, C, and H atoms are depicted in pink, red, gray, and white, respectively.

Microcalorimetry has been shown to be a powerful tool for studying adsorption phenomena in porous materials. It provides a direct measurement of the interaction energy between the adsorbent and the guest molecule and can be used to probe the chemical nature of the surface, highlight phase transitions and pore filling, and characterize specific adsorption sites.[27] In particular, microcalorimetry has been used to illustrate the flexibility of the MIL53 series[28] and the interaction of adsorbed species with open metal sites in the large-pore MIL100(Fe) system.[29]

In this work, we have used a combination of the ab initio calculations employing the recently developed DFT/CC method and microcalorimetry to study the adsorption mechanism of CO_2 in CuBTC at various coverages, focusing especially on the different adsorption sites and the corresponding enthalpies.

MATERIALS AND METHODS

Experimental Methods. *Sample Characterization.* CuBTC MOF (HKUST-1) was provided by the Korean Research Institute for Chemical Technology and was prepared by microwave synthesis.[17] The sample was activated by heating to 150 °C under secondary vacuum ($<1 \times 10^{-3}$ mbar). The apparent Brunauer−Emmett−Teller (BET) surface area was determined by adsorption of N_2 at 77 K in the relative pressure range of $P/P_0 = 0.0002-0.01$, following the guidelines proposed by Rouquerol et al.[30] The sample was found to have a surface area of 1628 m^2/g and a pore volume of 0.64 cm^3/g. These values are among the highest reported in the literature and are very close to the values reported by Chang et al.[17] for CuBTC prepared by microwave synthesis (1656 m^2/g).

Microcalorimetry. Adsorption enthalpies were measured experimentally using a Tian−Calvet-type microcalorimeter coupled with a homemade manometric gas dosing system.[31] This apparatus allows the simultaneous measurement of the adsorption isotherm and the corresponding differential enthalpies. Gas is introduced into the system using a step-by-step method, and each dose is allowed to stabilize in a reference volume before being brought into contact with the adsorbent, located in the microcalorimeter. The introduction of the adsorbate to the sample is accompanied by an exothermic thermal signal, measured by the thermopiles of the microcalorimeter. The peak in the calorimetric signal is integrated over time to give the total energy released during that adsorption step.

The adsorption of CO_2 on CuBTC was carried out at 30 °C and up to 15 bar. Around 0.2 g of sample was used, and this was outgassed at 150 °C for 16 h under secondary vacuum prior to the experiment. For each injection of gas, equilibrium was assumed to have been reached after 90 min. This was confirmed by the return of the calorimetric signal to its baseline (<5 μW). The gas used for the adsorption was obtained from Air Liquide and was of N48 quality (99.998% purity).

Computational Methods. A recently proposed combined DFT−ab initio computational scheme, the DFT/CC method,[24−26] was used in this study. It has been shown to provide an accurate description of the interaction of CuBTC with adsorbing molecules,[23] outperforming both DFT and DFT including dispersion corrections (DFT-D). The DFT/CC method is based on the pairwise representability of DFT error, ΔE, defined as

$$\Delta E = E_{\mathrm{CCSD(T)}} - E_{\mathrm{DFT}} \quad (1)$$

where $E_{\mathrm{CCSD(T)}}$ and E_{DFT} are the interaction energies calculated at the CCSD(T)/CBS and DFT/AVQZ levels of theory, respectively. An extension of DFT/CC method for the CO_2/CuBTC system is described below.

Within the DFT/CC method, the DFT error, ΔE, is expressed as a sum of atom−atom correction functions $\varepsilon_{ij}(R^{ij})$,

$$\Delta E = \sum_{ij} \varepsilon_{ij}(R_{ij}) \quad (2)$$

where R_{ij} is the distance between atoms i and j. No explicit functional form for the ε_{ij} correction functions is assumed; instead, a reproducible kernel Hilbert space interpolation is used.[32] In addition to the assumption about pairwise representability of DFT error (eq 2), the transferability of the correction functions from the reference system to the system of interest is assumed. Correction functions $\varepsilon_{\mathrm{OH}}$ ($\varepsilon_{\mathrm{CH}}$), $\varepsilon_{\mathrm{CC}}$ ($\varepsilon_{\mathrm{OC}}$), $\varepsilon_{\mathrm{OO}}$, and $\varepsilon_{\mathrm{OCu}}$ ($\varepsilon_{\mathrm{CCu}}$) were evaluated from one-dimensional potential energy curves of the $CO_2\cdots H_2$, $CO_2\cdots C_6H_6$, $CO_2\cdots CO_2$, and $CO_2\cdots Cu(HCOO)_2$ complexes, respectively. Details about the construction of correction functions are presented in the Supporting Information, whereas more detailed descriptions of the DFT/CC method can be found elsewhere.[24,33] The assumption of the correction transferability was tested by calculations carried out for a larger $(CO_2)_2\cdots Cu_2(HCOO)_4$ cluster model at the CCSD(T)/CBS level (in the PBE/AVDZ-optimized geometry). The interaction energy of the CO_2 molecule with the $Cu_2(HCOO)_4$ cluster model of −19.0 kJ mol^{-1} calculated at the DFT/CC level was found to be in excellent agreement with the CCSD(T)/CBS value of −18.8 kJ mol^{-1}.

Furthermore, as a higher-coverage behavior of the CO_2 molecule in CuBTC was also investigated in this study, the correct description of the CO_2-CO_2 lateral interactions is of

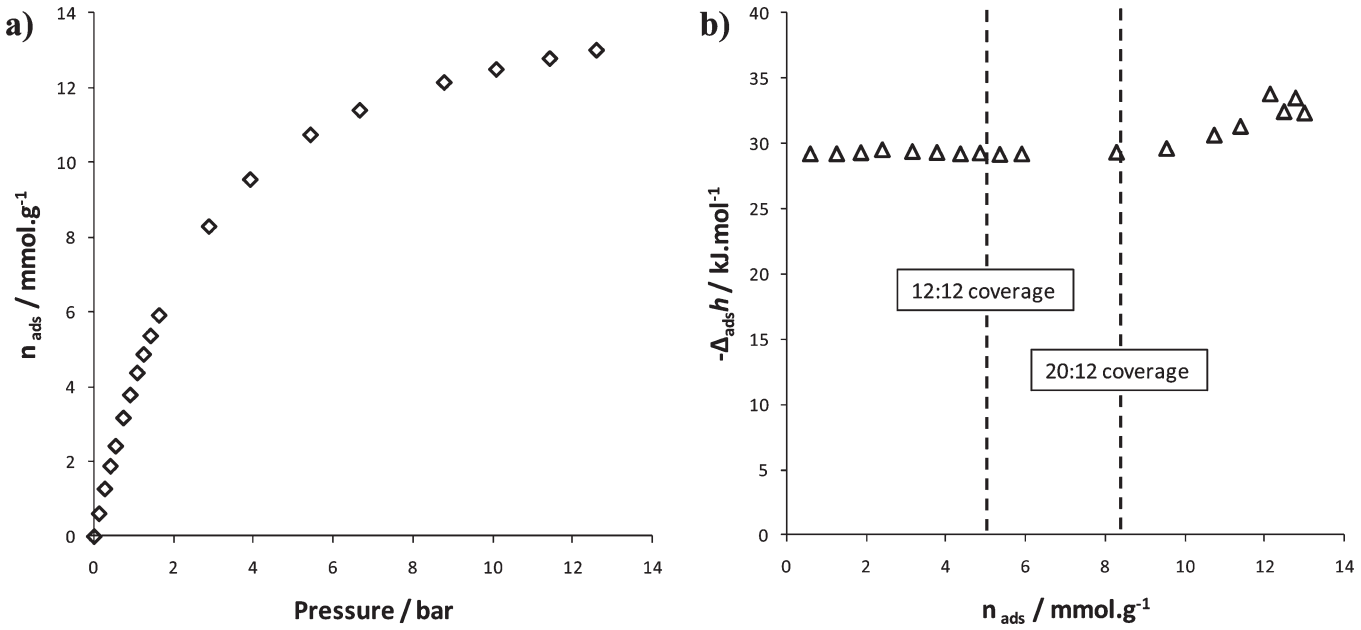

Figure 2. CO_2 adsorption at 303 K on CuBTC: (a) adsorption isotherm, (b) corresponding adsorption enthalpies.

great importance. The calculations of the CO_2 dimer interaction energies at both the CCSD(T)/CBS and DFT/CC levels were carried out for different relative orientations of the CO_2 molecules (see Table S1, Supporting Information), and a very good agreement between CCSD(T)/CBS and DFT/CC values was observed.

The zero-point vibrational energy correction for CO_2 in CuBTC has been estimated to be between 0.8 and 1.7 kJ mol^{-1}, values obtained at the PBE and LDA[34] levels, respectively. The reported interaction energies in the case of CO_2/Cu coverages of 1:12, 2:12, 3:12, 13:12, and 21:12 are defined as the interaction energy of the last CO_2 molecule

$$\Delta E_{\text{int}} = E[(CO_2)_n/\text{CuBTC}] - E[(CO_2)_{n-1}/\text{CuBTC}] - E(CO_2) \quad (3)$$

whereas for coverages of 12:12, 16:12, and 20:12, the average interaction energy per CO_2 molecule is reported as

$$\bar{E}_{\text{int}} = \{E[(CO_2)_n/\text{CuBTC}] - E(\text{CuBTC}) - nE(CO_2)\}/n \quad (4)$$

The pseudopotential-based correlation-consistent valence-X-ζ basis set with polarization functions by Peterson et al.,[35] cc-pVXZ-PP, was employed for Cu atoms, whereas the standard Dunning's correlation-consistent valence-X- ζ basis sets with polarization functions,[36] cc-pVXZ, was used for other atoms. The corresponding augmented correlation-consistent basis sets were also employed, namely, aug-cc-pVXZ-PP and aug-cc-pVXZ for Cu and other atoms, respectively. The above-mentioned mixed basis sets are denoted throughout the text as VXZ or AVXZ for the standard and augmented basis sets, respectively. The CCSD(T)/CBS estimate of the interaction energy of the $Cu_2(HCOO)_4(CO_2)_2$ model system was obtained using the correlation energy dependence on the cardinal number X ($E_X = E^{\text{CBS}} + AX^{-3}$). The HF/AVTZ energy was taken as the CBS limit for the uncorrelated part of the energy. The interaction energies were calculated at the CCSD(T)/AVDZ level, and the CCSD(T)/CBS was obtained from

$$\text{CCSD(T)/CBS} = [\text{CCSD(T)/AVDZ}] + (\text{MP2/CBS}) - (\text{MP2/AVDZ}) \quad (5)$$

using the MP2/CBS estimate obtained from MP2/AVTZ and MP2/AVDZ by means of the same extrapolation formula mentioned above.

The periodic DFT calculations of the interaction of the carbon dioxide molecule with CuBTC were modeled using the rhombohedral primitive cell (RPC) of CuBTC including two small tetrahedral cages and containing 156 framework atoms ($Cu_{12}O_{48}C_{72}H_{24}$). The optimized RPC lattice parameters ($a = b = c = 18.774$ Å, $\alpha = \beta = \gamma = 60°$, and $V = 4678.71$ $Å^3$) were taken from ref 23. The projector augmented wave approximation (PAW)[37] and the plane wave basis set with a kinetic energy cutoff of 600 eV were used; Brillouin-zone sampling was restricted to the Γ point. The Perdew–Burke–Ernzerhof (PBE) exchange–correlation functional[38,39] was employed. The periodic structures of the CuBTC with adsorbed carbon dioxide molecules were optimized with respect to all atomic positions considering fixed RPC lattice parameters. Calculations with cluster models and calculations with periodic models were performed with the Molpro 2009.1[40] and VASP 5.2[41] program suites, respectively.

RESULTS

Experimental Results. The adsorption isotherm of CO_2 on CuBTC at 303 K is shown in Figure 2a. The plot shows a classic Langmuir-type isotherm with an almost linear adsorption curve in the low-pressure region. The amount adsorbed at 5 bar (~10.3 mmol g^{-1}) is comparable to the highest values reported in the literature.[14,18,42]

The adsorption enthalpy for CO_2 as a function of loading is shown Figure 2b. Initially, the heat of adsorption remains very steady at approximately −29 kJ mol^{-1} before increasing gradually by 2−3 kJ mol^{-1} above 8 mmol g^{-1}. A flat curve for the enthalpy of adsorption is generally characteristic of an adsorbent

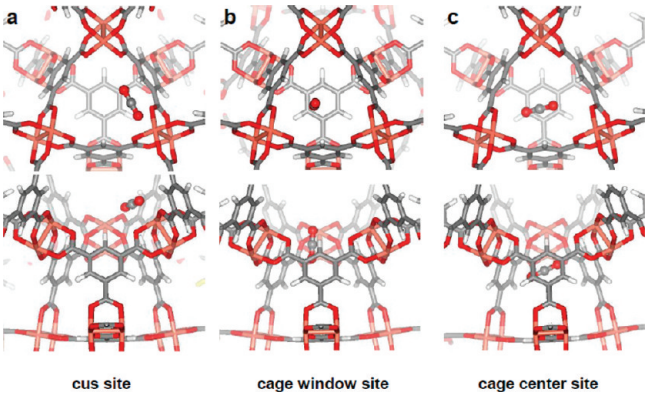

Figure 3. Structures of the CO_2 adsorption complexes on the (a) cus, (b) small cage window, and (c) small cage center sites. The upper and lower parts of the figure represent the views perpendicular and parallel, respectively, to one of the small cage openings.

Table 1. Characteristics of the CO_2 Adsorption Complexes on cus Sites for Various CO_2 Coverages

coverage (CO_2 per Cu)	adsorption site[a]	interaction energy[b] (kJ mol^{-1})
1:12	–	−28.2 (−9.5)[c]
2:12	(0, 1, 0, 0)	−32.0
3:12	(0, 0, 1, 0)	−35.9
12:12	(1, 3, 3, 1)	−29.8 (−9.3)[c]
	(0, 4, 4, 0)	−29.1
	(4, 0, 0, 4)	−31.5

[a] See the section Complete Occupation of the cus Sites (12:12 Coverage) for the notation used. [b] See Materials and Methods for the definition of the interaction energy for different coverages. [c] Interaction energies in parentheses calculated at the PBE level.

with an energetically homogeneous surface and no particularly strong adsorption sites; however, this is not the case for CuBTC, which is known to have coordinatively unsaturated metal sites. The unexpected results are discussed in the next subsection based on a theoretical investigation employing the DFT/CC method.

Computational Results. There are several adsorption sites available for CO_2 in CuBTC characterized by different adsorption enthalpies. It is shown below that the adsorption enthalpies of individual sites depend significantly on the amount of CO_2 adsorbed in the sample. It is therefore advantageous to describe the results for the CO_2 adsorption complexes for the low-coverage regime first, followed by the the complexes formed at higher coverages. The particular coverage is specified as X:12, where X is the number of CO_2 molecules in the CuBTC unit cell containing 12 cus sites.

Low-Coverage CO_2 Adsorption Behavior. The notation for CO_2 adsorption complexes in CuBTC introduced by Yildirim et al. is adopted here.[34] Three CO_2 adsorption sites have been identified (Figure 3): (i) sites in the close vicinity of the coordinatively unsaturated metal site are termed "coordinatively unsaturated sites" (cus sites), (ii) sites with the CO_2 molecule sitting in the one of the four triangular-shaped openings into the small tetrahedral cage are called "cage window sites", and (iii) sites in the center of a small tetrahedral cage are denoted as "cage center sites". The calculated characteristics (structural parameters and interaction energies) of the adsorption sites are reported in Tables 1 and 2, and the structural parameters used for the description of the adsorption complexes are shown in Figure 4.

Table 2. Characteristics of the CO_2 Adsorption Complexes on Cage Window and Cage Center Sites for Various CO_2 Coverages

coverage (CO_2 per Cu)	adsorption site characterization[a]	interaction energy[c] (kJ mol^{-1})	R(CO_2-Δ) (Å)	∠(CO_2-Δ) (°)
1:12	CW	−23.1 (−6.7)[d]	1.19	84.5
	CC	−23.2	3.47	23.5
13:12	CW_0	−24.4	1.18	90.0
	CW_1	−28.4	1.16	77.1
	CW_2	−27.6	1.42	73.2
	CW_3	−27.7	1.78	89.2
	CC	−25.2	3.44	23.6
16:12	cage 1	−30.0 (−30.5)[e]		
	CW_1		0.97	81.2
	CW_1		1.45	72.8
	CW_2		2.31	50.8
	CW_2		2.25	47.8
20:12	cage 1 and cage 2[b]	−29.4 (−27.1)[e]		
	CW_0		1.00	88.0
	CW_1		1.01	76.8
	CW_2		1.38	70.4
	CW_3		1.51	75.4

[a] Cage window and cage center sites denoted CW and CC, respectively. [b] Only the characteristics of the CO_2 molecules in the cage window sites of the second small cage are considered. [c] See Materials and Methods for the definition of the interaction energy for different coverages. [d] Interaction energy in parentheses calculated at the PBE level. [e] Interaction energies in parentheses calculated per one cage window site CO_2 molecule as defined by the reaction $^1/_4(CO_2)_{n-4}$CuBTC + CO_2 → $^1/_4(CO_2)_n$CuBTC.

The most stable CO_2 adsorption complex formed at low coverage (1:12) is the one formed on the cus site (ΔE_{int} = −28.2 kJ mol^{-1}). The stability of this CO_2 adsorption complex is driven by the interaction of CO_2 with the Cu^{2+} of the primary paddlewheel (R_{Cu-O} = 2.39 Å), and it is modulated by the electrostatic interaction with both the hydrogen of the trimesic acid and the Cu^{2+} cation of the secondary paddlewheel (R_{O-H} = 2.72 Å, R_{Cu-O} = 4.37 Å), as well as by the dispersion interaction with organic linkers (Figures 3 and 4). Althoug the CO_2 molecule remains linear, it is strongly tilted away from the Cu−Cu axis of the paddlewheel toward the Cu^{2+} ion of the neighboring paddlewheel (lying on the "edge" of the triangular-shaped opening to the small tetrahedral cage; ∠Cu−O−C = 123°). Note that the CO_2 adsorption complex with the end-on linear coordination (∠Cu−O−C = 174°) was localized as well; however, it is only a local minimum with ΔE_{int} = −21.9 kJ mol^{-1}.

Adsorption complexes on the cage window and cage center sites (see Figure 3) are almost isoenergetic at low coverage, about 5 kJ mol^{-1} less stable than the complex on the cus site. The CO_2 molecule in the cage window site is almost perpendicular to the cage opening and pulled slightly toward one of the copper atoms

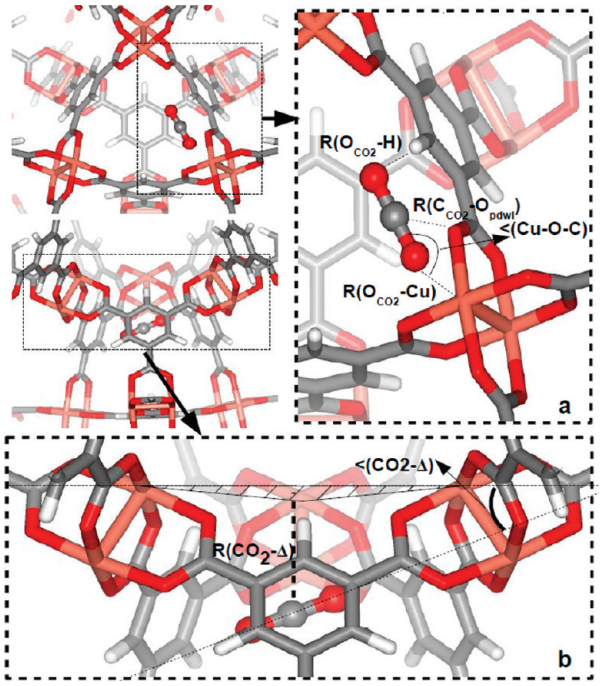

Figure 4. (a) Structure of the most stable CO_2 adsorption complex on the cus site and (b) definition of the structural parameters used for small cage window and cage center CO_2 adsorption sites. $R(CO_2\text{-}\Delta)$ is the distance of the carbon atom of the CO_2 molecule from the cage-entrance plane Δ defined by three Cu^{2+} ions in the cage window, and $\angle(CO_2\text{-}\Delta)$ is the angle between the C_∞ axis of CO_2 and the small cage-entrance plane. Cu, O, C, and H atoms are depicted in pink, red, gray, and white, respectively.

of the cage window (Figure 3b). Note that the symmetric CO_2 adsorption complex where the CO_2 molecular axis coincides with the C_3 axis of the small cage window was calculated to be only by ~0.7 kJ mol^{-1} less stable. The CO_2 adsorption complex formed inside the cage is almost parallel to the cage window, lying roughly in the plane formed by the three benzene rings forming the small cage walls (Figure 3c).

It follows that, in the low-coverage limit, the CO_2 molecules are preferentially adsorbed on cus sites. It is reasonable to assume that the first CO_2 molecule in the unit cell (UC) is on a cus site. The second CO_2 molecule in the UC (situation corresponding to 2:12 coverage) also preferentially adsorbs onto one of the 11 cus sites still available; on each of these 11 cus sites, the CO_2 molecule can adopt one of four different directions that are no longer equivalent because they are different with respect to the first CO_2 molecule. It turns out that all configurations with two CO_2 molecules per UC fall into one of the two energetically distinguishable cases: (i) In one case, both CO_2 molecules are located on the edges of the same triangular-shaped small cage opening, as in the situation shown in Figure 5a. The R_{C-C} distance between two CO_2 molecules is less than 4 Å, and it leads to an additional stabilization due to $CO_2\cdots CO_2$ interaction, $\Delta E_{int} = -32$ kJ mol^{-1}. A relatively large lateral interaction found for this CO_2 pair (−4.6 kJ mol^{-1} at the DFT/CC level) was also checked at the CCSD(T)/CBS level adopting the geometry from DFT/CC calculations; excellent agreement between the two methods was found (see Table S1 in the Supporting Information). (ii) In every other configuration of a pair of CO_2 molecules on cus sites, the CO_2 molecules are farther apart,

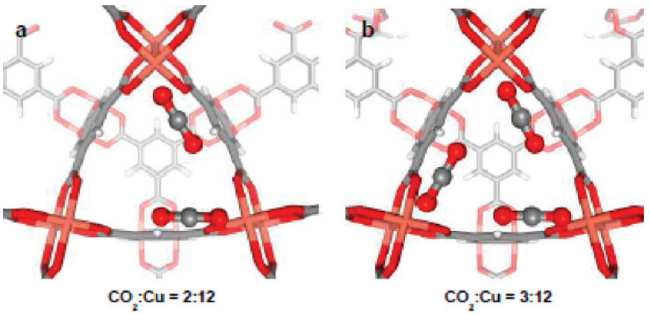

Figure 5. Structures of the CO_2 adsorption complexes on the cus sites for CO_2/Cu coverages of (a) 2:12 and (b) 3:12.

$R_{C-C} > 5.5$ Å, and the stabilization due to the lateral interaction does not exceed 1 kJ mol^{-1}. In line with the discussion above, three CO_2 molecules in a UC (3:12 coverage) are preferentially adsorbed (considering interaction energies) on the Cu^{2+} ions forming one small cage opening (Figure 5b). The interaction energy of the third CO_2 molecule in this case is $\Delta E_{int} = -35.9$ kJ mol^{-1}, about 7 kJ mol^{-1} more stable than other configurations on cus sites. The same arguments as above apply for additional CO_2 molecules in the coverage range from 4:12 to 11:12; therefore, they are not explicitly discussed here.

Complete Occupation of the cus Sites (12:12 Coverage). Considering now the situation where all cus sites in the UC are occupied by CO_2 molecules (12:12 coverage), it follows from the previous section that the energetically most stable configuration is the one where four of eight (triangular-shaped) small cage openings have all of their edges occupied by adsorbed CO_2 (Figure 5b) and the remaining four small cage openings do not contain any adsorbed CO_2 (on their edges). This configuration can be denoted $(4, 0, 0, 4)_{UC}$, where sequence of four integers denotes the numbers of small cage openings within the UC (eight in total) containing zero, one, two, and three CO_2 molecules, respectively. On the contrary, the least stable configuration (the one having the smallest lateral interactions) has one-half of the cage openings populated by two CO_2 molecules while the other half is filled with only a single CO_2 molecule, that is, the $(0, 4, 4, 0)_{UC}$ configuration. The average interaction energy per CO_2 molecule calculated for the $(4, 0, 0, 4)_{UC}$ and $(0, 4, 4, 0)_{UC}$ configurations at the DFT/CC level was −31.5 and −29.1 kJ mol^{-1}, respectively. Note a relatively small difference between the energies of the least and most stable configurations (2.4 kJ mol^{-1}) with 12 CO_2 molecules per UC. This suggests that the energetics of the particular configuration will have only a minor effect on the distribution of the configurations in CuBTC at this coverage range, especially at higher temperatures as the configurational entropy becomes more important.

Higher CO_2 Coverage. The CO_2 adsorption behavior for coverages higher than 12:12 is characterized by a gradual filling of the secondary adsorption sites, namely, the cage window and cage center sites. For the sake of simplicity, it is assumed that all 12 cus sites in the UC are filled first and only after that (starting at 13:12 coverage) can the cage window and cage center sites be occupied. Even with this simplification, the situation is complicated by the fact that there are many possible configurations of 12 CO_2 molecules on cus sites characterized by rather similar interaction energies (see above). To investigate the effects of different CO_2 configurations in cus sites on the CO_2 adsorption in cage sites, the $(1,3,3,1)_{UC}$ configuration is adopted.

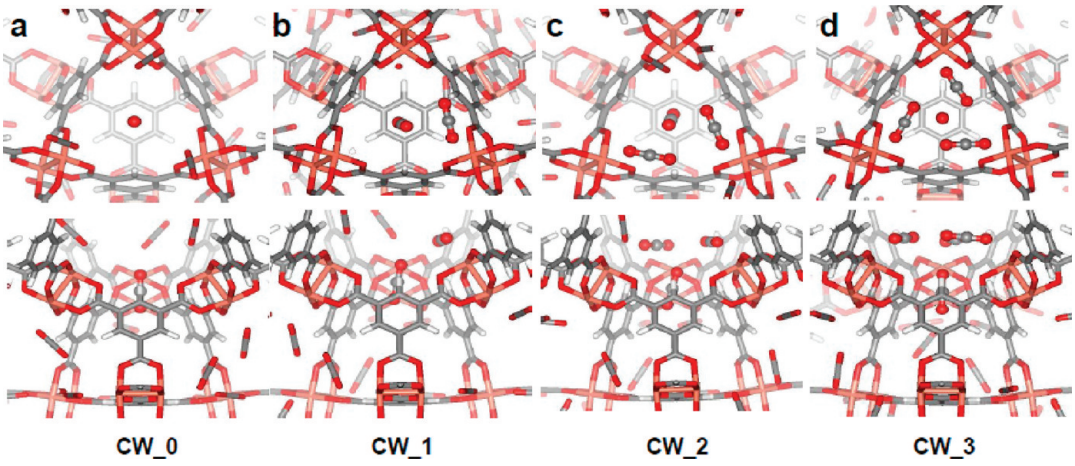

Figure 6. Structures of the CO_2 adsorption complexes for a CO_2/Cu coverage of 13:12 with different types of cage windows with respect to the number of cus CO_2 molecules present on the edges of the particular cage window: (a) zero, (b) one, (c) two, and (d) three CO_2 molecules. The upper and lower parts of the figure represent the views perpendicular and parallel, respectively, to one of the small cage openings.

This configuration contains four types of cage openings with respect to the number of cus CO_2 molecules on their edges. The different types of cage windows are denoted CW_x, where x is the number of cus CO_2 molecules on the edges of the particular cage opening (Figure 6). The average interaction energy per CO_2 molecule calculated for this particular configuration is -29.8 kJ mol^{-1}, which is precisely in the range set by the previous (extreme) configurations.

The presence of cus CO_2 molecules on the edges of the small cage window has a notable effect on the CO_2 adsorption in the cage sites. The interaction energy calculated for CO_2 adsorption in the CW_0 small cage window of -24.4 kJ mol^{-1} (Figure 6a) is only slightly higher than the corresponding interaction energy calculated at 1:12 CO_2 coverage. The interaction with the cage window site CW_1 is strengthened by a strong lateral interaction between a pair of CO_2 molecules (Figure 6b), resulting in $\Delta E_{int} = -28.4$ kJ mol^{-1}. (Note that this value is very close to the interaction energy found for a cus site at 1:12 coverage.) Similar values for the interaction energy are found for CO_2 adsorption on CW_1, CW_2, and CW_3 cage windows. This is likely due to the fact that the CO_2 molecule in the cage window site is pushed farther inside the small cage as the number of neighboring CO_2 molecules occupying cus sites increases; an increase in the R_{C-C} distance between CO_2 molecules from 3.9 to 4.3 Å is apparent from comparison of panels b and d in Figure 6. When CO_2 is adsorbed in CW_0 and CW_3 cage windows, the C_∞ axis coincides with the C_3 axis of the small cage window (Figure 6a,d), whereas in the case of CW_1 and CW_2, a moderate tilt of the CO_2 molecule off the C_3 axis is apparent (Figure 6b,c).

It is shown above that the CO_2 adsorption complexes in cage window sites are significantly stabilized (about 5 kJ mol^{-1}) by the presence of cus CO_2 molecules on the cage window edges. The stabilization effect is much less pronounced for CO_2 adsorption in cage center sites, which can be stabilized by at most 2 kJ mol^{-1} by CO_2 molecules in cus sites. The difference between the CO_2 adsorption complexes formed at cage window and cage center sites at 13:12 coverage can be understood simply by the fact that CO_2 molecules at cage center sites are farther from cus CO_2 molecules at the cage window edges. Therefore, only the CO_2 adsorption complexes formed at cage window sites were investigated for higher coverages.

For the sake of simplicity, the adsorption behavior of CO_2 molecules in cage sites was further investigated only for configurations with either completely filled or half-filled cage window sites in addition to all the cus sites being occupied; there are eight and four CO_2 molecules in cage window sites, respectively, in addition to the 12 CO_2 molecules in cus sites [UC in the $(1,3,3,1)_{UC}$ configuration]. In the case of the 16:12 coverage, there are about 70 distinguishable configurations of four CO_2 molecules in eight available cage window sites. To further investigate the effect of increasing CO_2-CO_2 lateral interactions (as its importance was shown above), a specific configuration of CO_2 molecules for the 16:12 coverage was chosen: all four CO_2 molecules in cage windows sites are sitting in the openings to the same small cage and the second small cage present in the CuBTC UC is empty. The average interaction energy per window site CO_2 molecule (see Table 2 for the definition of the average interaction energy) for the 16:12 coverage reaches -30.5 kJ mol^{-1}, and thus, it is even higher than the average interaction energy for the $(1,3,3,1)_{UC}$ cus monolayer (by 1 kJ mol^{-1}, Table 2). On the other hand, the average interaction energy per window site CO_2 molecule for the 20:12 coverage is only -27.1 kJ mol^{-1}. Note, however, that the interaction energy range for the aforementioned coverages is very much the same as the interaction energy range observed for the cus monolayer. It was further observed that the CO_2 molecules in cage window sites undergo changes with respect to their structural characteristics calculated for 13:12 configuration; some of the CO_2 molecules are only slightly displaced from their respective 13:12 configurations, whereas there are also cage window site CO_2 molecules that are pushed significantly inside the cage center, ending up halfway between the cage window site and the cage center site (see Figure S2, Supporting Information). The notable differences in both the average interaction energies and the amplitudes of the structural changes were found to stem from the different characters of the small tetrahedral cages (two in UC) in which the cage window site CO_2 molecules are accommodated; details about the CO_2 adsorption behavior for 16:12 and 20:12 coverage are presented in the Supporting Information.

Finally, the stability of the CO_2 molecule in the small cage center was reinvestigated for the 21:12 coverage (a single configuration only, with both cus and cage window sites fully

occupied); the calculated interaction energy is −32.6 kJ mol^{-1}, which is about 1−3 kJ mol^{-1} higher than the average interaction energy per CO_2 molecule for the monolayer and almost 10 kJ mol^{-1} higher than the interaction energy for the cage center site at zero coverage.

DISCUSSION

Three distinct CO_2 adsorption regimes have been identified computationally due to the heterogeneous nature of the surface of CuBTC (cus, small cage window, and cage center sites): (i) up to 12:12 coverage, filling of the cus sites; (ii) between 13:12 and 20:12 coverages, occupation of cage window sites; and (iii) above 20:12 coverage, filling of the centers of the small cages and large pores. The discussion of the computational results for a specific coverage region is complemented by a comparison with the relevant calorimetric data.

The low-coverage region is considered first. The calculated interaction energy for a single CO_2 molecule in the UC (1:12 coverage) is −28.2 kJ mol^{-1}. As the number of CO_2 molecules in the UC increases, the calculated interaction energies gradually increase as a consequence of the increasing importance of lateral interactions; the interaction energies for the 12:12 coverage range from −29.1 to −31.5 kJ mol^{-1} depending on the configuration of the CO_2 molecules. With respect to experimental data (Figure 2), both the "zero-coverage-limit" experimental adsorption enthalpy of −29 kJ mol^{-1} and the average adsorption enthalpy measured for the low-coverage region of −29.3 kJ mol^{-1} fall well within the energy range determined computationally, although no significant increase in the experimental adsorption enthalpy was observed going from 1:12 to 12:12 coverage. Note, however, that the higher value (−31.5 kJ mol^{-1}) of the calculated interaction energy corresponds to a rather extreme case in which all of the CO_2 molecules are localized in just four cage windows (largest lateral interactions). The number of occurrences of such a configuration is small compared to other possible, and only slightly less stable, distributions of the CO_2 molecules; hence, especially at higher temperatures, the entropy could render the most stable configurations less important. In addition, the experimental enthalpies remain relatively constant, indicating a fairly even distribution of CO_2 molecules between the cage windows in the coverage range below 13:12 and thus suggesting that a minor increase in the stability might not be sufficient to overcome an entropy contribution (at 30 °C).

Although the higher-coverage region from 13:12 to 20:12 corresponds to filling of the secondary adsorption sites (small cage windows), the presence of already adsorbed CO_2 molecules on the cus sites (cus monolayer) was shown to lead to an increase in the interaction energy of CO_2 in the cage window sites by up to 5 kJ mol^{-1}. Hence, for the 20:12 coverage, corresponding to the filling of all of the cage windows, an average interaction energy per CO_2 molecule of −29.4 kJ mol^{-1} was calculated. The corresponding experimental adsorption enthalpies remain constant (−29.3 kJ mol^{-1}) compared to the low-coverage-region adsorption heats, being thus well in line with the trend observed for the calculated CO_2 interaction energies.

A small gradual increase in adsorption enthalpy at CO_2 coverage above 21:12 is apparent from experimental data (Figure 2). Based on the results presented above, this is probably due to the increased importance of lateral interactions. The number of possible configurations of CO_2 molecules in CuBTC at higher CO_2 coverages is enormous; therefore, it is almost impossible to investigate this situation at the ab initio level. Only one particular configuration was investigated for the 21:12 CO_2 coverage: 12 CO_2 molecule on cus sites having a (1,3,3,1) distribution, 8 CO_2 molecules in cage window sites, and one CO_2 molecule in a cage center site. The calculated interaction energy for this 21st molecule at the cage center site is 32.6 kJ mol^{-1}, thus perfectly supporting our interpretation of experimental data based on the increased role of lateral interactions. Note that, if the CO_2 molecule in the cage center site is the only adsorbed molecule in the CuBTC unit cell, it has an interaction energy of only 23.2 kJ mol^{-1}; the stabilization due to lateral interactions is therefore almost 10 kJ mol^{-1}.

The results provided above can be directly compared with a recent neutron diffraction study of adsorption sites of CO_2 in CuBTC by Yildirim et al.[34] They reported diffraction data for two different CO_2 loadings (1.07 and 1.47 CO_2/Cu) locating a number of distinct adsorption sites and determining their occupancies for each CO_2 loading. Coordinatively unsaturated metal sites, cage window sites, and cage center sites were experimentally identified as the main CO_2 adsorption sites. Diffraction data collected for 1.07 CO_2/Cu (corresponding to ∼13:12 coverage) showed the CO_2 site occupancies to be 0.964 and 0.164 for cus and cage window sites, respectively. This is in very good agreement with the results reported above, and it provides further support for the assumption that cus sites are filled first. Furthermore, the reported structural characteristics of CO_2 adsorption complexes [strong tilt of the CO_2 molecule from the Cu−Cu axis of the paddlewheel toward the Cu^{2+} ion of neighboring paddlewheel, Cu−CO_2 distance, Cu−O−C angle, and $R(CO_2\text{-}\Delta)$ value] are in accordance with the calculated ones (see Tables 1 and 2 above and the Supporting Information for ref 34.)

The diffraction data collected for 1.47 CO_2/Cu (∼18:12 coverage) showed a non-negligible presence of the secondary CO_2 adsorption site identified as a small cage center site; CO_2 site occupancies were 0.974, 0.659, and 0.21 for cus, cage window, and cage center sites, respectively. The following interpretations can be drawn based on the results presented above: (i) Once the cus sites are fully occupied, the difference in stability between the cage window and cage center sites is only ∼3 kJ mol^{-1}, and as the cage window sites become populated, this difference is further reduced as result of the lateral interactions. (ii) Another interpretation originates from the observation that significant structural changes to the CO_2 adsorption complexes in the cage window sites take place in the case of the 16:12 coverage, where the final CO_2 structures are halfway between the structure of the "isolated" cage window site and the cage center site at 13:12 coverage (see Table 2 and Figure S2, Supporting Information). The structural refinement can identify such structures either as the cage window or the cage center sites, hence assigning some scattering length density to the cage center site. Such an assumption is further backed by the fact that the ratio of the occupations of the cage window and cage center sites is much closer to 3:1 than to 4:1 (four cage window sites and one cage center site per cage). Note that the two interpretations described above are not mutually exclusive and that the experimental observation might be due to a combination of both mechanisms. The excellent agreement between the experimental data obtained by Yildirim et al. and the results presented above indicates that the relative stabilities of the cus and cage window sites are well explained by the DFT/CC

calculations. As the nature of the CO_2 adsorption is very different for cus (electrostatic) and cage window sites (van der Waals), the agreement implies that the DFT/CC method is able to provide a balanced description of complicated systems having various types of interactions.

Although a number of simulation studies have considered the CO_2 adsorption behavior in CuBTC, only a few have reported quantities directly comparable to our simulation data, such as interaction energies and structures. At the same time, the reported values of the interaction energies depend heavily on the level of theory used and are somewhat ambiguous. The interaction energies calculated by the local density approximation (LDA) and generalized gradient approximation (GGA) are −33 and −7 kJ mol^{-1}, respectively.[34] An *NVT* simulation employing a combination of DREIDING and TraPPE force fields gives −15 and −22 kJ mol^{-1} for molecules in large pores and small cages, respectively.[43]

There are also a number of experimental studies reporting both adsorption isotherms and heats of adsorption for CO_2 on CuBTC at various coverages;[42−46] however, in many cases, the heats were obtained indirectly from adsorption isotherms measured at different temperatures using either the Clausius−Clapeyron equation[43,46] or a temperature-dependent isotherm equation.[45] Although these approaches can give reasonably accurate values for the heats of adsorption, they are limited by the quality of the fit of the experimental data and are therefore best done using data at many different temperatures. That being said, with the exception of the work in ref 43, all of the values reported in the literature are close to the enthalpies obtained in this study. Using the temperature-dependent form of the Sips equation, Aprea et al.[45] estimated a heat of adsorption assumed to be independent of loading at −25.9 kJ mol^{-1}. Wang and co-workers[44] determined isosteric heats by applying the Clausius−Clapeyron equation directly to experimentally measured isosteres at temperatures ranging from 120 to 290 K and pressures between 0.1 and 100 mbar and obtained a zero-coverage-limit adsorption heat value of −35 kJ mol^{-1}, which drops to −30 kJ mol^{-1} at 1 mmol/g (2:12 coverage) and then steadily decreases to bulk-phase sublimation heat of CO_2 (−25.3 kJ mol^{-1}) at about 10 mmol/g (24:12 coverage). Although the Clausius−Clapeyron equation assumes isosteric heats to be independent of temperature and completely reversible adsorption, a slightly different adsorption mechanism at these conditions is a likely cause for the minor discrepancies. At the same time, the presence of impurities in the framework such as a Cu_2O phase might explain the higher zero-coverage adsorption heat.[4,16]

Moellmer et al.[46] reported isosteric heats at different coverages determined in the temperature range of 308−343 K, and the zero-coverage heat (−29.2 kJ mol^{-1}) agrees perfectly with the value obtained in this study. At higher loadings, however, the calculated isosteric heats were found to decrease slightly with increasing coverage, whereas the experimental enthalpies measured here increased slightly. A possible explanation for this difference in tendency is the fact that the isotherms used to determine the isosteric heats were absolute rather than excess. Although the difference between excess and absolute amounts adsorbed remains small below 20 bar, the use of absolute amounts in the Clausius−Clapeyron equation is questionable.

Farrusseng et al.[43] reported heats of adsorption both calculated using the Clausius−Clapeyron equation (−12.1 kJ mol^{-1}) and measured using pulse−response experiments in an ultra-high-vacuum reactor system (−14.6 kJ mol^{-1}). These differ significantly from other values reported in the literature; however, this is to be expected as they estimated that the small tetrahedral cages were inaccessible in their sample. This is confirmed by the substantially lower amounts adsorbed (1.5 mmol g^{-1} at 313 K and 100 kPa) compared to those obtained by Moellmer et al.[46] (3.9 mmol g^{-1} at 308 K and 90 kPa) and in this study (3.8 mmol g^{-1} at 303 K and 90 kPa), even accounting for the differences in temperature.The only other adsorption heat measured directly was reported by Liang et al.[42] In their case, the enthalpy of adsorption was determined by differential thermal analysis (DTA), and the result (−30 kJ mol^{-1}) agrees very well with those of this study.

CONCLUSIONS

A rather unexpected dependence of the adsorption enthalpies on the CO_2 coverage has been found by microcalorimetry for CO_2 adsorption on CuBTC metal−organic framework. Adsorption enthalpies were found to remain almost unchanged at about −29 kJ mol^{-1} for coverages up to almost two CO_2 molecules per Cu^{2+} cus site. Together with the linear adsorption curve observed in the low-pressure region, this suggests that the adsorption sites in CuBTC are homogeneous. A completely different interpretation is given based on the theoretical investigation of the adsorption of CO_2 on CuBTC.

The CO_2 interaction with CuBTC has been described within the framework of a combined DFT−ab initio computation scheme. An excellent agreement between experimental and theoretical results reported here and excellent agreement of the calculated structures with the recently reported neutron diffraction data[34] allows us to draw the following conclusions:

(i) In the low-coverage regime (up to one CO_2 per Cu^{2+} site), CO_2 molecules adsorb onto cus sites. Only one CO_2 molecule can interact with each cus site. CO_2 molecules on cus sites are tilted toward the adjacent cus site, and their arrangement is such that the lateral interactions are maximized.

(ii) At higher coverages, up to CO_2/Cu = 20:12, CO_2 molecules preferentially occupy sites in the cage windows of small cages. Lateral interactions between CO_2 molecules in cage window sites and those already adsorbed on cus sites (about 5 kJ mol^{-1}) result in increased stability of CO_2 in cage windows sites, and as a result, the adsorption enthalpy remains unchanged.

(iii) At even higher coverages, CO_2 molecules adsorb in the center of small cages and in large cages. The lateral interactions between these molecules and those already adsorbed in cus sites and cage windows sites (amounting to almost 10 kJ mol^{-1}) are behind increasing adsorption enthalpies in the high-coverage regime, also observed experimentally.

The very good agreement between theoretical and experimental results should be also mentioned. The fact that the DFT/CC method used in this study provides a balanced description of CO_2 adsorption at rather different sites (electrostatic interaction with the coordinatively unsaturated metal site versus purely dispersion driven interaction in the cage window site) and that it properly accounts for lateral interactions is encouraging for future theoretical investigations of MOFs.

■ ASSOCIATED CONTENT

Supporting Information. Details on the construction of the DFT/CC correction functions [reference systems, CCSD(T)/CBS extrapolation scheme, etc.] and an expanded discussion of the higher-coverage CO_2 adsorption behavior. This material is available free of charge via the Internet at http://pubs.acs.org.

■ AUTHOR INFORMATION

Corresponding Author
*E-mail: petr.nachtigall@molecular.cz.

■ ACKNOWLEDGMENT

The research leading to these results received funding from the European Community's Seventh Framework Programme (FP7/2007-2013) under Grant 228862. MACADEMIA is a Large-Scale Integrating Project under the Nanosciences, Nanotechnologies, Materials and New Production Technologies Theme (www.macademia-project.eu). P.N. and L.G. also acknowledge the support of ME CR (Grants 7E09111 and MSM0021620857). J.S.C. acknowledges the financial support of KICOS and KRICT for the international collaboration program. We also thank You-Kyong Seo and Dr. Young Kyu Hwang for the synthesis.

■ REFERENCES

(1) Long, J. R.; Yaghi, O. M. *Chem. Soc. Rev.* **2009**, *38*, 1213–1214.
(2) Li, J. R.; Kuppler, R. J.; Zhou, H. C. *Chem. Soc. Rev.* **2009**, *38*, 1477–1504.
(3) Uemura, T.; Yanai, N.; Kitagawa, S. *Chem. Soc. Rev.* **2009**, *38*, 1228–1236.
(4) Alaerts, L.; Seguin, E.; Poelman, H.; Thibault-Starzyk, F.; Jacobs, P. A.; De Vos, D. E. *Chem.—Eur. J.* **2006**, *12*, 7353–7363.
(5) de Meester, P.; Fletcher, S. R.; Skapski, A. C. *Dalton Trans.* **1973**, 2575–2578.
(6) Chui, S. S. Y.; Lo, S. M. F.; Charmant, J. P. H.; Orpen, A. G.; Williams, I. D. *Science* **1999**, *283*, 1148–1150.
(7) Getzschmann, J.; Senkovska, I.; Wallacher, D.; Tovar, M.; Fairen-Jimenez, D.; Duren, T.; Van Baten, J. M.; Krishna, R.; Kaskel, S. *Microporous Mesoporous Mater.* **2010**, *136*, 50–58.
(8) Rowsell, J. L. C.; Yaghi, O. M. *J. Am. Chem. Soc.* **2006**, *128*, 1304–1315.
(9) Xiao, B.; Wheatley, P. S.; Zhao, X.; Fletcher, A. J.; Fox, S.; Rossi, A. G.; Megson, I. L.; Bordiga, S.; Regli, L.; Thomas, K. M.; Morris, R. E. *J. Am. Chem. Soc.* **2007**, *129*, 1203–1209.
(10) Vitillo, J. G.; Regli, L.; Chavan, S.; Ricchiardi, G.; Spoto, G.; Dietzel, P. D. C.; Bordiga, S.; Zecchina, A. *J. Am. Chem. Soc.* **2008**, *130*, 8386–8396.
(11) Li, Y.; Yang, R. T. *AIChE J.* **2008**, *54*, 269–279.
(12) Millward, A. R.; Yaghi, O. M. *J. Am. Chem. Soc.* **2005**, *127*, 17998–17999.
(13) Wang, S.; Yang, Q.; Zhong, C. *Sep. Purif. Technol.* **2008**, *60*, 30–35.
(14) Karra, J. R.; Walton, K. S. *J. Phys. Chem. C* **2010**, *114*, 15735–15740.
(15) Pérez-Mayoral, E.; Čejka, J. *ChemCatChem* **2011**, *3*, 157–159.
(16) Schlichte, K.; Kratzke, T.; Kaskel, S. *Microporous Mesoporous Mater.* **2004**, *73*, 81–88.
(17) Seo, Y.-K.; Hundal, G.; Jang, I. T.; Hwang, Y. K.; Jun, C.-H.; Chang, J.-S. *Microporous Mesoporous Mater.* **2009**, *119*, 331–337.
(18) Chowdhury, P.; Bikkina, C.; Meister, D.; Dreisbach, F.; Gumma, S. *Microporous Mesoporous Mater.* **2009**, *117*, 406–413.
(19) Karra, J. R.; Walton, K. S. *Langmuir* **2008**, *24*, 8620–8626.
(20) Wu, H.; Simmons, J. M.; Liu, Y.; Brown, C. M.; Wang, X.-S.; Shengqian, M.; Peterson, V. K.; Southon, P. D.; Kepert, C. J.; Zhou, H.-C.; Yildirim, T.; Zhou, W. *Chem.—Eur. J.* **2010**, *16*, 5205–5214.
(21) Dubbeldam, D.; Krishna, R.; Snurr, R. Q. *J. Phys. Chem. C* **2009**, *113*, 19317–19327.
(22) Yazaydin, A. O.; Benin, A. I.; Faheem, S. A.; Jakubczak, P.; Low, J. J.; Richard, R. W.; Snurr, R. Q. *Chem. Mater.* **2009**, *21*, 1425–1430.
(23) Grajciar, L.; Bludsky, O.; Nachtigall, P. *J. Phys. Chem. Lett.* **2010**, *1*, 3354–3359.
(24) Bludský, O.; Rubeš, M.; Soldán, P.; Nachtigall, P. *J. Chem. Phys.* **2008**, *128*, 114102.
(25) Rubes, M.; Kysilka, J.; Nachtigall, P.; Bludsky, O. *Phys. Chem. Chem. Phys.* **2010**, *12*, 6438–6444.
(26) Zukal, A.; Pulido, A.; Gil, B.; Nachtigall, P.; Bludsky, O.; Rubes, M.; Cejka, J. *Phys. Chem. Chem. Phys.* **2010**, *12*, 6413–6422.
(27) Maurin, G.; Llewellyn, P. L.; Bell, R. G. *J. Phys. Chem. B* **2005**, *109*, 16084–16091.
(28) Llewellyn, P. L.; Maurin, G.; Devic, T.; Loera-Serna, S.; Rosenbach, N.; Serre, C.; Bourrelly, S.; Horcajada, P.; Filinchuk, Y.; Ferey, G. *J. Am. Chem. Soc.* **2008**, *130*, 12808–12814.
(29) Yoon, J. W.; Seo, Y.-K.; Hwang, Y. K.; Chang, J.-S.; Leclerc, H.; Wuttke, S.; Bazin, P.; Vimont, A.; Daturi, M.; Bloch, E.; Llewellyn, P. L.; Serre, C.; Horcajada, P.; Greneche, J.-M.; Rodrigues, A. E.; Ferey, G. *Angew. Chem., Int. Ed.* **2010**, *49*, 5949–5952.
(30) Llewellyn, P. L.; Maurin, G.; Poyet, T.; Dufau, N.; Denoyel, R.; Rouquerol, F. *Adsorption* **2005**, *11*, 73–78.
(31) Llewellyn, P. L.; Maurin, G. *C. R. Chim.* **2005**, *8*, 283–302.
(32) Soldán, P.; Hutson, J. M. *J. Chem. Phys.* **2000**, *112*, 4415–4416.
(33) Bludský, O.; Rubeš, M.; Soldán, P. *Phys. Rev. B* **2008**, *77*, 092103.
(34) Wu, H.; Simmons, J. M.; Srinivas, G.; Zhou, W.; Yildirim, T. *J. Phys. Chem. Lett.* **2010**, *1*, 1946–1951.
(35) Peterson, K. A.; Puzzarini, C. *Theor. Chem. Acc.* **2005**, *114*, 283–296.
(36) Dunning, T. H. *J. Chem. Phys.* **1989**, *90*, 1007–1023.
(37) Blöchl, P. E. *Phys. Rev. B* **1994**, *50*, 17953–17979.
(38) Perdew, J. P.; Burke, K.; Ernzerhof, M. *Phys. Rev. Lett.* **1996**, *77*, 3865–3868.
(39) Perdew, J. P.; Burke, K.; Ernzerhof, M. *Phys. Rev. Lett.* **1997**, *78*, 1396–1396.
(40) Werner, H.-J.; Knowles, P. J.; Lindh, R.; Manby, F. R.; Schültz, M.; Celani, P.; Korona, T.; Berning, A. A.; Cooper, D. L.; Deegan, M. J. O.; Dobbyn, A. J.; Eckert, F.; Goll, E.; Hampel, C.; Hetzer, G.; Hrenar, T.; Knizia, G.; Koeppl, C.; Liu, Y.; Lloyd, A. W.; Palmieri, R. P.; Pfluger, K.; Pitzer, R.; Reiher, M.; Schumann, U.; Stoll, H.; Stone, A. J.; Tarroni, R.; Thorsteinsson, T.; Wang, M.; Wolf, A. *Molpro*, version 2009.1; University College Cardiff Consultants Limited: Cardiff, U.K., 2009.
(41) Kresse, G.; Hafner, J. *Phys. Rev. B* **1993**, *48*, 13115–13118.
(42) Liang, Z.; Marshall, M.; Chaffee, A. L. *Energy Fuels* **2009**, *23*, 2785–2789.
(43) Farrusseng, D.; Daniel, C.; Gaudillère, C.; Ravon, U.; Schuurman, Y.; Mirodatos, C.; Dubbeldam, D.; Frost, H.; Snurr, R. Q. *Langmuir* **2009**, *25*, 7383–7388.
(44) Wang, Q. M.; Shen, D. M.; Bülow, M.; Lau, M. L.; Deng, S. G.; Fitch, F. R.; Lemcoff, N. O.; Semanscin, J. *Microporous Mesoporous Mater.* **2002**, *55*, 217–230.
(45) Aprea, P.; Caputo, D.; Gargiulo, N.; Iucolano, F.; Pepe, F. *J. Chem. Eng. Data* **2010**, *55*, 3655–3661.
(46) Moellmer, J.; Moeller, A.; Dreisbach, F.; Glaeser, R.; Staudt, R. *Microporous Mesoporous Mater.* **2011**, *138*, 140–148.

Attachment D

THE JOURNAL OF PHYSICAL CHEMISTRY C

ARTICLE

pubs.acs.org/JPCC

Accurate Prediction of Methane Adsorption in a Metal−Organic Framework with Unsaturated Metal Sites by Direct Implementation of an ab Initio Derived Potential Energy Surface in GCMC Simulation

Linjiang Chen,[†] Lukáš Grajciar,[‡] Petr Nachtigall,[‡] and Tina Düren*[,†]

[†]Institute for Materials and Processes, School of Engineering, The University of Edinburgh, King's Buildings, Edinburgh, EH9 3JL, United Kingdom

[‡]Department of Physical and Macromolecular Chemistry, Faculty of Science, Charles University in Prague, Hlavova 2030, CZ-128 40 Prague 2, Czech Republic

Supporting Information

ABSTRACT: Whereas grand-canonical Monte Carlo (GCMC) simulations based on generic force fields provide good predictions of adsorption isotherms in metal−organic frameworks (MOFs), especially at higher temperature, they fail to correctly describe the adsorption mechanism in MOFs with coordinatively unsaturated sites (cus's) at low temperatures, even for nonpolar fluids such as methane. To address this problem, we directly implemented the potential energy surface calculated by a hybrid DFT/ab inito method in the GCMC simulations using the adsorption of methane on CuBTC as an example. A comparison with previously published in situ experiments shows that our approach not only quantitatively predicts adsorption isotherms for a wide range of temperatures and pressures but also provides the correct description of the adsorption mechanism, including adsorption on the cus's. We also show that care must be taken when selecting the ab initio method to be coupled with GCMC simulations to obtain accurate predictions.

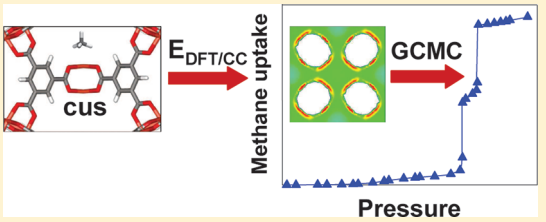

INTRODUCTION

There has been great interest in metal−organic frameworks (MOFs) in the past decade. Synthesized in a self-assembly process from metal corner units bridged by organic linkers, MOFs can be readily tailored for specific applications by choosing appropriate building blocks and/or by introducing functional groups.[1−4] MOFs have been assessed for a number of applications including gas storage and separation,[5−8] catalysis,[9,10] drug delivery,[11,12] optical and electronic applications,[13−15] and sensing.[16,17] The possibility of incorporating coordinatively unsaturated metal sites (cus's), also known as unsaturated metal centers or open metal sites, into the framework makes MOFs even more attractive for areas such as catalysis[18,19] and drug delivery (where cus's contribute to controlled release).[11] Coordinatively unsaturated sites also play an important role in the adsorption of various gases, including methane,[20−22] hydrogen,[23−25] and carbon dioxide,[26,27] especially at low loadings when host−guest interactions play a predominant role.

Molecular simulation has evolved into an important tool that not only allows predictions of macroscopic adsorption performance but also provides a detailed picture on the molecular scale that permits detailed exploration of the adsorption mechanism.[28−30] Most molecular simulation studies use Lennard-Jones parameters taken from generic force fields, such as UFF,[31] DREIDING,[32] and OPLS-AA,[33] that were not specifically developed for MOFs. Although these force fields do surprisingly well for many MOFs, they fail to correctly describe the interaction with cus's where the distance between the metal atom and the fluid molecule is often considerably less than the combined hard-sphere diameter.[20,34,35] In contrast, ab initio calculations provide an accurate description of the interactions and distances,[30,36,37] yet they allow only the description of the interaction of individual molecules with open metal sites and not the prediction of whole isotherms. To obtain quantitative predictions of adsorption isotherms in MOFs with cus's, two distinct approaches have been used. One is to refit the Lennard-Jones parameters of the metal atoms[38,39] or the partial charges of the framework[40] to experimental isotherms. Although this approach gives good predictions of adsorption isotherms at different temperatures, for example, questions remain about the transferability of these parameters to other fluids or—as experimental isotherms vary widely depending on the synthesis and activation procedure[41]—even to different samples of the same material. Furthermore, it is unclear whether this approach leads to a realistic representation of the adsorption mechanism. In the other approach, the potential for the cus's is derived directly from ab initio calculations.[42,43] However, great care must be taken when selecting a suitable method for the description of a particular system, as methods based on density function theory (DFT) can fail in the description of dispersion interactions and the charge distribution between organic linkers and metal cus's.[30,37]

Received: September 20, 2011
Published: October 18, 2011

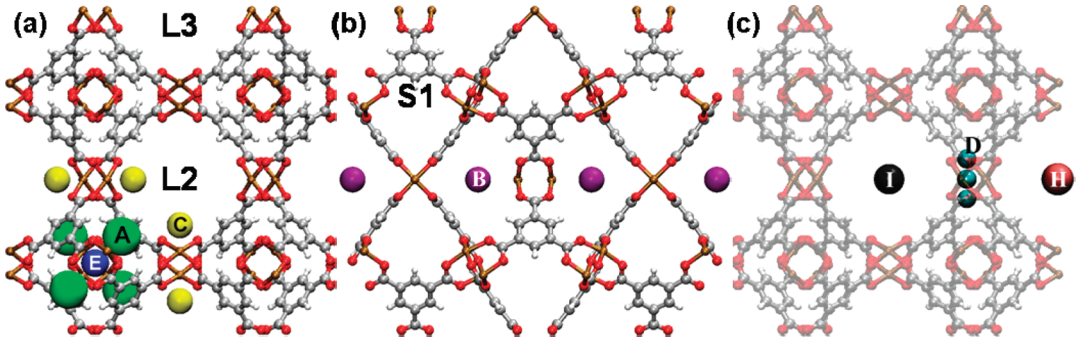

Figure 1. Structure of CuBTC viewed from the (a,c) front and (b) side: gray, carbon; white, hydrogen; brown, copper; red, oxygen. Experimental adsorption sites are represented by colored spheres: sites E (blue), I (black), and H (pink) are located at the center of pores S1, L2, and L3, respectively; sites A (green) and D (cyan) are located at the center of the windows of S1 and L2, respectively; two secondary adsorption sites G and F are close to sites A and D, respectively (not shown); site B (purple), the main adsorption site in L2, is close to the corner of two neighboring BTC ligands connected by copper ions; site C (yellow), the main adsorption site in L3, is located close to the Cu^{II} coordinatively unsaturated site.

Here, we directly combine ab initio methods with classical grand-canonical Monte Carlo (GCMC) simulations by implementing the potential energy surface (PES) calculated from ab initio calculations in a GCMC simulation and thus removing the ambiguity and inaccuracies resulting from generic force fields. In our approach, the combined dispersive and electrostatic fluid−framework interactions are directly taken from ab initio calculations. To illustrate our method, we studied the adsorption of methane in CuBTC[44] at 77 K. We chose this system because (1) the importance of cus's, even for nonpolar fluids such as methane, has been observed experimentally;[20,22,27,35] (2) methane is a nearly spherical molecule, so the orientation dependence of the methane−framework potential energy can be neglected, which significantly reduces computational costs; and (3) detailed information about the adsorption sites is available from experimental in situ X-ray diffraction (XRD) experiments.[20] We used the same notations for the pores and adsorption sites in CuBTC as specified in reference 20. In brief, the CuBTC framework contains three types of pores: S1, with a diameter of 4.9 Å (calculated as the diameter of the largest sphere that fits into the cavity without overlapping with the framework atoms)[45] and center at (0.25, 0.25, 0.25) (Wyckoff notation); L2, with a diameter of 10.5 Å and center at (0.5, 0.5, 0.5); and L3, with a diameter of 12.2 Å and center at (0.0, 0.0, 0.0). A total of nine adsorption sites were identified from neutron diffraction experiments, as shown in Figure 1. Their crystallographic positions are reported in Table S1 of the Supporting Information. The distance observed experimentally between CD_4 and the copper ion is 3.075 Å. As this distance is considerably smaller than the Lennard-Jones parameter σ_{CH_4-Cu} [$0.5(\sigma_{CH_4} + \sigma_{Cu}) = 3.422$ Å], it is obvious that the UFF-based GCMC simulation cannot reproduce adsorption on the cus's.

COMPUTATIONAL DETAILS

In recent work,[37] we compared the suitability of various theoretical methods and models for the description of water adsorption on cus's in copper(II) benzene-1,3,5-tricarboxylate (CuBTC) and demonstrated that the hybrid DFT/ab initio method DFT/CC[46−48] provides an accurate description. Furthermore, this method was recently shown to give accurate descriptions of CO_2 interaction with cus's and other sites in CuBTC.[30] Here, we use DFT/CC to obtain the methane−framework PES by placing the carbon atom of a single methane molecule in a random configuration on specific grid points and calculating the interaction energies with the CuBTC framework. The potential energy grid was then used to calculate the CuBTC−CH_4 interaction in the GCMC simulations. For comparison, we also simulated adsorption isotherms using classical, generic force fields and using the PES obtained at the DFT level.

Ab Initio Host−Guest Interaction Potential. The methane−framework potential energy surface was represented on a precalculated three-dimensional Cartesian grid neglecting the orientation dependence of the interaction potential (which is small, as methane is a spherical molecule) and keeping the CuBTC framework rigid. The methane−framework potential energy was calculated at the DFT/CC level as

$$E_{int} = E(\text{CuBTC}\cdots\text{CH}_4) - E(\text{CuBTC}) - E(\text{CH}_4) + \Delta E_{DFT/CC} \quad (1)$$

where $E(CH_4)$, E(CuBTC), and $E(\text{CuBTC}\cdots\text{CH}_4)$ are the total energies of the CH_4 molecule, CuBTC framework, and CH_4/CuBTC system, respectively, calculated at the PBE level with the periodic model (see below). $\Delta E_{DFT/CC}$ is the DFT/CC correction described below. The frozen monomer approximation was adopted, employing the CCSD(T)/AVQZ-optimized geometry of CH_4 and the experimental geometry of CuBTC.

First, the interaction potential was evaluated on the equally spaced 2-Å grid with the exclusion of the grid points in close contact with the framework (less than 1.5 Å from the framework atoms). Based on these values, a refinement of the grid was performed, introducing a denser grid especially in the vicinity of adsorption sites A−C and E. The grid was constructed from about 2000 grid points for which the interaction potential was explicitly evaluated. By taking into account the symmetry of the individual sites, the number of grid points was increased to a few tens of thousands. Finally, to obtain the equally spaced 0.25-Å grid used in the GCMC simulations, a three-dimensional linear interpolation was used to determine the potential energy between a methane molecule and the CuBTC framework.

DFT/CC Method. We used the recently proposed DFT/CC method[46−48] for the calculation of the methane−framework interaction potential, as it was found previously[30,37] to perform significantly better than both the (pure) DFT and the (dispersion-corrected) DFT-D approaches. The DFT/CC method is based on the pairwise representability of the DFT error, ΔE,

defined as

$$\Delta E = E_{CCSD(T)} - E_{DFT} \quad (2)$$

where $\Delta E_{CCSD(T)}$ and ΔE_{DFT} are the interaction energies calculated at the CCSD(T)/CBS and DFT/AVQZ levels of theory, respectively. Within the DFT/CC method, the DFT error, ΔE, is expressed as the sum of the atom−atom correction functions $\varepsilon_{ij}(R_{ij})$

$$\Delta E = \sum_{ij} \varepsilon_{ij}(R_{ij}) \quad (3)$$

where R_{ij} is the distance between atoms i and j. No explicit functional form for the ε_{ij} correction functions is assumed; instead, a reproducible kernel Hilbert space interpolation is used.[49] In addition to the assumption about pairwise representability of the DFT error (eq 3), transferability of the correction functions from the reference system to the system of interest is assumed. An extension of the DFT/CC method for the CH_4/CuBTC system is described below, whereas a more detailed description of the DFT/CC method can be found elsewhere.[46,50]

To evaluate the DFT/CC corrections (eq 3), the PBE/AVQZ and CCSD(T)/CBS calculations on the reference set were carried out; for details, see the Supporting Information. The correction functions ε_{HH}, ε_{HC}, ε_{CH}, ε_{CC}, ε_{HO}, ε_{CO}, and ε_{CCu} (ε_{HCu}) were evaluated from the one-dimensional potential energy curves of $H_2\cdots H_2$, $H_2\cdots C_6H_6$, $CH_4\cdots H_2$, $CH_4\cdots C_6H_6$, $H_2\cdots CO_2$, $CH_4\cdots CO_2$, and $CH_4\cdots Cu(HCOO)_2$ reference complexes, respectively. The DFT/CC reference complexes are shown in Figure S1 in the Supporting Information. The assumption of the DFT/CC correction transferability was tested by calculations carried out for a larger $(CH_4)_2\cdots Cu_2(HCOO)_4$ cluster model at the CCSD(T)/CBS level (on the PBE/VTZ-optimized geometry). The interaction energy of the CH_4 molecule with the $Cu_2(HCOO)_4$ cluster model of −13.50 kJ mol^{-1} calculated at the DFT/CC level was found to be in excellent agreement with the CCSD(T)/CBS value of −13.48 kJ.mol^{-1}.

The periodic DFT calculations of the interaction of a methane molecule with CuBTC were modeled using the experimental rhombohedral primitive cell (RPC; $a = b = c = 18.627$ Å, $\alpha = \beta = \gamma = 60°$, and $V = 4570.205$ Å^3) of CuBTC including two small tetrahedral cages and containing 156 framework atoms (of which 12 were copper, 48 oxygen, 24 hydrogen, and 72 carbon atoms). The projector augmented wave (PAW)[51] approximation and a plane-wave basis set with a kinetic energy cutoff of 600 eV were used; Brillouin-zone sampling was restricted to the Gamma point. The Perdew−Burke−Ernzerhof (PBE) exchange−correlation functional was employed.[52] Calculations with cluster models and calculations with periodic models were performed with the Molpro 09[53] and VASP 5.2[54] program suites, respectively.

GCMC Simulations. Methane adsorption in CuBTC was studied using GCMC simulations implemented in the multipurpose simulation code MUSIC.[55] Details of the method are given elsewhere.[56] The atomistic representation of the CuBTC framework was constructed from the experimental crystallographic data[44] with all atoms kept fixed at their positions during the simulation. In the DFT/CC-PES GCMC simulations, the methane−framework interaction was determined from the pretabulated potential determined by DFT/CC. For comparison, we also carried out simulations using three classical force fields

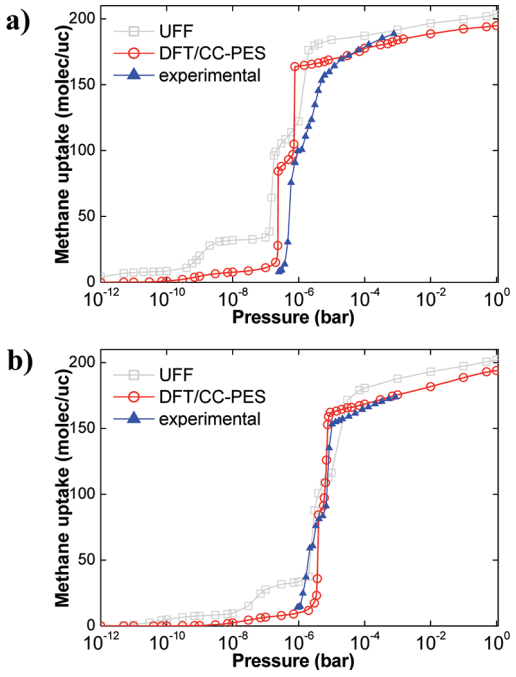

Figure 2. Methane adsorption isotherms for CuBTC at (a) 77 and (b) 87 K. Note that the isotherms are represented on a logarithmic pressure axis to better show the adsorption behavior at low pressures. Experimental data were taken from the work of Getzschmann et al.[20]

for the framework (UFF,[31] DREIDING,[32] and OPLS-AA[33]). The model used for methane was derived by Goodbody et al. and used a united-atom description of the methane molecules (denoted UA); that is, one methane molecule was represented by a single sphere ($\sigma_{CH_4} = 3.73$ Å, $\varepsilon_{CH_4}/k_B = 148.00$ K).[57] To check the influence of the methane model, methane was modeled as a five-atom molecule from the TraPPE-EH force field[58] for one of the isotherms shown in Figure S2 (Supporting Information). All methane−methane interactions and all generic-force-field-based methane−framework interactions were modeled using the standard 12−6 Lennard-Jones (LJ) potential. The Lorentz−Berthelot combining rules were used to calculate the LJ cross-parameters. Interactions beyond 18.650 Å were neglected. Each simulation consisted of an equilibration period of 2.0×10^7 iterations followed by a production run of a further 2.0×10^7 iterations, carefully ensuring that equilibrium was reached.

To compare the simulation and the experimental results, the absolute amount adsorbed from a GCMC simulation was converted into the excess amount adsorbed using the method of Myers and Monson.[59] The excess amount of methane adsorbed, n_{excess}, is given by

$$n_{excess} = n_{abs} - \frac{pV_{pore}}{ZRT} \quad (4)$$

where n_{abs} is the absolute amount adsorbed, p is the bulk pressure, V_{pore} is the pore volume, Z is the compressibility factor, and T is the temperature. The Peng−Robinson equation of state was used to estimate Z. The accessible pore volume, V_{pore}, was taken to be equal to the experimentally determined value of 0.72 cm^{3}g^{-1}.[20]

To determine the occupancies of the different adsorption sites, a sphere of radius $R = 0.316$ Å was defined around each experimental adsorption site. Any methane molecule falling into

dx.doi.org/10.1021/jp2090878 |J. Phys. Chem. C 2011, 115, 23074–23080

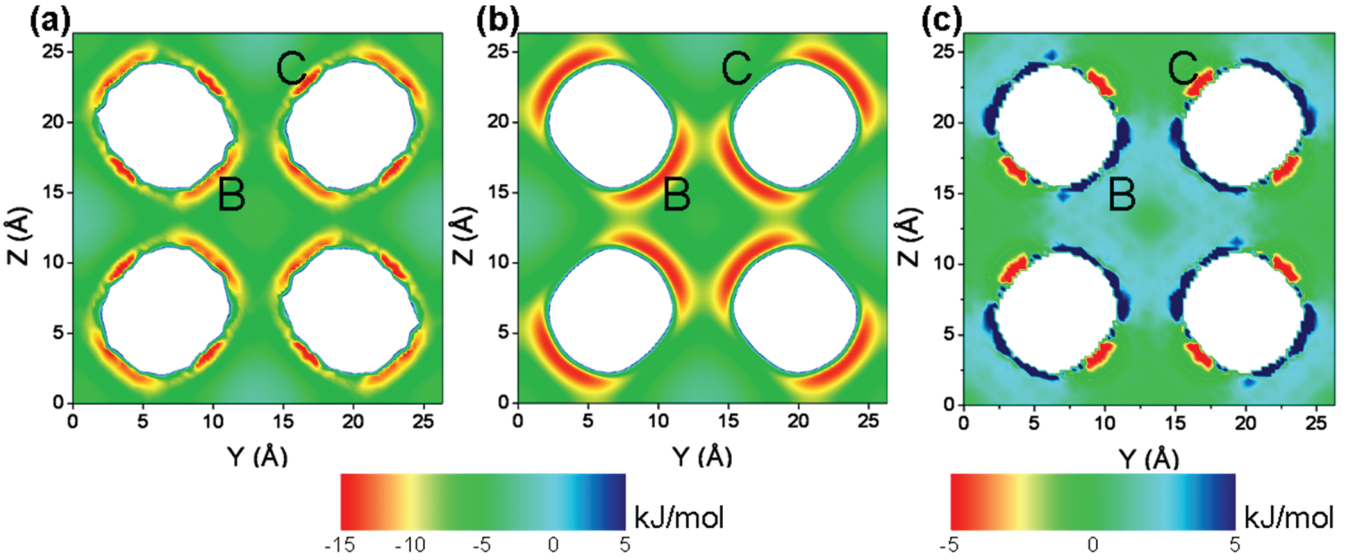

Figure 3. Contour plots of the potential energy between a methane molecule and the CuBTC framework on the (200) plane for (a) DFT/CC-PES, (b) UFF and (c) the difference, E(DFT/CC-PES) − E(UFF). Adsorption sites B and C (at the cus's) are labeled. The white space corresponds to the CuBTC framework.

this sphere during the simulation was counted toward the occupancy of the corresponding site. Larger values for R would result in the same methane molecule being assigned to two different experimental adsorption sites, especially for the secondary sites G and F, which are close to sites A and D, respectively.

RESULTS AND DISCUSSION

We compare the results from our ab initio-based PES GCMC simulations with experimental results from recent work by Getzschmann et al.,[20] which serves as an excellent benchmark for assessing our method, as both adsorption isotherms and adsorption sites were determined experimentally and simulations using the UFF force field in the same work highlighted the shortcomings of using parameters from the generic UFF force field.

Methane adsorption isotherms obtained from both DFT/CC and UFF-based GCMC simulations at 77 and 87 K are shown in Figure 2. Experimentally, it was determined that CuBTC contains 88 favorable adsorption sites for methane: 40 are located in the small S1 pores [one in the center (site E) and one in each of the four windows (site A) of the eight S1 pores] and 48 are located at the cus's. The step in the experimental isotherm at 85 molecules per unit cell (uc) was attributed to the filling of these sites.[20] In contrast, simulations based on the UFF force field showed a step at 40 molecules/uc corresponding to the filling of the small S1 pores and failed to capture adsorption on the cus's. Figure S2 in the Supporting Information shows that this failure to correctly predict the adsorption mechanism is not unique to the UFF force field but applies to all other generic force fields tested. In contrast, the DFT/CC-PES simulations captured the shape of the isotherms including the step and the maximum uptake at both 77 and 87 K very well. The DFT/CC-PES GCMC simulations were also performed for higher temperatures (up to 373 K) with pressures up to 200 bar. Again, quantitative agreement with the experimental isotherms was obtained (Figure S3 in the Supporting Information).

To illustrate the difference between the fluid−framework potential energy derived from UFF and DFT/CC, contour plots for the (200) planes (Miller indices) are given in Figure 3. Note that the lower (i.e., more negative) the potential energy, the stronger the interaction. The differences are clearly observable. Site C, the adsorption site for the cus's, shows a very strong interaction for the DFT/CC-PES whereas it is absent from the PES derived from the UFF force field. Another remarkable difference, which has a significant impact on the adsorption mechanism, is that site B, the main adsorption site inside the large L2 pore, is characterized by a weaker interaction between methane and the framework in the DFT/CC-PES (compare Figure 3c).

To confirm that the DFT/CC-PES leads to a correct description of the adsorption mechanism, we determined the adsorption sites for methane in CuBTC at three loadings, namely, 8, 88, and 176 molecules/uc, corresponding to the steps in the adsorption isotherm at 77 K. For the last loading, experimental data from in situ XRD measurements are available from reference 20.

A comparison of the occupancy of the different adsorption sites together with their potential energies is given in Table 1. The DFT/CC-PES simulation results quantitatively capture the experimentally determined adsorption sites at a loading of 176 molecules/uc, including the open metal sites (site C). For this site, the DFT/CC-PES simulation gives an occupancy of 96% corresponding to 46.25 of the 48 cus's being occupied by methane, which is in very good agreement with the experimental result (93%). The simulated average distance between methane molecules and the copper ion of the cus is 3.097 Å, in excellent agreement with the experimental value of 3.075 Å.[20] This gives us confidence that the DFT/CC-PES GCMC simulations provide a correct description of the adsorption mechanism of methane at 77 K in CuBTC. It is worth pointing out that the characteristic steps in the adsorption isotherm are caused by the difference in potential energies of the main adsorption sites, and we continue by contrasting the adsorption mechanism predicted from the DFT/CC-PES with that predicted using the UFF force field. At low loading (8 molecules/uc), the two methods predict the same adsorption mechanism, where the centers of the eight S1 pores (site E) are the most attractive sites for methane because of the enhanced dispersion interaction in the small pores. The other site

Table 1. Potential Energy and Loading of CH_4 Molecules Identified for Each Adsorption Site at Different Loadings

	potential energy (kJ/mol)		8 molecules/uc		88 molecules/uc		176 molecules/uc		
site	DFT/CC	UFF[a]	DFT/CC	UFF[a]	DFT/CC	UFF[a]	DFT/CC	UFF[a]	expt[b]
A	−14.20	−17.49	1.12	1.21	31.37	31.12	22.38	20.57	24.76
B	−10.45	−12.66	0.00	0.00	1.88	38.25	47.62	48.00	48.00
C	−13.23	N/A	0.00	0.00	46.75	0.00	46.25	0.00	44.63
D	−8.05	−10.88	0.00	0.00	0.00	10.88	29.12	32.13	27.80
E	−18.70	−22.70	6.88	6.79	8.00	2.63	8.00	8.00	6.39
F	−7.90	−10.04	0.00	0.00	0.00	2.12	4.87	19.88	4.00
G	−12.59	−16.33	0.00	0.00	0.00	0.00	10.12	12.15	11.76
H	−1.50	−2.02	0.00	0.00	0.00	0.00	3.52	31.27	4.00
I	−3.36	−4.04	0.00	0.00	0.00	3.00	4.12	4.00	*c*

[a] Results from the UFF-based simulations done in this work. [b] Experimental results from ref 20, where 171.21 of 176 molecules/uc were resolved. (Note that this is the only loading for which occupancies were reported in ref 20.) [c] Not reported in ref 20.

that becomes occupied at this loading—but to a much lesser extent—is site A, the center of the windows to the small cavities, of which 32 are present in the CuBTC unit cell. At higher loadings, the differences in the adsorption mechanisms predicted by the two methods become apparent. Whereas both methods predict a nearly 100% occupancy of site E, the center of the small S1 pore, the DFT/CC-PES simulations show that the next adsorption sites to be occupied are the cus's (sites C) and not sites B and D, the sites in the large L2 pore, as predicted by the UFF-based simulations. Note that the UFF-based simulations completely fail to capture the occupancy of the cus's at all loadings, whereas the DFT/CC-PES simulations show that the cus's start being populated at loadings as low as 25 molecules/uc but, in the case of methane, are not the first sites to be occupied. After the S1 pores and the cus's are saturated, the larger L2 and L3 pores start being filled.

Despite not capturing the adsorption on the cus's, the UFF-based simulations provide surprisingly good predictions for higher methane loadings. The reason for this is that the potential energy predicted from the UFF force field is consistently lower (i.e., more attractive) than the DFT/CC potential energy in the large L2 and L3 pores (except for the cus's in L3), especially at site B, as illustrated in Figure 3c. This leads to the large L2 pores (sites B, D, and F) being heavily populated starting from relatively low pressures and is the reason for the step in the isotherm at a loading of 104 molecules/uc. Toward saturation, site H, the center of the large L3 pore, plays an increasing role in accommodating methane molecules in the UFF-based simulations, where methane molecules were observed to reorder themselves to be extremely close-packed.[20] These artifacts largely compensate for the missing strong adsorption sites at the cus's and could well explain the generally good agreement between simulation and experimental results at higher temperatures, where the isotherms are much less sensitive to the precise description of the adsorption mechanism because of the higher mobility of the methane molecules.

It needs to be emphasized here that the choice of ab initio method has a critical influence on the accuracy of the predictions. Neither DFT, DFT-D2,[60] nor DFT-D3[61] derived PES lead to a correct prediction of the adsorption isotherm, as illustrated in Figure 4. The adsorption isotherm obtained from the DFT-derived adsorbate−adsorbent interaction potential is completely wrong. Adsorption isotherms obtained with the interaction potential based on DFT-D-type models are significantly better;

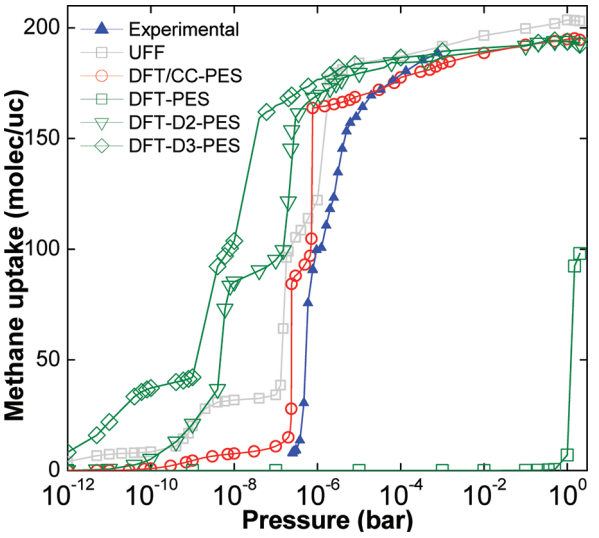

Figure 4. Comparison of methane adsorption isotherms at 77 K calculated using potential energy surfaces derived from different ab initio methods with experimental data. Experimental results were taken from reference 20. The isotherm calculated with the UFF force field was added for comparison.

nevertheless, they are far less accurate than those obtained with standard force fields (compare Figure 4 and Figure S2 in the Supporting Information). Although it is well-known that DFT is not capable of accurately describing dispersion interactions,[62] even the commonly adopted empirical dispersion-corrected DFT-D methods of Grimme et al.[60,61] are not a suitable choice because the lack of accounting for dispersion is only part of the problem. In addition, standard exchange−correlation functionals fail to properly describe electron density distribution between anionic organic linker and transition-metal cations.[37] It should therefore be stressed again that the choice of an ab initio level of theory used for the adsorbate−adsorbent interaction is critical and that the accurate description of the adsorbate interaction with the open-shell transition-metal cus's requires more involved methods than just standard DFT or DFT-D approaches.

CONCLUSIONS

In summary, we successfully used a DFT/CC-based potential energy surface directly implemented in GCMC simulations to

predict the adsorption of methane in CuBTC. The amount adsorbed as well as (and more importantly) the adsorption mechanism were captured accurately when compared to available experimental results. Most importantly, the interaction with the cus's was correctly described, which cannot be achieved by using any classical force field. Our approach is not restricted to the system studied in this work and can be extended to other MOFs with open metal sites, as well as other fluids.

■ ASSOCIATED CONTENT

Supporting Information. Computational details about the construction of the DFT/CC potential energy surface. Simulated methane adsorption isotherms for (1) higher temperatures, T = 285, 303, 333, 353, and 373 K, from DFT/CC-PES GCMC and (2) different generic force fields at 77 K. This material is available free of charge via the Internet at http://pubs.acs.org.

■ AUTHOR INFORMATION

Corresponding Author
*E-mail: tina.duren@ed.ac.uk.

■ ACKNOWLEDGMENT

We thank David Fairen-Jimenez for helpful discussions. The research leading to these results received funding from the European Community's Seventh Framework Programme (FP7/2007-2013) under Grant 228862. MACADEMIA is a Large-scale Integrating Project under the Nanosciences, Nanotechnologies, Materials and New Production Technologies Theme (www.macademia-project.eu). T.D. and L.C. also thank the EPSRC for funding (EP/G062129/1), and P.N. and L.G. acknowledge the support of ME CR (Grants 7E09111 and MSM0021620857).

■ REFERENCES

(1) Rosseinsky, M. J. *Microporous Mesoporous Mater.* **2004**, *73*, 15.
(2) Natarajan, S.; Mahata, P. *Chem. Soc. Rev.* **2009**, *38*, 2304.
(3) Farha, O. K.; Hupp, J. T. *Acc. Chem. Res.* **2010**, *43*, 1166.
(4) Meek, S. T.; Greathouse, J. A.; Allendorf, M. D. *Adv. Mater.* **2011**, *23*, 249.
(5) Li, J. R.; Kuppler, R. J.; Zhou, H. C. *Chem. Soc. Rev.* **2009**, *38*, 1477.
(6) Murray, L. J.; Dinca, M.; Long, J. R. *Chem. Soc. Rev.* **2009**, *38*, 1294.
(7) Li, J.-R.; Ma, Y.; McCarthy, M. C.; Sculley, J.; Yu, J.; Jeong, H.-K.; Balbuena, P. B.; Zhou, H.-C. *Coord. Chem. Rev.* **2011**, *255*, 1791.
(8) Düren, T.; Sarkisov, L.; Yaghi, O. M.; Snurr, R. Q. *Langmuir* **2004**, *20*, 2683.
(9) Lee, J.; Farha, O. K.; Roberts, J.; Scheidt, K. A.; Nguyen, S. T.; Hupp, J. T. *Chem. Soc. Rev.* **2009**, *38*, 1450.
(10) Ranocchiari, M.; van Bokhoven, J. A. *Phys. Chem. Chem. Phys.* **2011**, *13*, 6388.
(11) McKinlay, A.; Morris, R.; Horcajada, P.; Férey, G.; Gref, R.; Couvreur, P.; Serre, C. *Angew. Chem., Int. Ed.* **2010**, *49*, 6260.
(12) Horcajada, P.; Chalati, T.; Serre, C.; Gillet, B.; Sebrie, C.; Baati, T.; Eubank, J. F.; Heurtaux, D.; Clayette, P.; Kreuz, C.; Chang, J. S.; Hwang, Y. K.; Marsaud, V.; Bories, P. N.; Cynober, L.; Gil, S.; Ferey, G.; Couvreur, P.; Gref, R. *Nat. Mater.* **2010**, *9*, 172.
(13) Allendorf, M. D.; Bauer, C. A.; Bhakta, R. K.; Houk, R. J. T. *Chem. Soc. Rev.* **2009**, *38*, 1330.
(14) Sadakiyo, M.; Yamada, T.; Kitagawa, H. *J. Am. Chem. Soc.* **2009**, *131*, 9906.
(15) White, K. A.; Chengelis, D. A.; Gogick, K. A.; Stehman, J.; Rosi, N. L.; Petoud, S. *J. Am. Chem. Soc.* **2009**, *131*, 18069.
(16) Chen, B. L.; Yang, Y.; Zapata, F.; Lin, G. N.; Qian, G. D.; Lobkovsky, E. B. *Adv. Mater.* **2007**, *19*, 1693.
(17) Allendorf, M. D.; Houk, R. J. T.; Andruszkiewicz, L.; Talin, A. A.; Pikarsky, J.; Choudhury, A.; Gall, K. A.; Hesketh, P. J. *J. Am. Chem. Soc.* **2008**, *130*, 14404.
(18) Horcajada, P.; Surblé, S.; Serre, C.; Hong, D. Y.; Seo, Y. K.; Chang, J. S.; Grenèche, J. M.; Margiolaki, I.; Férey, G. *Chem. Commun.* **2007**, 2820.
(19) Schlichte, K.; Kratzke, T.; Kaskel, S. *Microporous Mesoporous Mater.* **2004**, *73*, 81.
(20) Getzschmann, J.; Senkovska, I.; Wallacher, D.; Tovar, M.; Fairen-Jimenez, D.; Düren, T.; van Baten, J. M.; Krishna, R.; Kaskel, S. *Microporous Mesoporous Mater.* **2010**, *136*, 50.
(21) Wu, H.; Zhou, W.; Yildirim, T. *J. Am. Chem. Soc.* **2009**, *131*, 4995.
(22) Guo, Z. Y.; Wu, H.; Srinivas, G.; Zhou, Y. M.; Xiang, S. C.; Chen, Z. X.; Yang, Y. T.; Zhou, W.; O'Keeffe, M.; Chen, B. L. *Angew. Chem., Int. Ed.* **2011**, *50*, 3178.
(23) Dinca, M.; Long, J. R. *J. Am. Chem. Soc.* **2005**, *127*, 9376.
(24) Xiao, B.; Wheatley, P. S.; Zhao, X.; Fletcher, A. J.; Fox, S.; Rossi, A. G.; Megson, I. L.; Bordiga, S.; Regli, L.; Thomas, K. M.; Morris, R. E. *J. Am. Chem. Soc.* **2007**, *129*, 1203.
(25) Dietzel, P. D. C.; Panella, B.; Hirscher, M.; Blom, R.; Fjellvag, H. *Chem. Commun.* **2006**, 959.
(26) Caskey, S. R.; Wong-Foy, A. G.; Matzger, A. J. *J. Am. Chem. Soc.* **2008**, *130*, 10870.
(27) Dietzel, P. D. C.; Besikiotis, V.; Blom, R. *J. Mater. Chem.* **2009**, *19*, 7362.
(28) Düren, T.; Bae, Y. S.; Snurr, R. Q. *Chem. Soc. Rev.* **2009**, *38*, 1237.
(29) Keskin, S.; Liu, J.; Rankin, R. B.; Johnson, J. K.; Sholl, D. S. *Ind. Eng. Chem. Res.* **2009**, *48*, 2355.
(30) Grajciar, L.; Wiersum, A. D.; Llewellyn, P. L.; Chang, J.-S.; Nachtigall, P. *J. Phys. Chem. C* **2011**, *115*, 17925.
(31) Rappe, A. K.; Casewit, C. J.; Colwell, K. S.; Goddard, W. A.; Skiff, W. M. *J. Am. Chem. Soc.* **1992**, *114*, 10024.
(32) Mayo, S. L.; Olafson, B. D.; Goddard, W. A. *J. Phys. Chem.* **1990**, *94*, 8897.
(33) Jorgensen, W. L.; Maxwell, D. S.; TiradoRives, J. *J. Am. Chem. Soc.* **1996**, *118*, 11225.
(34) Yazaydin, A. O.; Snurr, R. Q.; Park, T. H.; Koh, K.; Liu, J.; LeVan, M. D.; Benin, A. I.; Jakubczak, P.; Lanuza, M.; Galloway, D. B.; Low, J. J.; Willis, R. R. *J. Am. Chem. Soc.* **2009**, *131*, 18198.
(35) Wu, H.; Simmons, J. M.; Liu, Y.; Brown, C. M.; Wang, X. S.; Ma, S.; Peterson, V. K.; Southon, P. D.; Kepert, C. J.; Zhou, H. C.; Yildirim, T.; Zhou, W. *Chem.—Eur. J.* **2010**, *16*, 5205.
(36) Valenzano, L.; Civalleri, B.; Chavan, S.; Palomino, G. T.; Areán, C. O.; Bordiga, S. *J. Phys. Chem. C* **2010**, *114*, 11185.
(37) Grajciar, L.; Bludský, O.; Nachtigall, P. *J. Phys. Chem. Lett.* **2010**, *1*, 3354.
(38) Yang, Q. Y.; Zhong, C. L. *J. Phys. Chem. B* **2005**, *109*, 11862.
(39) Jorge, M.; Lamia, N.; Rodrigues, A. E. *Colloids Surf. A: Physicochem. Eng. Aspects* **2010**, *357*, 27.
(40) Castillo, J. M.; Vlugt, T. J. H.; Calero, S. *J. Phys. Chem. C* **2008**, *112*, 15934.
(41) Liu, J.; Culp, J. T.; Natesakhawat, S.; Bockrath, B. C.; Zande, B.; Sankar, S. G.; Garberoglio, G.; Johnson, J. K. *J. Phys. Chem. C* **2007**, *111*, 9305.
(42) Yang, Q. Y.; Zhong, C. L. *J. Phys. Chem. B* **2006**, *110*, 655.
(43) Fischer, M.; Kuchta, B.; Firlej, L.; Hoffman, F.; Fröba, M. *J. Phys. Chem. C* **2010**, *114*, 19116.
(44) Chui, S. S. Y.; Lo, S. M. F.; Charmant, J. P. H.; Orpen, A. G.; Williams, I. D. *Science* **1999**, *283*, 1148.
(45) Gelb, L. D.; Gubbins, K. E. *Langmuir* **1999**, *15*, 305.
(46) Bludský, O.; Rubeš, M.; Soldan, P.; Nachtigall, P. *J. Chem. Phys.* **2008**, *128*, 114102.

(47) Rubeš, M.; Kysilka, J.; Nachtigall, P.; Bludský, O. *Phys. Chem. Chem. Phys.* **2010**, *12*, 6438.
(48) Zukal, A.; Pulido, A.; Gil, B.; Nachtigall, P.; Bludský, O.; Rubeš, M.; Čejka, J. *Phys. Chem. Chem. Phys.* **2010**, *12*, 6413.
(49) Soldan, P.; Hutson, J. M. *J. Chem. Phys.* **2000**, *112*, 4415.
(50) Bludský, O.; Rubeš, M.; Soldán, P. *Phys. Rev. B* **2008**, *77*, 092103.
(51) Blöchl, P. E. *Phys. Rev. B* **1994**, *50*, 17953.
(52) Perdew, J. P.; Burke, K.; Ernzerhof, M. *Phys. Rev. Lett.* **1996**, *77*, 3865.
(53) Werner, H.-J.; Knowles, P. J.; Lindh, R.; Manby, F. R.; Schültz, M.; Celani, P.; Korona, T.; Berning, A. A.; Cooper, D. L.; Deegan, M. J. O.; Dobbyn, A. J.; Eckert, F.; Goll, E.; Hampel, C.; Hetzer, G.; Hrenar, T.; Knizia, G.; Koeppl, C.; Liu, Y.; Lloyd, A. W.; Palmieri, R. P.; Pfluger, K.; Pitzer, R.; Reiher, M.; Schumann, U.; Stoll, H.; Stone, A. J.; Tarroni, R.; Thorsteinsson, T.; Wang, M.; Wolf, A. *Molpro*, version 2009.1; University College Cardiff Consultants Limited: Cardiff, U.K., 2009.
(54) Kresse, G.; Hafner, J. *Phys. Rev. B* **1993**, *48*, 13115.
(55) Gupta, A.; Chempath, S.; Sanborn, M. J.; Clark, L. A.; Snurr, R. Q. *Mol. Simul.* **2003**, *29*, 29.
(56) Frenkel, D.; Smit, B. *Understanding of Molecular Simulation: from Algorithms to Applications*, 2nd ed.; Academic Press: San Diego, CA, 2002.
(57) Goodbody, S. J.; Watanabe, K.; Macgowan, D.; Walton, J. P. R. B.; Quirke, N. *J. Chem. Soc., Faraday Trans.* **1991**, *87*, 1951.
(58) Chen, B.; Siepmann, J. I. *J. Phys. Chem. B* **1999**, *103*, 5370.
(59) Myers, A. L.; Monson, P. A. *Langmuir* **2002**, *18*, 10261.
(60) Grimme, S. *J. Comput. Chem.* **2006**, *27*, 1787.
(61) Grimme, S.; Antony, J.; Ehrlich, S.; Krieg, H. *J. Chem. Phys.* **2010**, *132*, 154104.
(62) Kristyan, S.; Pulay, P. *Chem. Phys. Lett.* **1994**, *229*, 175.

Attachment E

THE JOURNAL OF PHYSICAL CHEMISTRY C

Article

pubs.acs.org/JPCC

Adsorption of Propane and Propylene on CuBTC Metal–Organic Framework: Combined Theoretical and Experimental Investigation

Miroslav Rubeš,[‡] Andrew D. Wiersum,[§] Philip L. Llewellyn,[§] Lukáš Grajciar,[‡] Ota Bludský,[†] and Petr Nachtigall*[,‡]

[‡]Department of Physical and Macromolecular Chemistry, Faculty of Science, Charles University in Prague, Hlavova 2030, CZ-128 40, Prague 2, Czech Republic

[§]Laboratoire MADIREL (UMR 7246), Aix-Marseille Univ. & CNRS, Centre de St Jérôme, 13397 Marseille Cedex 20, France

[†]Institute of Organic Chemistry and Biochemistry, Academy of Sciences of the Czech Republic, Flemingovo nám. 2, Prague 6, 162 10, Czech Republic

Supporting Information

ABSTRACT: A combined experimental and theoretical investigation of propane and propylene adsorption in the metal–organic framework CuBTC is presented. The dependence of adsorption enthalpies on the adsorbed amount was determined by microcalorimetry up to 8 mmol g^{-1} coverage (roughly C_3H_n/Cu^{2+} ratio of 1.5). Trends observed experimentally were interpreted on the basis of accurate calculations carried out at the hybrid DFT–ab initio level. Three types of adsorption sites were identified; however, qualitatively different results were obtained for propane and propylene. Propane preferentially adsorbs at the cage center sites ($-\Delta H^\circ$ = 43 kJ mol^{-1}), followed by adsorption at the cage window sites (31 kJ mol^{-1}), while the interaction with the coordinatively unsaturated sites (CUS) is relatively weak (24 kJ mol^{-1}). On the contrary, propylene preferentially interacts with the CUS (56 kJ mol^{-1}), while the adsorption at the cage center and cage window sites was found to be only 45 and 34 kJ mol^{-1}, respectively. Due to the topology of CuBTC, lateral interactions are significantly more important among the adsorbates located at the cage center and cage window sites (populated in the case of propane) than among adsorbates at the CUS and cage center sites (populated in the case of propylene). Therefore, adsorption energies obtained for coverages above 6 mmol g^{-1} of adsorbed amount were larger for propane than for propylene. Consequently, the presence of small cages makes the CuBTC MOF less suitable for propane/propylene separation than MOFs having the Cu^{2+} CUS but without small cages (e.g., CPO-27).

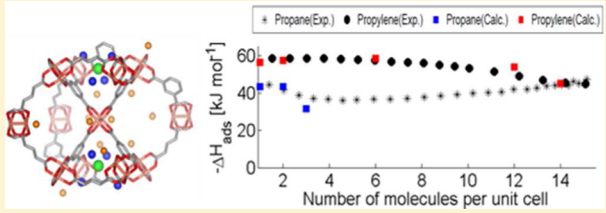

INTRODUCTION

Metal–organic frameworks (MOFs) are widely investigated due to their potential applications in various areas, including separation and purification, gas storage, catalysis, or drug delivery.[1−4] There is a relatively large group of MOFs containing coordinatively unsaturated sites (CUS), e.g., MIL-100, MIL-101, CPO-27, or HKUST-1, exhibiting unique properties in adsorption and even in catalysis.[5−10] The CuBTC MOF (often denoted HKUST-1)[11] is one of the earliest reported stable MOFs, and it has been often investigated experimentally and computationally. CuBTC is now considered as a reference MOF containing CUS. Adsorption of many gases in CuBTC, including small molecules such as H_2, H_2O, CO_2, or CH_4, has been investigated both experimentally and computationally, focusing on the adsorption on the CUS.[12−15] It has been recognized that the agreement between experimental and computational results deteriorates with the increasing role of the CUS in adsorption.

The CuBTC MOF has been also considered for propane/propylene separation.[1,16−20] The reported experimental isosteric heats for propane and propylene (mostly obtained by means of the simple Clausius–Clapeyron relation) show significant differences; they are in the range of 27–38 and 33–51 kJ mol^{-1} for propane and propylene, respectively.[17,18,20]

The presence of the Cu^{2+} CUS makes the theoretical description of adsorption in CuBTC rather challenging. It has been shown that the accuracy of commonly employed force fields is not sufficient for methane adsorption in CuBTC,[21] and the problem of force fields is mostly due to their inaccuracy in the description of the interaction with the CUS. In the case of propane/propylene adsorption in CuBTC, the situation is even more complicated due to the presence of the propylene double bond that can form a partial dative bond with the CUS. The preferential adsorption for propylene and isobutene has been explained by formation of partially dative bond between CUS and π-molecular orbitals.[17,19,22] However, the accuracy of a force field (commonly Lennard-Jones) to describe correctly this partial dative bond is questionable even after the parameter readjustment.

Received: February 14, 2013
Revised: April 29, 2013
Published: April 29, 2013

   dx.doi.org/10.1021/jp401600v | J. Phys. Chem. C 2013, 117, 11159–11167

The recently developed DFT/CC method[23] has been successfully used to accurately describe adsorption in MOFs containing CUS; accurate adsorption enthalpies for H_2O, CO, CO_2, and CH_4 in the CuBTC MOF were reported.[15,21,24,25] It has been shown that the addition of a dispersion component missing in standard exchange-correlation functionals fixes only part of the problem in the density functional theory (DFT) description of the adsorbate−CUS interaction. It is thus the goal of the present study to describe the adsorption of propane and propylene in CuBTC MOF with high accuracy; the DFT/CC correction scheme is adopted for that purpose. Adsorption enthalpies calculated for various adsorption sites and various adsorbate loadings are compared with newly acquired accurate experimental adsorption enthalpies obtained for a broad range of adsorbed amount using a Tian−Calvet-type microcalorimeter.

EXPERIMENTAL AND THEORETICAL METHODS

Sample Characterization. CuBTC MOF (HKUST-1) was provided by the Korean Research Institute for Chemical Technology and was prepared by microwave synthesis.[26] The sample was activated by heating to 150 °C under secondary vacuum (<1.10−3 mbar). Apparent BET surface area was determined by adsorption of N_2 at 77 K in the relative pressure range P/P_0 = 0.0002−0.01, following the guidelines proposed by Rouquerol et al.[27] The sample was found to have a surface area of 1628 m^2/g and a pore volume of 0.64 cm^3/g. These values are among the highest reported in the literature and are very close to the values reported by Chang et al.[26] for CuBTC prepared by microwave synthesis (1656 m^2/g).

Microcalorimetry. Adsorption enthalpies were measured experimentally using a Tian−Calvet-type microcalorimeter coupled with an in-house manometric gas dosing system.[28] This apparatus allows the simultaneous measurement of the adsorption isotherm and the corresponding differential enthalpies. Gas is introduced into the system using a step-by-step method, and each dose is allowed to stabilize in a reference volume before being brought into contact with the adsorbent, located in the microcalorimeter. The introduction of the adsorbate to the sample is accompanied by an exothermic thermal signal, measured by the thermopiles of the microcalorimeter. The peak in the calorimetric signal is integrated over time to give the total energy released during that adsorption step.

The adsorption of propane and propylene on CuBTC was carried out at 30 °C and up to 8 bar. Around 0.2 g of sample was used and this was outgassed at 150 °C for 16 h under secondary vacuum prior to the experiment. For each injection of gas, equilibrium was assumed to have been reached after 150 min. This was confirmed by the return of the calorimetric signal to its baseline (<5 μW).

Calculations. The experimentally determined CuBTC structure has a cubic symmetry with lattice parameter of 26.3 Å.[11] For the computational convenience this cell has been reduced to the rhombohedral primitive cell containing 156 framework atoms with cell parameters optimized in previous work ($a = b = c$ = 18.774 Å, $\alpha = \beta = \gamma = 60°$).[15] Three different adsorption sites depicted in Figure 1 were investigated: (i) coordinatively unsaturated sites (CUS), where the adsorbate interacts primarily with unsaturated Cu^{2+} cations, (ii) cage window sites located at the entrance window into the small cages, and (iii) cage center sites at the center of small cages. Note that the reduced cell contains 12, 8, and 2 CUS, cage window, and cage center sites, respectively (Figure 1). Besides single propane and propylene adsorption characteristics, we have also addressed the adsorption of more than one molecule of adsorbate in CuBTC to evaluate the importance of lateral interactions. Interaction energies and adsorption enthalpies were calculated for the process

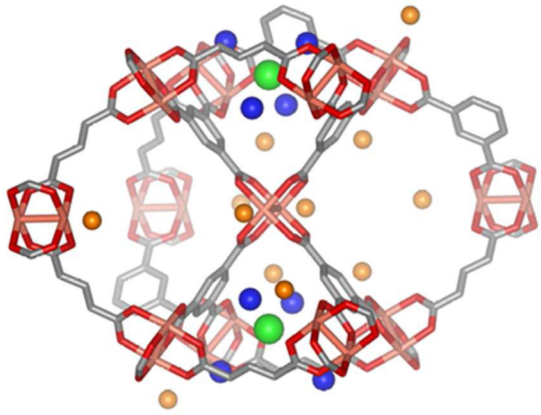

Figure 1. CuBTC adsorption sites: the 12 CUS sites in the unit cell (indicated by orange balls) are located just above the Cu^{2+} cations in the large (L3) cage; there are two small (S1) cages, each of them with one cage center site (green sphere) and four cage windows sites (blue spheres).

$$(n-1)C_3H_x/\text{CuBTC} + C_3H_x \rightarrow nC_3H_x/\text{CuBTC}$$

where n is number of adsorbed molecules and x = 6 or 8. Deformation energies (E_{def}) were calculated as the difference between the energy calculated for adsorbate (adsorbent) at the geometry optimized for the adsorption complex and at the geometry optimized for the isolated adsorbate (adsorbent). For each adsorption site several geometry optimizations (at least three) with different starting geometries were performed to find the lowest energy structure for the particular adsorption site.

The periodic DFT/CC calculations[23] (see below) were performed with the PBE exchange-correlation functional.[29] The Kohn−Sham equations were solved using the projector augmented wave (PAW) of Blöchl[30] setting the planewave basis set kinetic energy cutoff to 600 eV. The Γ-point sampling of the first Brillouin zone was found to be sufficient to yield converged results.[15] A threshold of 0.01 eV $Å^{-1}$ on forces was used in the geometry optimization. In case of propane and propylene adsorption on CuBTC, the spin polarization has been neglected due to the small difference in interaction energies (not exceeding 2 kJ mol^{-1}, see results reported in Table 1) between spin-polarized (high-spin solution) and non-spin-polarized calculations. The ΔZPVE has been evaluated using the finite differences approach with two displacements of 0.01 Å for each degree of freedom; the CuBTC framework atoms were kept fixed, only taking into account the degrees of freedom associated with adsorbate (propane or propylene). Furthermore, the ΔZPVE for more than one adsorbed molecule has been estimated from single molecule adsorption at a given adsorption site. The periodic calculations were performed with the VASP 5.2 package.[31]

The cluster-model calculations at the DFT and CCSD(T) levels of theory were required for the construction of DFT/CC correction functions. The standard Dunning's correlation-consistent valence-X-ζ basis sets with polarization functions were used for H, C, and O atoms,[32] while for the Cu atoms the

dx.doi.org/10.1021/jp401600v | J. Phys. Chem. C 2013, 117, 11159−11167

Table 1. Adsorption Characteristics for a Single Molecule of Propane or Propylene Adsorbed at the Three Different Adsorption Sites in CuBTC[a]

molecule	CuBTC adsorption site	E_{def} CuBTC[b]	E_{def} C_3H_n[c]	E_{int}	$-\Delta H°(0K)$
propane	cage	0.17	0.05	−45.2 (−0.2)	43.3
	window	0.08	0.04	−33.3 (2.32)	31.0
	CUS	0.69	0.67	−25.3 (−4.9)	24.3
propylene	center	0.26	0.02	−46.3 (−2.9)	44.7
	window	0.48	0.37	−36.1 (5.8)	34.0
	CUS	10.15	1.01	−59.9 (−27.0)	56.4

[a]The DFT/CC deformation energies (E_{def}), interaction energies (E_{int}), and adsorption enthalpies ($-\Delta H°(0K)$) in kJ mol^{-1} are reported. The PBE interaction energies for DFT/CC geometries are presented in parentheses. [b]The deformation energy of CuBTC is defined as the difference in energy of CuBTC without any adsorbate calculated at the geometry optimized with and without adsorbate. [c]The deformation energy of propane/propylene is defined as the difference in energy of C_3H_n calculated at the geometry of adsorption complex and at the geometry obtained for a free molecule.

pseudopotential-based correlation-consistent valence-X-ζ basis set with polarization functions was employed.[33] The basis sets are denoted VXZ, where X = D, T, and Q stands for double, triple, and quadruple basis sets, respectively, and the corresponding augmented basis sets are denoted AVXZ. In order to avoid basis set deficiencies the CCSD(T) energies were extrapolated to the complete basis set (CBS) limit and corresponding DFT calculations with PBE functional were performed with the large AVQZ basis sets. The CBS estimate was obtained by means of a simple correlation energy dependence on the basis set cardinal number X ($E_X = E_{CBS} + AX^{-3}$).[34] The uncorrelated part (HF) was extrapolated using a two-point formula proposed by Halkier et al.,[35] or in some cases, the HF/AVQZ energy was taken as a CBS estimate. The standard ΔMP2 extrapolation was used to obtain CCSD(T)/CBS estimates (see eq 1 and the Supporting Information for more details):

$$\mathrm{CCSD(T)/CBS} = \mathrm{CCSD(T)/AVXZ} + (\mathrm{MP2/CBS} - \mathrm{MP2/AVXZ}) \quad (1)$$

The interaction energies for cluster models are all counterpoise corrected by the standard Boys and Bernardi procedure.[36] The CCSD(T) and DFT cluster model calculations were performed with Molpro 09[37] and Gaussian 09[38] program suites, respectively.

DFT/CC Method. DFT/CC has been used to describe the adsorption of propane and propylene on CuBTC. The DFT/CC computational approach is described only briefly here; however, additional details can be found elsewhere.[15,23] The DFT/CC correction scheme is based on the pairwise representability of the DFT error (ΔE), which is expressed as follows:

$$\Delta E = E_{CCSD(T)} - E_{DFT} \quad (2)$$

where $E_{CCSD(T)}$ and E_{DFT} are interaction energies calculated at the CCSD(T)/CBS and the DFT/AVQZ levels of theory, respectively. The DFT error, ΔE, is then expressed as a sum of pairwise atom−atom correction functions $\varepsilon_{ij}(R_{ij})$

$$\Delta E = \sum_{ij} \varepsilon_{ij}(R_{ij}) \quad (3)$$

where R_{ij} is the distance between atoms i and j. There is no assumption about the functional form of ε_{ij}; instead, the reciprocal power reproducing kernel Hilbert space[39,40] (RP-RKHS) interpolation is used. The essential prerequisite in the DFT/CC approach is the choice of the reference set of molecules from which the atom−atom corrections are generated. Correction functions derived previously for methane adsorption in CuBTC (ref 21) are used herein for propane adsorption; the reference set consisting of H_2, C_2H_4, C_6H_6, CO_2, and $Cu(HCOO)_2$ was used for the construction of the correction functions for sp^2 carbon atoms in propylene (see the Supporting Information for details).

Transferability of the DFT/CC Correction Functions. The transferability of the correction functions for the propane and propylene interaction with CuBTC was investigated for four intermolecular complexes not included in the reference set (Figures 2 and S4, Supporting Information). The transferability

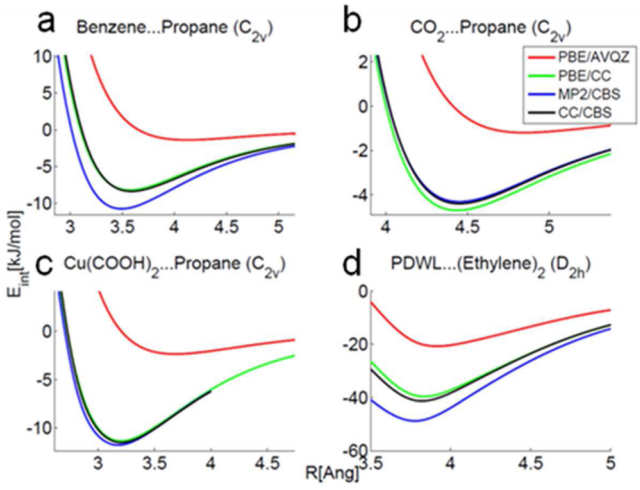

Figure 2. Transferability tests of the DFT/CC correction scheme for four complexes outside the reference set. The distance R (in Å) is defined as a center of mass separation between monomers; corresponding structures are depicted in Figure S4 (Supporting Information).

of the correction functions for H and C atoms of sp^3 carbon (obtained previously for methane) was tested for the interaction of propane with benzene (Figure 2a), CO_2 (Figure 2b), and $Cu(HCOO)_2$ (Figure 2c). An excellent agreement between the DFT/CC and CCSD(T)/CBS results was found, with the largest deviation of only 0.3 kJ mol^{-1} observed for the CO_2···propane complex. This suggests that correction functions obtained for methane interaction with CuBTC[21] can be used to describe the interaction of saturated hydrocarbon with CuBTC. The $Cu_2(HCOO)_4$ paddle-wheel (PDWL) complex with ethylene was used to investigate the transferability of the

dx.doi.org/10.1021/jp401600v | J. Phys. Chem. C 2013, 117, 11159−11167

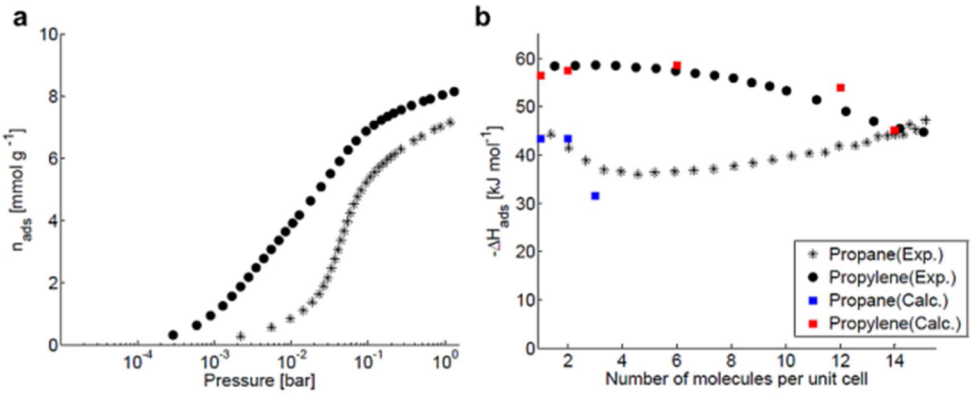

Figure 3. Propane and propylene adsorption isotherms measured at 303 K (a) and corresponding experimental adsorption enthalpies (b). The calculated adsorption heats ($-\Delta H°(0K)$) are added to part b for comparison with experimental results.

correction functions for sp^2 carbon atoms (Figure 2d). The largest deviation of the DFT/CC interaction energy from the CCSD(T)/CBS one is found at the potential minimum; the DFT/CC value is 1.7 kJ mol^{-1} underestimated, and that corresponds to 4% error in the interaction energy. It can be concluded that DFT/CC provides a very accurate description of the propane and propylene interactions with CuBTC; however, a small underestimation (1−2 kJ mol^{-1}) should be expected for the interaction of propylene with the CUS.

RESULTS

Microcalorimetry. Adsorption isotherms for propane and propylene obtained at 30 °C are shown in Figure 3a; the corresponding pseudodifferential adsorption enthalpies as a function of loading are shown in Figure 3b. The propylene adsorption energy ($-\Delta H°$) decreases from about 58 kJ mol^{-1} (low coverage region) to 45 kJ mol^{-1} at a coverage of 15 propylene molecules per unit cell (UC). A rather different dependence of the adsorption enthalpies on the loading is observed for propane: the adsorption energy decreases from 44 to 36 kJ mol^{-1} for loadings up to three C_3H_8 molecules per UC and then steadily increases with increasing loading up to 50 kJ mol^{-1} for 16 propane molecules per UC. These results are discussed below on the basis of a theoretical investigation employing DFT/CC calculations (described above).

Adsorption of a Single Propane or Propylene Molecule in CuBTC MOF. The most stable adsorption complexes of propane and propylene in the cage center, in the cage window, and on the coordinatively unsaturated sites are reported in Figure 4, and the corresponding adsorption enthalpies are summarized in Table 1. In the case of propane, the preferential adsorption site is in the center of the small octahedral cage ($-\Delta H°$ = 43.3 kJ mol^{-1}), where one of the CH_3 groups is pointing to the cage window (Figure 4a) to maximize the dispersion interactions with the BTC linkers. The interaction between propane and CuBTC is about 12 kJ mol^{-1} weaker when it adsorbs at the cage window site (Figure 4b); one methyl group is located in the cage window while the rest of the molecule points into the large cage of CuBTC. The adsorption enthalpy of propane on the CUS is only 24 kJ mol^{-1}. The interaction of propane with the Cu^{2+} cation results in a structure where the central carbon atom of propane is above the Cu^{2+} cation at a distance of 2.8 Å (Figure 4c). The relatively small interaction energy found for the adsorption on the CUS is due to the geometry of this complex where both CH_3 groups of propane are far from BTC linkers, resulting in a smaller dispersion interaction. Results reported in Table 1 show that neither ΔZPVE nor deformation energies are significant for propane adsorption complexes in CuBTC.

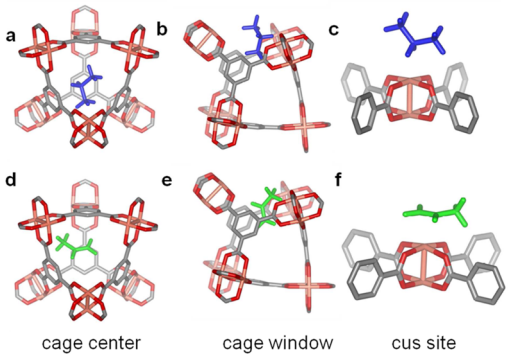

Figure 4. The geometries of adsorption complexes of propane and propylene obtained at the DFT/CC level: (a) propane at the cage center site, (b) propane at the window site, (c) propane at the CUS, (d) propylene at the cage center site, (e) propylene at the cage window site, and (f) propylene at the CUS. Propane and propylene are depicted in blue and green, respectively, and framework Cu, O, and C atoms are depicted in orange, red, and gray, respectively.

Adsorption enthalpies of 44.7 and 34.0 kJ mol^{-1} were calculated for propylene adsorption in the cage center and cage window sites, respectively. There are many similarities between the adsorption of propane and propylene in the cage center and cage windows sites, including the adsorption enthalpies that differ by less than 3 kJ mol^{-1} for each site. However, the adsorption of propylene at the cage center site is about 11 kJ mol^{-1} more favorable than at the cage window site. Two propylene adsorption complexes can be distinguished at the cage center: the complex where the CH_3 group points toward the window (Figure 4d) is about 3 kJ mol^{-1} more stable than the complex where the CH_2 group is directed toward the cage window. Similarly, it can be expected that two propylene adsorption complexes can be distinguished for the cage window site. However, only the complex having the CH_2 group inside the cage window (Figure 4e) has been found, while the corresponding complex with the CH_3 group inside the cage window was not observed; all the attempts to find such a complex resulted in the propylene drifting inside the cage and forming the cage center complex with the CH_2 group pointing toward the cage window.

dx.doi.org/10.1021/jp401600v | J. Phys. Chem. C 2013, 117, 11159−11167

The adsorption of propane and propylene molecules on a CUS is rather different: while the propane adsorption complex on the CUS is significantly less stable than adsorption complexes at the cage center and cage windows sites, the propylene molecule binds preferentially on the CUS (Figure 4f) with large adsorption enthalpy $-\Delta H^\circ$ = 56 kJ mol^{-1}. The formation of a partial dative bond between the propylene π-orbital and the Cu^{2+} cation is behind the increased stability. The partial dative bond character is also evidenced by the small distance between the center of the propylene double bond and the Cu^{2+} cation (2.4 Å) and by increased deformation energy due to the pyramidalization of the PDWL unit (Figure S5, Supporting Information). There is a small preference for the CH_3 group to orient itself toward the cage window (Figure 4f), but this stationary point is only 1 kJ mol^{-1} more stable than the structure where the CH_3 group goes into the main channel of CuBTC. It is expected that the rotational barriers of propylene around the Cu−Cu bond axis are rather small.

Adsorbate−Adsorbate Interactions: Adsorption of 2−14 Molecules. Lateral interactions between propane or propylene molecules adsorbed in CuBTC must be taken into consideration. At the same time, partial site blocking should be expected when an adsorbate molecule is adsorbed on a specific site and it partially blocks adjacent sites (e.g., a molecule in the cage center site partially blocks adjacent cage window site; see the subsection above and Figure 5). It follows that for increasing adsorbate loading the differential heats of adsorption can either increase (stabilization due to lateral interactions) or decrease (either due to the occupancy of strongly binding sites or due to a partial site blocking). The importance of lateral interactions was investigated computationally; the adsorption enthalpies calculated at the DFT/CC level for higher loadings are summarized in Table 2.

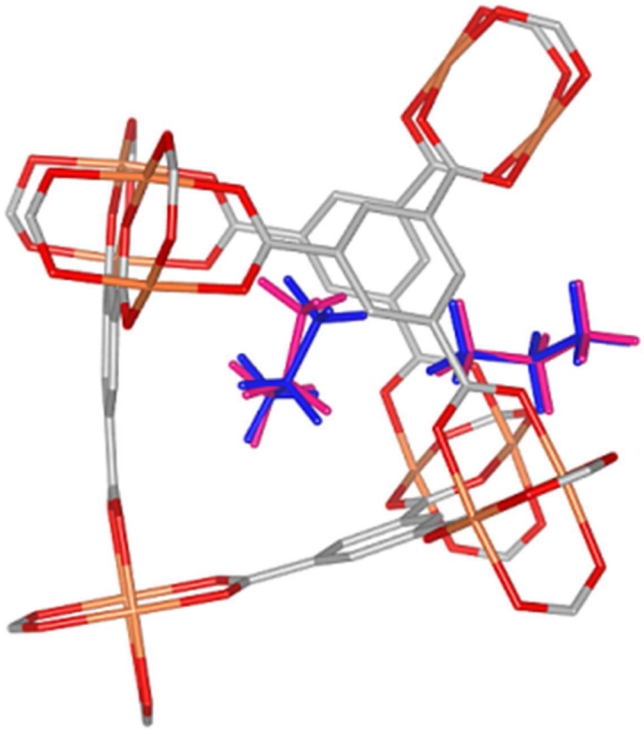

Figure 5. The structure of propane adsorption complexes at the cage center and cage window sites: structures obtained by geometry optimization of single propane molecule in UC (shown in blue) and structures obtained by geometry optimization of two propane molecules in UC (shown in pink). The difference between the structures is due to the partial site blocking and lateral interactions.

Up to three propane molecules in the CuBTC unit cell have been considered. Due to the large differences in adsorption enthalpies reported in Table 1 for the individual adsorption sites, it is assumed that the first two molecules of propane adsorb at the cage-center sites. The two cage-center sites in the UC are far apart; thus, lateral interactions are negligible and no site blocking can occur (Table 2). Upon the full occupation of the cage-center sites, the next molecule of propane adsorbs either at the cage-window site or on the CUS. Calculated adsorption enthalpies for the third molecule are 31.5 and 24.8 kJ mol^{-1} for the cage window and coordinatively unsaturated sites, respectively. Both these enthalpies are very close (within 0.5 kJ mol^{-1}) to corresponding values reported in Table 1 for the adsorption of a single propane molecule in the UC. However, in the case of the third molecule adsorbing at the cage-window site, this agreement is only due to the cancelation of lateral interactions with the effect of partial site blocking (Table 2). It is evident that propane molecules adsorbed on adjacent sites are significantly stabilized by lateral interactions, e.g., molecules in cage center and adjacent cage window sites are stabilized by 3.8 kJ mol^{-1} and a pair of molecules on CUS and cage window sites is stabilized by 4.3 kJ mol^{-1} (Table 2). However, this lateral stabilization is in some cases compensated by partial site blocking (see above).

In the case of propylene, the CUS are preferred adsorption sites due to the formation of a partial dative bond between propylene double bond and Cu^{2+} cation. Results reported in Table 2 show that there is a small stabilization due to the simultaneous adsorption of two propylene molecules on a pair of adjacent sites (about 0.6 kJ mol^{-1}); however, when two propylene molecules are adsorbed on a pair of Cu^{2+} cations in the same paddle-wheel unit, the adsorption enthalpy drops significantly from 56 kJ mol^{-1} found for a single propylene molecule on a paddle wheel to 47 kJ mol^{-1} for the second propylene molecule. This is due to the pyramidalization of the entire paddle wheel upon the adsorption of a single propylene molecule; this pyramidalization is lost when both Cu^{2+} cations interact with propylene (Figure S5, Supporting Information). Assuming that the first 12 molecules adsorb on CUS (full occupation of the CUS) after which additional molecules adsorb at cage center sites, the corresponding adsorption enthalpy is 45.1 kJ mol^{-1}, similar to $-\Delta H^\circ$ = 44.7 kJ mol^{-1} found for a single propylene molecule in the UC adsorbed at the cage site. The same conclusions about the importance of lateral interactions drawn above for propane can be also made for propylene.

DISCUSSION

The dependence on loading of the adsorption enthalpies for propane and propylene measured experimentally (Figure 3) can be interpreted on the basis of a very good agreement between the experimental and calculated results (Figure 3 and Tables 1 and 2, respectively). The mechanism for propylene adsorption is the following: (i) propylene adsorbs first on CUS, and adsorption energies may first slightly increase due to lateral interactions (only for very low coverages); (ii) the gradual decrease of adsorption energies observed experimentally for loadings ranging from 3 to 12 molecules/UC is due to the uneven adsorption enthalpies for the first and the second propylene molecule on the CUS of a single paddle wheel (58

dx.doi.org/10.1021/jp401600v | J. Phys. Chem. C 2013, 117, 11159−11167

Table 2. Adsorption Characteristics Obtained for Several Molecules of Propane (Propylene) Adsorbed Simultaneously on CuBTC[a]

molecule	$n(C_3H_n)$ CUS + cage + window[b]	E_{def}[c]	$E_{lateral}$	E_{int}	av E_{int}[d]	$-\Delta H°(0K)$	av $-\Delta H°(0K)$[d]
propane	0 + 2 + 0	0.5	−0.1	−45.2	−45.2	43.3	43.3
	1 + 0 + 1	1.7	−4.3		−30.9		29.3
	0 + 2 + 1	0.7	−3.8	−33.8	−41.4	31.5	39.4
	1 + 2 + 0	1.9	−0.7	−25.8	−38.7	24.8	37.1
exp.	(1.38)						44.3
propylene	2 + 0 + 0	22.2	−2.2	−61.0	−60.5	57.5	57.0
	2 + 0 + 0[e]	9.5	0.0	−50.4	−55.1	46.9	51.6
	6 + 0 + 0	64.9	−19.9	−62.1	−61.2	58.6	57.7
	12 + 0 + 0	57.1	−54.6		−57.5		54.0
	12 + 2 + 0	58.1	−64.0	−46.7	−56.1	45.1	52.9
exp.	(1.52)						58.4

[a]The DFT/CC deformation energies (E_{def}), lateral interactions ($E_{lateral}$), interaction energies (E_{int}), and adsorption enthalpies ($-\Delta H°(0K)$) are reported in kJ mol^{-1}. [b]Number of propane/propylene molecules adsorbed on the coordinatively unsaturated, cage center, and cage window sites. [c]The deformation energy of CuBTC is defined as the difference in energy of CuBTC without any adsorbate calculated at the geometry optimized with and without adsorbate. [d]Average interaction energy (adsorption enthalpy) calculated for n molecules adsorbed simultaneously. [e]Two propylene molecules adsorbed on the same PDWL unit.

and 47 kJ mol^{-1}, respectively); (iii) the further decrease of the adsorption energies (down to 45 kJ mol^{-1}) is due to the occupation of cage center sites at 12−14 molecules/UC loading; and (iv) adsorption of propylene on the cage window sites is strongly stabilized by lateral interactions (both cage center and coordinatively unsaturated sites are mostly occupied before the adsorption on the cage window sites takes place) that increase with increasing propylene loading. Note that the experimental results (Figure 3) are in excellent agreement with the results obtained at the DFT/CC level (Tables 1 and 2).

The mechanism for propane adsorption is the following: (i) propane first adsorbs in the cage center sites (up to two molecule/UC, $-\Delta H°$ = 43 kJ mol^{-1}), (ii) adsorption energies decrease for loadings ranging from 2−10 molecules/UC due to the adsorption in cage window sites that is energetically less favorable than the adsorption at the cage center sites, and (iii) the increasing role of lateral interactions for higher propane loadings results in an increase in the adsorption energies. Note that the DFT/CC calculations were performed for up to three propane molecules per UC; they are in quantitative agreement with experimental data; however, the adsorption mechanism proposed for higher propane loadings is based only on qualitative considerations. Note that the dependence of adsorption heats of propane follows a very similar trend as previously reported for methane adsorption in CuBTC.[41]

The mechanisms of adsorption presented above results from qualitative considerations based on accurately calculated DFT/CC adsorption enthalpies. An improved insight into the mechanism of C_3 hydrocarbon adsorption could be achieved by means of GCMC simulations employing a suitable force field. However, it has been recently shown that the common force fields used to describe the adsorption of methane on CuBTC fails to describe the system reliably.[21] New force fields for the description of hydrocarbon adsorption on CuBTC must be developed[42] and only then is it meaningful to carry out GCMC simulations. The development of reliable force fields is in progress, and the DFT/CC data reported here will serve as a benchmark.

The adsorption of propane and propylene on CuBTC (and on other MOFs containing CUS) has been investigated computationally in a number of studies; however, significantly less accurate methods than the DFT/CC model employed here were used. Propane adsorption on CuBTC was simulated using a force field (a combination of DREIDING and UFF) and GCMC; a reasonable agreement between simulated and experimental adsorption isotherms was found only for low loadings and at a relatively low temperature (283 K), while for higher temperatures and higher loadings the experimental and simulated results diverged significantly.[43] The disagreement between experimental and simulated data can be easily understood when interaction energies obtained with the force field for the zero-coverage limit ($-\Delta U$ = 12.8, 46.9, and 44.0 kJ mol^{-1} for the coordinatively unsaturated, cage center, and cage window sites, respectively) are compared with those obtained with the DFT/CC method herein (24.3, 43.3, 31.0 kJ mol^{-1}, Table 1). The interaction energies calculated with this force field are underestimated by 50% and overestimated by 50% for the coordinatively unsaturated and cage window sites, respectively. It is evident that the molecular simulations employing simple force fields cannot correctly predict the adsorption sites in CuBTC, and this has been previously demonstrated for the adsorption of methane on CuBTC, for which neutron diffraction data are also available.[21] A different combination of force fields in the MC and MD investigation of propane adsorption in CuBTC led to adsorption heats of −49 kJ mol^{-1}, which is also overestimated.[44]

It is clear that force fields cannot properly describe the interaction of saturated hydrocarbons with the CUS, and it is far more problematic to use force fields for the adsorption of unsaturated hydrocarbons on CuBTC. The failure of the standard force fields to describe the interaction with the CUS, in particular for the interaction with a π orbitals, was recognized by Jorge et al.[17] They suggested using two sets of ε/k_B for the Cu atom: 2.5 and 875 K for the interaction with the sp^2 and sp^3 carbon, respectively.[19] Nevertheless, the simulated adsorption isotherms for propylene were still underestimated at low pressures and overestimated at higher pressure (with respect to experimental data). The poor performance of standard force fields to describe olefin/CuBTC interactions motivated the development of a new force fields based on ab initio data. Fischer et al.[16] fitted the potential between π-orbitals and CUS based on the DFT data augmented with dispersion corrections; through this approach the interaction energy between ethylene and the CUS is about 33 kJ mol^{-1}, which is significantly

underestimated compared to the accurate CCSD(T)/CBS results (41 kJ mol^{-1}) reported in Figure 2d. It is becoming clear that commonly employed DFT functionals have problems in properly describing the interactions of adsorbates with CUS, in particular those formed by transition metal cations such as Cu^{2+} in CuBTC.[15,21,24,25] Very good results were obtained with the force fields fitted on the MP2 calculations recently for Mg-MOF-74.[6] It should be noted, however, that the interaction of olefins with the Cu^{2+} CUS is strongly overestimated at the MP2/CBS level (−49 kJ mol^{-1}) compared to reference CCSD(T)/CBS calculations (−41 kJ mol^{-1}) (see Figure 2).

Regarding experimental adsorption enthalpies for propane and propylene on CuBTC, a number of groups have reported isosteric heats of adsorption calculated from isotherms measured at multiple temperatures, and these are summarized in Table 3.[17,18,20,44−47] From this it is apparent that for propylene, in particular, there is quite a disparity in the values reported in the literature, highlighting the need for accurate adsorption enthalpies obtained by direct measurement.

Table 3. Adsorption Energies Extrapolated to Zero Coverage ($-\Delta H_{zero}$) and Average Adsorption Energies ($-\Delta H_{av}$) for Propane and Propylene on CuBTC Compared with Literature Data[a]

	propane		propylene	
ref	$-\Delta H_{zero}$	$-\Delta H_{av}$	$-\Delta H_{zero}$	$-\Delta H_{av}$
Wagener et al.[20]	–	33	–	30
Lamia et al.[17]	–	29	54[b]	42
Wehring et al.[44]	–	31	–	43
Yoon et al.[18]	35	35	50	48
Ferreira et al.[45]	20[b]	34	60[b]	40
Plaza et al.[46]	26[b]	33	43	39
Plaza et al.[47]	28	30	54[b]	42
this work	45	38	58	55 → 45

[a]All values are expressed in kJ mol^{-1}. [b]Extrapolated from first two data points; however, significantly different from measured data.

For propane, the average adsorption energies are generally in the range of 30−35 kJ mol^{-1}, which is approximately 5 kJ mol^{-1} lower than the values obtained by calorimetry. The general trend observed is for the isosteric heats to remain more or less constant or increase slightly with loading, in agreement with the microcalorimetric measurements at higher loadings; however, the stronger interaction with the first few molecules observed by microcalorimetry is below the lowest loading for the isosteric heats reported in the literature. For propylene, the average adsorption energies range from 33 to 48 kJ mol^{-1}, while the isosteric heats extrapolated to zero coverage vary between 43 and ca. 60 kJ mol^{-1}. The tendency in most cases correctly shows the decrease in adsorption energy as a function of loading; however, this decrease is rather more abrupt than that observed by microcalorimetry.

There are a number of possible explanations for these differences. In the first place, they could be related to the quality of the sample used in the experiments. Previous studies have shown the wide range of surface areas and pore volumes obtained for CuBTC synthesized using different methods and synthesis conditions, with particularly in certain cases the tetrahedral cages being inaccessible.[48,49] The more abrupt decrease in adsorption enthalpies as a function of loading could be related to the partial blocking of some of the stronger adsorption sites. Alternatively, the variations could be artifacts introduced by the limitations of using the Clausius−Clapeyron equation to determine isosteric heats. This method is particularly dependent on not only the quality of the experimental data but also the quality of the fit used to determine the isosteres. Because of the rapid uptake of both propane and propylene on CuBTC at low pressure, it can be difficult to obtain many reliable points of the isotherms at low loadings and, hence, an accurate fit for calculating isosteric heats. In these cases it is essential to carry out direct measurements using microcalorimetry in order to have a reliable and detailed picture of the adsorption energies as a function of loading.

CONCLUSIONS

The dependence of the adsorption enthalpies on loading for propane and propylene on CuBTC was measured experimentally using a Tian−Calvet-type microcalorimeter up to approximately 8 mmol g^{-1} of propane/propylene in CuBTC (about 17 molecules in the reduced rhobohedral unit cell corresponding to a C_3H_n/Cu^{2+} ratio of 1.5). Qualitatively different results for propane and propylene were observed: adsorption enthalpies for propylene are first relatively constant and then they steadily decrease from 58 to 45 kJ mol^{-1}, while the adsorption enthalpies of propane first decrease from 44 to 36 kJ mol^{-1} (at about 2 mmol g^{-1} adsorbed amount) and then they steadily increase up to 49 kJ mol^{-1}.

The same three types of adsorption complexes were identified based on the DFT/CC investigation for both propane and propylene—coordinatively unsaturated, cage center, and cage windows sites. The stabilities of propane and propylene adsorption complexes on particular site types are qualitatively different: calculated $-\Delta H^{\circ}$ on coordinatively unsaturated, cage center and cage window sites are 56, 45, and 34 kJ mol^{-1}, respectively, for propylene, and they are 24, 43, and 31, respectively, for propane. Adsorption enthalpies were also calculated for higher propane/propylene loadings. On the basis of a very good agreement between experimental and calculated results the following adsorption mechanisms were proposed: propylene preferentially adsorbs on the CUS; cage center sites are occupied next (note that there seem to be only quite small lateral interactions between adsorbates at CUS and cage center sites) and cage window sites are occupied only at higher loading. Propane preferentially binds at the cage center sites, followed by adsorption at cage window sites; since there are significant lateral interactions between the adsorbates in the cage center and cage window sites, the adsorption enthalpies increase with increasing propane loading.

Due to the significant contribution of the partially dative bond between propylene π-orbitals and the Cu^{2+} cation, the propylene interaction with the CuBTC is significantly stronger than the propene interaction up to a coverage of 4−5 mmol g^{-1}. However, due to the increasing lateral interactions between propane molecules in cage center and cage window sites, the adsorption heats of propane are larger than those of propylene at higher loadings. Consequently, the CuBTC MOF does not have the optimum properties for propane/propylene separation. While the presence of Cu^{2+} CUS is beneficial for good propane/propylene separation, the presence of small cages (where molecules in cage center and cage window sites show favorable lateral interactions) makes the C_3 separation less efficient. This suggests that MOFs with Cu^{2+} CUS sites but no small cages (e.g., CPO-27[50]) could be more suitable for propane/propylene separation than the CuBTC MOF

dx.doi.org/10.1021/jp401600v | J. Phys. Chem. C 2013, 117, 11159−11167

investigated here.[7] It should also be noted, however, that while the presence of CUS in the adsorbent improves its ability to separate the two molecules, the stronger interaction of these sites with propylene significantly increases the difficulty in regenerating the adsorbent in a large column. For this reason, while adsorbents with CUS could be interesting from a purification point of view, the need for a high vacuum and/or heating during the regeneration step is likely to be prohibitive to these materials being used for a bulk separation using a PSA-type process.

The DFT/CC calculations employed here in combination with the periodic model are based on accurate coupled cluster calculations performed on a smaller model. These calculations clearly show that the standard exchange−correlation functional cannot be used to accurately describe the interaction of olefins with the Cu^{2+} CUS; even MP2 calculations overestimate the interaction by about 8 kJ mol^{-1}.

■ ASSOCIATED CONTENT

Supporting Information

Details about the DFT/CC reference sets and DFT/CC transferability. This material is available free of charge via the Internet at http://pubs.acs.org.

■ AUTHOR INFORMATION

Corresponding Author

*E-mail: petr.nachtigall@molecular.cz.

Notes

The authors declare no competing financial interest.

■ ACKNOWLEDGMENTS

The work has been funded by MACADEMIA (www.macademia-project.eu). MACADEMIA is a 4-year Large-Scale Integrating Collaborative Project, funded under the EU Seventh Framework Programme for Research and Development, under the Nanosciences, Nanotechnologies, Materials and New Production Technologies Theme ([FP7/2007-2013] under grant agreement no. 228862). Work in Prague was also supported by ME CR (grants ME10032 and MSM0021620857) and GA CR (P106/12/G015). Calculations were partially performed at MetaCentrum and CERIT-SC computational facilities (MSM/LM2010005 and OP VaVpI CZ. 1.05/3.2.00/08.0144).

■ REFERENCES

(1) Wu, H. H.; Gong, Q. H.; Olson, D. H.; Li, J. Commensurate Adsorption of Hydrocarbons and Alcohols in Microporous Metal Organic Frameworks. *Chem. Rev.* **2012**, *112*, 836−868.

(2) Ferey, G.; Serre, C.; Devic, T.; Maurin, G.; Jobic, H.; Llewellyn, P. L.; De Weireld, G.; Vimont, A.; Daturi, M.; Chang, J. S. Why Hybrid Porous Solids Capture Greenhouse Gases? *Chem. Soc. Rev.* **2011**, *40*, 550−562.

(3) Duren, T.; Sarkisov, L.; Yaghi, O. M.; Snurr, R. Q. Design of New Materials for Methane Storage. *Langmuir* **2004**, *20*, 2683−2689.

(4) Li, J. R.; Sculley, J.; Zhou, H. C. Metal−Organic Frameworks for Separations. *Chem. Rev.* **2012**, *112*, 869−932.

(5) Opanasenko, M.; Dhakshinamoorthy, A.; Shamzhy, M.; Nachtigall, P.; Horacek, M.; Garcia, H.; Cejka, J. Comparison of the Catalytic Activity of MOFs and Zeolites in Knoevenagel Condensation. *Catal. Sci. Technol.* **2013**, *3*, 500−507.

(6) Dzubak, A. L.; Lin, L. C.; Kim, J.; Swisher, J. A.; Poloni, R.; Maximoff, S. N.; Smit, B.; Gagliardi, L. Ab Initio Carbon Capture in Open-Site Metal−Organic Frameworks. *Nat. Chem.* **2012**, *4*, 810−816.

(7) Bae, Y. S.; Lee, C. Y.; Kim, K. C.; Farha, O. K.; Nickias, P.; Hupp, J. T.; Nguyen, S. T.; Snurr, R. Q. High Propene/Propane Selectivity in Isostructural Metal−Organic Frameworks with High Densities of Open Metal Sites. *Angew. Chem., Int. Ed.* **2012**, *51*, 1857−1860.

(8) Perez-Mayoral, E.; Musilova, Z.; Gil, B.; Marszalek, B.; Polozij, M.; Nachtigall, P.; Cejka, J. Synthesis of Quinolines Via Friedlander Reaction Catalyzed by CuBTC Metal−Organic-Framework. *Dalton Trans.* **2012**, *41*, 4036−4044.

(9) Vermoortele, F.; Ameloot, R.; Alaerts, L.; Matthessen, R.; Carlier, B.; Fernandez, E. V. R.; Gascon, J.; Kapteijn, F.; De Vos, D. E. Tuning the Catalytic Performance of Metal−Organic Frameworks in Fine Chemistry by Active Site Engineering. *J. Mater. Chem.* **2012**, *22*, 10313−10321.

(10) Pérez-Mayoral, E.; Čejka, J. $[Cu_3(BTC)_2]$: A Metal−Organic Framework Catalyst for the Friedländer Reaction. *ChemCatChem* **2011**, *3*, 157−159.

(11) Chui, S. S. Y.; Lo, S. M. F.; Charmant, J. P. H.; Orpen, A. G.; Williams, I. D. A Chemically Functionalizable Nanoporous Material $[Cu_3(TMA)_2(H_2O)_3]_n$. *Science* **1999**, *283*, 1148−1150.

(12) Vitillo, J. G.; Regli, L.; Chavan, S.; Ricchiardi, G.; Spoto, G.; Dietzel, P. D. C.; Bordiga, S.; Zecchina, A. Role of Exposed Metal Sites in Hydrogen Storage in MOFs. *J. Am. Chem. Soc.* **2008**, *130*, 8386−8396.

(13) Millward, A. R.; Yaghi, O. M. Metal−Organic Frameworks with Exceptionally High Capacity for Storage of Carbon Dioxide at Room Temperature. *J. Am. Chem. Soc.* **2005**, *127*, 17998−17999.

(14) Karra, J. R.; Walton, K. S. Molecular Simulations and Experimental Studies of CO_2, CO, and N_2 Adsorption in Metal−Organic Frameworks. *J. Phys. Chem. C* **2010**, *114*, 15735−15740.

(15) Grajciar, L.; Bludsky, O.; Nachtigall, P. Water Adsorption on Coordinatively Unsaturated Sites in CuBTC MOF. *J. Phys. Chem. Lett.* **2010**, *1*, 3354−3359.

(16) Fischer, M.; Gomes, J. R. B.; Froba, M.; Jorge, M. Modeling Adsorption in Metal−Organic Frameworks with Open Metal Sites: Propane/Propylene Separations. *Langmuir* **2012**, *28*, 8537−8549.

(17) Lamia, N.; Jorge, M.; Granato, M. A.; Paz, F. A. A.; Chevreau, H.; Rodrigues, A. E. Adsorption of Propane, Propylene and Isobutane on a Metal−Organic Framework: Molecular Simulation and Experiment. *Chem. Eng. Sci.* **2009**, *64*, 3246−3259.

(18) Yoon, J. W.; Jang, I. T.; Lee, K. Y.; Hwang, Y. K.; Chang, J. S. Adsorptive Separation of Propylene and Propane on a Porous Metal−Organic Framework, Copper Trimesate. *B. Kor. Chem. Soc.* **2010**, *31*, 220−223.

(19) Jorge, M.; Lamia, N.; Rodrigues, A. E. Molecular Simulation of Propane/Propylene Separation on the Metal−Organic Framework CuBTC. *Colloid. Surf. A* **2010**, *357*, 27−34.

(20) Wagener, A.; Schindler, M.; Rudolphi, F.; Ernst, S. Metal−Organic Coordination Polymers for the Adsorptive Separation of Propane/Propylene Compounds. *Chem. Ing. Tech.* **2007**, *79*, 851−855.

(21) Chen, L.; Grajciar, L.; Nachtigall, P.; Dueren, T. Accurate Prediction of Methane Adsorption in a Metal−Organic Framework with Unsaturated Metal Sites by Direct Implementation of an Ab Initio Derived Potential Energy Surface in GCMC Simulation. *J. Phys. Chem. C* **2011**, *115*, 23074−23080.

(22) Hartmann, M.; Kunz, S.; Himsl, D.; Tangermann, O.; Ernst, S.; Wagener, A. Adsorptive Separation of Isobutene and Isobutane on $Cu_3(BTC)_2$. *Langmuir* **2008**, *24*, 8634−8642.

(23) Bludsky, O.; Rubes, M.; Soldan, P.; Nachtigall, P. Investigation of the Benzene-Dimer Potential Energy Surface: DFT/CCSD(T) Correction Scheme. *J. Chem. Phys.* **2008**, *128*, 114102.

(24) Grajciar, L.; Wiersum, A. D.; Llewellyn, P. L.; Chang, J.-S.; Nachtigall, P. Understanding CO_2 Adsorption in CuBTC MOF: Comparing Combined DFT−Ab Initio Calculations with Microcalorimetry Experiments. *J. Phys. Chem. C* **2011**, *115*, 17925−17933.

(25) Rubes, M.; Grajciar, L.; Bludsky, O.; Wiersum, A. D.; Llewellyn, P. L.; Nachtigall, P. Combined Theoretical and Experimental Investigation of CO Adsorption on Coordinatively Unsaturated Sites in CuBTC MOF. *ChemPhysChem* **2012**, *13*, 488−495.

(26) Seo, Y.-K.; Hundal, G.; Jang, I. T.; Hwang, Y. K.; Jun, C.-H.; Chang, J.-S. Microwave Synthesis of Hybrid Inorganic−Organic Materials Including Porous $Cu_3(BTC)_2$ from Cu(II)−Trimesate Mixture. *Microporous Mesoporous Mater.* **2009**, *119*, 331−337.
(27) Llewellyn, P. L.; Maurin, G.; Poyet, T.; Dufau, N.; Denoyel, R.; Rouquerol, F. Do the Differential Enthalpies of Adsorption Vary between 77 and 302 K? An Experimental Case Study of Argon and Nitrogen on Two Faujasite Type Zeolites. *Adsorption* **2005**, *11*, 73−78.
(28) Llewellyn, P. L.; Maurin, G. Gas Adsorption Microcalorimetry and Modelling To Characterise Zeolites and Related Materials. *C. R. Chim.* **2005**, *8*, 283−302.
(29) Perdew, J. P.; Burke, K.; Ernzerhof, M. Generalized Gradient Approximation Made Simple. *Phys. Rev. Lett.* **1996**, *77*, 3865−3868.
(30) Blochl, P. E. Projector Augmented-Wave Method. *Phys. Rev. B* **1994**, *50*, 17953−17979.
(31) Kresse, G.; Hafner, J. Ab-Initio Molecular-Dynamics for Open-Shell Transition Metals. *Phys. Rev. B* **1993**, *48*, 13115−13118.
(32) Woon, D. E.; Dunning, T. H. Gaussian-Basis Sets for Use in Correlated Molecular Calculations. 3. The Atoms Aluminum through Argon. *J. Chem. Phys.* **1993**, *98*, 1358−1371.
(33) Peterson, K. A.; Puzzarini, C. Systematically Convergent Basis Sets for Transition Metals. II. Pseudopotential-Based Correlation Consistent Basis Sets for the Group 11 (Cu, Ag, Au) and 12 (Zn, Cd, Hg) Elements. *Theor. Chem. Acc.* **2005**, *114*, 283−296.
(34) Helgaker, T.; Klopper, W.; Koch, H.; Noga, J. Basis-Set Convergence of Correlated Calculations on Water. *J. Chem. Phys.* **1997**, *106*, 9639−9646.
(35) Halkier, A.; Helgaker, T.; Jorgensen, P.; Klopper, W.; Olsen, J. Basis-Set Convergence of the Energy in Molecular Hartree−Fock Calculations. *Chem. Phys. Lett.* **1999**, *302*, 437−446.
(36) Boys, S. F.; Bernardi, F. Calculation of Small Molecular Interactions by Differences of Separate Total Energies. Some Procedures with Reduced Errors. *Mol. Phys.* **1970**, *19*, 553−566.
(37) Werner, H. J.; Amos, R. D.; Bernhardsson; A.; Berning, A.; Celani, P. L.; Cooper, D.; Deegan, M. J. O.; Dobbyn, A. J.; Eckert, F.; Hampel, C.; Hetzer, G.; Knowles, P. J.; Korona, T.; Lindh, R.; Lloyd, A. W.; McNicholas, S. J.; Manby, F. R.; Meyer, W.; Mura, M. E.; Nicklaß, A.; Palmieri, P.; Rauhut, G.; Schütz, M.; Schumann, U.; Stoll, H.; Stone, A. J.; Tarroni, R.; Thorsteinsson, T. *MOLPRO, version 2009.1. A Package of Ab Initio Programs*; University College Cardiff Consultants Limited: Wales, U.K., 2009.
(38) Frisch, M. J.; Trucks, G. W.; Schlegel, H. B.; Scuseria, G. E.; Robb, M. A.; Cheeseman, J. R.; Montgomery, J. A., Jr.; Vreven, T.; Kudin, K. N.; Burant, J. C.; Millam, J. M.; Iyengar, S. S.; Tomasi, J.; Barone, V.; Mennucci, B.; Cossi, M.; Scalmani, G.; Rega, N.; Petersson, G. A.; Nakatsuji, H.; Hada, M.; Ehara, M.; Toyota, K.; Fukuda, R.; Hasegawa, J.; Ishida, M.; Nakajima, T.; Honda, Y.; Kitao, O.; Nakai, H.; Klene, M.; Li, X.; Knox, J. E.; Hratchian, H. P.; Cross, J. B.; Bakken, V.; Adamo, C.; Jaramillo, J.; Gomperts, R.; Stratmann, R. E.; Yazyev, O.; Austin, A. J.; Cammi, R.; Pomelli, C.; Ochterski, J. W.; Ayala, P. Y.; Morokuma, K.; Voth, G. A.; Salvador, P.; Dannenberg, J. J.; Zakrzewski, V. G.; Dapprich, S.; Daniels, A. D.; Strain, M. C.; Farkas, O.; Malick, D. K.; Rabuck, A. D.; Raghavachari, K.; Foresman, J. B.; Ortiz, J. V.; Cui, Q.; Baboul, A. G.; Clifford, S.; Cioslowski, J.; Stefanov, B. B.; Liu, G.; Liashenko, A.; Piskorz, P.; Komaromi, I.; Martin, R. L.; Fox, D. J.; Keith, T.; Al-Laham, M. A.; Peng, C. Y.; Nanayakkara, A.; Challacombe, M.; Gill, P. M. W.; Johnson, B.; Chen, W.; Wong, M. W.; Gonzalez, C.; and Pople, J. A. *Gaussian 09*; Gaussian, Inc.: Wallingford CT, 2004.
(39) Ho, T. S.; Rabitz, H. A General Method for Constructing Multidimensional Molecular Potential Energy Surfaces from Ab Initio Calculations. *J. Chem. Phys.* **1996**, *104*, 2584−2597.
(40) Soldan, P.; Hutson, J. M. On the Long-Range and Short-Range Behavior of Potentials from Reproducing Kernel Hilbert Space Interpolation. *J. Chem. Phys.* **2000**, *112*, 4415−4416.
(41) Wu, H.; Simmons, J. M.; Liu, Y.; Brown, C. M.; Wang, X. S.; Ma, S.; Peterson, V. K.; Southon, P. D.; Kepert, C. J.; Zhou, H. C.; Yildirim, T.; Zhou, W. Metal−Organic Frameworks with Exceptionally High Methane Uptake: Where and How Is Methane Stored? *Chem.—Eur. J.* **2010**, *16*, 5205−5214.
(42) Chen, L. J.; Morrison, C. A.; Duren, T. Improving Predictions of Gas Adsorption in Metal-Organic Frameworks with Coordinatively Unsaturated Metal Sites: Model Potentials, Ab Initio Parameterization, and GCMC Simulations. *J. Phys. Chem. C* **2012**, *116*, 18899−18909.
(43) Garcia-Perez, E.; Gascon, J.; Morales-Florez, V.; Castillo, J. M.; Kapteijn, F.; Calero, S. Identification of Adsorption Sites in Cu-BTC by Experimentation and Molecular Simulation. *Langmuir* **2009**, *25*, 1725−1731.
(44) Wehring, M.; Gascon, J.; Dubbeldam, D.; Kapteijn, F.; Snurr, R. Q.; Stallmach, F. Self-Diffusion Studies in CuBTC by PFG NMR and MD Simulations. *J. Phys. Chem. C* **2010**, *114*, 10527−10534.
(45) Ferreira, A. F. P.; Santos, J. C.; Plaza, M. G.; Lamia, N.; Loureiro, J. M.; Rodrigues, A. E. Suitability of Cu-BTC Extrudates for Propane-Propylene Separation by Adsorption Processes. *Chem. Eng. J.* **2011**, *167*, 1−12.
(46) Plaza, M. G.; Ferreira, A. F. P.; Santos, J. C.; Ribeiro, A. M.; Mueller, U.; Trukhan, N.; Loureiro, J. M.; Rodrigues, A. E. Propane/Propylene Separation by Adsorption Using Shaped Copper Trimesate MOF. *Microporous Mesoporous Mater.* **2012**, *157*, 101−111.
(47) Plaza, M. G.; Ribeiro, A. M.; Ferreira, A.; Santos, J. C.; Lee, U. H.; Chang, J.-S.; Loureiro, J. M.; Rodrigues, A. E. Propylene/Propane Separation by Vacuum Swing Adsorption Using Cu-BTC Spheres. *Sep. Purif. Technol.* **2012**, *90*, 109−119.
(48) Chowdhury, P.; Bikkina, C.; Meister, D.; Dreisbach, F.; Gumma, S. Comparison of Adsorption Isotherms on Cu-BTC Metal Organic Frameworks Synthesized from Different Routes. *Microporous Mesoporous Mater.* **2009**, *117*, 406−413.
(49) Farrusseng, D.; Daniel, C.; Gaudillère, C.; Ravon, U.; Schuurman, Y.; Mirodatos, C.; Dubbeldam, D.; Frost, H.; Snurr, R. Q. Heats of Adsorption for Seven Gases in Three Metal−Organic Frameworks: Systematic Comparison of Experiment and Simulation. *Langmuir* **2009**, *25*, 7383−7388.
(50) Bloch, E. D.; Queen, W. L.; Krishna, R.; Zadrozny, J. M.; Brown, C. M.; Long, J. R. Hydrocarbon Separation in a Metal−Organic Framework with Open Iron(II) Coordination Sites. *Science* **2012**, *335*, 1606−1610.

Attachment F

CHEMPHYSCHEM

DOI: 10.1002/cphc.201100602

Combined Theoretical and Experimental Investigation of CO Adsorption on Coordinatively Unsaturated Sites in CuBTC MOF

Miroslav Rubeš,[a] Lukáš Grajciar,[a] Ota Bludský,[b] Andrew D. Wiersum,[c] Philip L. Llewellyn,[c] and Petr Nachtigall*[a]

The adsorption of CO in metal–organic framework CuBTC material is investigated by a combination of theoretical and experimental approaches. The adsorption enthalpy of CO on CuBTC determined experimentally to be $-29\ kJ\,mol^{-1}$ at the zero-coverage limit is in very good agreement with the adsorption enthalpy calculated at the combined DFT–ab initio level with the periodic model. Calculations show that polycarbonyl complexes cannot be formed on regular coordinatively unsaturated sites in CuBTC. Experimental IR spectra of the CO probe molecule adsorbed in CuBTC are interpreted based on calculated CO stretching frequencies. Calculations show that long-range interactions are insignificant for the CO/CuBTC system and that this system can be accurately modeled with just a $Cu_2(HCOO)_4$ cluster model of the paddle wheel. The reliability of various methods for the description of CO interaction with the Cu^{2+} site in CuBTC is discussed based on the experimental results and accurate coupled-cluster calculations. It is shown that standard exchange-correlation functionals do not provide a reliable description of CO interaction with coordinatively unsaturated Cu^{2+} sites in CuBTC.

1. Introduction

Metal–organic frameworks (MOFs) are currently investigated with respect to their potential applications utilizing both their porosity and the presence of coordinatively unsaturated (CUS) sites.[1] The MOF HKUST-1, Cu_3(1,3,5-benzenetricarboxylate)$_2$, often referred to as CuBTC, has become a reference MOF material that has often been investigated both experimentally and theoretically.[2] The presence of Cu^{2+} CUS sites, together with the presence of large and small cages, makes this material attractive for gas adsorption,[2d,g,3] gas separation,[2c,h,i] and even for catalysis.[2j,4]

The active sites in catalysis and adsorption are often investigated by IR spectroscopy with CO as a probe molecule,[5] in particular in microporous materials where the use of many powerful surface characterization techniques is precluded.[6] The CO probe molecule has also been tested for numerous MOFs,[7] including CuBTC.[2a,8] Assignment of relatively rich spectra in the CO stretching region has been discussed; nevertheless, not all of the IR features were conclusively interpreted. There is an agreement on the interpretation of the main band located at about 2170–2178 cm^{-1} that is assigned to carbonyl groups formed on Cu^{2+} sites in CuBTC.[2a,8] However, there are several suggestions to explain the shift of this band from 2178 cm^{-1} to lower energy with increasing CO coverage.[8,9]

On the computational side, adsorption of various molecules (including H_2, N_2, CO, CO_2, and hydrocarbons) on CuBTC has been investigated using various combinations of models and methods.[2b,d,e,10] 1) Cluster models have been used in combination with the density functional theory (DFT) based method[10c] or with standard ab initio post-Hartree–Fock (HF) methods such as perturbation theory or even coupled clusters.[2e,f,11] Such ab initio calculations can be used for benchmarking computationally less expensive DFT methods and for verification and/or re-parameterization of force fields. 2) Periodic models have been used in combination with either force fields[2b,d,10b,e,g] or the DFT method.[10a,d,f,11]

An accurate description of CO interaction with CUS sites in CuBTC is a particularly challenging problem for computational chemistry for the following reasons: long-range interactions (that can be correctly captured only with periodic models) may be important, the electronic structure of open-shell transition-metal cations (Cu^{2+}) must be properly described, interaction of CO with Cu^{2+} sites has some covalent (dative) character, and, last but not least, the presence of unpaired electrons on two adjacent Cu^{2+} cations calls for multireference wavefunctions. It is an interesting question whether cluster models combined with highly accurate electronic structure methods (such as

[a] Dr. M. Rubeš, L. Grajciar, Prof. P. Nachtigall
Department of Physical and Macromolecular Chemistry
Faculty of Science, Charles University in Prague
Hlavova 2030, 12840 Prague 2 (Czech Republic)
Fax: (+420) 221 951 289
E-mail: petr.nachtigall@molecular.cz

[b] Dr. O. Bludský
Center for Biomolecules and Complex Molecular Systems
Institute of Organic Chemistry and Biochemistry, AS ČR
Flemingovo nám. 2, 16610 Prague (Czech Republic)

[c] A. D. Wiersum, Dr. P. L. Llewellyn
Laboratoire Chimie Provence
Université d'Aix-Marseille I, II et III, CNRS (UMR 6264)
Centre de St Jérôme, 13397 Marseille Cedex 20 (France)

Supporting information for this article is available on the WWW under http://dx.doi.org/10.1002/cphc.201100602. CuBTC = Cu_3(1,3,5-benzenetricarboxylate)$_2$; MOF = metal–organic framework.

coupled clusters) or periodic models in combination with less accurate DFT methods or force fields should be used for the reliable description of adsorption on open-shell transition-metal sites. To address this question it is essential to have reliable experimental data to compare with the theoretical results. However, no experimental adsorption enthalpies are available for CO adsorption on CuBTC in the literature to the best of our knowledge.

The accurate description of CO interaction with CUS sites in HKUST-1 is presented here. The reliability of the methods is investigated first with the cluster models representing the Cu^{2+} site; the accuracy of various methods is evaluated with respect to highly precise coupled-cluster (CC) calculations. The multireference character of the wavefunction is also discussed. Based on the cluster model calculations a method to be used in the periodic model is proposed. The periodic model is then used for calculations of adsorption enthalpies and the results are compared with experimental data obtained from microcalorimetry measurements for the low CO coverage regime. Experimental results are essential for the assessment of the accuracy of various models and methods used for calculations of CO adsorption enthalpy and frequencies on the CuBTC model.

2. Results

Theoretical results obtained with cluster models of the paddle wheel (PDWL) are described first. The performance of the exchange-correlation functional is discussed based on the agreement with the multireference CASPT2 calculations. The accuracy of the DFT/CC method, used for the calculations on the periodic model of CuBTC, is discussed in the light of accurate CCSD(T)/CBS calculations carried out for cluster models. Experimental results are reported in the last section.

Cluster Model Calculations

As described in the Computational and Experimental Section, the DFT calculations for the singlet (S) state were carried out either for the closed-shell singlet (S_{CS}) or for the broken-symmetry solution (S_{BS}; Table 1). The PBE-(S_{CS}) results are in qualitative disagreement with CASPT2 reference results; firstly, the singlet state is above the triplet (T) state and, secondly, the ΔE_{ST} values depend on the number of CO molecules interacting with the PDWL. Similar problems were found for other exchange-correlation functionals. The S_{CS} state will not be considered any further herein, since it cannot provide a reliable description of the system. On the contrary, the PBE calculations carried out for the singlet within the broken-symmetry approximation, PBE(S_{BS}), result in a qualitatively correct sign of ΔE_{ST} and only a moderate dependence on the number of CO molecules. However, the ΔE_{ST} is significantly (about 10 kJ mol^{-1}) overestimated.

Table 1. Singlet–triplet energy gap (ΔE_{ST}, with respect to the triplet state) [kJ mol^{-1}] for bare PDWL, CO/PDWL, and $(CO)_2$/PDWL complexes. The structures were optimized under the C_{4v} symmetry constraint with the VDZ basis set.

Method	PDWL	CO/PDWL	$(CO)_2$/PDWL
CASPT2(S_{MR})[a]	−1.9	−1.7	−1.6
PBE(S_{CS})[b]	13.0	5.2	8.0
PBE(S_{BS})[c]	−11.4	−13.0	−12.6

[a] Multireference singlet state. [b] Single-reference closed-shell singlet state. [c] Broken-symmetry singlet solution.

The characteristics of CO adsorption complexes on PDWL are summarized in Table 2. The reliability of the DFT method will be discussed with respect to the CASPT2/AVDZ level. The reported DFT characteristics are not expected to change substantially with increasing basis set size, since the VDZ and AVDZ interaction energies are within 1 kJ mol^{-1}. Note that for the T state, the CASPT2/AVDZ gives interaction energies in good agreement with the accurate CCSD(T)/CBS level (see Figure 1 and discussion below) as a consequence of the fortuitous error compensation (small basis set versus insufficient treatment of electron correlation). Therefore, the CASPT2/AVDZ results reported in Table 2 are expected to be rather close to accurate CCSD(T)/CBS results.

Table 2. CO interaction with Cu^{2+} sites modeled by the PDWL cluster; the deformation energy (E_{def}), counterpoise (CP)-corrected interaction energy (E_{int}), and enthalpy change ($-\Delta H^0$(0 K)) are defined per CO molecule.[a]

Methods	n(CO)[b]	Pyramidalization[c] [Å]	r_{Cu-C} [Å]	$\Delta\nu$(CO)[d] [cm^{-1}]	E_{def}[e] [kJ mol^{-1}]	E_{int} [kJ mol^{-1}]	$-\Delta H^0$(0 K) [kJ mol^{-1}]
CASPT2(S_{MR})	1	0.190/0.082	2.326	44[g]	3.0	−31.4	27.8[h]
CASPT2(T) ≡ MP2	1	0.190/0.082	2.327	44	3.0	−31.6	28.0
B3LYP(S_{BS})	1	0.209/0.091	2.329	42	3.6	−19.4	16.2
B3LYP(T)	1	0.206/0.090	2.332	42	3.5	−19.5	16.2
PBE(S_{BS})[f]	1	0.254/0.016	2.092	10	11.7	−29.9	27.7
PBE(T)	1	0.215/0.022	2.137	18	8.7	−28.4	25.9
CASPT2(S_{MR})	2	0.156	2.354	41[g]	3.5	−30.1	26.6[h]
CASPT2(T) ≡ MP2	2	0.156	2.353	41	3.5	−30.2	26.7
B3LYP(T)	2	0.173	2.362	38	4.3	−18.1	15.0
PBE(S_{BS})[f]	2	0.173	2.159	11	11.5	−26.0	23.9
PBE(T)	2	0.156	2.182	16	10.0	−25.5	23.2

[a] The C_{4v} constrained optimization was performed with the VDZ basis set. Resulting geometries were used for evaluations of CP-corrected interaction energies with the larger AVDZ basis set. [b] Number of CO molecules interacting with PDWL; one CO molecule is on each Cu^{2+} site when two molecules interact with PDWL. [c] Pyramidalization is defined as the Cu^{2+} distance from the plane defined by four carboxylic oxygen atoms interacting with Cu^{2+}. The two entries shown for n(CO) = 1 refer to pyramidalization on Cu^{2+} cations with and without a CO molecule. The bare PDWL pyramidalization amounts to 0.115, 0.125, 0.087, and 0.080 Å at the CASPT2, B3LYP, PBE(S_{BS}), and PBE(T) levels, respectively. [d] Vibration frequency shifts of interacting CO molecules defined with respect to free CO at the same level of theory. Experimental shifts of 35 and 31 cm^{-1} were reported for lower and higher CO coverage, respectively.[8,9] [e] E_{def} is defined in the Computational Section. [f] PBE(S_{BS}) CP-corrected interaction energies are estimated from basis set superposition error (BSSE) uncorrected values due to convergence issues. [g] CO frequencies calculated from a two-dimensional grid. [h] ΔE_{ZPVE} calculated for the MP2 triplet state (ZPVE = zero-point vibrational energy).

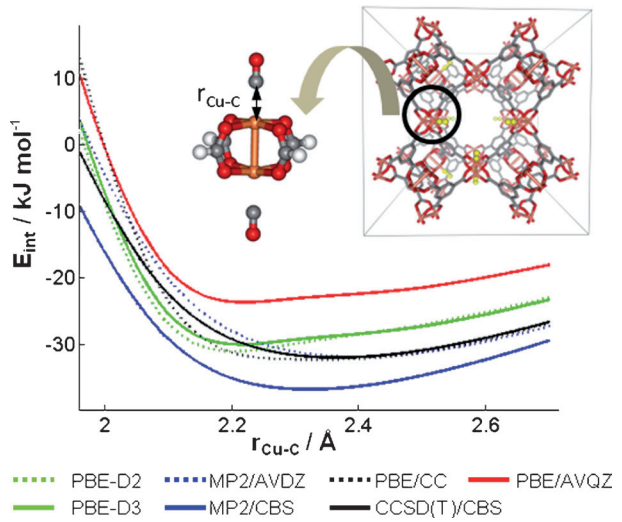

Figure 1. Interaction energy of CO with Cu^{2+} CUS site calculated with the $(CO)_2/Cu_2(HCOO)_4$ cluster model of PDWL (left inset) representing the CUS site in CuBTC (right inset). Calculations were performed for the triplet electronic state at different levels of theory as a function of r_{Cu-C} distance (frozen monomer approximation adopted). Methods are defined in the Computational Section; PBE-D2 and PBE-D3 refer to dispersion correction schemes proposed in ref. [12].

The characteristics calculated for S and T electronic states at the CASPT2 level are almost indistinguishable. The same observation can be made for the B3LYP results; however, small differences between the results obtained for T and S states at the PBE level are apparent. The interaction between CO and PDWL is substantially underestimated at the B3LYP level. On the contrary, the interaction energies calculated at the PBE level are underestimated only by about 2–5 kJ mol^{-1}.

Large deformation energies observed at the PBE level result from the largest change of pyramidalization upon interaction with CO molecules (Table 2). The extent of geometrical changes of PDWL upon formation of $(CO)_n$/PDWL complexes is quantified by the pyramidalization on Cu^{2+} and by the deformation energy (E_{def}). The pyramidalization is defined as the distance of the Cu^{2+} cation from the plane defined by four adjacent carboxylic oxygen atoms. As the pyramidalization increases, we observe both that the Cu–Cu distance increases and that the Cu–C distance decreases. The B3LYP and CASPT2 Cu–C distances are about 0.2 Å longer than the PBE ones. Deformation energies calculated at the PBE level are significantly larger than those obtained at the CASPT2 level.

All methods predict a blue shift in the CO stretching frequencies with respect to the free CO (Table 2). The CASPT2 CO frequency shifts amount to 44 and 41 cm^{-1} for one and two adsorbed CO molecules, respectively. The CO frequency shifts calculated at the B3LYP level are in good agreement (within 3 cm^{-1}) with the CASPT2 results. However, the blue shift is considerably underestimated at the PBE level. All methods predict a small shift to lower CO stretching frequency upon adsorption of the second CO molecule, with the exception of the PBE(S_{BS}) level.

The comparison of the PBE/CC results with benchmark calculations for the triplet state of PDWL with two CO molecules (one on each side) is depicted in Figure 1. The frozen monomer approximation has been adopted (see Computational Section). The CCSD(T)/CBS interaction energy amounts to −32.0 kJ mol^{-1} with equilibrium Cu–C distance of 2.37 Å. The MP2/CBS interaction energies are about 5 kJ mol^{-1} overestimated with respect to CCSD(T)/CBS values and also the Cu–C distances are shorter by 0.05 Å. However, note that the MP2/AVDZ interaction energy and equilibrium distance are close to CCSD(T)/CBS values, even though, as mentioned above, the agreement is based on error cancellation in the MP2 approach. The PBE interaction energies are about 8 kJ mol^{-1} underestimated with respect to CCSD(T)/CBS. However, the substantial underestimation of the interaction energy at the PBE level is inconsistent with the short Cu–C equilibrium distance. The DFT/CC approach corrects the deficient behavior of the PBE functional to a large extent. Thus, the interaction energy and equilibrium distance are very close to benchmark CCSD(T)/CBS values. A closer inspection of the behavior of the DFT/CC potential energy curve reveals that transferability of pairwise correction functions is not as good as in the previously reported cases of PDWL interacting with water and CO_2.[2e,f] It can also be noted that DFT with empirical dispersion correction (often referred to as DFT-D[12]) improves the interaction energies, but the short equilibrium Cu–C distances remain essentially unchanged.

The PBE/CC error estimate presented in Figure 1 is based on the fixed monomer geometries. Note, however, that the DFT/CC approach inherently assumes that the error in DFT description is not significantly altered upon some changes in monomer geometries in the complex. The artificially large relative change of PDWL pyramidalization upon CO adsorption at the PBE level indicates that this assumption is not fully satisfied. The full PBE/CC optimization of the $(CO)_2$/PDWL complex gives an interaction energy of −33.7 kJ mol^{-1} and Cu–C equilibrium distance of 2.286 Å. The PBE/CC error estimate can be obtained by comparison with MP2/AVDZ interaction energies (supposedly close to CCSD(T)/CBS) for the optimized PDWL complex with two CO molecules (see Table 2). It can be concluded that PBE/CC interaction energy is about 3.5 kJ mol^{-1} overestimated and the Cu–C equilibrium distance is shorter by 0.07 Å.

CO Adsorption in CuBTC: Periodic DFT/CC Model

Neither PBE nor B3LYP functionals describe accurately all the aspects of the $(CO)_n$–PDWL interaction. The B3LYP significantly underestimates the interaction energies, while the more accurate interaction energies obtained at the PBE level are only on account of a large change of PDWL pyramidalization upon interaction with CO. To accurately describe the CO adsorption in CuBTC within the periodic DFT approach, the DFT description should be corrected. The primary focus will be on correcting the PBE behavior because the size of the primitive cell of CuBTC makes the calculations at the B3LYP level computationally expensive. The deficient behavior of the PBE functional is corrected within the DFT/CC correction scheme.

The results of CO adsorption in CuBTC represented by a periodic model are summarized in Table 3. The high-spin ferromagnetic solution has been used to keep it consistent with our benchmark calculations for the PDWL model in the triplet electronic state. The interaction energy calculated for the first CO molecule is $-35.8\,kJ\,mol^{-1}$, very similar to the value found for the PDWL cluster model at the same level of theory. It indicates that long-range interactions (defined as interactions with atoms outside the PDWL where CO is bound) are very small. It also suggests that the cluster model of PDWL represents well the CUS site of the CuBTC framework and that it can be used for the investigation of CO interaction with CuBTC. Note, however, that such a conclusion cannot be generalized; a recent study of CO_2 adsorption in CuBTC revealed rather large importance of long-range interactions, including lateral interactions.[2f]

Table 3. CO interaction with CUS sites in CuBTC described by periodic PBE and PBE/CC models.

Methods	n(CO)[a]	Pyramidalization[b] [Å]	r_{Cu-C} [Å]	E_{def}[c] [kJ mol^{-1}]	E_{int} [kJ mol^{-1}]	$-\Delta H^0$(0 K)[d] [kJ mol^{-1}]
PBE	1	0.232/0.022	2.130	10.2	−26.8	24.3
PBE/CC	1	0.188/0.036	2.263	5.4	−35.8	33.3
PBE	2	0.168/0.161	2.190/2.196	5.2	−23.6	21.3
PBE/CC	2	0.141/0.136	2.298/2.295	2.8	−33.8	31.5

[a] Number of CO molecules interacting with PDWL; one CO molecule is on each Cu^{2+} site when two molecules interact with PDWL. [b] Pyramidalization is defined as the Cu^{2+} distance from the plane defined by four carboxylic oxygen atoms interacting with Cu^{2+}. [c] E_{def} is defined in the Computational Section. [d] ΔE_{ZPVE} is taken from the PBE(T) results of the PDWL model.

The adsorption enthalpies $-\Delta H^0$ calculated at the DFT/CC level with the periodic model amount to 33.3 and 31.5 $kJ\,mol^{-1}$ for the first and second CO molecules adsorbed on the same PDWL unit, respectively. Based on the discussion of the PBE/CC accuracy presented above, the best estimate of $-\Delta H^0$ is 30 and 28 $kJ\,mol^{-1}$ for one and two CO molecules, respectively, on one PDWL unit. The formation of polycarbonyl complexes (two CO molecules interacting with one Cu^{2+} cation) was also investigated at the PBE and PBE/CC levels of theory and with the periodic model. However, such complexes were found to be unstable and geometry optimization always led to dissociation of one of the CO molecules away from Cu^{2+}; attempts to find polycarbonyl complexes with the cluster model of PDWL also failed.

Microcalorimetry

To validate the theoretical study, adsorption uptakes and direct energy measurements were carried out. The adsorption isotherms of CO on CuBTC at 303 K from the large-dose and small-dose experiments are shown in Figure 2 (hollow and filled symbols, respectively). The two isotherms are in perfect agreement, thereby showing the regenerability of the sample and reliability of the experimental setup. The plot shows a classic Langmuir-type isotherm with a relatively shallow slope. A Henry's constant of 1.55 $mmol\,g^{-1}\,bar^{-1}$ has been calculated for the almost linear section in the low-pressure region, compared to 5.25 $mmol\,g^{-1}\,bar^{-1}$ for CO_2, for example.[2f] The amounts adsorbed are comparable to the values reported in the literature.[1d,10b] Note that at 6 bar, the sample is far from reaching its saturation capacity.

Adsorption enthalpies measured during the large-dose experiment show an initial enthalpy of almost $-40\,kJ\,mol^{-1}$, which drops to below $-30\,kJ\,mol^{-1}$ at a coverage of 0.4 $mmol\,g^{-1}$ followed by a slight but constant decrease of $-1.7\,kJ\,mol^{-1}$ per $mmol\,g^{-1}$ of gas adsorbed as the coverage increases. To investigate the high initial enthalpy, the experiment was repeated with small doses. Again, a very high initial enthalpy was observed, this time in excess of $-63\,kJ\,mol^{-1}$, after which the adsorption enthalpy dropped immediately to $-29\,kJ\,mol^{-1}$ at a coverage of 0.1 $mmol\,g^{-1}$. This very high initial enthalpy can be attributed to the presence of Cu^{+} impurities in the sample, which will be discussed further in the next section. At higher coverages, the two experiments are in good agreement.

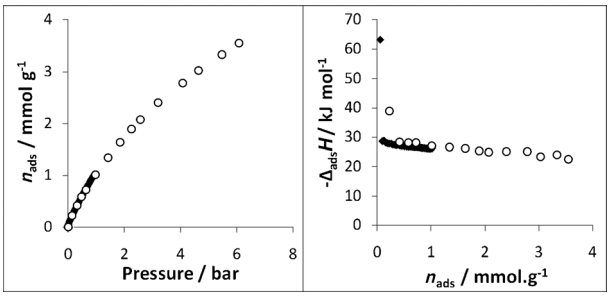

Figure 2. CO adsorption at 303 K on CuBTC: large doses (○) and small doses (◆). Adsorption isotherm (left) and the corresponding adsorption enthalpies (right).

3. Discussion

The experimentally detected IR band at 2178 cm^{-1} is assigned to a CO interaction with a CUS site of the CuBTC.[2a,8,9] This band is 35 cm^{-1} blue-shifted with respect to free CO; however, the calculated shift in CO stretching frequency is about 10 cm^{-1} overestimated at the MP2 and B3LYP levels. This discrepancy mainly stems from the insufficient basis set size used in the PDWL model calculations; Table S1 in the Supporting Information shows that a larger basis set brings the frequency down by 7 cm^{-1}, in good agreement with experimental results. The PBE(T) calculations underestimate the shift in CO frequency by a factor of 2 and the larger basis set would not bring any significant improvement. The poor description at the PBE level might be connected with the short Cu–C equilibrium dis-

tances, which indicate a more favorable σ-bonding interaction.[13] The overestimated σ-bonding interaction is consistent with large PDWL pyramidalization observed at the PBE level. Also, PBE tends to effectively increase the electron density on the Cu^{2+} cation.[2e] This artificial charge delocalization (electron density flow from organic linkers to the metal cation) found at the PBE level might lead to some π back-donation from Cu to CO, which results in the decrease of the CO frequency shift. The mixing of the exact exchange into the DFT functional decreases the charge delocalization onto the Cu^{2+} cation;[2e] thus, B3LYP gives CO frequency shifts significantly improved with respect to the PBE ones.

The theoretical assignment of the other experimentally observed IR bands is more difficult. The formation of polycarbonyl species on the CUS sites can be ruled out based on the calculations reported above, contrary to some propositions based on experimental IR spectra.[2a,8b] This is not surprising, because just one adsorbed CO molecule on the Cu^{2+} cation saturates the octahedral coordination sphere of the cation. At low coverage, only one CO molecule is adsorbed per PDWL and it is characterized by ν(CO) = 2178 cm^{-1}. With increasing CO coverage, complexes having a CO on each Cu^{2+} of the same PDWL occur and such complexes are characterized by ν(CO) in the range 2170–2174 cm^{-1}; a small shift of the CO frequency due to the presence of the second CO molecule on the PDWL is due to an indirect interaction caused by the change in Cu^{2+} pyramidalization. The other experimentally determined IR bands, namely the band around 2125 cm^{-1} and two smaller bands around 2195 and 2155 cm^{-1}, should not arise as a result of the CO interaction with regular CUS sites in CuBTC.

Our assignment does not agree with the conclusion of Liu and Zhong,[10c] who assigned the band at 2125 cm^{-1} to the CO complex on Cu^{2+} CUS sites. However, there are several reasons why the band at 2125 cm^{-1} cannot correspond to this complex. The high initial enthalpy of the microcalorimetric measurements suggests the presence of a small number of defects in the form of Cu^{+} sites in the sample. Similar microcalorimetric measurements for the adsorption of CO on highly loaded Cu^{+}-ZSM-5 gave enthalpies of −103 and −64 kJ mol^{-1} for the formation of monocarbonyl and dicarbonyl complexes, respectively, with part of the monocarbonyl complexes being irreversible under simple vacuum.[14] Such defects in CuBTC have already been observed by IR spectroscopy by Prestipino et al.,[9] who detected the presence of a small amount of strongly bonded CO on Cu^{+} sites at low pressure which was resistant to prolonged outgassing at 77 K. From the adsorption enthalpies obtained with small doses (Figure 2) it is possible to estimate the ratio of Cu^{+} to Cu^{2+} ions in the same sample, which is most likely less than 1:80. Thus, the band at 2125 cm^{-1} is usually assigned to the interaction of CO with Cu^{+} sites in the form of Cu_2O impurities, because the typical red Cu_2O nanoparticles have been observed after the synthesis of the CuBTC and this agrees well with previously reported CO frequency shifts on this type of surface.[2a,13,15] Furthermore, the CO interaction with Cu^{+} is strong enough to be persistent at room temperature upon evacuation,[16] and it should be noted that about an order of magnitude larger extinction coefficient is expected for CO complexes on Cu^{+} than on Cu^{2+} cations.[5] Moreover, Liu and Zhong[10c] assigned the IR bands based on absolute values of calculated harmonic CO frequencies, which is rather peculiar.

The best estimate reported above for the calculated adsorption enthalpy for the zero-coverage limit is −30 kJ mol^{-1}, obtained with the periodic PBE/CC model. This result is, however, rather different from comparable computational values reported in the literature: Karra and Walton have reported an isosteric heat of 17.5 kJ mol^{-1} based on their GCMC simulation employing a combination of several force fields.[10b] The periodic DFT calculations of Watanabe and Sholl gave a binding energy of 46.3 kJ mol^{-1}.[10d] Based on the B3LYP calculations, Liu and Zhong reported CO interaction with the PDWL cluster model of −27.7 kJ mol^{-1}.[10c] It is apparent that the reliable experimental adsorption enthalpies reported in the Results section are absolutely essential for further discussion. The experimentally determined adsorption enthalpy at zero-coverage limit is −29 kJ mol^{-1}. This is in very good agreement with the DFT/CC results reported above. The experimental value is also close to the cluster model results of Liu and Zhong;[10c] however, this agreement is rather fortuitous since their calculations are not corrected for BSSE (we have estimated this error to be about 12 kJ mol^{-1} for the VDZP quality basis set). The B3LYP results reported in Table 2 for cluster models do indeed show a $-\Delta H^0$ value of 16.2 kJ mol^{-1}. Watanabe and Sholl[10d] employed a periodic model with PW91 functional along with antiferromagnetic solution and their interaction energy is about 20 kJ mol^{-1} larger than the corresponding value obtained at the PBE level (Table 3). Note that the results reported in Table 3 were obtained for the high-spin ferromagnetic solution, because the state is well defined and convergence to the adequate state is guaranteed; based on cluster calculations (Table 1) the difference between interaction energies obtained with ferromagnetic and antiferromagnetic spin couplings should not exceed 2 kJ mol^{-1}. Also, the experimentally reported coupling between PDWL units in CuBTC is rather weak.[17] The interaction energy of 46.3 kJ mol^{-1} reported in Ref. [10d] was obtained for the antiferromagnetic state; it is quite a challenging task to converge the solution to appropriate spin couplings for every PDWL in the unit cell. Note a large difference between the closed-shell and broken-symmetry singlet PBE results reported in Table 1. The discrepancy between interaction energies reported here and the interaction energies of Watanabe and Sholl[10d] can be possibly attributed to the convergence issues associated with the antiferromagnetic solution.

Results reported in Tables 2 and 3 indicate that the effect of long-range interactions is very small. To quantify the differences between the periodic and $Cu_2(HCOO)_4$ cluster model, the PBE and PBE/CC calculations on the cluster model were repeated with a saturated basis set (VQZ). It shows that the interaction strength of the first CO molecule actually decreases upon going from the cluster to periodic model from −29.6 to −26.8 kJ mol^{-1} at the PBE level and it remains unchanged (−36.1 and −35.8 kJ mol^{-1}) at the PBE/CC level. It follows that the long-range dispersion interactions accounted for at the PBE/CC level (about −3 kJ mol^{-1}) just compensate the changes

due to the electronic structure effects described at the DFT level.

Recently, it has been shown that the interaction of water with CuBTC can be successfully modeled using a cluster of water with copper formate ($Cu_2(HCOO)_4$) having a PDWL structure.[2e] A rather similar conclusion can be drawn here for CO interaction with CuBTC. It follows that the interaction of small molecules (CO, H_2O, and most likely H_2 and N_2) with CUS sites in CuBTC can be accurately described with the cluster model. However, just a slightly larger molecule, such as CO_2, requires a significantly larger model than the $Cu_2(HCOO)_4$ cluster.[2f]

4. Conclusions

The adsorption enthalpy of CO on CuBTC was determined experimentally to be $-29\,kJ\,mol^{-1}$ at zero-coverage limit and it slightly but steadily decreases with increasing CO coverage. Experimental adsorption enthalpies are in very good agreement with those calculated at the combined DFT–ab initio level using the recently developed DFT/CC method.[18] It is demonstrated that an accurate theoretical description of the CO interaction with CUS sites in CuBTC is rather complicated and requires theoretical modeling that goes beyond the standard DFT or standard force fields.

Based on a very good agreement between DFT/CC adsorption enthalpies obtained for the periodic model, $-\Delta H^0 = 30$ and $28\,kJ\,mol^{-1}$ for the first and the second CO molecule on one PDWL unit, respectively, the accuracy of models and methods can be commented on. The long-range effects are rather small and the interaction of CO with CuBTC can be well described with the cluster model of the PDWL. While a relatively small cluster model can represent the CuBTC material, the accurate description of the electronic structure of the system is rather demanding. 1) A multireference wavefunction or at least broken-symmetry solution must be used for the description of the PDWL with antiferromagnetically coupled electrons. 2) The ferromagnetic coupling of electrons (that can be represented by a single Slater determinant) in a PDWL can be used for the description of interaction with CO. 3) The CCSD(T)/CBS level provides a highly accurate description of the system in the triplet electronic state (ferromagnetic coupling). 4) The MP2/CBS level overestimates the interaction with CO. 5) Standard generalized gradient approximation (GGA)-type exchange-correlation functionals exaggerate the electron density flow from the organic linker to the Cu^{2+} cation and such an error cannot be simply corrected by empirical dispersion correction terms.

Calculations show that only the band in the IR spectra at $2170–2178\,cm^{-1}$ is due to the CO adsorption complexes on regular CUS sites in CuBTC, while the other bands observed experimentally must be due to the defect sites or to weakly (dispersion) bound CO. The shift of the band at $2178\,cm^{-1}$ towards a lower frequency at increased CO coverage is due to the formation of adsorption complexes having one CO molecule on each of the two Cu^{2+} sites of one PDWL; frequency lowering is due to the smaller pyramidalization.

Computational and Experimental Section

CuBTC Sample: CuBTC MOF (HKUST-1) was provided by the Korea Research Institute for Chemical Technology and was prepared by microwave synthesis.[19] The sample was activated by heating to 150 °C under secondary vacuum ($< 1.10^{-3}$ mbar). The apparent BET surface area was determined by adsorption of N_2 at 77 K in the relative pressure range $P/P_0 = 0.0002–0.01$, following the guidelines proposed by Rouquerol et al.[20] The sample was found to have a surface area of $1628\,m^2\,g^{-1}$ and a pore volume of $0.64\,cm^3\,g^{-1}$. These values are among the highest reported in the literature and are very close to the values reported by Seo et al.[19] for CuBTC prepared by microwave synthesis ($1656\,m^2\,g^{-1}$).

Microcalorimetry: Adsorption enthalpies were measured experimentally using a Tian–Calvet-type microcalorimeter coupled with a homemade manometric gas-dosing system.[21] This apparatus allowed the simultaneous measurement of the adsorption isotherm and the corresponding differential enthalpies. Gas is introduced into the system using a step-by-step method and each dose is allowed to stabilize in a reference volume before being brought into contact with the adsorbent located in the microcalorimeter. The introduction of the adsorbate to the sample is accompanied by an exothermic thermal signal, measured by the thermopiles of the microcalorimeter. The peak in the calorimetric signal is integrated over time to give the total energy released during that adsorption step.

Two separate experiments were carried out at 30 °C using large (0.6 bar) doses up to 6 bar and small (0.1 bar) doses up to 1 bar, respectively. Around 0.2 g of sample was used and this was outgassed at 150 °C for 16 h under secondary vacuum prior to each experiment. For each injection of gas, equilibrium was assumed to have been reached after 90 min. This was confirmed by the return of the calorimetric signal to its baseline ($< 5\,\mu W$). The gas used for the adsorption was obtained from Air Liquide and was of N47 quality (99.997% purity).

Calculations: The model complex $(CO)_{n=1,2}/Cu_2(HCOO)_4$ (see inset of Figure 1) has been described with the standard Dunning's correlation-consistent valence-*X*-ζ basis set with polarization functions,[22] while for the Cu atoms the pseudopotential-based correlation-consistent valence-*X*-ζ basis set with polarization functions has been employed.[23] The basis sets will be collectively denoted as V*X*Z, where *X* stands for double, triple, and quadruple basis sets. The corresponding augmented basis sets will be accordingly denoted as AV*X*Z throughout the work.

The complete active space second-order perturbation theory with two electrons in two active orbitals (CASPT2(2,2)) optimization of $(CO)_{n=0,1,2}/Cu_2(HCOO)_4$ complexes was performed for the multireference singlet (S_{MR}) and triplet (T) electronic states.[24] Note that the CASPT2(2,2) calculation in the triplet electronic state is equivalent to the second-order perturbation theory of Møller–Plesset (MP2[25]) in this particular case. The geometry optimization at the DFT level was performed with B3LYP[26] and PBE[27] functionals. The behavior of the single-reference closed-shell singlet (S_{CS}), broken-symmetry singlet (S_{BS}), and triplet (T) electronic states was investigated. Geometry optimization was performed under the C_{4v} symmetry constraint (Figure 1) employing the VDZ basis set. Only the C-down adsorption complexes were considered since they are twice as stable as O-down complexes at the MP2/VDZ level. The resulting interaction energies were evaluated with a larger AVDZ basis set and they were counterpoise (CP) corrected by means of the standard procedure of Boys and Bernardi.[28] For discussion of geometry changes of the PDWL or CuBTC upon interaction with CO mole-

cules the deformation energy (E_{def}) was evaluated. The deformation energy is defined as the energy required to move PDWL or framework CuBTC atoms from their optimal position with no CO molecules adsorbed to the position optimal for the formation of CO-adsorbed species. The CO frequencies and the zero-point vibrational energy (ZPVE) were evaluated within the harmonic approximation. In the case of the CASPT2(S_{MR}) calculations the Hessian was evaluated numerically on a two-dimensional 25-point grid, by varying Cu–C and C–O distances with the steps 0.01 and 0.005 Å, respectively.

The benchmark CCSD(T) interaction energies at the complete basis set (CBS) limit were obtained for the $(CO)_2$/PDWL complex with D_{4h} symmetry. The PDWL monomer was optimized at PBE(S_{CS})/AVTZ (pyramidalization amounts up to 0.094 Å) and CO at CCSD(T)/AVQZ level of theory. The CBS estimate was obtained by means of a simple correlation energy dependence on the basis set cardinal number X ($E_X = E_{CBS} + AX^{-3}$).[29] The uncorrelated part (HF) of the calculation was extrapolated by means of a two-point formula proposed by Halkier et al., with $\alpha = 1.63$.[30] The HF/CBS and MP2/CBS estimates were obtained from VTZ and VQZ calculations. The interaction energies were calculated at the CCSD(T)/AVDZ level, and the corresponding CCSD(T)/CBS was obtained as follows [Eq. (1)]:

$$\mathrm{CCSD(T)/CBS} = \mathrm{CCSD(T)/AVDZ} + (\mathrm{MP2/CBS} - \mathrm{MP2/AVDZ}) \quad (1)$$

The periodic DFT calculations were performed with the PBE functional for the ferromagnetic case (i.e. unpaired spins on 12 copper atoms in the unit cell were aligned in the same direction). The rhombohedral primitive cell containing 156 framework atoms has been adopted with cell parameters optimized in previous work ($a = b = c = 18.774$ Å, $\alpha = \beta = \gamma = 60^\circ$).[2e] The projector augmented wave (PAW)[31] and the kinetic energy cutoff of 600 eV were used. The Γ-point sampling of the first Brillouin zone was found to be sufficient to yield converged results.
The cluster model calculations were performed with Molpro 09[32] and Gaussian 09[33] program suites and periodic calculations were performed in the VASP 5.2[34] package.

DFT/CC Method: Recently, we have shown that nonlocal correlation (i.e. dispersion) remedies only part of the problem in the DFT description of the water interaction with PDWL or CuBTC.[2e] It is thus necessary to go beyond standard dispersion-corrected DFT schemes to correct the deficient DFT behavior for these types of complexes. The DFT/CC[18] correction scheme is based on the pairwise representability of the DFT error (ΔE), which is expressed as follows [Eq. (2)]:

$$\Delta E = E_{CCSD(T)} - E_{DFT} \quad (2)$$

where $E_{CCSD(T)}$ and E_{DFT} are interaction energies calculated at the CCSD(T)/CBS and DFT/AVQZ levels of theory, respectively. It can be seen that Equation (2) can be applied in a general manner, and thus it is not confined to just addressing the lack of dispersion in "standard" GGAs or hybrid DFT functionals. The DFT error, ΔE, is then expressed as a sum of pairwise atom–atom correction functions $\varepsilon_{ij}(R_{ij})$ [Eq. (3)]:

$$\Delta E = \sum_{ij} \varepsilon_{ij}(R_{ij}) \quad (3)$$

where R_{ij} is the distance between atoms i and j. There is no assumption about the functional form of the ε_{ij}; instead the reciprocal-power reproducing kernel Hilbert space (RP-RKHS)[35] interpolation is used. The essential prerequisite in the DFT/CC approach is the choice of the reference set of molecules from which the atom–atom corrections are generated. The correction functions ε_{CH} (ε_{OH}), ε_{CC} (ε_{OC}), ε_{OO}, and ε_{CuC} (ε_{CuO}) were evaluated from one-dimensional potential energy curves of CO···H_2, CO···C_6H_6, CO···CO_2, and CO···Cu-$(HCOO)_2$. The details about the construction of correction functions are given in the Supporting Information. The transferability (i.e. the quality of the resulting correction functions) was checked for the $(CO)_2$/PDWL complex and compared with the CCSD(T)/CBS results. Furthermore, the DFT/CC approach was used in periodic DFT calculations to obtain accurate estimates of adsorption enthalpies.

Acknowledgements

The research leading to these results received funding from the European Community's Seventh Framework Programme (FP7/2007-2013) under grant agreement no. 228862. MACADEMIA is a large-scale integrating project under the Nanosciences, Nanotechnologies, Materials, and New Production Technologies Theme (www.macademia-project.eu). P.N. and L.G. also acknowledge the support of ME CR (grants 7E09111 and MSM0021620857). A.D.W. and P.L.L. would like to thank researchers of KRICT (Korea Research Institute of Chemical Technology) for the microwave synthesis of CuBTC and the sample provision. Work at the Institute of Organic Chemistry and Biochemistry (OB) was supported by the Ministry of Education, Youth, and Sports (MEYS) under Grant No. LC512 and Research Project No. Z4055 0506.

Keywords: ab initio calculations · adsorption · density functional calculations · metal–organic frameworks · microcalorimetry

[1] a) N. Rosi, J. Eckert, M. Eddaoudi, D. Vodak, J. Kim, M. O'Keeffe, O. Yaghi, *Science* **2003**, *300*, 1127; b) G. Férey, *Chem. Soc. Rev.* **2008**, *37*, 191; c) A. R. Millward, O. M. Yaghi, *J. Am. Chem. Soc.* **2005**, *127*, 17998; d) Q. M. Wang, D. M. Shen, M. Bulow, M. L. Lau, S. G. Deng, F. R. Fitch, N. O. Lemcoff, J. Semanscin, *Microporous Mesoporous Mater.* **2002**, *55*, 217.

[2] a) L. Alaerts, E. Seguin, H. Poelman, F. Thibault-Starzyk, P. A. Jacobs, D. E. De Vos, *Chem. Eur. J.* **2006**, *12*, 7353; b) J. M. Castillo, T. J. H. Vlugt, S. Calero, *J. Phys. Chem. C* **2008**, *112*, 15934; c) A. F. P. Ferreira, J. C. Santos, M. G. Plaza, N. Lamia, J. M. Loureiro, A. E. Rodrigues, *Chem. Eng. J.* **2011**, *167*, 1; d) J. Getzschmann, I. Senkovska, D. Wallacher, M. Tovar, D. Fairen-Jimenez, T. Duren, J. M. van Baten, R. Krishna, S. Kaskel, *Microporous Mesoporous Mater.* **2010**, *136*, 50; e) L. Grajciar, O. Bludsky, P. Nachtigall, *J. Phys. Chem. Lett.* **2010**, *1*, 3354; f) L. Grajciar, A. D. Wiersum, P. Llewellyn, J.-S. Chang, P. Nachtigall, *J. Phys. Chem. C* **2011**, *115*, 17925; g) F. Gul-E-Noor, B. Jee, A. Poppl, M. Hartmann, D. Himsl, M. Bertmer, *Phys. Chem. Chem. Phys.* **2011**, *13*, 7783; h) L. Hamon, E. Jolimaitre, G. D. Pirngruber, *Ind. Eng. Chem. Res.* **2010**, *49*, 7497; i) Z. J. Liang, M. Marshall, A. L. Chaffee, *Energy Fuels* **2009**, *23*, 2785; j) E. Pérez-Mayoral, J. Čejka, *ChemCatChem* **2011**, *3*, 157.

[3] J. Moellmer, A. Moeller, F. Dreisbach, R. Glaeser, R. Staudt, *Microporous Mesoporous Mater.* **2011**, *138*, 140.

[4] K. Schlichte, T. Kratzke, S. Kaskel, *Microporous Mesoporous Mater.* **2004**, *73*, 81.

[5] K. I. Hadjiivanov, G. N. Vayssilov, *Adv. Catal.* **2002**, *47*, 307.

[6] A. Zecchina, C. O. Arean, *Chem. Soc. Rev.* **1996**, *25*, 187.

[7] L. Valenzano, B. Civalleri, S. Chavan, G. T. Palomino, C. Arean, S. Bordiga, *J. Phys. Chem. C* **2010**, *114*, 11185.

[8] a) S. Bordiga, L. Regli, F. Bonino, E. Groppo, C. Lamberti, B. Xiao, P. S. Wheatley, R. E. Morris, A. Zecchina, *Phys. Chem. Chem. Phys.* **2007**, *9*,

2676; b) N. Drenchev, E. Ivanova, M. Mihaylov, K. Hadjiivanov, *Phys. Chem. Chem. Phys.* **2010**, *12*, 6423.
[9] C. Prestipino, L. Regli, J. G. Vitillo, F. Bonino, A. Damin, C. Lamberti, A. Zecchina, P. L. Solari, K. O. Kongshaug, S. Bordiga, *Chem. Mater.* **2006**, *18*, 1337.
[10] a) H. Wu, J. M. Simmons, G. Srinivas, W. Zhou, T. Yildirim, *J. Phys. Chem. Lett.* **2010**, *1*, 1946; b) J. R. Karra, K. S. Walton, *J. Phys. Chem. C* **2010**, *114*, 15735; c) D. H. Liu, C. L. Zhong, *J. Phys. Chem. Lett.* **2010**, *1*, 97; d) T. Watanabe, D. S. Sholl, *J. Chem. Phys.* **2010**, *133*, 094509; e) Q. Yang, C. Zhong, *J. Phys. Chem. B* **2006**, *110*, 17776; f) S. C. Xiang, W. Zhou, J. M. Gallegos, Y. Liu, B. L. Chen, *J. Am. Chem. Soc.* **2009**, *131*, 12415; g) D. Farrusseng, C. Daniel, C. Gaudillere, U. Ravon, Y. Schuurman, C. Mirodatos, D. Dubbeldam, H. Frost, R. Q. Snurr, *Langmuir* **2009**, *25*, 7383.
[11] K. Sillar, A. Hofmann, J. Sauer, *J. Am. Chem. Soc.* **2009**, *131*, 4143.
[12] a) S. Grimme, *J. Comput. Chem.* **2006**, *27*, 1787; b) S. Grimme, J. Antony, S. Ehrlich, H. Krieg, *J. Chem. Phys.* **2010**, *132*, 154104.
[13] K. Hadjiivanov, H. Knozinger, A. Milushev, *Catal. Commun.* **2002**, *3*, 37.
[14] V. Bolis, A. Barbaglia, S. Bordiga, C. Lamberti, A. Zecchina, *J. Phys. Chem. B* **2004**, *108*, 9970.
[15] A. Zecchina, D. Scarano, S. Bordiga, G. Spoto, C. Lamberti, *Adv. Catal.* **2001**, *46*, 265.
[16] R. Bulánek, H. Drobna, P. Nachtigall, M. Rubes, O. Bludsky, *Phys. Chem. Chem. Phys.* **2006**, *8*, 5535.
[17] a) X. X. Zhang, S. S. Y. Chui, I. D. Williams, *J. Appl. Phys.* **2000**, *87*, 6007; b) A. Poppl, S. Kunz, D. Himsl, M. Hartmann, *J. Phys. Chem. C* **2008**, *112*, 2678.
[18] a) O. Bludský, M. Rubes, P. Soldan, P. Nachtigall, *J. Chem. Phys.* **2008**, *128*, 114102; b) M. Rubeš, J. Kysilka, P. Nachtigall, O. Bludsky, *Phys. Chem. Chem. Phys.* **2010**, *12*, 6438.
[19] Y. K. Seo, G. Hundal, I. T. Jang, Y. K. Hwang, C. H. Jun, J. S. Chang, *Microporous Mesoporous Mater.* **2009**, *119*, 331.
[20] F. Rouquerol, J. Rouquerol, K. Sing, *Adsorption by Powders and Porous Solids*, Academic Press, London, **1999**.
[21] P. Llewellyn, G. Maurin, *C. R. Chim.* **2005**, *8*, 283.
[22] D. E. Woon, T. H. Dunning, *J. Chem. Phys.* **1993**, *98*, 1358.
[23] K. A. Peterson, C. Puzzarini, *Theor. Chem. Acc.* **2005**, *114*, 283.
[24] P. Celani, H. J. Werner, *J. Chem. Phys.* **2000**, *112*, 5546.
[25] C. Møller, M. S. Plesset, *Phys. Rev.* **1934**, *46*, 618.
[26] A. D. Becke, *J. Chem. Phys.* **1993**, *98*, 5648.
[27] J. P. Perdew, K. Burke, M. Ernzerhof, *Phys. Rev. Lett.* **1996**, *77*, 3865.
[28] S. F. Boys, F. Bernardi, *Mol. Phys.* **1970**, *19*, 553.
[29] T. Helgaker, W. Klopper, H. Koch, J. Noga, *J. Chem. Phys.* **1997**, *106*, 9639.
[30] A. Halkier, T. Helgaker, P. Jorgensen, W. Klopper, J. Olsen, *Chem. Phys. Lett.* **1999**, *302*, 437.
[31] P. E. Blöchl, *Phys. Rev. B* **1994**, *50*, 17953.
[32] Molpro (version 2009.1), H. J. Werner, R. D. Amos, A. Bernhardsson, A. Berning, P. Celani, D. L. Cooper, M. J. O. Deegan, A. J. Dobbyn, F. Eckert, C. Hampel, G. Hetzer, P. J. Knowles, T. Korona, R. Lindh, A. W. Lloyd, S. J. McNicholas, F. R. Manby, W. Meyer, M. E. Mura, A. Nicklaß, P. Palmieri, R. Pitzer, G. Rauhut, M. Schütz, U. Schumann, H. Stoll, A. J. Stone, R. Tarroni, T. Thorsteinsson, A Package of Ab Initio Programs, University College Cardiff Consultants Limited, Wales, UK, **2009**.
[33] Gaussian 03 (Revision A.02), M. J. Frisch, G. W. Trucks, H. B. Schlegel, G. E. Scuseria, M. A. Robb, J. R. Cheeseman, J. A. Montgomery, Jr., T. Vreven, K. N. Kudin, J. C. Burant, J. M. Millam, S. S. Iyengar, J. Tomasi, V. Barone, B. Mennucci, M. Cossi, G. Scalmani, N. Rega, G. A. Petersson, H. Nakatsuji, M. Hada, M. Ehara, K. Toyota, R. Fukuda, J. Hasegawa, M. Ishida, T. Nakajima, Y. Honda, O. Kitao, H. Nakai, M. Klene, X. Li, J. E. Knox, H. P. Hratchian, J. B. Cross, V. Bakken, C. Adamo, J. Jaramillo, R. Gomperts, R. E. Stratmann, O. Yazyev, A. J. Austin, R. Cammi, C. Pomelli, J. W. Ochterski, P. Y. Ayala, K. Morokuma, G. A. Voth, P. Salvador, J. J. Dannenberg, V. G. Zakrzewski, S. Dapprich, A. D. Daniels, M. C. Strain, O. Farkas, D. K. Malick, A. D. Rabuck, K. Raghavachari, J. B. Foresman, J. V. Ortiz, Q. Cui, A. G. Baboul, S. Clifford, J. Cioslowski, B. B. Stefanov, G. Liu, A. Liashenko, P. Piskorz, I. Komaromi, R. L. Martin, D. J. Fox, T. Keith, M. A. Al-Laham, C. Y. Peng, A. Nanayakkara, M. Challacombe, P. M. W. Gill, B. Johnson, W. Chen, M. W. Wong, C. Gonzalez, J. A. Pople, Gaussian, Inc., Wallingford, CT, **2004**.
[34] a) G. Kresse, J. Hafner, *Phys. Rev. B* **1993**, *48*, 13115; b) G. Kresse, D. Joubert, *Phys. Rev. B* **1999**, *59*, 1758.
[35] a) T. S. Ho, H. Rabitz, *J. Chem. Phys.* **1996**, *104*, 2584; b) P. Soldán, J. M. Hutson, *J. Chem. Phys.* **2000**, *112*, 4415.

Received: August 3, 2011
Revised: September 15, 2011
Published online on December 13, 2011

Attachment G

DOI: 10.1002/cssc.201200270

Controlling the Adsorption Enthalpy of CO_2 in Zeolites by Framework Topology and Composition

Lukáš Grajciar,[a] Jiří Čejka,[b] Arnošt Zukal,[b] Carlos Otero Areán,[c] Gemma Turnes Palomino,[c] and Petr Nachtigall*[a]

Zeolites are often investigated as potential adsorbents for CO_2 adsorption and separation. Depending on the zeolite topology and composition (Si/Al ratio and extra-framework cations), the CO_2 adsorption heats at low coverages vary from -20 to -60 kJ mol^{-1}, and with increasing surface coverage adsorption heats either stay approximately constant or they quickly drop down. Experimental adsorption heats obtained for purely siliceous porous solids and for ion-exchanged zeolites of the structural type MFI, FER, FAU, LTA, TUN, IMF, and -SVR are discussed in light of results of periodic density functional theory calculations corrected for the description of dispersion interactions. Key factors influencing the stability of CO_2 adsorption complexes are identified and discussed at the molecular level. A general model for CO_2 adsorption in zeolites and related materials is proposed and data reported in literature are evaluated with regard to the proposed model.

Introduction

Oil, natural gas, and coal together account for, at present, about 80% of the primary energy supply. It is worthwhile noting that these three carbon-based energy sources (known as fossil fuels) made the rapid development of our technological civilization possible, leading to the present level of well-being and comfort. However, CO_2 produced by burning fossil fuels, together with that generated by several industrial processes (cement manufacturing, iron and steel production, and petrochemical plants, among others), results in it being presently vented into the atmosphere at a rate of about 28 billion tons per year. The consequent increase in the greenhouse effect, which can adversely affect climate, is causing worldwide concern. Replacing fossil fuels with renewable, and cleaner, energy sources could provide a way out of this problem in the long run, but we still need a mid-term solution to allow the humanity to continue using fossil fuels until cost-effective renewable energy can be implemented on a large scale. Carbon dioxide capture and sequestration (CCS)[1] could constitute part of that mid-term solution, particularly if current research in this area brings about a significant reduction of cost.

Implementation of CCS from the flue gases of stationary sources (such as fossil-fuel power plants) can be accomplished by using liquid amine-based (or ammonia-based) chemical absorbents,[2] but, besides being energy intensive and expensive,[3] that technology can pose environmental hazards derived from accidental spills;[4] hence, it is convenient to search for less expensive and safer CO_2-capturing media. Among them, porous solids capable of separating CO_2 from flue gases by physical adsorption (instead of chemical absorption) constitute a main topic of current research.

Besides separating CO_2 from N_2 in flue gases of power stations, porous adsorbents are also used to separate CO_2 from methane in natural gas and landfill gas. In both cases pressure swing adsorption (PSA) processes can be used,[5] which have the potential to be less energy intensive than regeneration of chemical CO_2 absorbents. The main types of porous materials currently under active research for CO_2 separation are porous carbons,[6] metal–organic frameworks (MOFs),[6a,7] zeolites,[8] and amine-functionalized ordered mesoporous silica.[6a,8a,9] Propelled by the need to find a cost-effective solution for CCS, research on CO_2 sorbents is currently attracting considerable attention,[9a,b,10] and several excellent reviews on this research field (including both physical and chemical sorbents for CO_2) have appeared.[8a,d,11] Among porous materials for CO_2 capture, nowadays MOFs constitute the main focus of very active research.[12] Nevertheless, for several reasons (see below), zeolites continue to be attractive in this field. Herein, we focus on the mechanism of CO_2 adsorption in zeolites and mesoporous silicas.

The main advantages of zeolites are low cost and high thermal stability, as well as easy cation exchange, which facilitate the tuning of gas–solid interaction energy. Such interaction energy is the main factor to consider when screening porous

[a] L. Grajciar, Prof. P. Nachtigall
Department of Physical and Macromolecular Chemistry
Faculty of Science, Charles University in Prague
Hlavova 2030, CZ-128 40 Prague 2 (Czech Republic)
Fax: (+420) 221-951-289
E-mail: petr.nachtigall@molecular.cz

[b] Prof. J. Čejka, Dr. A. Zukal
J. Heyrovský Institute of Physical Chemistry
Academy of Sciences of the Czech Republic
Dolejškova 3, Prague 8, 182 23 (Czech Republic)

[c] Prof. C. Otero Areán, G. Turnes Palomino
Department of Chemistry
University of the Balearic Islands
Palma de Mallorca (Spain)

Supporting Information for this article is available on the WWW under http://dx.doi.org/10.1002/cssc.201200270.

adsorbents for gas separation by PSA processes; the differential stability of adsorption complexes formed by different components of a gas mixture should be large enough to enhance separation selectivity, while keeping the stability low enough to facilitate regeneration of the adsorbent with low energy expenditure. To find the most suitable adsorbent for a particular application, it is essential to understand the mechanism of CO_2 adsorption at the molecular level.

The interaction of CO_2 with alkali-metal-exchanged zeolites has been investigated computationally by employing DFT and various models of adsorbent (e.g., bare metal cations,[13] large cluster models,[14] periodic models of zeolites[15]) or interatomic potentials and grand canonical Monte Carlo simulations (GCMC).[16] While GCMC simulations give access to thermodynamic features relevant to higher coverage and temperature, the accuracy of these simulations depends heavily on the quality of the interatomic potential parameters employed. Several interatomic potentials were used to describe the interaction of CO_2 with zeolite adsorbents, and in the majority of cases these interatomic potentials were adjusted to reproduce experimental adsorption isotherms or adsorption heats. The use of DFT (employing standard generalized-gradient approximation (GGA)-type exchange-correlation functionals) is even more problematic: first, because only data relevant for the zero coverage limit is obtained and, second, because of the inability of GGA functionals to account properly for dispersion interactions, which constitutes a major drawback.

The main goal of the investigation reported herein was to combine the highly accurate ab initio description of the interaction of CO_2 with zeolites with experimentally determined adsorption heats to understand the mechanism of CO_2 interaction with zeolites at the molecular level. For that purpose, we combined experimentally determined isosteric heats of adsorption with DFT/coupled cluster (CC)[17] calculations (recently shown to give a very accurate description of adsorbate–adsorbent interactions[18]) on periodic zeolite models. The role of different factors that determine the gas–solid interaction energy, such as zeolite topology and zeolite chemical composition, is thus analyzed. Purely siliceous polymorphs and several alkali-metal-exchanged zeolites (sodium-exchanged zeolites, in particular) with different framework topologies and Si/Al ratios were both investigated.

Experimental Section

Materials

Zeolite Na-A (Si/Al ratio = 1) reported in this contribution was obtained from the National Bureau of Standards (US).[19] Zeolites Li-Y, K-Y, and CsY were prepared by ion exchange of a parent Na-Y sample with an Si/Al ratio of 2.5.[15a] Zeolite ZSM-5 was purchased from Zeolyst. Other zeolites, namely, ferrierite,[20] MCM-22,[21] ZSM-11,[22] TNU-9,[22] IM-5,[22] and SSZ-74,[22] as well as the mesoporous molecular sieve SBA-15,[23] were synthesized in the J. Heyrovsky Institute of Physical Chemistry (Prague). All molecular sieves were transformed into the sodium form by ion exchange with sodium nitrate (0.5 M, 100 mL of the aqueous solution per 1 g of material; ion exchange was carried out at room temperature for 4 h and repeated four times). Li, Cs, and K forms were then prepared from the parent Na forms under the same conditions by using the respective metal nitrates or chlorides. After ion exchange, the samples were thoroughly washed with distilled water and dried overnight.

Adsorption measurements

Adsorption isotherms of nitrogen at 77 K and carbon dioxide in the temperature range from 273 to 333 K were recorded by using an ASAP 2020 (Micromeritics) static volumetric apparatus. To attain sufficient accuracy in the accumulation of the adsorption data, the ASAP 2020 instrument was equipped with pressure transducers covering the 0.133, 1.33, and 133 kPa ranges. Generally, before the adsorption measurements, the individual samples were outgassed under a turbomolecular pump vacuum by using a heating program that afforded slow removal of humidity at a relatively low temperature. Starting at ambient temperature, the samples were outgassed at 383 K until a residual pressure of 0.5 Pa was attained. After further heating at 383 K for 1 h, the temperature was increased up to 623 K and maintained for 8 h. A homemade thermostat capable of maintaining the temperature of the sample within an accuracy of ± 0.01 K was used for the measurements of carbon dioxide adsorption at 273, 293, 313, and 333 K. The corresponding nitrogen adsorption isotherm was obtained prior to measurements with carbon dioxide, for which the sample was regenerated. The outgassing procedure was performed at 523 K for 12 h under a turbomolecular pump vacuum. The only exception to this sample activation procedure was that used for the Na-A zeolite, which, like other low-silica zeolites, tended to form (irreversibly) surface carbonates.[8g,24] For this reason the sample was saturated with CO_2 prior to the experiments and left to stand until surface carbonate formation ended. Subsequently, free CO_2 was outgassed and volumetric adsorption measurements were started. Further details about this activation procedure can be found elsewhere.[19]

Calculations

Results reported herein for CO_2 interaction with Silicalite-1, Na-ZSM-5, siliceous LTA, and Na-Y adsorbents were all obtained by using a periodic model and the DFT method implemented in the VASP program package[25] and augmented for the description of dispersion interactions[17] (described below). The exchange-correlation functional of Perdew, Becke, and Ernzerhof (PBE)[26] was employed together with the projector-augmented wave approximation (PAW) of Blöchl[25c,27] and the plane wave basis set with a kinetic energy cutoff of 400 eV. Brillouin-zone sampling was restricted to the Γ point. The same level of theory was also used in recent theoretical investigations of CO_2 adsorption in alkali-metal-exchanged FER zeolites[15b,20,28] and in zeolite Na-LTA.[19]

Calculations on Silicalite-1 were performed with the orthorhombic unit cell (UC) optimized previously ($Si_{96}O_{192}$, $a = 20.241$ Å, $b = 20.001$ Å, $c = 13.514$ Å).[29] A UC of the same volume was also used as a model of the high-silica Na-ZSM-5, represented by $Si_{96-n}Al_nNa_nO_{192}$ ($n = 1$ and 2). The Y zeolite was represented by a reduced UC with the composition $Si_{35}Al_{13}Na_{13}O_{96}$ (Si/Al = 2.69:1) and cell parameters $\alpha = \beta = \gamma = 60^\circ$ and $a = b = c = 17.37$ Å. The experimental cubic UC was used for calculations on purely siliceous LTA ($a = b = c = 11.87$ Å).[30] Calculations on Na-A and various ferrierites were described previously.[19,20,28]

Dispersion forces contribute substantially to the total interaction energy between CO_2 and microporous adsorbents,[16a,b,d] and hence, they have to be accounted for in calculations. It was recent-

ly shown that standard exchange-correlation functionals (not accounting for nonlocal interactions) strongly underestimate the total interaction energy between zeolites and adsorbed CO_2. Hence, an appropriate correction for dispersion interactions must necessarily be applied.[20,28] A combined DFT/CC method recently developed was shown to give results in a very good agreement with experimental data,[20,28] and for this reason it was adopted in the present investigation. The DFT/CC method is based on the pairwise representability of the DFT error, $\Delta E_{DFT/CC}$, defined as the difference between the precise CCSD(T) and DFT interaction energy [Eq. (1)]:[18a,31]

$$\Delta E_{DFT/CC} = \Delta E_{CC} - \Delta E_{DFT} = \sum_{ij} \varepsilon_{ij}(R_{ij}) \quad (1)$$

in which ΔE_{DFT} and ΔE_{CC} are interaction energies calculated for the reference system at the DFT and coupled cluster CCSD(T) levels, respectively, ε_{ij} are the correction functions depending on the interatomic distances R_{ij}, and i and j runs over atoms in adsorbent and adsorbate, respectively. The correction functions for CO_2 interaction with zeolites can be found in the Supporting Information of Ref. [31], together with more details about this method.

The geometry of each CO_2 adsorption complex was optimized at the DFT/CC level; atomic positions of both adsorbate and adsorbent were fully relaxed, while the size and shape of the UC were constrained. The zero-point vibrational energy corrections, ΔE_{ZPVE}, were evaluated within the harmonic approximation considering nine degrees of freedom for the CO_2 molecule; the second derivatives were calculated numerically by using ± 0.005 Å displacements. An almost constant value of ΔE_{ZPVE} was found for CO_2 interactions with FER zeolites;[20] therefore, a constant value of $\Delta E_{ZPVE} =$ 1 and 2 kJ mol^{-1} was used for Silicalite-1 and Na-MFI, respectively. Adsorption enthalpies ΔH^0 [Eq. (3)] were calculated for the process shown in Equation (2) as a sum of interaction energies calculated at the DFT level (ΔE_{DFT}), DFT/CC correction term ($\Delta E_{DFT/CC}$), and correction for the zero-point vibrational energy (ΔE_{ZPVE}):

$$(CO_2)_g + \text{Zeolite} \rightarrow CO_2 \cdots \text{Zeolite} \quad (2)$$

$$\Delta H^0 = \Delta E_{DFT} + \Delta E_{DFT/CC} + \Delta E_{ZPVE} \quad (3)$$

It must be stressed that all calculations discussed herein (both new results reported for Silicalite-1, Na-MFI, Na-FAU, and siliceous LTA and recently published results for Na-LTA, M-FER, and siliceous FER) were carried out at the same level of theory (DFT/CC) and consistent model (periodic model of each particular UC). Therefore, the results obtained can be directly compared with each other.

Notation used for adsorption sites

The cationic CO_2 adsorption sites in zeolites are discussed, in particular, for zeolites belonging to the structural type MFI, FER, FAU, and LTA, for which, first, there are both experimental and theoretical results available and, second, these zeolites cover the entire range of allowed Si/Al ratios (from 1 to ∞). Two types of extra-framework cation positions can be distinguished:[32] 1) channel wall sites, where cations are located on top of, or inside, a ring located on the surface of the channel; and 2) intersection sites, where cations are located on the edge formed by two intersecting channels. Compared with cations located at intersection sites, those located in channel wall sites typically interact with more framework oxygen atoms, are buried deeper into the channel surface, and have a lower ability to bind molecules of adsorbate. Examples of channel wall sites and intersection sites can be found in Figure 1 (e.g., Z6/T10 and I2/T6 sites, respectively). Some necessary details about specific zeolites investigated herein are briefly reviewed below.

Na-ZSM-5: The CO_2 adsorption complexes formed on the Na^+ cation located in the vicinity of framework AlO_4 tetrahedra in the T4, T6, T10, T11, and T12 positions (adopting the numbering scheme from Ref. [33]) were considered (Figure 1). A detailed description of these Na^+ sites in Na-ZSM-5 can be found in Ref. [29]. Notation for cation sites introduced previously was adopted:[34] intersection sites, sites in the main channel, and sites in the zigzag channel are denoted as "I", "M", and "Z" sites, respectively (Figure 1).

(Li-, Na-, K-)FER: All details about the models and methods used for the investigation of FER zeolites can be found in Refs. [20] (Li-FER, Na-FER, and K-FER) and [28] (siliceous FER).

Na-Y: Framework Al distribution was generated randomly within the constraints defined by the Löwenstein and Dempsey rules.[35] The distribution that matched the results of ^{29}Si NMR spectroscopy obtained for the Y zeolite with Si/Al = 2.7:1 was selected for calculations. Na^+ cations were distributed in the following way: 3, 8, and 2 in sites I, II, and I′, respectively.[36] Note that this is a unique cation distribution where all sites II are fully occupied and one of four sites I is replaced by a pair of I′ sites. Note also that only eight Na^+ cations in sites II are accessible for CO_2 molecules.

Na-A: Calculations on the CO_2/Na-A system were described in detail in Ref. [19]; the following notation for Na^+ sites was adopted: Na^+ cations located inside the 6-ring, in the 8-ring, and on top of the 4-ring were denoted S1, S2, and S3, respectively.

Generalized model for CO_2 adsorption in zeolites

Based on a systematic investigation of carbon monoxide adsorption in metal-exchanged zeolites by a combination of experimental

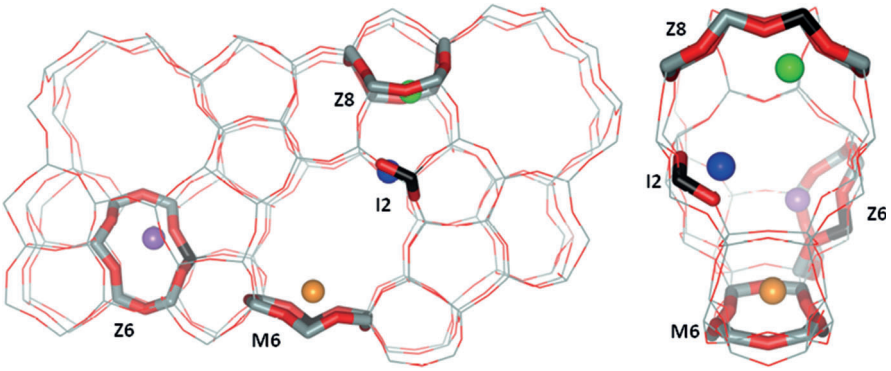

Figure 1. Extra-framework cation sites for Na^+ in Na-ZSM-5, viewed along the main channel (left) and the zigzag channel (right). The Na^+ cation located in the Z8, Z6, M6, and I2 site is depicted as a green, violet, orange, and blue ball, respectively. The Z8 and Z6 sites are located in the zigzag channel, whereas the M6 site is in the main channel; the I2 site is in the channel intersection. Framework Si, Al, and O atoms are shown in gray, black, and red, respectively.

and theoretical methods, a general model for adsorption in microporous materials was proposed by some of us.[37] This model was recently verified for CO_2 interacting with alkali-metal-exchanged zeolites.[20] It was shown that dispersion interactions between the adsorbate and the adsorbent played a much greater role in the case of CO_2 (where they accounted roughly for about one half of the overall interactions) than in the case of CO. The original model described elsewhere[37] was adopted herein, emphasizing features relevant to the CO_2 molecule: increased importance of dispersion interactions and electrostatic interactions due to the electric quadrupole moment. Note that both oxygen atoms bear a negative charge, an ideal situation for simultaneous interaction of the CO_2 molecule with two extra-framework cations. The interaction of CO_2 with microporous adsorbents can be formally divided into three contributions, as shown in Figure 2; these are described in more detail below.

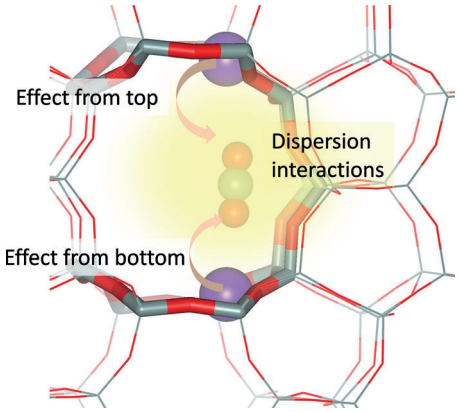

Figure 2. Generalized model of CO_2 interacting with a zeolite. CO_2 interacts with the primary extra-framework metal cation (violet ball at the bottom of the figure) and it can also interact with a secondary extra-framework metal cation (violet ball at the top of the figure) if there happens to be one. Dispersion interactions between the CO_2 molecule and the zeolite also play an important role, as there are many framework atoms all around the CO_2 molecule, both within a distance corresponding to the sum of atomic van der Waals radii and also at a longer distance.

Effect from bottom: This effect accounts for the interaction of CO_2 with the primary extra-framework metal cation. In the case of alkali or alkaline-earth-metal cations in zeolites, effects from bottom are dominated by the electrostatic interaction between the metal cation and the CO_2 quadrupole. Therefore, the importance of this effect increases with increasing cation charge, decreasing cation size, and decreasing coordination of extra-framework cations to framework oxygen atoms. The adsorption site where the CO_2 molecule interacts with only one extra-framework cation was denoted as the single cation (SC) site.

Effect from top: When two extra-framework cations are separated by a distance between 5 and 10 Å (depending on cation size and charge), the CO_2 molecule can interact with both cations simultaneously. Such a site, where CO_2 interacts with two cations at the same time, was denoted as the dual cation (DC) site. An example of CO_2 adsorption on a DC site is shown in Figure 2. For zeolites with very high concentration of accessible extra-framework cations (e.g., LTA), the CO_2 molecule can simultaneously interact even with more than two extra-framework cations;[19] the corresponding adsorption sites were denoted as multiple cation (MC) sites.

Dispersion interactions: Dispersion interactions are maximal when interacting atoms are at a distance equal to the sum of van der Waals radii and they decay quickly (r^{-6} in the asymptotic region) with increasing atom separation. Thus, dispersion interactions are particularly important for adsorption in microporous channels, since the molecule of the adsorbate (CO_2) is surrounded by framework atoms.

In the case of CO_2 adsorption, both effects, from the top and bottom, are predominantly of electrostatic origin, and hence, they are described by standard DFT functionals with good accuracy. Conversely, dispersion interactions are not correctly described when using common exchange-correlation functionals within generalized-gradient approximation and the correction for the accurate description of dispersion interactions is required. The DFT/CC correction scheme described above was adopted herein. It should be mentioned that the DFT/CC method is defined as a global correction of DFT (not only dispersion energy correction). However, for the systems investigated herein the dominant part of the DFT/CC correction accounted for the lack of dispersion energy. Therefore, in the discussion below the ΔE_{DFT} and $\Delta E_{DFT/CC}$ contributions are considered to be a measure of electrostatic and dispersion interactions, respectively, between the adsorbent and adsorbate.

Results and Discussion

The strength and mechanism of CO_2 interaction with zeolites depend on many parameters, and different types of interactions dominate isosteric heats of adsorption for zeolites with different concentrations of extra-framework cations. It is therefore advantageous to classify the zeolitic materials based on their composition: 1) purely siliceous materials (Si/Al$\rightarrow\infty$), 2) high-silica zeolites (Si/Al$>$12), 3) zeolites with intermediate Si/Al ratios (12$>$Si/Al$>$4), and 4) Al-rich zeolites (Si/Al$<$4). The results reported herein, along with abundant literature reports, are discussed below following this classification.

CO_2 adsorption in purely siliceous molecular sieves

There are no extra-framework cations present in siliceous materials. Therefore, the analysis of the results obtained for these materials should reveal the character and importance of CO_2 interactions with the zeolitic framework. Isosteric heats of CO_2 adsorption in purely siliceous microporous materials have been reported for several structures, including MFI, BEA, and LTA topologies.[30,38] They are summarized in Table 1 together with the results for the mesoporous purely siliceous material SBA-15. Experimental results can be compared with adsorption enthalpies, ΔH_{ads} (0 K), calculated at the DFT/CC level for LTA (Si/Al$\rightarrow\infty$) and MFI (Si/Al$\rightarrow\infty$) and with those previously reported for FER (Si/Al$\rightarrow\infty$).[28] A more detailed description of the calculated results is given in the Supporting Information.

Calculated and experimental results are in good agreement and, importantly, their relative values are correctly reproduced. Calculations show that the interaction between CO_2 and silicalite is dominated by dispersion interactions that account for at least 80% of the overall interaction and in some cases (e.g., CO_2 interaction with the 8-ring in FER reported in Ref. [28]) dispersion interactions account for almost 100% of adsorbate–ad-

Table 1. CO_2 adsorption heats in pure-silica zeotypes.

Zeotype topology	Density[a] [SiO_2 per 1000 Å^3]	Q_{st} ($0 \leftarrow \theta$)[b] [kJ mol^{-1}]	ΔH_{ads} (0 K)[c] [kJ mol^{-1}]
MFI	18.4	27,[d] 29[e]	26–28
FER	17.6		23–25[f]
BEA	15.3	21[g]	–
LTA	14.2	21[h]	20–22
SBA-15	11.0[i]	26[j]	–

[a] From the Database of Zeolite Structures.[39] [b] Experimental isosteric heats of adsorption at the low coverage limit. [c] Adsorption enthalpies calculated at the DFT/CC level. [d] From Refs. [38a, c]. [e] From Ref. [38b]. [f] From Ref. [28]. [g] From Ref. [38c]. [h] From Ref. [30]. [i] Half of the density of amorphous silica. [j] From Ref. [10b].

sorbent interactions. Consequently, the CO_2 molecules are adsorbed in the vicinity of the channel or cavity wall at the distance given approximately by the sum of van der Waals radii,[40] as shown in Figure 3a for CO_2 adsorbed in LTA (Si/Al$\rightarrow\infty$). CO_2 is located inside the LTA supercage close to the D4R unit to maximize dispersion interactions (geometry with the maximum number of framework atoms at the van der Waals contact with atoms of the adsorbate). The structure of the CO_2 adsorption complexes found in the main channel of MFI (Si/Al$\rightarrow\infty$) is depicted in Figure 3b; the CO_2 molecule is located in the main channel, as far as possible from the channel intersections and the orientation of the CO_2 molecule is such that the number of framework atoms in its vicinity is maximal. Calculations also indicate that the potential energy surface (PES) for CO_2 diffusion through the channels is relatively flat corresponding to the fact that the PES is mostly determined by the dispersion interactions. It should also be mentioned that based on DFT/CC periodic calculations a somewhat peculiar structure has been reported for FER (Si/Al$\rightarrow\infty$), where CO_2 is located in the middle of an 8-ring window (see Figure 6a in Ref. [28]). A similar structure was also found here for LTA (Si/Al$\rightarrow\infty$); the stability of this structure is driven by an optimal van der Waals distance between the carbon atom of CO_2 and the eight oxygen atoms of the 8-ring window.

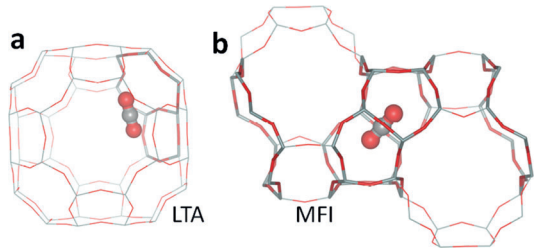

Figure 3. Adsorption of CO_2 in purely siliceous materials: LTA (a) and MFI (b). Atoms of the CO_2 molecule are depicted as balls; framework Si and O atoms are shown as gray and red wires, respectively. Atoms of the 6-ring and D4R of LTA closest to adsorbed CO_2 are depicted in tube mode (a). MFI is viewed along the zigzag channel direction; Si and O atoms on the main channel surface are shown in a tube mode (b).

It follows that adsorption heats of CO_2 in purely siliceous zeotypes should increase with decreasing size of the channel or cavity and with increasing thickness of the channel wall. Indeed, data reported in Table 1 shows that Q_{st} correlates with the zeolite density; nonetheless, this correlation does not hold for mesoporous SBA-15. The framework density of SBA-15 is 7.9 SiO_2 per 1000 Å^3; however, it is more meaningful to consider a density of 11.0 SiO_2 per 1000 Å^3, which is half of the density of the SBA-15 wall (amorphous silica): CO_2 adsorbs on the wall of SBA-15 mesopores and it interacts with the atoms of the wall on one side of the CO_2 molecule, whereas there are no atoms to interact with on the other side. Clearly, the CO_2 adsorption heat on a smooth SBA-15 mesopore wall should not exceed 20 kJ mol^{-1}; a significantly larger experimentally determined value thus indicates that the surface of the wall is corrugated and that CO_2 is not adsorbed on the flat silica surface. This is in line with recent reports evaluating the surface roughness of SBA-15 molecular sieves.[41]

CO_2 adsorption in high-silica zeolites

The concentration of extra-framework cations in high-silica zeolites is expected to be too low to allow the formation of DC sites suitable for adsorption of CO_2 (this is true only for samples with a homogeneous concentration of framework aluminum throughout the crystal; this point is addressed in a greater detail below). Assuming there are no DC sites in a high-silica sample, the interaction of CO_2 with the zeolite is driven by the (specific) electrostatic interaction with the extra-framework cations at SC sites and it is further increased by the (nonspecific) dispersion interaction with the zeolite framework. Therefore, adsorption heats are driven by the effect from bottom, which reflects the coordination of the extra-framework cation with the framework.

Interactions of CO_2 with alkali-metal cations in a high-silica FER zeolite were investigated previously by a combination of experimental and theoretical approaches.[20] It was shown that the effect from bottom on the adsorption enthalpy of CO_2 decreased with increasing cation size. It is also known from a previous investigation of carbon monoxide interaction with lithium-exchanged zeolites that the effect from bottom is larger in ZSM-5 than that in FER (see, e.g., Refs. [42] and [29] for Na-FER and Na-ZSM-5, respectively, or Refs. [43] and [44] for Li-FER and Li-ZSM-5, respectively). For this reason, we have investigated CO_2 adsorption in a high-silica Na-ZSM-5 zeolite computationally by employing the DFT/CC method and a periodic DFT model; results are summarized in Table 2.

The Na^+ cation at the Z6/T10 site is located on top of a 6-ring on the wall of the zigzag channel (Figure 4a) and it is coordinated to four framework oxygen (O_f) atoms. Consequently, the interaction of CO_2 with this Na^+ cation is the weakest among all investigated Na^+ sites in Na-ZSM-5 ($-\Delta E_{DFT}=$ 22 kJ mol^{-1}). The strongest CO_2 interaction is found for the I2/T6 intersection site (Figure 4b), where the Na^+ cation is coordinated to only two O_f atoms. The electrostatic component of the interaction energy (corresponding mostly to the CO_2 interaction with the extra-framework cation) for the I2/T6 site is

Table 2. Calculated characteristics of CO_2 adsorption complexes formed in the Na-ZSM-5 zeolite.[a]

Al position	Na^+ site[b]	CO_2 location[c]	r(Na–O_f)[d] [Å]	r(Na–OCO) [Å]	E_{int}(DFT)[e] [kJ mol^{-1}]	$\Delta E_{DFT/CC}$[f] [kJ mol^{-1}]	ΔH^0(0 K)[g] [kJ mol^{-1}]
SC site							
T10	Z6	CH	2.36, 2.39, 2.40, 2.68	2.326	−22.4	−24.2	−45
T4	Z6	CH	2.29, 2.34, 2.63, 2.69	2.324	−25.7	−24.2	−48
T11	M6	I	2.31, 2.32, 2.49, 2.51	2.320	−27.6	−19.2	−45
T12	Z8	I	2.33, 2.33, 2.63	2.347	−31.0	−17.4	−46
T6	I2	W	2.28, 2.29	2.345	−32.2	−20.3	−51
DC site							
T10	I2		2.24, 2.27	2.397	−47.1	−18.4	−64
T12	Z8		2.31, 2.33, 2.55	2.424			

[a] Calculated at the DFT/CC level by employing a periodic model of the MFI UC. [b] For notation, see Figure 1. [c] Location of the CO_2 molecule within the zeolite channel system; CH, I, and W represent the CO_2 molecule in the channel, on the intersection, and on the wall at the channel crossing, respectively. [d] Distance between the Na^+ cation and framework oxygen atoms. [e] Interaction energy between CO_2 and Na-ZSM5 calculated at the DFT level. [f] DFT/CC correction of DFT interaction energy, mostly due to the dispersion interaction. [g] Adsorption enthalpy at 0 K calculated as $E_{int}(DFT) + \Delta E_{DFT/CC} + \Delta ZPVE$; a zero-point vibrational energy correction of 2 kJ mol^{-1} calculated previously for the CO_2/Na-FER system was used.[15b]

10 kJ mol^{-1} larger than that for the Z6/T10 site (Table 2). Calculations thus show that the effect from bottom is indeed significant in MFI-type zeolites. The results summarized in Table 2 also show a good correlation between cation coordination with the framework and its ability to bind CO_2; channel wall sites (Z6/T10, Z6/T4, M6/T11, and Z8/T12) are all characterized by a smaller value of $-\Delta E_{DFT}$ than that of the intersection site (I2/T6). However, the situation is more complex when the dispersion component of the CO_2–framework interaction is also considered. When CO_2 interacts with the Na^+ cation at the channel wall site (where the electrostatic interaction with CO_2 is weaker), and when the localization of Na^+ within the zeolite channel system allows, the CO_2 molecule is located as far as possible from the channel intersection to maximize the dispersion component of its interaction with the framework. The dispersion interaction is maximal when CO_2 is in the zigzag channel (Figure 4a), where there is the maximum number of framework atoms around the adsorbate. As seen from the results given in Table 2, the dispersion interaction ($-\Delta E_{DFT/CC}$) is comparable with, or even larger than, the electrostatic interaction ($-\Delta E_{DFT}$) for sites Z6/T10 and Z6/T4. The dispersion interaction for these sites is up to 7 kJ mol^{-1} larger than that for intersection sites. Consequently, the difference in adsorption enthalpy (last column of Table 2) for the channel wall and intersection sites is not as large.

The isosteric heats of adsorption of CO_2 on M-ZSM-5 (Si/Al = 30; M = Li, Na, K) were recently investigated.[38b] The reported results for Na-ZSM-5 can be directly compared with those quoted in Table 2. Experimental isosteric heats reported for Na-ZSM-5 (Si/Al = 30) start at 49 kJ mol^{-1} and they gradually decrease to 46 and 44 kJ mol^{-1} at CO_2/Na ratios of 0.5:1.0 and 1.0:1.0, respectively.[38b] The difference between the isosteric heats at the low coverage limit (which correspond to the energetically most favorable sites) and those obtained for CO_2/Na = 1:1 ($\theta = 1$ indicates the least stable CO_2 adsorption complexes are formed) can be taken as a measure of the effect from bottom. The difference of 5 kJ mol^{-1} observed experimentally is in perfect agreement with the results reported in Table 2. Experimental and computational results are in very good agreement, not only qualitatively but also quantitatively (difference of about 2 kJ mol^{-1}). Experimental results reported in Reference [38b] also showed a rather large effect from bottom for Li-ZSM-5; about 10 kJ mol^{-1} measured as the difference between Q_{st} at low coverage and at $\theta = 1$, which is almost twice as much as the difference observed for Na-ZSM-5 and K-ZSM-5. The isosteric heat of CO_2 on Li-ZSM-5 (Si/Al = 30) drops down to 27 kJ mol^{-1} (value reported for Silicalite-1), which is already below the coverage 1.5:1 = CO_2/Li[38b] and is much faster than in the case of Na- and K-ZSM-5 (Si/Al = 30) samples. This indicates that the adsorption capacity of Li^+ sites in Li-ZSM-5 is smaller, which is due to the preference of small Li^+ cations for channel wall sites[32,34] that do not allow the formation of geminal adsorption complexes;[29,44] with increasing cation size there is a growing preference for intersection sites where geminal complexes can be easily formed. Consequently, the increasing preference for intersection sites found for larger cations[34] leads to increased population of geminal complexes and an increased number of CO_2 molecules directly interacting with extra-framework cations. Note also that the CO_2 adsorption complexes on DC sites are not formed in Na-ZSM-5 (Si/Al = 30), although calculations showed that such complexes were about 10 kJ mol^{-1} more stable than those of CO_2 adsorption complexes on the SC sites.

The detailed description of CO_2 adsorption in ZSM-5 zeolites given above is remarkably similar to that reported for high-silica ferrierites.[20,28] We believe that this is a general model that can be used for the description of CO_2 adsorption in any high-silica zeolite. Experimental results for several sodium-exchanged high-silica zeolites are collected in Figure 5, showing the dependence of isosteric heats on CO_2 loading (expressed as the number of CO_2 molecules per extra-framework cation). The results for Na-ZSM-5 (Si/Al = 35), Na-ZSM-11 (Si/Al = 35), Na-TNU-9 (Si/Al = 35), Na-IM-5 (Si/Al = 30), and Na-SSZ-74 (Si/Al = 100) are reported. All of these zeolites have relatively similar topologies: the channel system of all of them is formed by a three-dimensional network of 10-ring channels (limited in the third dimension for IM-5). All of these high-silica zeolites are also available with similar Si/Al ratios (except for SSZ-74, which can only be synthesized with a very high Si/Al ratio). The exact location of alkali-metal cations in the channel systems is not known. Isosteric adsorption heats at low coverages

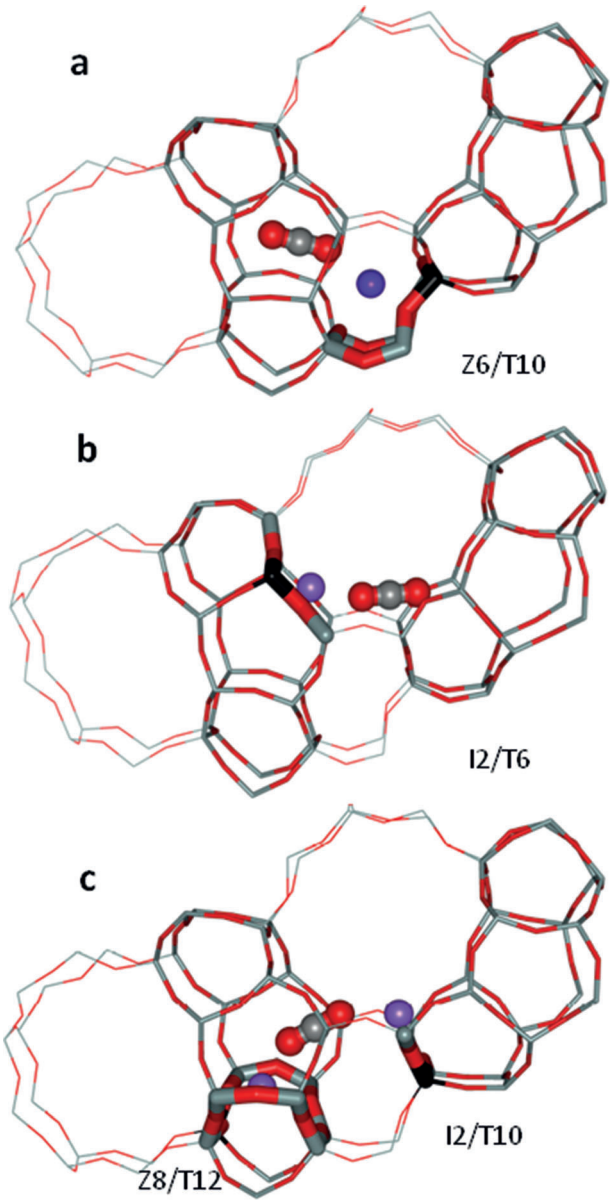

Figure 4. CO_2 adsorption complexes on Na-ZSM-5. CO_2 atoms and Na^+ cations are depicted as balls, see caption of Figure 1 for color scheme. ZSM-5 is viewed along the main channel; the zigzag channel surface is shown in tube mode. The CO_2 adsorption complexes on the Na^+ cation in the channel wall site Z6/T10 (a) and in the intersection site I2/T6 (b) are shown, together with the adsorption complex on a DC site (c).

obtained for TNU-9, IM-5, ZSM-5, and ZSM-11 are between 40 and 45 kJ mol^{-1}. The values of adsorption heats at low coverages indicate the absence (or only a very limited concentration) of DC sites in these zeolites. For higher coverages, the adsorption heats decrease to about 30 kJ mol^{-1}, which is typical for CO_2 adsorption in siliceous microporous solids.

CO_2 adsorption in zeolites with intermediate Si/Al ratios

The largest heterogeneity of CO_2 adsorption sites can be found in zeolites with intermediate Si/Al ratios. The same set of SC sites as those found in high-silica materials are also available here (intersection and channel wall sites differing in metal cation/framework coordination) and, in addition, with increasing extra-framework cation concentration (decreasing Si/Al ratio) the number of DC sites increases. Therefore, the isosteric heat of adsorption measured for such zeolites does not depend only on the cation size and coordination (effect from bottom), but also on the cation concentration and attendant presence of DC sites (effect from top). It should be noted that the ratio of SC and DC cation sites depends, in addition to cation concentration, on the zeolite topology and even (in some cases) on the synthetic method (see below).

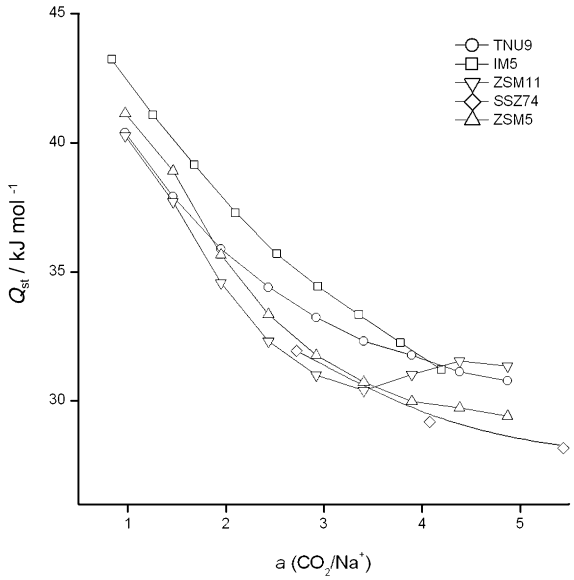

Figure 5. Isosteric heats of carbon dioxide adsorption in high-silica Na-zeolites. The adsorbed amount is expressed as the number of CO_2 molecules per Na^+ cation.

Experimental isosteric heats obtained for Li-, Na-, and K-exchanged ferrierites with two different Si/Al ratios [FER (Si/Al = 8.6) and FER (Si/Al = 27) samples] are shown in Figure 6. Results reported for the high-silica Na-FER sample are similar to those reported in Figure 5 for different high-silica zeolites. Conversely, results reported for the Na-FER sample with Si/Al = 8.6:1 are distinctly different (Figure 6). The higher isosteric heats obtained at low coverage of CO_2 were recently ascribed to CO_2 adsorption complexes on DC sites.[20] Formation of CO_2 adsorption complexes on DC sites was also supported by IR spectroscopy, which showed a shift of $\Delta\nu_3$ (asymmetric stretching vibration) to a higher value than that observed for CO_2 adsorption on SC sites, in agreement with theoretical predictions.[15b, 20, 28, 45]

Adsorption of CO_2 in alkali-metal-exchanged FER zeolites was also investigated recently by using calorimetric measurements, which allowed the determination of isosteric heats for very low amounts of adsorbed CO_2 (about 1 CO_2 per 100 extra-framework cations, $\theta = 0.01$ of a monolayer).[46] Isosteric heats obtained at low coverage for Li-FER (Si/Al = 8.6) and Li-FER (Si/Al = 27) were equal, indicating that the amount of DC sites was negligible in both samples. Conversely, for Na-FER and K-

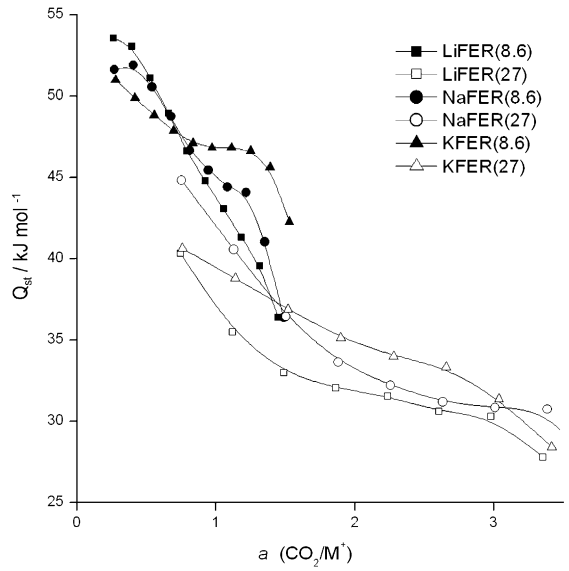

Figure 6. Isosteric heats of carbon dioxide adsorption in ferrierites. The adsorbed amount is expressed as the number (a) of CO_2 molecules per cation.

FER zeolites, adsorption heats at the $\theta \rightarrow 0$ limit measured for FER (8.6) samples were about 10 kJ mol^{-1} larger than those obtained for FER (27) samples. The difference between Li-FER and Na- and K-FER zeolites is understandable in light of a previous investigation of alkali-metal-cation coordination in zeolites.[43–44] First, the optimum distance between a pair of extra-framework cations to set up a DC site for the CO_2 molecule is 6.5, 7.3, and 8.3 Å for Li, Na, and K cations, respectively (as determined by cluster model calculations). Second, the Li^+ cation preferably occupies the channel wall sites, in particular the 6-ring, where it can fit in the middle of the ring, and thus, maximize its interaction with the zeolite framework; the probability of formation of a DC site is thus further decreased.

Experimental data reported for CO_2 adsorption on Na-FER and K-FER zeolites indicate the presence of a small amount (however, experimentally detectable) of DC sites even for the FER (Si/Al = 27) zeolites.[20,46] The presence of DC sites in some high-silica zeolites leads to a large increase of Q_{st} at low amounts of CO_2 adsorbed. Large values of Q_{st} were reported for $\theta \rightarrow 0$ for other zeolites with a large Si/Al ratio; for example, Q_{st} = 49 kJ mol^{-1} for K-ZSM-5 (Si/Al = 14)[13a] and 61 kJ mol^{-1} for Na-ZSM-5 (Si/Al = 14).[47] Therefore, we also investigated the possible formation of CO_2 adsorption complexes on DC sites in Na-ZSM-5. Instead of a systematic investigation of DC sites in Na-ZSM-5 (which is computationally very demanding), we only considered one particular pair of Na^+ cations described recently for CO adsorption in Na-ZSM-5.[29] A very stable CO_2 adsorption complex ($-\Delta H^0$ = 64 kJ mol^{-1}) was found (Table 2) for this DC site in agreement with experimental reports; the corresponding structure is depicted in Figure 4c.

It has been reported recently that the dependence of Q_{st} on the amount of CO_2 adsorbed was also influenced by the template synthesis procedure.[48] Two FER samples with almost identical Si/Al ratios (Si/Al = 15.6), but synthesized with different templates, showed a qualitatively different Q_{st} dependence of the amount of CO_2 adsorbed. In particular, one of the samples showed a constant value of Q_{st} irrespective of the amount of CO_2 adsorbed, which was explained in terms of a very regular distribution of aluminum atoms in the zeolite framework (which are situated as far as possible from one another).

CO_2 adsorption in Al-rich zeolites

A combination of volumetric gas adsorption measurements, variable-temperature (VTIR) spectroscopy,[49] and periodic DFT calculations was used to investigate CO_2 adsorption on the zeolite Na-A (Si/Al = 1:1).[19] The main findings can be summarized as follows: Due to the large number of Na^+ cations accessible for adsorbate molecules in each zeolite supercage, all of the adsorbed CO_2 molecules interact with more than one extra-framework cation, thus forming adsorption complexes on DC and MC sites. A possible SC site was also found computationally; however, the calculated adsorption enthalpy (-23 kJ mol^{-1}) was only about half of that found for DC and MC sites (-44 to -55 kJ mol^{-1}). The CO_2 molecule in the SC site would be directed towards the center of the supercage, which results in a small dispersion interaction energy (-6 kJ mol^{-1}) compared with that shown by CO_2 adsorbed on DC and MC sites (-21 to -23 kJ mol^{-1}). Therefore, and in agreement with experimental results, CO_2 only adsorbs on DC or MC sites in Na-A.

Qualitatively different conclusions were drawn, based on combined experimental and computational results for CO_2 adsorption on Na-Y.[15a] In this case, no CO_2 adsorption complexes on DC sites were found. This observation was explained by the fact that Na^+ cations in adjacent SII sites (inside the zeolite supercage) were 9.9 Å apart from each other, a significantly longer distance than the optimum separation (7.3 Å) for a DC site.

The calculations referred to above were performed by Pirngruber et al. for a model of the Y zeolite with Si/Al = 5:1.[15a] As reported in the Experimental Section, we performed periodic DFT/CC calculations for CO_2 adsorption on Na-Y (Si/Al = 2.7:1); the results obtained are summarized in Table 3. There are eight accessible Na^+ cations in our model, which is the same as in the model used by Pirngruber et al.[15a] Our calculations confirmed that there were no DC sites available for CO_2 adsorption, not even when the Si/Al ratio was as small as 2.7:1. The most stable CO_2 adsorption complex (denoted B in Table 3) is depicted in Figure 7; the CO_2 molecule interacts with a Na^+ cation in site II and the dispersion interaction with the framework is maximized when the molecule is tilted towards a 4-ring in the supercage wall. Note that an adsorption complex with a structure similar to that reported in Ref. [15a], which points towards the center of the supercage, was also found (C in Table 3) to be a local minimum (only 1 kJ mol^{-1} less stable than complex B). Further investigations showed that the relative stability of adsorption complexes in Na-Y (Na/Al = 2.7:1) depended on the particular configuration of framework Al and Na^+ atoms. It is not possible to say which of these complexes represents the global minimum on the PES without fur-

Table 3. Calculated characteristics of CO_2 adsorption complexes formed in FAU-type zeolites.[a]

CO_2 site	CO_2 location[b]	r(Na–O_f)[c] [Å]	r(Na–OCO) [Å]	E_{int}(DFT)[d] [kJ mol^{-1}]	$\Delta E_{DFT/CC}$[e] [kJ mol^{-1}]	ΔH^0(0 K)[f] [kJ mol^{-1}]
A	supercage wall	*2.25*, *2.26*, 2.36	2.399	−20.0	−17.2	−35
B	supercage wall	*2.25*, *2.26*, 2.35	2.381	−21.3	−19.8	−39
C	supercage center	*2.25*, *2.26*, 2.37	2.413	−22.1	−17.5	−38

[a] Calculated at the DFT/CC level by employing a periodic model of the FAU primitive cell. [b] See Figure 7. [c] Distance between the Na^+ cation and framework oxygen atoms; O atoms of AlO_4 tetrahedra are in italic. [d] Interaction energy between CO_2 and FAU calculated at the DFT level. [e] DFT/CC correction of DFT interaction energy, mostly due to the dispersion interaction. [f] Adsorption enthalpy at 0 K calculated as E_{int}(DFT) + $\Delta E_{DFT/CC}$ + ΔZPVE; a zero-point vibrational energy correction of 2 kJ mol^{-1} calculated previously for the CO_2/Na-FER system was used.[15b]

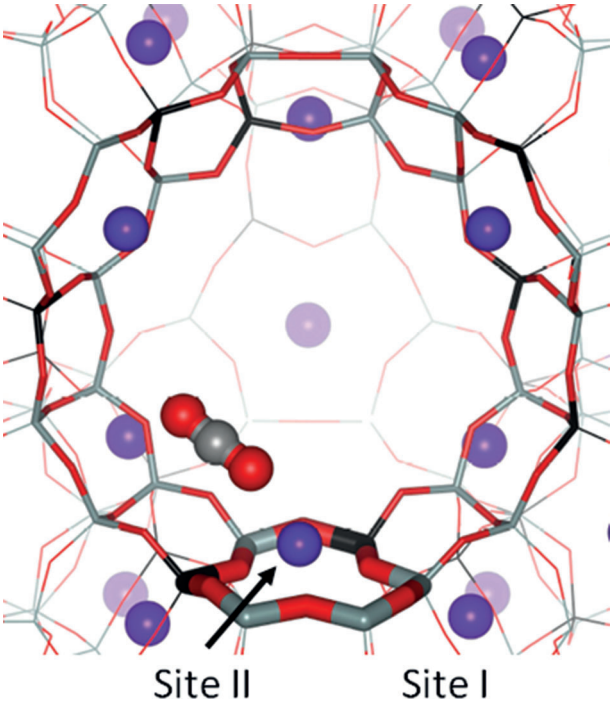

Figure 7. CO_2 adsorption complex on Na-Y. CO_2 atoms and Na^+ cations are depicted as balls, see caption of Figure 1 for color scheme. The CO_2 molecule interacts with a Na^+ cation at site II and is tilted towards a 4-ring situated in the supercage wall.

ther investigation. However, it can be safely concluded that no DC sites are available in Na-Y (Si/Al = 2.7:1). The adsorption of CO_2 on DC sites in Na-Y can be expected only when sites III become occupied by Na^+ cations and that can only be expected for Si/Al < 2:1.[36]

The dependence of isosteric heats on CO_2 loading for zeolites NaA, NaX, and NaY is shown in Figure 8. In the case of NaA zeolite, Q_{st} quickly decreases with increasing a; a relatively low pore volume and high concentration of Na^+ cations result in only about 0.6 CO_2/Na^+ ratio at 10^5 Pa. High and quickly decreasing Q_{st} observed for the NaX zeolite can be attributed to a large concentration of Na^+ in SIII′ sites. Upon the saturation of Na^+ cations in SIII′ sites, the isosteric heats reported for NaX become very similar to those found for the NaY zeolite; CO_2 molecules interact dominantly with Na^+ cations at SII sites. An increase in Q_{st} observed for NaY for $a > 0.8$ should be attributed to the increasing importance of lateral interactions.

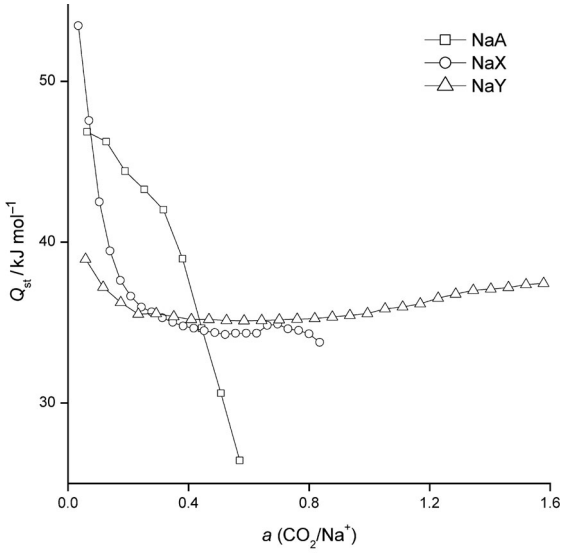

Figure 8. Isosteric heats of CO_2 adsorption in NaA, NaX, and NaY zeolites. The adsorbed amount is expressed as the number of CO_2 molecules per Na^+ cation.

CO_2 adsorption in micro- and mesoporous materials: General aspects

The results reported above show that a clear understanding of the mechanisms of CO_2 adsorption in zeolites can only be attained when the framework topology on the one side, and the extra-framework cation size, charge, concentration, and distribution, on the other, are simultaneously analyzed. Some general aspects of the interaction of CO_2 with micro- and mesoporous materials are critically reviewed below.

The strongest electrostatic interaction is expected for the smallest alkali-metal cation. However, in some cases, the same zeolite sample ion-exchanged to the Na, K, or Cs form gives higher Q_{st} than that of the Li form, see, for example, Figure 6 for FER (Si/Al = 27). This behavior can be explained by one of the following effects: First, the concentration of extra-framework cations is such that the amount of DC sites in the Li form of the zeolite is negligible, whereas there is an experimentally detectable amount of DC sites in another alkali-metal form of this zeolite. Second, Li^+ cations are only located at the channel wall sites, whereas larger cations are located at the intersection sites as well.

For a particular framework topology, the Q_{st} value increases with increasing cation concentration. First, increased cation concentration may result in occupation of intersection sites

that are not populated at lower cation concentrations (e.g., sites III vs. sites II in FAU). However, even this generalization is not 100% valid; the synthetic procedure can influence the framework Al distribution, and thus, isosteric heats also depend on zeolite synthetic conditions.[48]

Zeolite topology has a large effect on isosteric heats. First, zeolites in which extra-framework cations occupy sites on the channel intersection are characterized by large Q_{st} values; a larger Q_{st} value is found for the intersection of two 10-rings (e.g., MFI) than that for the intersection of 10- and 8-ring channels (e.g., FER). Second, DC sites are already formed for Si/Al > 10 (e.g., FER) in zeolites with narrow channels, whereas for zeolites with a large cavity (e.g., FAU) a value of Si/Al < 2 is required.

The arguments given above should help us to understand the differences in isosteric heats reported for zeolites and related materials. The fact that FAU zeolites with a relatively high concentration of extra-framework cations are characterized by rather low Q_{st} values[15a,16c,50] is still somewhat puzzling and is discussed in greater detail below. There are only DC and MC sites in Na-A (Si/Al = 1:1), and there is even a significant fraction of DC sites in Na-FER (Si/Al = 8.6) and Na-ZSM-5 (Si/Al = 14:1) zeolites. Conversely, there are no DC sites in Na-FAU (Si/Al = 2.7). This rather surprising result can be understood as follows: 1) Only some Na^+ cations in Na-FAU (Si/Al = 2.7:1) are accessible for the CO_2 molecules (8 SII sites in the model adopted herein); hence the effective Na^+ concentration for CO_2 adsorption in FAU-type zeolites (considering only the accessible Na^+ cations) can be significantly lower than the actual Si/Al ratio corresponding to the zeolite chemical composition. 2) For a broad range of Si/Al ratio, Na^+ cations are regularly distributed among sites II, I, and I′ (with nearly 100% occupancy of sites II); sites I and I′ are not accessible to CO_2, and nearest SII sites are almost 10 Å apart from each other, which is too large a distance for a CO_2 molecule to interact with both Na^+ cations simultaneously. The CO_2 adsorption mechanism is qualitatively different in K-FAU (Si/Al = 2.7:1). The K^+ ions are too large to fit inside the 6-ring; thus, site II is shifted above the ring towards the supercage, and consequently, adjacent K^+ cations in sites II are only 8.6 Å apart,[15a] which is close enough to constitute a DC site for CO_2.

Differences between micro- and mesoporous materials are discussed below based on the CO_2 isosteric heats measured for alkali-metal-exchanged Al-SBA-15 (Figure 9). Interpretation of these results is complicated by the fact that there is no information about the structure of the surface of the mesopores. The relatively low values of isosteric heats reported in Figure 9 indicate that there are no DC sites in any of the Al-SBA-15 samples. The lower value of the isosteric heat observed for the Al-SBA-15/Li^+ sample (relative to that of Al-SBA-15/Na^+ and Al-SBA-15/K^+) indicates that Li^+ cations are relatively well coordinated with the framework oxygen atoms, while Na^+ and K^+ cations are more exposed towards the mesopore free space and more accessible for molecules of CO_2.

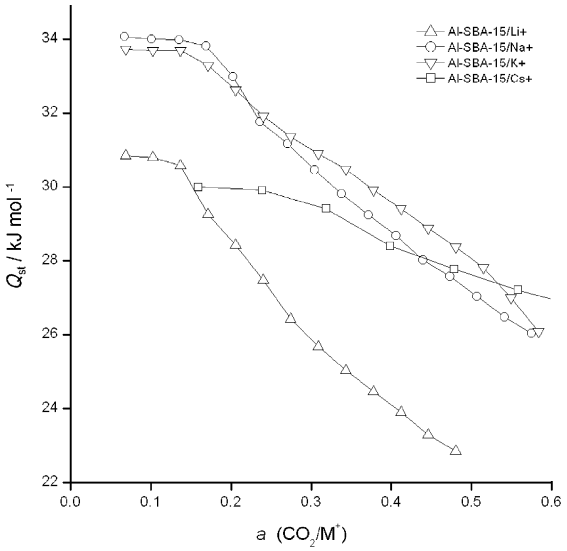

Figure 9. Isosteric heats of carbon dioxide adsorption on alkali-metal-cation-doped Al-SBA-15. The adsorbed amount is expressed as the number of CO_2 molecules per cation.

Conclusions

Based on the analysis of numerous experimental and theoretical results collected for zeolites with different structures and compositions, key factors influencing the CO_2 interaction with zeolites were identified. There are three dominant effects determining heats of adsorption of CO_2:

1) Effects from bottom: The strongest interaction can be expected with extra-framework cations with a large charge/ionic radius ratio; however, the cation must also be sufficiently exposed in the zeolite channel (or cavity) to efficiently interact with CO_2. Increasing coordination of the extra-framework metal cation with the framework leads to a decreased interaction energy with CO_2. It follows that extra-framework cations on channel intersections usually show larger values of $-\Delta H^0$ than those located on channel walls. The number of framework Al atoms in the vicinity of the extra-framework cation being considered can also play a role.
2) Effects from top: The charge distribution in CO_2 makes this molecule an ideal adsorbate to interact simultaneously with two extra-framework cations in DC sites. Adsorption of CO_2 on these sites is stronger than that on SC sites. The DC site is formed when two extra-framework cations are at a suitable distance from each other to form a linear $M^+\cdots O{=}C{=}O\cdots M^+$ adsorption complex (the optimum distance for such a CO_2 adsorption complex is 6.5, 7.3, and 8.3 Å for Li^+, Na^+, and K^+, respectively). The concentration of dual cation (DC) sites depends mainly on the Si/Al ratio, which dictates the average concentration of extra-framework cations. However, it also depends on zeolite topology and on the distribution of Al atoms in the zeolite framework.

3) Dispersion interactions: van der Waals dispersion interactions between CO_2 and framework atoms are behind the relatively large CO_2 adsorption enthalpy observed, even for purely siliceous zeolites. Dispersion interactions depend on the zeolite topology (channel diameter) and on channel wall thickness (framework density). In some cases, these interactions can account for more than 50% of the overall interaction energy between CO_2 and zeolites, even for relatively low Si/Al ratios.

It follows that for applications requiring large CO_2 adsorption heats, zeolites showing either the maximal effect from bottom (e.g., Li^+ cations on the intersection site formed by two 10-ring channels) or zeolites with a large number of DC sites (e.g., a pair of Na^+ cations in two neighboring 8-ring in FER) should be used. For cases where constant adsorption heats are required, it becomes more complicated to find a suitable zeolite; a lower cation concentration should be used (to avoid the formation of DC sites) and as homogeneous a distribution of extra-framework cations as possible is desirable.

Acknowledgements

The work of J.C. and A.Z. was supported by the Grant Agency of the Czech Republic (GACR 203/08/0604). The work of P.N. and L.G. was supported by GACR (203/09/0134) and by grant MSM0021620857 from ME CR.

Keywords: adsorption · carbon dioxide · density functional theory · zeolites

[1] a) R. B. Alley, T. Berntsen, N. L. Bindoff, Z. Chen, A. Chidthaisong, P. Friedlingstein, J. M. Gregory, G. C. Hegerl, M. Heimann, B. Hewitson, B. J. Hoskins, F. Joos, J. Jouzel, V. Kattsov, U. Lohmann, M. Manning, T. Matsuno, M. Molina, N. Nicholls, J. Overpeck, D. Qin, G. Raga, V. Ramaswamy, J. Ren, M. Rusticucci, S. Solomon, R. Somerville, T. F. Stocker, P. A. Stott, R. J. Stouffer, P. Whetton, R. A. Wood, D. Wratt *Summary for Policymakers*, in *Climate Change: The Physical Science Basis* (Eds.: S. Solomon, D. Qin, M. Manning, Z. Chen, M. Marquis, K. B. Averyt, M. Tignor, H. L. Miller), IPCC 2007: Cambridge University Press, Cambridge, **2007**; b) S. A. Rackley, *Carbon Capture and Storage*, Elsevier, Amsterdam, **2010**; c) J. M. Klara, J. E. Plunkett, *Int. J. Greenhouse Gas Control* **2010**, *4*, 112 – 118.

[2] a) D. Aaron, C. Tsouris, *Sep. Sci. Technol.* **2005**, *40*, 321 – 348; b) G. Pellegrini, R. Strube, G. Manfrida, *Energy* **2010**, *35*, 851 – 857; c) R. Strube, G. Pellegrini, G. Manfrida, *Energy* **2011**, *36*, 3763 – 3770; d) A. A. Olajire, *Energy* **2010**, *35*, 2610 – 2628.

[3] a) E. J. Stone, J. A. Lowe, K. P. Shine, *Energy Environ. Sci.* **2009**, *2*, 81 – 91; b) K. Z. House, C. F. Harvey, M. J. Aziz, D. P. Schrag, *Energy Environ. Sci.* **2009**, *2*, 193 – 205; c) R. Strube, G. Manfrida, *Int. J. Greenhouse Gas Control* **2011**, *5*, 710 – 726; d) J. Davison, *Energy* **2007**, *32*, 1163 – 1176.

[4] a) B. Thitakamol, A. Veawab, A. Aroonwilas, *Int. J. Greenhouse Gas Control* **2007**, *1*, 318 – 342; b) M. Karl, R. F. Wright, T. F. Berglen, B. Denby, *Int. J. Greenhouse Gas Control* **2011**, *5*, 439 – 447.

[5] a) A. L. Chaffee, G. P. Knowles, Z. Liang, J. Zhany, P. Xiao, P. A. Webley, *Int. J. Greenhouse Gas Control* **2007**, *1*, 11 – 18; b) R. T. Yang, *Gas Separation by Adsorption Processes*, Butterworths, Boston, **1987**.

[6] a) N. Hedin, L. J. Chen, A. Laaksonen, *Nanoscale* **2010**, *2*, 1819 – 1841; b) R. P. Ribeiro, T. P. Sauer, F. V. Lopes, R. F. Moreira, C. A. Grande, A. E. Rodrigues, *J. Chem. Eng. Data* **2008**, *53*, 2311 – 2317; c) C. Lu, H. Bai, B. Wu, F. Su, J. F. Hwang, *Energy Fuels* **2008**, *22*, 3050 – 3056; d) L. Zhou, X. Liu, J. Li, N. Wang, Z. Wang, Y. Zhou, *Chem. Phys. Lett.* **2005**, *413*, 6 – 9.

[7] a) P. L. Llewellyn, S. Bourrelly, C. Serre, A. Vimont, M. Daturi, L. Hamon, G. De Weireld, J. S. Chang, D. Y. Hong, Y. K. Hwang, S. H. Jhung, G. Ferey, *Langmuir* **2008**, *24*, 7245 – 7250; b) A. O. Yazaydin, R. Q. Snurr, T. H. Park, K. Koh, J. Liu, M. D. LeVan, A. I. Benin, P. Jakubczak, M. Lanuza, D. B. Galloway, J. J. Low, R. R. Willis, *J. Am. Chem. Soc.* **2009**, *131*, 18198 – 18199; c) O. K. Farha, A. O. Yazaydin, I. Eryazici, C. D. Malliakas, B. G. Hauser, M. G. Kanatzidis, S. T. Nguyen, R. Q. Snurr, J. T. Hupp, *Nat. Chem.* **2010**, *2*, 944 – 948; d) J. R. Li, J. Sculley, H. C. Zhou, *Chem. Rev.* **2012**, *112*, 869 – 932; e) Y. S. Bae, R. Q. Snurr, *Angew. Chem.* **2011**, *123*, 11790 – 11801; *Angew. Chem. Int. Ed.* **2011**, *50*, 11586 – 11596.

[8] a) D. M. D'Alessandro, B. Smit, J. R. Long, *Angew. Chem.* **2010**, *122*, 6194 – 6219; *Angew. Chem. Int. Ed.* **2010**, *49*, 6058 – 6082; b) S. Cavenati, C. A. Grande, A. E. Rodrigues, *J. Chem. Eng. Data* **2004**, *49*, 1095 – 1101; c) P. J. E. Harlick, F. H. Tezel, *Microporous Mesoporous Mater.* **2004**, *76*, 71 – 79; d) S. Choi, J. H. Drese, C. W. Jones, *ChemSusChem* **2009**, *2*, 796 – 854; e) A. Ghoufi, L. Gaberova, J. Rouquerol, D. Vincent, P. L. Llewellyn, G. Maurin, *Microporous Mesoporous Mater.* **2009**, *119*, 117 – 128; f) S. T. Yang, J. Kim, W. S. Ahn, *Microporous Mesoporous Mater.* **2010**, *135*, 90 – 94; g) T. Montanari, E. Finocchio, E. Salvatore, G. Garuti, A. Giordano, C. Pistarino, G. Busca, *Energy* **2011**, *36*, 314 – 319; h) M. R. Delgado, C. O. Arean, *Energy* **2011**, *36*, 5286 – 5291.

[9] a) P. J. E. Harlick, A. Sayari, *Ind. Eng. Chem. Res.* **2006**, *45*, 3248 – 3255; b) V. Zeleňák, M. Badaničová, D. Halamová, J. Čejka, A. Zukal, N. Murafa, G. Goerigk, *Chem. Eng. J.* **2008**, *144*, 336 – 342; c) A. Zukal, J. Jagiello, J. Mayerova, J. Cejka, *Phys. Chem. Chem. Phys.* **2011**, *13*, 15468 – 15475.

[10] a) P. J. E. Harlick, A. Sayari, *Ind. Eng. Chem. Res.* **2007**, *46*, 446 – 458; b) A. Zukal, I. Dominguez, J. Mayerova, J. Cejka, *Langmuir* **2009**, *25*, 10314 – 10321.

[11] a) G. Férey, C. Serre, T. Devic, G. Maurin, H. Jobic, P. L. Llewellyn, G. De Weireld, A. Vimont, M. Daturi, J. S. Chang, *Chem. Soc. Rev.* **2011**, *40*, 550 – 562; b) Q. A. Wang, J. Z. Luo, Z. Y. Zhong, A. Borgna, *Energy Environ. Sci.* **2011**, *4*, 42 – 55; c) L. Valenzano, B. Civalleri, K. Sillar, J. Sauer, *J. Phys. Chem. C* **2011**, *115*, 21777 – 21784.

[12] a) A. R. Millward, O. M. Yaghi, *J. Am. Chem. Soc.* **2005**, *127*, 17998 – 17999; b) S. Keskin, T. M. van Heest, D. S. Sholl, *ChemSusChem* **2010**, *3*, 879 – 891; c) P. D. C. Dietzel, V. Besikiotis, R. Blom, *J. Mater. Chem.* **2009**, *19*, 7362 – 7370; d) L. Grajciar, A. D. Wiersum, P. L. Llewellyn, J.-S. Chang, P. Nachtigall, *J. Phys. Chem. C* **2011**, *115*, 17925 – 17933.

[13] a) B. Bonelli, B. Civalleri, B. Fubini, P. Ugliengo, C. O. Arean, E. Garrone, *J. Phys. Chem. B* **2000**, *104*, 10978 – 10988; b) E. Garrone, B. Bonelli, C. Lamberti, B. Civalleri, M. Rocchia, P. Roy, C. O. Arean, *J. Chem. Phys.* **2002**, *117*, 10274 – 10282; c) P. Galhotra, J. G. Navea, S. C. Larsen, V. H. Grassian, *Energy Environ. Sci.* **2009**, *2*, 401 – 409.

[14] D. F. Plant, G. Maurin, I. Deroche, L. Gaberova, P. L. Llewellyn, *Chem. Phys. Lett.* **2006**, *426*, 387 – 392.

[15] a) G. D. Pirngruber, P. Raybaud, Y. Belmabkhout, J. Cejka, A. Zukal, *Phys. Chem. Chem. Phys.* **2010**, *12*, 13534 – 13546; b) A. Pulido, P. Nachtigall, A. Zukal, I. Dominguez, J. Cejka, *J. Phys. Chem. C* **2009**, *113*, 2928 – 2935.

[16] a) E. D. Akten, R. Siriwardane, D. S. Sholl, *Energy Fuels* **2003**, *17*, 977 – 983; b) A. Hirotani, K. Mizukami, R. Miura, H. Takaba, T. Miya, A. Fahmi, A. Stirling, M. Kubo, A. Miyamoto, *Appl. Surf. Sci.* **1997**, *120*, 81 – 84; c) G. Maurin, P. L. Llewellyn, R. G. Bell, *J. Phys. Chem. B* **2005**, *109*, 16084 – 16091; d) D. F. Plant, G. Maurin, I. Deroche, P. L. Llewellyn, *Microporous Mesoporous Mater.* **2007**, *99*, 70 – 78.

[17] O. Bludský, M. Rubeš, P. Soldán, P. Nachtigall, *J. Chem. Phys.* **2008**, *128*, 114102.

[18] a) M. Rubeš, J. Kysilka, P. Nachtigall, O. Bludský, *Phys. Chem. Chem. Phys.* **2010**, *12*, 6438 – 6444; b) L. Grajciar, O. Bludský, P. Nachtigall, *J. Phys. Chem. Lett.* **2010**, *1*, 3354 – 3359.

[19] A. Zukal, C. O. Arean, M. R. Delgado, P. Nachtigall, A. Pulido, J. Mayerová, J. Cejka, *Microporous Mesoporous Mater.* **2011**, *146*, 97 – 105.

[20] A. Zukal, A. Pulido, B. Gil, P. Nachtigall, O. Bludsky, M. Rubes, J. Cejka, *Phys. Chem. Chem. Phys.* **2010**, *12*, 6413 – 6422.

[21] A. Zukal, J. Pawlesa, J. Cejka, *Adsorption* **2009**, *15*, 264 – 270.

[22] A. Zukal, J. Mayerova, M. Kubu, *Top. Catal.* **2010**, *53*, 1361 – 1366.

[23] A. Zukal, J. Mayerova, J. Cejka, *Phys. Chem. Chem. Phys.* **2010**, *12*, 5240 – 5247.

[24] T. Montanari, G. Busca, *Vib. Spectrosc.* **2008**, *46*, 45 – 51.

[25] a) G. Kresse, J. Hafner, *Phys. Rev. B* **1994**, *49*, 14251 – 14269; b) G. Kresse, J. Furthmuller, *Comput. Mater. Sci.* **1996**, *6*, 15 – 50; c) G. Kresse, D. Joubert, *Phys. Rev. B* **1999**, *59*, 1758 – 1775.

[26] J. P. Perdew, K. Burke, M. Ernzerhof, *Phys. Rev. Lett.* **1996**, *77*, 3865 – 3868.
[27] P. E. Blöchl, *Phys. Rev. B* **1994**, *50*, 17953 – 17979.
[28] C. Otero Areán, M. R. Delgado, G. F. Bibiloni, O. Bludský, P. Nachtigall, *ChemPhysChem* **2011**, *12*, 1435 – 1443.
[29] C. O. Arean, M. R. Delgado, K. Frolich, R. Bulanek, A. Pulido, G. F. Bibiloni, P. Nachtigall, *J. Phys. Chem. C* **2008**, *112*, 4658 – 4666.
[30] M. Palomino, A. Corma, F. Rey, S. Valencia, *Langmuir* **2010**, *26*, 1910 – 1917.
[31] A. Pulido, M. R. Delgado, O. Bludsky, M. Rubes, P. Nachtigall, C. O. Arean, *Energy Environ. Sci.* **2009**, *2*, 1187 – 1195.
[32] P. Nachtigall, K. Frolich, H. Drobna, O. Bludsky, D. Nachtigallova, R. Bulanek, *J. Phys. Chem. C* **2007**, *111*, 11353 – 11362.
[33] D. H. Olson, G. T. Kokotailo, S. L. Lawton, W. M. Meier, *J. Phys. Chem.* **1981**, *85*, 2238 – 2243.
[34] J. Kučera, P. Nachtigall, *Phys. Chem. Chem. Phys.* **2003**, *5*, 3311 – 3317.
[35] a) W. Loewenstein, *Am. Mineral.* **1954**, *39*, 92 – 96; b) W. Dempsey, G. H. Kuhl, D. H. Olson, *J. Phys. Chem.* **1969**, *73*, 387 – 390.
[36] T. Frising, P. Leflaive, *Microporous Mesoporous Mater.* **2008**, *114*, 27 – 63.
[37] a) D. Nachtigallová, O. Bludský, C. Otero Areán, R. Bulánek, P. Nachtigall, *Phys. Chem. Chem. Phys.* **2006**, *8*, 4849 – 4852; b) C. Otero Areán, M. R. Delgado, C. L. Bauca, L. Vrbka, P. Nachtigall, *Phys. Chem. Chem. Phys.* **2007**, *9*, 4657 – 4661.
[38] a) J. A. Dunne, R. Mariwala, M. Rao, S. Sircar, R. J. Gorte, A. L. Myers, *Langmuir* **1996**, *12*, 5888 – 5895; b) R. Bulánek, K. Frolich, E. Frydova, P. Cicmanec, *J. Therm. Anal. Calorim.* **2011**, *105*, 443 – 449; c) S. Bourrelly, G. Maurin, P. L. Llewellyn in *Molecular Sieves: From Basic Research to Industrial Applications, Parts A and B, Vol. 158* (Eds.: J. Cejka, N. Zilkova, P. Nachtigall), Elsevier, Amsterdam, **2005**, pp. 1121 – 1128.
[39] http://www.iza-struture.org/databases/.
[40] A. Bondi, *J. Phys. Chem.* **1964**, *68*, 441 – 451.
[41] a) A. Zukal, H. Siklova, J. Cejka, *Langmuir* **2008**, *24*, 9837 – 9842; b) C. J. Gommes, H. Friedrich, M. Wolters, P. E. de Jongh, K. P. de Jong, *Chem. Mater.* **2009**, *21*, 1311 – 1317; c) I. G. Shenderovich, G. Buntkowsky, A. Schreiber, E. Gedat, S. Sharif, J. Albrecht, N. S. Golubev, G. H. Findenegg, H. H. Limbach, *J. Phys. Chem. B* **2003**, *107*, 11924 – 11939; d) A. A. Gurinov, Y. A. Rozhkova, A. Zukal, J. Cejka, I. G. Shenderovich, *Langmuir* **2011**, *27*, 12115 – 12123.
[42] P. Nachtigall, M. R. Delgado, K. Frolich, R. Bulanek, G. T. Palomino, C. L. Bauca, C. O. Arean, *Microporous Mesoporous Mater.* **2007**, *106*, 162 – 173.
[43] P. Nachtigall, R. Bulanek, *Appl. Catal. A* **2006**, *307*, 118 – 127.
[44] D. Nachtigallová, P. Nachtigall, O. Bludský, *Phys. Chem. Chem. Phys.* **2004**, *6*, 5580 – 5587.
[45] O. Bludský, P. Nachtigall, V. Spirko, *Collect. Czech. Chem. Commun.* **2011**, *76*, 669 – 682.
[46] R. Bulánek, K. Frolich, E. Frydova, P. Cicmanec, *Top. Catal.* **2010**, *53*, 1349 – 1360.
[47] B. Bonelli, B. Onida, B. Fubini, C. O. Arean, E. Garrone, *Langmuir* **2000**, *16*, 4976 – 4983.
[48] P. Nachtigall, L. Grajciar, J. Perez-Pariente, A. B. Pinar, A. Zukal, J. Cejka, *Phys. Chem. Chem. Phys.* **2012**, *14*, 1117 – 1120.
[49] a) C. Otero Areán, O. V. Manoilova, G. T. Palomino, M. R. Delgado, A. A. Tsyganenko, B. Bonelli, E. Garrone, *Phys. Chem. Chem. Phys.* **2002**, *4*, 5713 – 5715; b) P. Nachtigall, M. R. Delgado, D. Nachtigallova, C. O. Arean, *Phys. Chem. Chem. Phys.* **2012**, *14*, 1552 – 1569.
[50] G. Maurin, Y. Belmabkhout, G. Pirngruber, L. Gaberova, P. Llewellyn, *Adsorption* **2007**, *13*, 453 – 460.

Received: April 15, 2012
Published online on August 10, 2012

Attachment H

PCCP

Cite this: *Phys. Chem. Chem. Phys.*, 2012, **14**, 1117–1120

www.rsc.org/pccp

COMMUNICATION

Control of CO_2 adsorption heats by the Al distribution in FER zeolites: effect of synthesis conditions†

Petr Nachtigall,[a] Lukáš Grajciar,[a] Joaquín Pérez-Pariente,[b] Ana B. Pinar,[b] Arnošt Zukal[c] and Jiří Čejka*[c]

Received 5th September 2011, Accepted 16th November 2011
DOI: 10.1039/c1cp22816a

Proper combination of template and optimized reaction conditions provides zeolite FER with homogeneous distribution of Al in the framework; this results in a new zeolite adsorbent exhibiting a constant heat of CO_2 adsorption.

Adsorption of CO_2 in various materials, including zeolites, functionalized silicas, metal oxides, carbon based materials and metal–organic frameworks, is currently being investigated with respect to environmental issues related to green-house gases capture and storage.[1–7] Many of these materials suffer from a substantial energetic heterogeneity,[8] adsorption heat is particularly high at low coverages and it quickly decreases with an increase in the amount of adsorbed CO_2. This site heterogeneity in alkali-metal exchanged zeolites has been recently interpreted in terms of the presence of *dual* cation sites,[2,9] where adsorbate molecules can simultaneously interact with two extra-framework metal cations. This is energetically favorable for molecules like CO_2 since each of its oxygen atoms can interact with one extra-framework cation. As a result, adsorption heats are significantly higher for *dual* cation sites than for ordinary *single* cation sites (adsorbate interacts only with one extra-framework cation).

The Li^+, Na^+, and K^+ exchanged zeolite ferrierites (FER framework type) with two different Si/Al ratios have been recently investigated by a combination of experimental and computational techniques, and the dependence of experimental adsorption heats on the CO_2 coverage was discussed in light of combined DFT/*ab initio* calculations.[2] The strength of the interaction of CO_2 with alkali-metal cations in zeolites depends on (i) the size and charge of the cation,[2] (ii) the concentration of cations in the channel system, which determines the possibility of formation of dual cation sites (where a molecule interacts with two extra-framework cations at the same time),[6] (iii) the size of the zeolite channel/cavity being reflected in the amount of dispersion interaction between CO_2 and framework[10] and (iv) the coordination of the extra-framework cation to framework oxygen atoms.[1] The majority of these parameters depend on the Al distribution in the zeolite framework. For a particular zeolite topology and an extra-framework cation, the position of Al in the framework determines the coordination and location of the extra-framework metal cations (the cation sites).

It follows that CO_2 is a suitable probe molecule to investigate the existence (and population) of dual cation sites. When the distance between a pair of Na^+ cations is in the range of 6–8 Å, its interaction with a CO_2 molecule is significantly strengthened (an increment of *ca.* 10 kJ mol^{-1} in the adsorption energy occurs).[6] Furthermore, the population of dual cation sites, as revealed by CO_2 adsorption, provides information about the distribution of framework Al atoms. The absence of dual cation sites in high-silica samples is an indication of *homogeneous* distribution of framework aluminium, *i.e.* Al atoms occupy T positions which are as far as possible form each other. Thus, the associated charge-compensating extra-framework cations are separated by a distance that is too long to allow the formation of dual cation sites.

A new synthesis strategy[11,12] has been designed to tailor the distribution of acid sites in zeolite FER.[13] This strategy, based on the use of suitable organic structure directing agents, in the absence of alkaline cations, could lead to the preparation of zeolites with the acid site distribution tuned for each specific catalytic application. Pyridine adsorption experiments monitored by FTIR showed that the distribution of acid sites (bridging hydroxyl groups) between the non-accessible positions of the FER cavity and the more open environment of the 10-ring channel in FER samples is strongly dependent on the combination of organic structure directing agents employed in its synthesis, and on the presence of sodium cations in the synthesis gel.[13] A good correlation between acid sites accessibility and catalytic activity of the samples has been found.[13,14]

It is the goal of this paper to show that not only the accessibility of Brønsted sites but also the homogeneity of Al distribution in the FER zeolite can be controlled with the synthesis strategy previously developed.[11,12] CO_2 adsorption is employed as a tool to seek information about the homogeneity of Al distribution, which, together with the Si/Al ratio (and thus with extra-framework cations concentration), determines

[a] *Department of Physical and Macromolecular Chemistry, Faculty of Science, Charles University of Prague, Hlavova 2030, Prague 2, 128 00, Czech Republic*
[b] *Instituto de Catálisis y Petroleoquímica, CSIC, C/Marie Curie 2, 28049-Cantoblanco, Spain*
[c] *J. Heyrovský Institute of Physical Chemistry, Academy of Sciences of the Czech Republic, v.v.i., Dolejškova 3, 182 23 Prague 8, Czech Republic. E-mail: jiri.cejka@jh-inst.cas.cz; Fax: 00420-28658-2307; Tel: 00420-26605-3795*
† Electronic supplementary information (ESI) available. See 10.1039/c1cp22816a

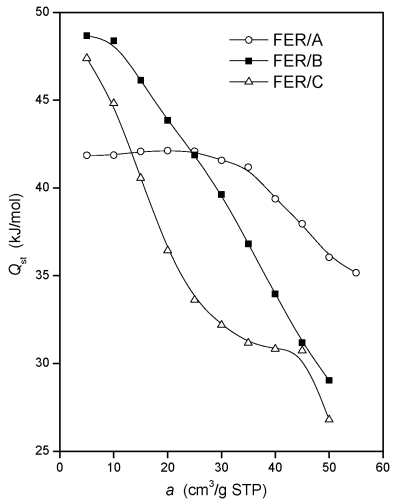

Fig. 1 Dependence of isosteric heats on the adsorbed amount of CO_2 for samples FER/A, FER/B and FER/C.

the existence of dual cation sites, and this, in turn, is reflected on the adsorption heats.

The dependence of CO_2 isosteric adsorption heats on the adsorbed amount for two FER samples with a similar Si/Al ratio (15.4 ± 0.2) prepared following our synthesis strategy to control the acid sites distribution[11–13] is depicted in Fig. 1. The FER/B sample exhibits the typical dependence of q_{st} on CO_2 coverage; a gradual decrease in q_{st} with an increase in the CO_2 : Na ratio evidences energetic heterogeneity of adsorption sites in this sample. A completely different situation is observed for the FER/A sample, for which q_{st} is almost constant from the onset of the adsorption isotherm up to the adsorbed amount of ~22.3 cm^3 g^{-1} STP corresponding to CO_2 coverage $\theta = 1$ (number of adsorbed CO_2 molecules equals the number of Na^+ cations).

Experimental data shown in Fig. 1 are discussed based on the results of combined DFT/*ab initio* theoretical investigation. A compilation of the adsorption enthalpies (ΔH^0) calculated for the most stable Na^+ sites (Fig. 2) in the vicinity of each of the four framework Al atoms is presented in Table 1. Adsorption enthalpies for the first and the second CO_2 molecule interacting with the single Na^+ cation site and for CO_2 adsorbed on the dual cation sites are shown.[2] Note that $-\Delta H^0$ values obtained for single cation sites are rather similar regardless the position of framework Al; the difference between the smallest and largest values of $-\Delta H^0$ is only 5 kJ mol^{-1} (Table 1). In contrast, the CO_2 adsorption on dual cation sites is characterized by adsorption enthalpies 10–12 kJ mol^{-1} greater than on the corresponding isolated Na^+ sites; except for the P6 site (Al in T4 position) where the Na^+ cation is tightly coordinated to the 6-ring and adsorption enthalpies are thus smaller.[15] Note that the adsorption enthalpy of the second CO_2 molecule on the Na^+ cation is 3–7 kJ mol^{-1} smaller than the corresponding value for the mono-CO_2 adsorption complex.

Table 1 Adsorption enthalpies, $-\Delta H^0$, calculated for CO_2 adsorption on Na^+ cations in the vicinity of Al in each of the four distinguishable framework sites (in kJ mol^{-1})

Al position[a]	Na^+ site[b]	1st CO_2[c] single Na^+	2nd CO_2[d] single Na^+	1st CO_2[e] dual Na^+
T1	I2	44	41	56
T2	I2	45	39	55
T3	M7	47	40	58[f]
T4	P6	42	38	46

[a] Numbering scheme from Atlas of Zeolite Structures is adopted.[16] [b] For site definition see Fig. 2. [c] One CO_2 molecule on a single Na^+ site. [d] $-\Delta H^0$ for the adsorption of a second CO_2 molecule on a single Na^+ site. [e] Adsorption on dual cation sites; both Na^+ cations are in the site type denoted in the second column. [f] Na^+ cations located in M7 and I2 sites.

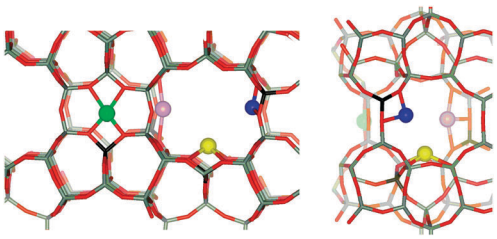

Fig. 2 Definition of Na^+ sites in Na-FER; view along the main (left) and perpendicular (right) channels. Na^+ cations in I2/T1, I2/T2, M7/T3, and P6/T4 sites are depicted as blue, violet, yellow, and green balls, respectively. Framework O, Si, and Al atoms are depicted in red, grey, and black colors, respectively.

Results reported in Fig. 1 for CO_2 coverage $\theta < 1$ could be, at least in principle, explained simply by the differences in $-\Delta H^0$ for individual single Na^+ sites (Table 1). It could be argued that all Na^+ cations are in the same site type (that requires also framework Al atoms in particular positions) in the sample FER/A whereas Na^+ cations (and framework Al) are distributed among all available sites in the FER/B sample. Consequently, former and latter cation distributions should result in a constant and decreasing isosteric heat, respectively (Fig. 1). However, such arguments must be ruled out: firstly, calculated differences in $-\Delta H^0$ are smaller than experimentally observed differences (sample FER/B) and, secondly, the results obtained for higher coverage are entirely inconsistent with such interpretation: the isosteric heats obtained for sample FER/B for coverage $\theta > 1$ are significantly lower than those of the sample FER/A and this contradicts the results reported in Table 1 for geminal complexes and as well as previous computational studies.[17] Adsorption enthalpies calculated for the geminal CO_2 complexes ($-\Delta H^0$ for the adsorption of the second CO_2 molecule on the Na^+ cation) are rather similar (within 3 kJ mol^{-1}). In general, the Na^+ cations coordinated inside the 6-ring on the channel wall (P6/T4 site in the case of Na-FER, Table 1) show lower ability to bind the first adsorbate molecule as well as the second adsorbate molecule (see Table 1 and ref. 6, 15 and 17 showing the same behaviour for other zeolites and adsorbates). Assuming that the constant and lower isosteric heats observed for the FER/A sample are due to Na^+ location exclusively in sites showing lower adsorption enthalpy, such a sample must show also lower isosteric heats for higher coverages. Since the FER/A sample shows higher isosteric heats than sample FER/B for $\theta > 1$, the interpretation proposed above must be ruled out.

The only reasonable explanation of the experimental results reported in Fig. 1 is based on the different involvement of dual cation sites in the adsorption of CO_2 molecules in each

ferrierite sample. Large values of adsorption enthalpies at low CO_2 coverage ($\theta < 1$) can be attributed to the formation of CO_2 adsorption complexes on dual cation sites (FER/B). The presence of dual cation sites generally increases adsorption enthalpies for $\theta < 1$ and also results summarized in Table 1 show that CO_2 adsorption complexes on dual cation sites are about 10 kJ mol^{-1} more stable than the corresponding CO_2 adsorption complexes on single Na^+ sites. It has been shown that Na^+ cations in Na-FER can interact with up to two CO_2 molecules at the same time.[6] Since the CO_2 molecule adsorbed on the dual site interacts with two cations, the available Na^+ sites are occupied faster and once the Na^+ sites are occupied additional CO_2 molecules cannot interact directly with extra-framework cations. Consequently, the presence of dual cation sites leads to a decrease in the adsorption enthalpies for coverage $\theta > 1$ to a value expected for a purely siliceous sample with the same topology. The adsorption enthalpy of CO_2 in siliceous FER of 25–26 kJ mol^{-1} has been reported.[10] (It should be noted that arguments given above hold only for zeolites with a sufficiently high Si/Al ratio.)

To further illuminate the explanation proposed above, a case example is depicted in Fig. 3. This figure is just a schematic representation, which aims to illustrate the concept of dual and single cation sites for CO_2 adsorption. For the sake of simplicity, two Na^+ cations per unit cell (one Na^+ per FER cage) are considered which corresponds to Si/Al = 17. The upper part of this figure depicts the situation where all the cations are distributed evenly in such a way that there is just one Na^+ in each FER cage (homogeneous distribution); Na^+ cations are far from each other and dual cation sites do not exist. Therefore, each Na^+ cation can form a geminal complex with two CO_2 molecules. A qualitatively different situation is schematically depicted in Fig. 3b, where the location of Na^+ cations is such that each Na^+ cation is surrounded by two other Na^+ cations establishing the dual cation sites for

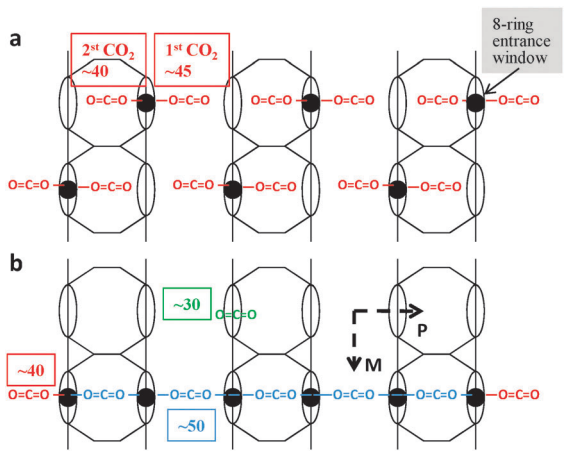

Fig. 3 Schematic representation of Na^+ cation distribution in Na-FER. Direction of the main (M) and perpendicular (P) channels is shown by arrows. Na^+ cations are depicted as black spheres. They are placed in the 8-ring entrance window of the FER cage. Part (a) shows the homogeneous distribution of Na^+ cations; lower part (b) shows the situation where Na^+ cations occupy adjacent entrance windows. Adsorbed CO_2 molecules are also depicted for *dual* cation sites (blue), single cation sites (red) and for non-specific interaction with framework (green). Estimated adsorption enthalpies for individual adsorption types are also shown (in kJ mol^{-1}).

CO_2 adsorption. Thus, each Na^+ cation can interact with two CO_2 molecules, however, on average there is just one CO_2 molecule per Na^+ cation. Considering first the situation depicted in Fig. 3a, q_{st} should be relatively constant for CO_2 adsorption up to $\theta \approx 1$ (there are no dual cation sites) and it should drop down only by about 5 kJ mol^{-1} for coverages in the range from $\theta = 1$ to $\theta = 2$. And this is exactly the situation depicted in Fig. 1 for experimental sample FER/A. Considering now the situation depicted in Fig. 3b, q_{st} should be again constant for CO_2 adsorption up to $\theta \approx 1$, however, much higher than in the previous case (only CO_2 adsorption complexes on dual cation sites are being formed). At coverage exceeding $\theta = 1$ the isosteric heats should sharply drop down to values below 30 kJ mol^{-1} since no Na^+ cations are accessible for CO_2 molecules any longer. This is of course an extreme situation where there are only dual cation sites in the sample and it certainly does not correspond to experimental results reported for sample FER/B in Fig. 1. However, experimental dependence of q_{st} on coverage can be understood in the following way: there are many dual cation sites available in the sample, however, there is still a certain fraction of Na^+ cations not involved in dual cation sites (and thus capable to participate in the formation of germinal adsorption complexes).

The interpretation of experimental results (Fig. 1) based on the relative population of single and dual cation sites described above can be further elaborated. The samples FER/A and FER/B described here have Si/Al = 15.4 ± 0.2, corresponding to *ca.* 2.2 Al atoms per unit cell (each unit cell contains 36 T atoms). Due to the topology and dimension of FER (a = 19.15, b = 14.30, c = 7.58 Å), the formation of Na^+ dual cation sites for CO_2 adsorption can only be avoided for a maximum of 2 Na^+ cations in UC. Therefore, for the FER samples with Si/Al < 17 the formation of dual cation sites is unavoidable. The fact that for the sample FER/A the dual cation sites are not observed (isosteric heats for $\theta < 0.18$ were not obtained, therefore we cannot exclude a small amount of *dual* cation sites at very low CO_2 coverage) is particularly remarkable. It can be only interpreted in terms of a very regular distribution of framework Al (with narrow distribution of Al–Al distances). This sample (FER-PYRR in ref. 13) presents the lowest percentage of accessible acid sites among the FER samples prepared with different combinations of SDAs in our previous work.[13] This implies that most of the acid sites in this sample are located in the inner part of the ferrierite cavity, not accessible for the pyridine probe molecule employed in the FTIR study reported in that article. Bearing in mind that the FER framework contains two cavities per unit cell, there would be at most 1 Al atom in each cavity, which could in turn counter balance the charge of only one Na^+ cation. This is consistent with the results discussed above, since this homogeneous distribution of aluminium would prevent the formation of dual cation sites for CO_2 adsorption, as the distance between two consecutive cavities which would contain Na^+ cations is more than 12 Å (as measured between two cavities in the same diagonal). This is too long to allow the interaction of a CO_2 molecule with two adjacent Na^+ cations.

To further support the arguments given *vide supra,* the isosteric heats as a function of CO_2 coverage for the FER/C

sample having Si/Al = 26.8 are also given in Fig. 1.[6] The existence of dual cation sites even in this high-silica FER is apparent from isosteric heats obtained at $\theta < \frac{1}{2}$. Since there are only 1.3 Na^+ cations in UC of FER/C, the isosteric heats quickly drop down below 35 kJ mol^{-1} at an adsorbed amount of 20 cm^3 g^{-1}, that for FER/C corresponds to $\theta > 1.5$.

It can be summarized that the results presented above provide clear evidence that the synthesis strategy designed in ref. 11–13 allows controlling the distribution of aluminium in zeolite FER. The synthesis of FER using exclusively pyrrolidine as the SDA (FER/A = FER-PYRR) provided the most even (homogeneous) distribution of aluminium. This resulted in the constant isosteric heats obtained for CO_2 coverage up to $\theta = 1$. In contrast, for sample FER/B (FER-BMP-TMA), the dependence of isosteric heat on the adsorbed amount of CO_2 is similar to the behaviour usually observed for conventional FER samples.

Experimental and theoretical section

Synthesis of FER zeolites was performed in fluoride medium from gels with Si/Al ratio = 15.7, containing either pyrrolidine (FER/A) or both 1-benzyl-1-methylpyrrolidinium hydroxide and tetramethylammonium hydroxide (FER/B) as structure directing agents (SDAs). The molar gel composition for the sample with bmpOH and TMAOH as SDAs was: 0.969 SiO_2 : 0.031 Al_2O_3 : 0.06 TMAOH : 0.48 bmpOH : 0.48 HF : 4.6 H_2O. For details see ESI.†

Adsorption isotherms of nitrogen at 77 K and carbon dioxide in the temperature range from 273 to 333 K were recorded using an ASAP 2020 (Micromeritics) static volumetric apparatus.

The home-made thermostat maintaining the temperature of the sample with accuracy ±0.01 K was used for the measurement of carbon dioxide adsorption at 273, 293, 313 and 333 K. The carbon dioxide isotherms at given temperatures were measured on the same sample, which was used for the nitrogen adsorption measurements.

Calculations were performed within the periodic DFT model employing VASP program package,[18] PBE exchange-correlation functional[19] and DFT/CC correction method[20] to account for dispersion interactions. Computational strategy is described briefly in ESI†; all details can be found in ref. 2.

Acknowledgements

Dr C. Marquez-Alvarez is acknowledged for his help with ammonia adsorption and FTIR measurements to asses that the ion exchange was complete. Funding (project MAT2009-13569) from the Spanish Ministry of Science and Innovation (MICINN) is greatly acknowledged. PN acknowledges the support of the GACR (203/09/0134) and the ME CR (LC512 and MSM0021620857). JČ and AZ thank the Grant Agency of the Czech Republic for financial support (203/08/0604).

Notes and references

1 A. Zukal, C. O. Arean, M. R. Delgado, P. Nachtigall, A. Pulido, J. Mayerova and J. Čejka, *Microporous Mesoporous Mater.*, 2011, **146**, 97–105.
2 A. Zukal, A. Pulido, B. Gil, P. Nachtigall, O. Bludsky, M. Rubes and J. Čejka, *Phys. Chem. Chem. Phys.*, 2010, **12**, 6413.
3 C. O. Arean and M. R. Delgado, *Appl. Surf. Sci.*, 2010, **256**, 5259.
4 J. van den Bergh, M. Mittelmeijer-Hazeleger and F. Kapteijn, *J. Phys. Chem. C*, 2010, **114**, 9379.
5 M. Palomino, A. Corma, F. Rey and S. Valencia, *Langmuir*, 2010, **26**, 1910.
6 A. Pulido, P. Nachtigall, A. Zukal, I. Dominguez and J. Čejka, *J. Phys. Chem. C*, 2009, **113**, 2928.
7 A. Pulido, M. R. Delgado, O. Bludsky, M. Rubes, P. Nachtigall and C. O. Arean, *Energy Environ. Sci.*, 2009, **2**, 1187.
8 S. Choi, J. H. Drese and C. W. Jones, *ChemSusChem*, 2009, **2**, 796.
9 E. Garrone, R. Bulanek, K. Frolich, C. O. Arean, M. R. Delgado, G. T. Palomino, D. Nachtigallova and P. Nachtigall, *J. Phys. Chem. B*, 2006, **110**, 22542.
10 C. O. Arean, M. R. Delgado, G. F. Bibiloni, O. Bludsky and P. Nachtigall, *ChemPhysChem*, 2011, **12**, 1435.
11 A. B. Pinar, L. Gomez-Hortiguela and J. Perez-Pariente, *Chem. Mater.*, 2007, **19**, 5617.
12 A. B. Pinar, J. Perez-Pariente and L. Gomez-Hortiguela, *WO Patent*, 2008116958-A1, 2008.
13 A. B. Pinar, C. Marquez-Alvarez, M. Grande-Casas and J. Perez-Pariente, *J. Catal.*, 2009, **263**, 258.
14 C. Marquez-Alvarez, A. B. Pinar, R. Garcia, M. Grande-Casas and J. Perez-Pariente, *Top. Catal.*, 2009, **52**, 1281.
15 P. Nachtigall, M. R. Delgado, K. Frolich, R. Bulanek, G. T. Palomino, C. L. Bauca and C. O. Arean, *Microporous Mesoporous Mater.*, 2007, **106**, 162.
16 Ch. Baerlocher and L. B. McCusker, Database of Zeolite Structures: http://www.iza-structure.org/databases/.
17 C. O. Arean, D. Nachtigallova, P. Nachtigall, E. Garrone and M. R. Delgado, *Phys. Chem. Chem. Phys.*, 2007, **9**, 1421.
18 G. Kresse and J. Hafner, *Phys. Rev. B*, 1993, **48**, 13115.
19 J. P. Perdew, K. Burke and M. Ernzerhof, *Phys. Rev. Lett.*, 1996, **77**, 3865.
20 O. Bludsky, M. Rubes, P. Soldan and P. Nachtigall, *J. Chem. Phys.*, 2008, **128**, 114102.

